R-8390

N71-16047

NASA CR 116047

PERFORMANCE ANALYSIS OF PROPULSION SYSTEMS

FINAL REPORT

(17 June 1969 through 18 October 1970)

By

J. A. Wrubel

Prepared For
George C. Marshall Space Flight Center
Marshall Space Flight Center,
Alabama 35812

November 1970

Contract NAS8-24568

Rocketdyne, A Division of
North American Rockwell Corporation
6633 Canoga Avenue, Canoga Park, California 91304

R-8390

PERFORMANCE ANALYSIS OF PROPULSION SYSTEMS

Final Report

(17 June 1969 through 18 October 1970)

By

J. A. Wrubel

Prepared For

George C. Marshall Space Flight Center
Marshall Space Flight Center
Alabama 35812

November 1970

Contract NAS8-24568

Rocketdyne, a Division of
North American Rockwell Corporation
6633 Canoga Avenue, Canoga Park, California 91304

FOREWORD

The effort described in this report was performed under G.O. 09208 from 17 June 1969 through 18 October 1970, and was technically managed by the Marshal Space Flight Center for the National Aeronautics and Space Administration under Contract No. NAS8-24568.

The contributions of Dr. G. A. Hosack, Mr. R. L. Proffit, Dr. W. F. Herget, Mr. G. L. Cline, Mr. W. S. Bose, Mr. E. J. Ostrowski, Mr. R. J. Guthrie, Mr. J. P. Dougherty, Mr. B. T. McDunn, Mr. J. T. Sabol, Mr. S. Zeldin, Mr. E. Embree, Mr. R. Weir, Mr. F. Traub, Mr. E. Pape, Mr. D. E. Hawkins, Mr. L. Maciel, Dr. L. J. Zajac, and Mr. W. H. Nurick to the technical effort are gratefully acknowledged.

This report was approved for formal printing via Telecon from T. F. Greenwood, NASA Technical Manager, to J. A. Wrubel, Rocketdyne Responsible Engineer, on 14 January 1971.

ABSTRACT

The improved understanding of gas-stream turbulent mixing is contingent upon obtaining a more comprehensive description of the resultant flow field and a more precise evaluation of the turbulent transport properties. Under Contract NAS7-521 a facility for study of this phenomenon was constructed and checked out. Characterization and diagnostic experiments together with some data analysis were accomplished under the present contract, NAS8-24568, and are described herein.

The flow field experimentally studied was the two-dimensional mixing of fuel-rich supersonic hydrogen-oxygen combustion products and a subsonic heated air-stream. The mixing was accomplished in a chamber accessible to both optical- and probe-type instrumentation systems. A total of 36 tests have been conducted which included studies of (1) film coolant interaction, (2) the two-dimensionality of the flow, (3) air temperature effects, (4) velocity ratio effects, (5) airstream turbulence effects, and (6) configuration effects. The data gathered consisted of (1) test section static pressure, (2) mixing layer temperature, (3) partial pressure of H_2O, (4) photographic information (UV, IR, color, and Schlieren), and (5) facility operation.

CONTENTS

ILLUSTRATIONS

FIGURE

TABLES

INTRODUCTION

Technological developments are required for advanced vehicle propulsion systems. One of the required technology development efforts, which is the subject of this study, is the improved understanding of high-speed gas mixing. Both fundamental and applied knowledge of turbulent mixing are required by engine designers to optimize the design of composite propulsion systems such as ramjets, scramjets, and air-augmented rockets. In addition, this information is applicable to the study of rocket engine exhaust plume afterburning. Here it can be utilized in such diverse fields as missile base heating and radio-frequency communication interference.

An extensive body of phenomenological theory on turbulent mixing exists. However, the proof of the validity of these theories, which are usually formulated in terms of an eddy transport coefficient or eddy viscosity, is greatly impeded by the limited knowledge of turbulent transport properties. This is particularly true in the case of mixing involving chemical reactions, as in flames. Therefore, the goal of this investigation is to experimentally determine in detail the developing free shear layer in a particular turbulent mixing process with combustion. The data thus obtained will be used to generate a comprehensive description of the flow field and to determine the turbulent transport properties of the mixing process.

In the past, probe-type instrumentation systems have been the primary source of data collection. These systems have the common disadvantage of disrupting the flow field in the vicinity of the measurement station which in turn introduces an inherent uncertainity into these data. This fundamental problem is overcome through utilization of optical instrumentation devices which can gather the same data, except velocity, without disturbing the flow field. These devices have been successfully used at Rocketdyne for a number of years.

The principal optical instruments (spectroradiometer and photographic pyrometer) utilized on this program were designed and constructed by Rocketdyne to conduct spectroscopic studies of rocket plume radiation. Measurements are taken through appropriate internal optics from a line of sight through the region of interest. When the region is enclosed by non-transparent hardware, windows must be utilized. Window materials are selected that ensure transmission of the particular specie radiation. Quartz is most commonly utilized because of its excellent mechanical and optical properties and is transparent to radiation from 2000 angstrons to 3 microns. Other more costly materials are required for transmission beyond this range.

The spectroradiometer is a versatile instrument, capable of both spatial and spectral scanning for quantitative emission and absorption measurements from the ultraviolet to the infrared spectral regions. It consists of a grating monochromator, detectors, entrance optics, radiation calibration sources, a turning fork radiation chopper capable of rapid startup or stop, and a zone ranging device, which enables the instrument to spatially scan across the exhaust plume. It can be used in a conventional manner to obtain spectral radiance and spectral absorption coefficients of a body of gas as a function of wavelength. Also, it can be used at a fixed wavelength to obtain spectral radiance, absorption coefficients, temperatures, and partial pressures of species as a function of spatial position.

The ultraviolet photographic pyrometer produces a photographic record of the spatial distribution of the apparent spectral radiance of the mixing region, or its equivalent brightness temperature, at low spectral resolution. Included in its field of view are both the hot gases to be measured and a radiation standard. The radiation standard consists of a calibrated tungsten filament lamp and a set of neutral density filters. The optical components of the pyrometer all transmit or reflect ultraviolet light.

These Rocketdyne-developed optical instruments were applied to the study of a 2-dimensional mixing layer between supersonic LOX/GH_2 combustion products and a subsonic heated airstream*. Under an earlier contract (NAS7-521), "Performance Analysis of Composite Propulsion Systems," the following was accomplished:

1. Hardware Design - Design of a suitable hydrogen-oxygen combustor, test section, and associated subsystems that ensure uniform parallel two-dimensional flow.

2. Test Hardware Fabrication. Construction of major components required for the experiments.

*This propellant combination is optically clean, i.e., it does not contain solid particles. Although flows containing solid particles can be handled by appropriate techniques, the complexities introduced do not warrant the study of propellant systems containing solid particles at this time.

3. Test Stand Buildup - Construction of a heated air supply, assembly of a control console, mounting of the test hardware, and mating of required supply lines (propellant, coolant, etc.) to the experimental configuration.

4. Facility Checkout - Preparation of the experiment operating manual and facility activation (cold flow and full-scale hot flow checkout tests).

5. Instrumentation Installation - Installation of the spectroradiometer, LASS (Large Aperture Spectrometer/Spectrograph), photographic pyrometer, test-section static pressure taps, and manometer bank.

6. Probe Instrumentation - The evaluation and procurement of special probe-type instrumentation devices for the determination of velocity and total pressure.

A detailed description of the accomplishment of these tasks is given in Refs. 1 and 2. For continuity, selected sections will be abstracted for inclusion in this report.

The present program was initiated on 17 June 1969 and the following which is described in this report was accomplished.

1. Traversing Mechanism Design and Fabrication - Design and construction of a traversing mechanism for probe-type instrumentation required to complete data collection requirements.

2. Testing - Conduction of 36 hot fire tests for the determination of:
    (a) the two-dimensionality of the flow
    (b) the effect of test-section film coolant on the mixing process

(c) a description of the basic configuration

(d) the effect of changes in air temperature

(e) the effect of changes in the air turbulence level

(f) the influence of velocity ratio.

3. Data Analysis - Test data reduction and presentation of the data into a usable form for subsequent calculation of the turbulent transport properties.

Utilization was made of the flow system fabricated and checked out under the previous contract. The above mentioned optical instrumentation systems and a 50-tube manometer bank were utilized for the determination of:

1. mixing layer temperature
2. mixing layer H_2O partial pressure
3. test section static pressure

The determination of the presence of any instabilities, background photographic data, and monitoring of facility operation were accomplished using "state-of-the-art" devices.

A detailed description of these results together with some background information is included in this report.

SUMMARY

This report discusses accomplishments made under NAS8-24568, "Performance Analysis of Propulsion Systems," which is a logical extension to the NAS7-521 contract, "Performance Analysis of Composite Propulsion Systems," described in Ref. 1 and 2. Figures 1 through 3 show the assembled test section, flow facility, zone radiometer, and schlieren apparatus.

A total of 36 full-scale tests were conducted with the apparatus and included studies of:

1. film coolant interaction
2. the two-dimensionality of the flow
3. air temperature effects
4. velocity ratio effects
5. airstream turbulence effects
6. configuration effects.

The data gathered consisted of:

1. test section static pressure
2. mixing layer temperature
3. partial pressure of H_2O
4. photographic information (UV, IR, color, and schlieren data)
5. facility operation.

These results represent the very first collection of mixing data utilizing non-interference techniques. Specialized use of optical instruments fulfilled the data

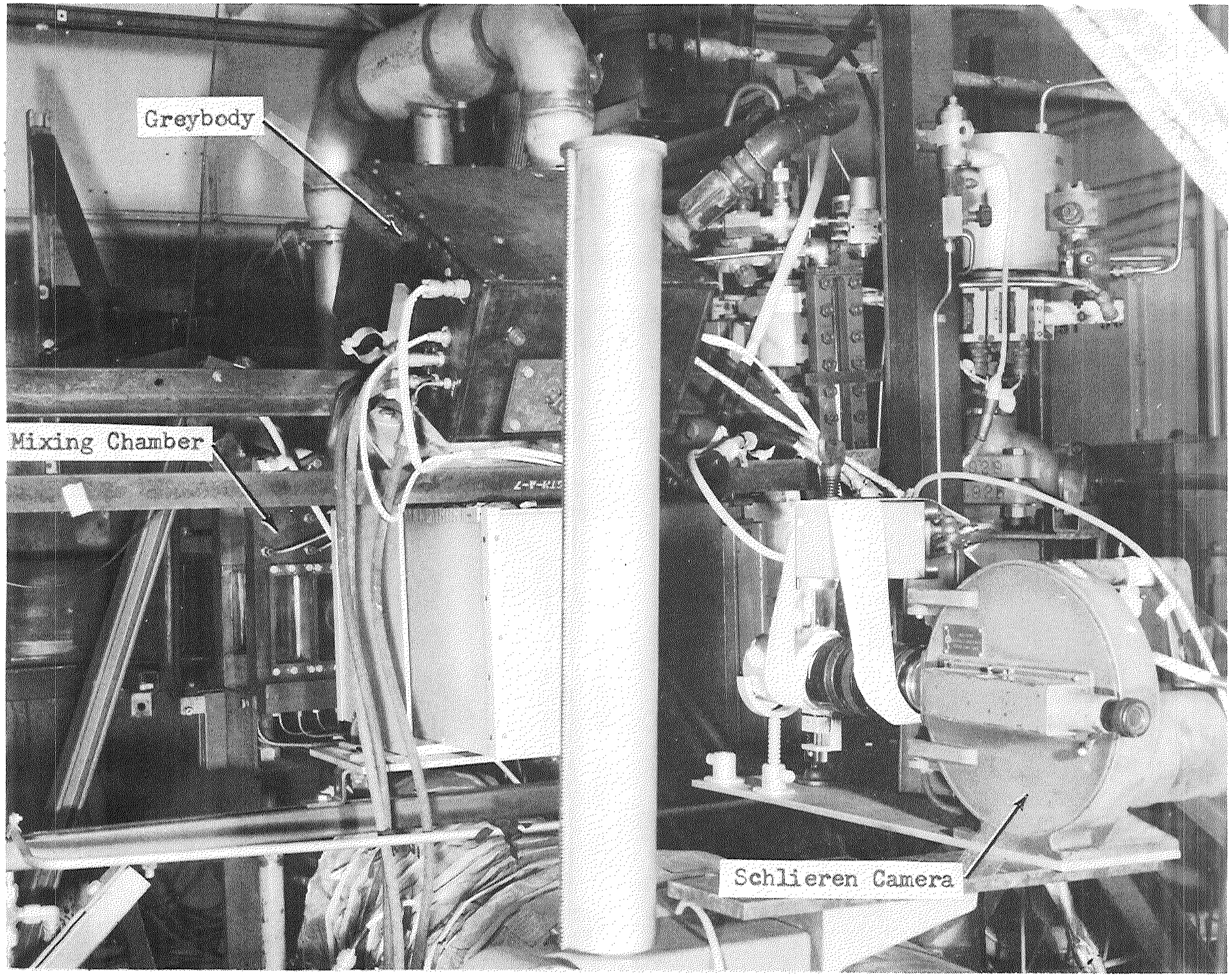

Figure 1. Test Section and Flow Facility (Right Side)

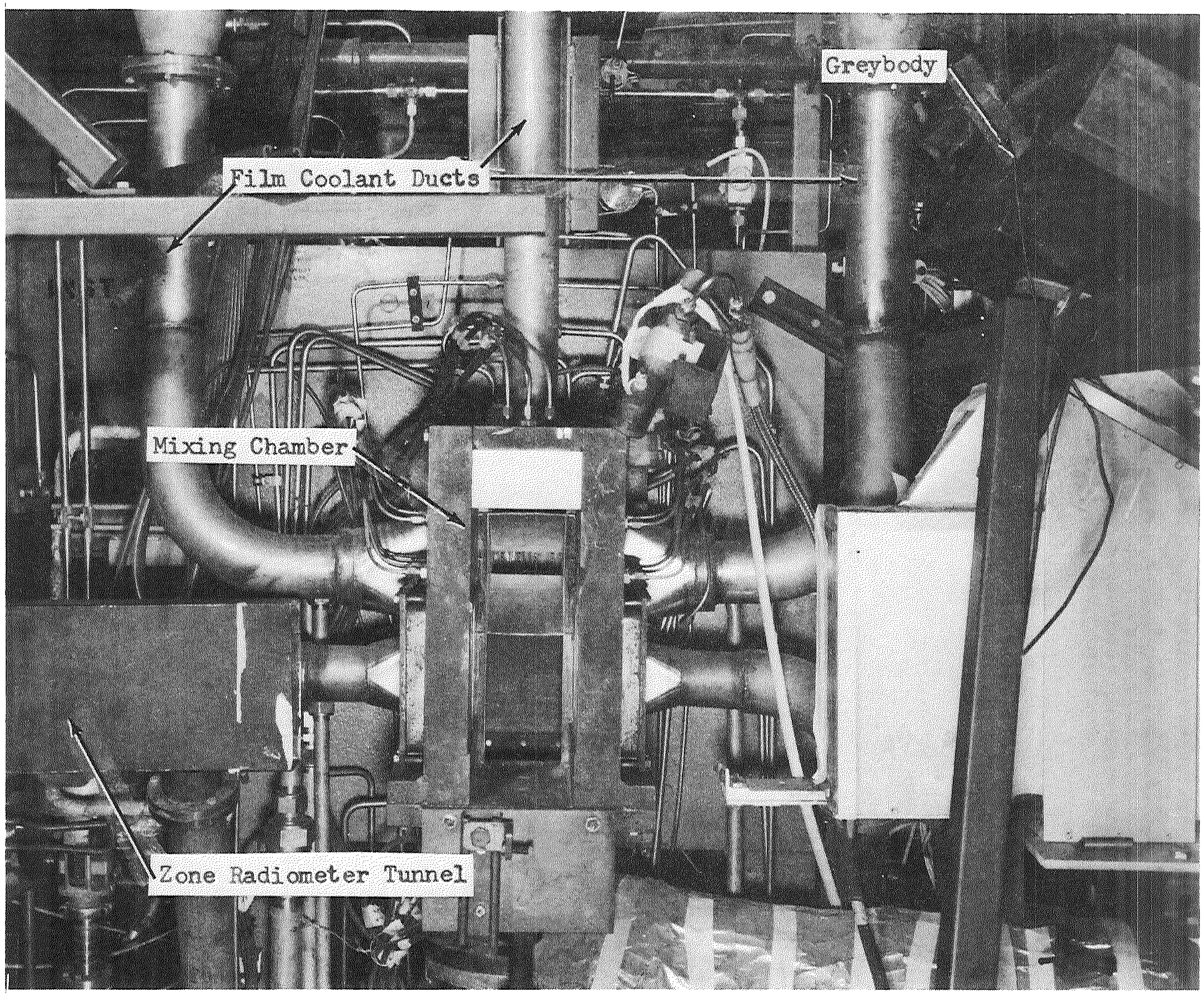

Figure 2. Test Section and Flow Facility (Front)

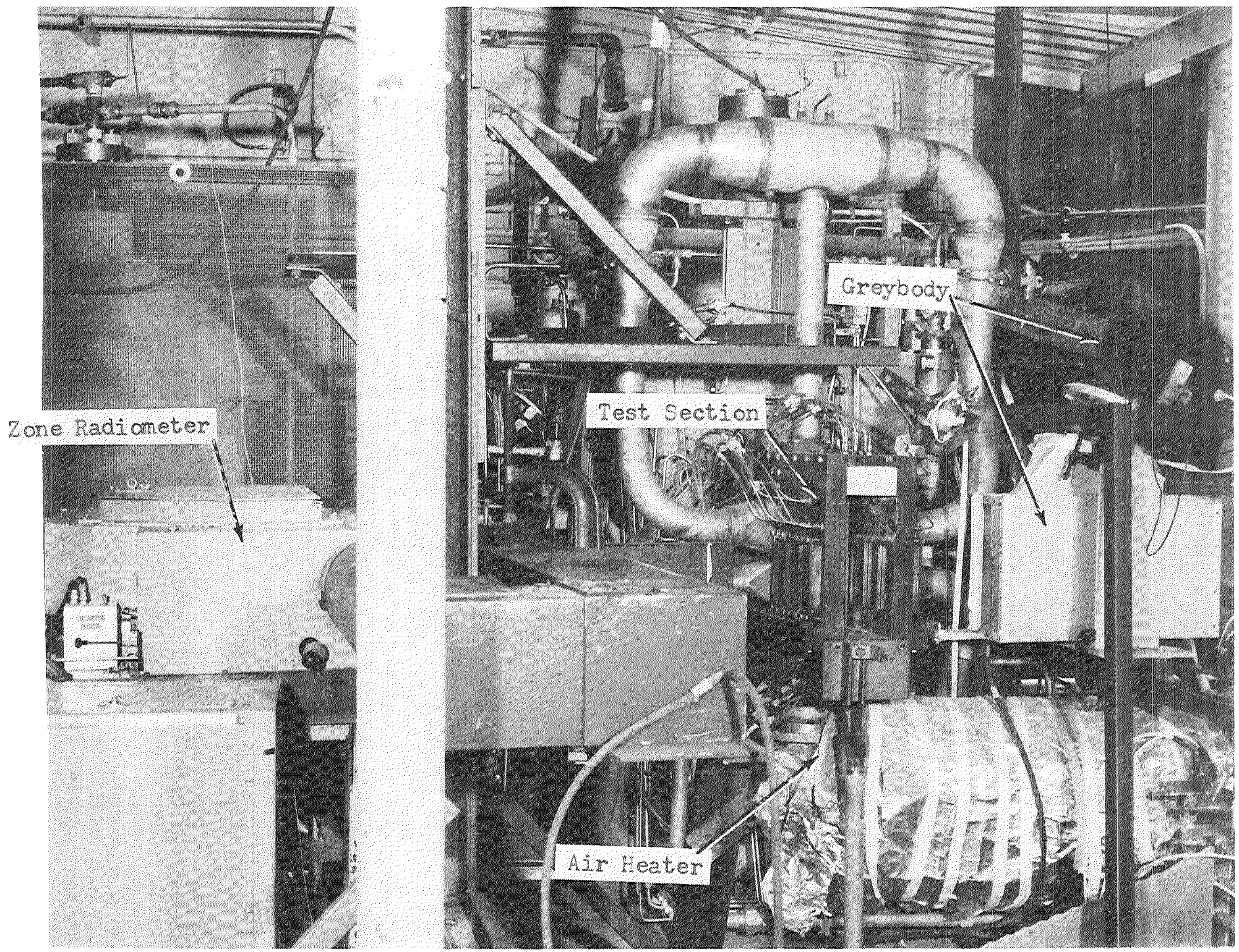

Figure 3. Test Section and Flow Facility (Left Side)

requirements without resorting to probe-type devices.

Data analysis was confined to explanation of trends displayed in the data and the production of cross plots yielding temperature and specie concentration maps. The ultimate reduction of the data to turbulent transport properties was not a contractual requirement. A detailed description of the present effort is given in ensuing sections of this report.

Under the previous contract a flow facility and test hardware were designed, fabricated, and checked out; optical instrumentation systems were installed and adapted for use; special instrumentation devices and their components were specified and procured; and facility data reduction procedures were established and computerized.

The test hardware, as fabricated, consisted of an existing water-cooled two-dimensional combustor (injector and body) with a specially designed water-cooled, ideally contoured nozzle. The injector consisted of 32 liquid-on-gas (impinging) triplet elements. The injector-to-throat distance was 11 inches. Based on previous firings with this injector, it was estimated that a c* efficiency of 97 percent would be obtained. The combustor attaches to the upper half of a fully instrumented windowed test section. The lower half of the test section accommodates a subsonic stream of hot air that flows beside and mixes with the combustion products in the test section. The air nozzle is located at the exit plane of the combustor nozzle. Film-cooled windows permit observation of the mixing region. Analytical results supplied by the contract technical manager and those calculated from Rocketdyne computer programs were utilized in the test section and combustor nozzle design.

The major test stand subsystems included: (1) coolant water lines and supply, (2) liquid oxygen lines and supply, (3) hypergol (TEAB) lines and supply, (4) gaseous hydrogen lines, (5) film coolant lines, (6) air lines and supply, and (7) an air heater. With the exception of a heated air supply and an adequate supply of coolant water, all subsystems were readily available to the test pad. A low-pressure water tank (200 gallons, 1500 psi) and an air blower were procured and installed; a specially designed steady-state air heater was designed and fabricated. The heater was attached to the air blower, which served as the air supply. A full-scale combustor, exhaust nozzle, and test section mock-up was installed in the thrust mount and all propellants, pressurants, and coolants were plumbed from their supply outlets to the test apparatus.

After the CEN/TS and the flow facility were fully checked out, the optical instrumentation systems were modified for use on this program and installed in the test pit. The spectroradiometer (zone radiometer) was mounted behind a blast wall in the test pit and the other optical instruments were located at a more remote site.

EXPERIMENTAL APPARATUS AND FLOW FACILITY

EXPERIMENTAL APPARATUS

The design of the experimental apparatus was predicated on the basis that the primary source of data collection would be through optical means. Therefore, great care was taken in the design phase to ensure that reliable optical data could be obtained. The combustor propellant flowrates of 6.5 lb/sec at a mixture ratio of 5 were conservatively based upon calculations performed to determine the required specie concentration for a fixed optical path with a reasonable flow height. This propellant flowrate was nearly identical to that deliverable by an existing Rocketdyne two-dimensional LOX-GH_2 test motor; therefore, this motor was utilized as the combustor. The combustor consisted of an impinging triplet injector (32 liquid on gas impinging elements) with a water-cooled body having a flow passage 3.54 inches wide by 2.03 inches high.

With the combustor design established, the design problem was reduced to the determination of a combustor exhaust nozzle, air nozzle, and mixing chamber that would ensure two-dimensional parallel flow and permit adequate observation by the optical instrumentation. The best design consisted of an integral arrangement of these three items and was designated combustor exhaust nozzle/test section (CEN/TS). Firing durations of 10 seconds, which were required for adequate optical data acquisition, necessitated the use of film coolant to maintain the CEN/TS hardware. The integral design made insertion of film coolant into the mixing chamber a relatively simple matter. Care was taken to minimize mixing between the film coolant and the propellant streams of interest.

The requirement of a two-dimensional flow system dictated that the two-dimensional combustor exhaust nozzle must produce uniform parallel flow with no cross flow. This was accomplished with the aid of a computer-calculated ideally contoured nozzle. The exhaust nozzle fulfilling these requirements was generated from calculations made with the Rocketdyne two-dimensional bell nozzle program. These calculations were compared to similar calculations provided by the contract technical manager and excellent agreement for contour curvature was obtained. The design detail of the combustor exhaust nozzle prior to final machining is shown in Fig. 4*. The design for mixture ratio 5 is the -3 configuration. Final machining operations reduce the nozzle tip thickness at the exit to 0.060 inch but did not change the inside contour of the nozzle. The "knife-edge" lip permitted smooth transition to the parallel stream mixing region.

The air flowrate was selected such that the air flow area was approximately equal to the exhaust area of the combustor nozzle. An air flowrate of approximately 2 lb/sec satisfied this condition. The design detail of one side of the air nozzle is shown in Fig. 5. The gradual convergence to a relatively long, flat configuration at the nozzle exit induces the air to flow two-dimensionally and parallel. The nozzle width at convergence is 3.54 inches which is identical to the width of the combustor exhaust nozzle. The air nozzle is attached to the side wall of the CEN/TS.

*It should be noted that fabrication limitations imposed by the cooling passages required that the nozzle expansion section be shortened by 25 percent. This length reduction was initiated at the midpoint of the expansion.

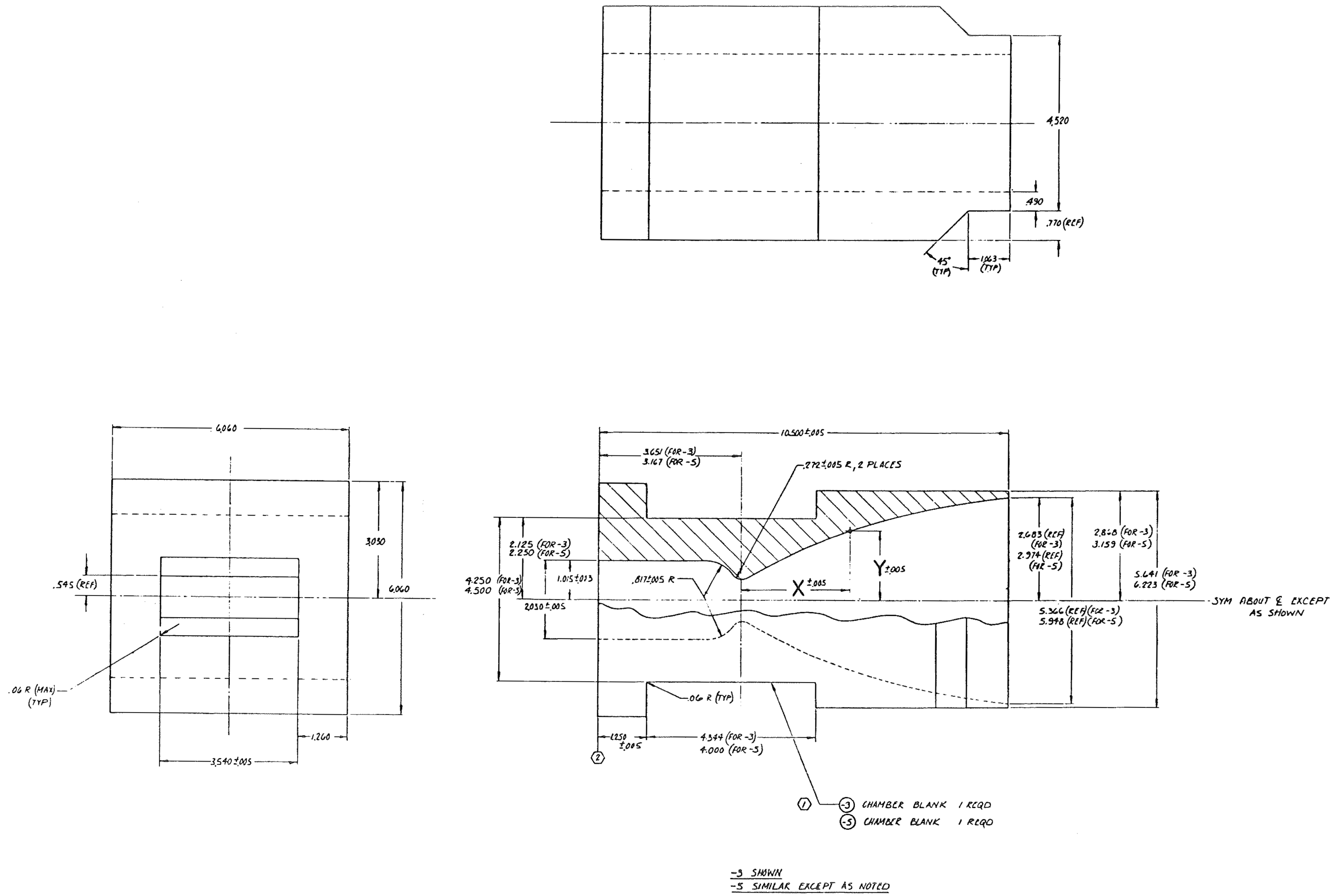

DETAIL -3	
X	Y
.000	.545
.020	.546
.040	.548
.061	.552
.084	.558
.107	.567
.131	.578
.155	.591
.178	.604
.201	.616
.246	.641
.290	.665
.355	.702
.422	.739
.490	.777
.588	.832
.668	.876
.756	.924
.856	.977
.969	1.038
1.129	1.120
1.298	1.203
1.472	1.285
1.658	1.368
1.856	1.452
2.072	1.538
2.305	1.630
2.562	1.725
2.843	1.826
3.152	1.923
3.319	1.975
3.495	2.027
3.679	2.078
3.873	2.135
4.077	2.188
4.292	2.239
4.519	2.290
4.758	2.341
5.011	2.396
5.276	2.448
5.558	2.497
5.852	2.540
6.166	2.590
6.498	2.638
6.849	2.683

Figure 4. Two-Dimensional Combustor Exhaust Nozzle

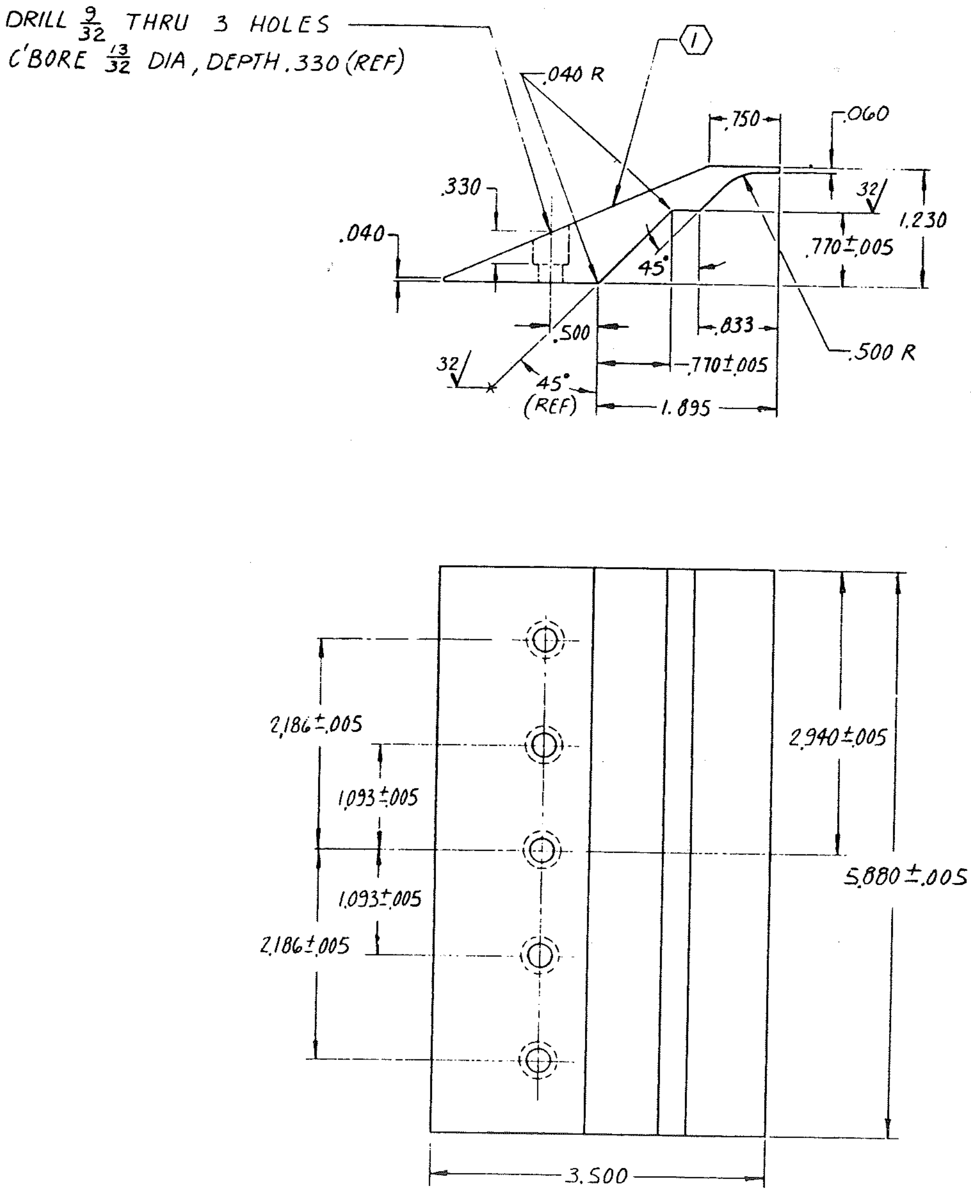

Figure 5. Air Nozzle Detail

The CEN/TS design layout is illustrated in Fig. 6 and an isometric illustration of it is presented in Fig. 7. The CEN/TS mates to the combustor and incorporates an air nozzle located on the bottom side at the exit plane of the LOX/GH_2 combustor nozzle. GN_2 film coolant is injected at the top of the exhaust product stream to prevent erosion of the test section top plate. Film coolant is also inserted along the sides of the combustor and air stream to protect the side walls from the hot combustion products. The side wall film coolant is injected parallel to the main streams and at velocities that minimize mixing between these streams. The film coolant on the air side was injected at approximately the same pressure and velocity as the air stream. Mixing between the combustor exhaust products and its film coolant stream was minimized by injecting the coolant at the test section pressure but at sonic velocity. Due primarily to cost considerations, the mixing chamber length was limited to approximately 9 inches which is also the stability limit (Ref. 3) of the film coolant streams. A summary of nominal parameters and dimensions for the combustor and CEN/TS is presented in Table I.

The location of the viewing ports was based upon results from a computer program (Ref. 4) describing gas-phase mixing with combustion for the design configuration. The mixing layer temperature contours for a LOX/GH_2 combustion products stream at a mixture ratio of 5 mixing with a parallel subsonic air stream of 1000 K is illustrated in Fig. 8. The locations of the air and combustion products streams are reversed in the actual physical configuration. The mixing chamber dimensions and the location of the view ports are overlaid on the temperature map illustrating the relationship of the mixing chamber to the analytically predicted mixing zone. The viewing ports allow observation of 25 percent of the combustor exhaust stream and 75 percent of the air stream. This enables viewing of the entire

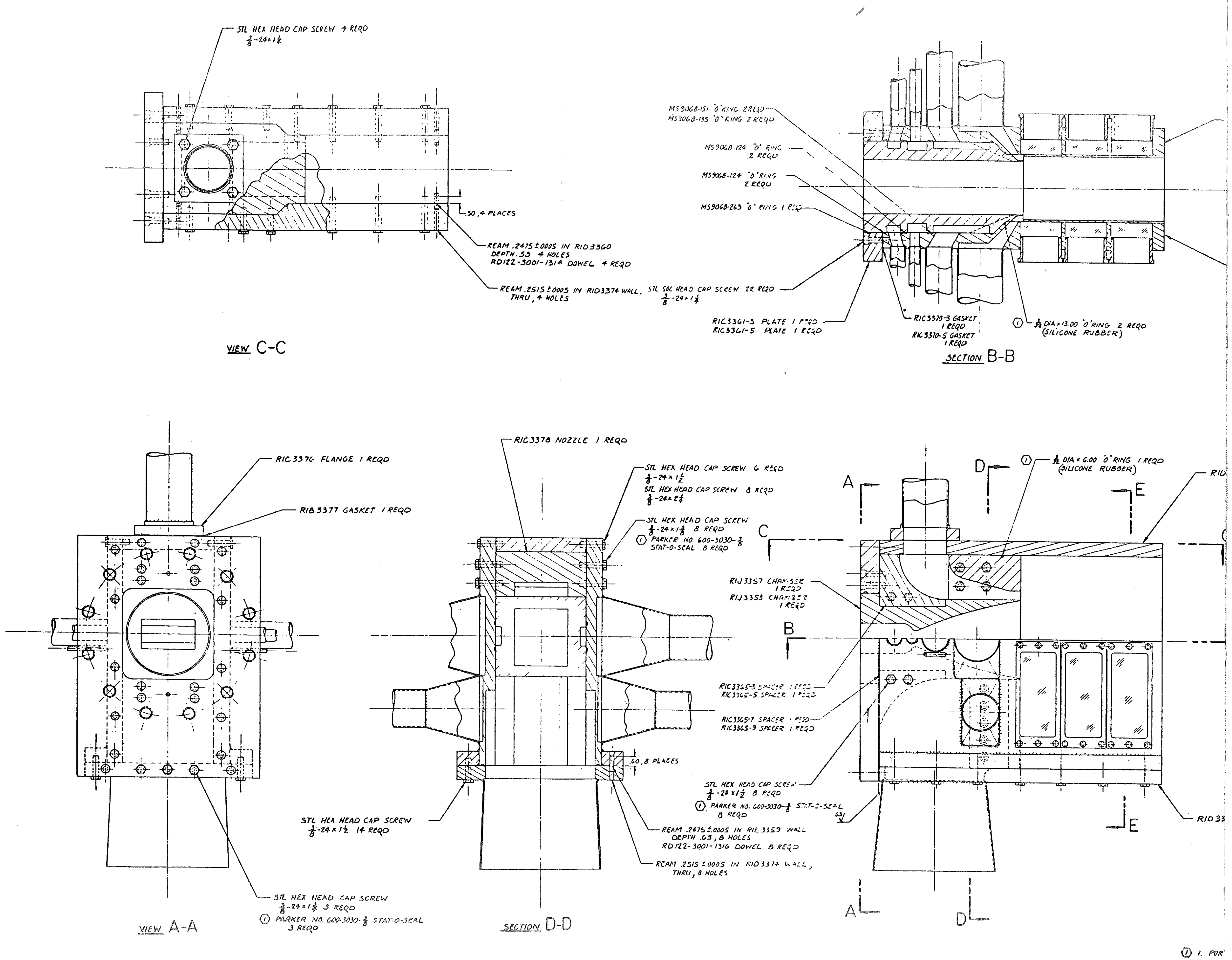

STL HEX HEAD CAP SCREW 4 REQD 3/8-24x1 1/4
.50, 4 PLACES
REAM .2475±.0005 IN RID3360 DEPTH .55 4 HOLES RD122-3001-1314 DOWEL 4 REQD
REAM .2515±.0005 IN RID3374 WALL, THRU, 4 HOLES
VIEW C-C
MS9068-151 "O" RING 2 REQD
MS9068-135 "O" RING 2 REQD
MS9068-124 "O" RING 2 REQD
MS9068-124 "O" RING 2 REQD
MS9068-263 "O" RING 1 REQD
STL SOC HEAD CAP SCREW 22 REQD 3/8-24x1 1/4
RIC3361-3 PLATE 1 REQD
RIC3361-5 PLATE 1 REQD
RIC3370-3 GASKET 1 REQD
RK3370-5 GASKET 1 REQD
1/8 DIA x 13.00 "O" RING 2 REQD (SILICONE RUBBER)
SECTION B-B
RIC3376 FLANGE 1 REQD
RIB3377 GASKET 1 REQD
STL HEX HEAD CAP SCREW 3/8-24x1 1/2 14 REQD
STL HEX HEAD CAP SCREW 3/8-24x1 3/4 3 REQD
PARKER NO. 600-3030-3/8 STAT-O-SEAL 3 REQD
VIEW A-A
RIC3378 NOZZLE 1 REQD
STL HEX HEAD CAP SCREW 6 REQD 3/8-24x1 1/2
STL HEX HEAD CAP SCREW 8 REQD 3/8-24x2 1/4
STL HEX HEAD CAP SCREW 3/8-24x1 3/4 8 REQD
PARKER NO. 600-3030-3/8 STAT-O-SEAL 8 REQD
.60, 8 PLACES
REAM .2475±.0005 IN RIC3359 WALL DEPTH .63, 8 HOLES RD122-3001-1316 DOWEL 8 REQD
REAM .2515±.0005 IN RID3374 WALL, THRU, 8 HOLES
SECTION D-D
1/8 DIA x 6.00 "O" RING 1 REQD (SILICONE RUBBER)
RIJ3357 CHAMBER 1 REQD
RIJ3359 CHAMBER 1 REQD
RIC3365-3 SPACER 1 REQD
RIC3365-5 SPACER 1 REQD
RIC3365-7 SPACER 1 REQD
RIC3365-9 SPACER 1 REQD
STL HEX HEAD CAP SCREW 3/8-24x1 1/2 8 REQD
PARKER NO. 600-3030-3/8 STAT-O-SEAL 8 REQD
63
A A B C D D E E
RID
RID33
1. POR

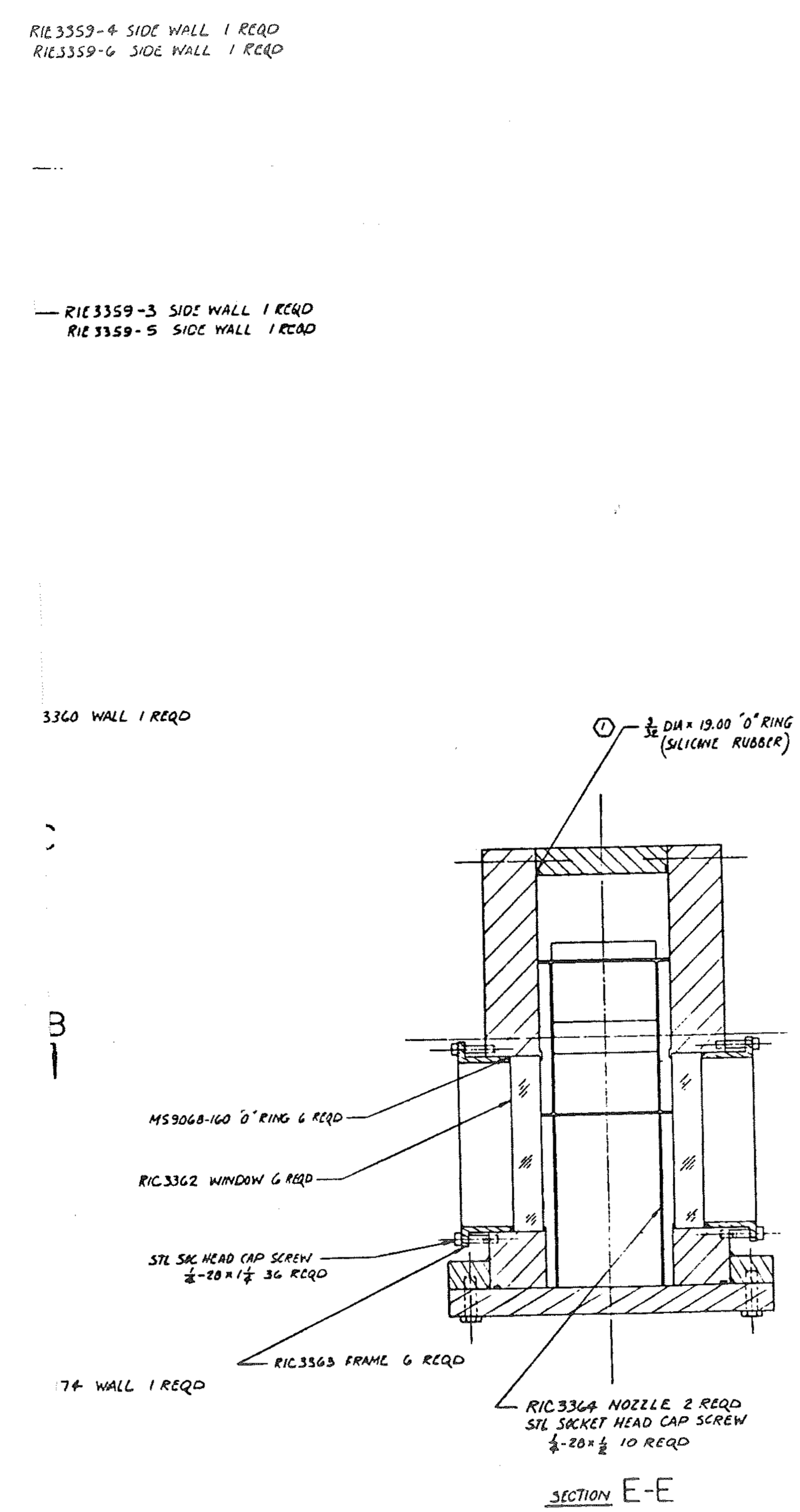

-21 ASSY	-11 ASSY	PART NO.	DESCRIPTION
1	1	RIC3378	NOZZLE
1	1	RIB3377	GASKET
1	1	RIC3376	FLANGE
1	1	RID3374	WALL
	1	RIC3370-5	GASKET
1		RIC3370-3	GASKET
	1	RIC3365-9	SPACER
1		RIC3365-7	SPACER
	1	RIC3365-5	SPACER
1		RIC3365-3	SPACER
2	2	RIC3364	NOZZLE
6	6	RID3363	FRAME
6	6	RIC3362	WINDOW
	1	RIC3361-5	FRONT PLATE
1		RIC3361-3	FRONT PLATE
1	1	RID3360	TOP WALL
	1	RIC3359-22	SIDE WALL
	1	RIC3359-21	SIDE WALL
1		RIC3359-12	SIDE WALL
1		RIC3359-11	SIDE WALL
	1	RIJ3358	CHAMBER
1		RIJ3357	CHAMBER

Figure 6. CEN/TS Assembly

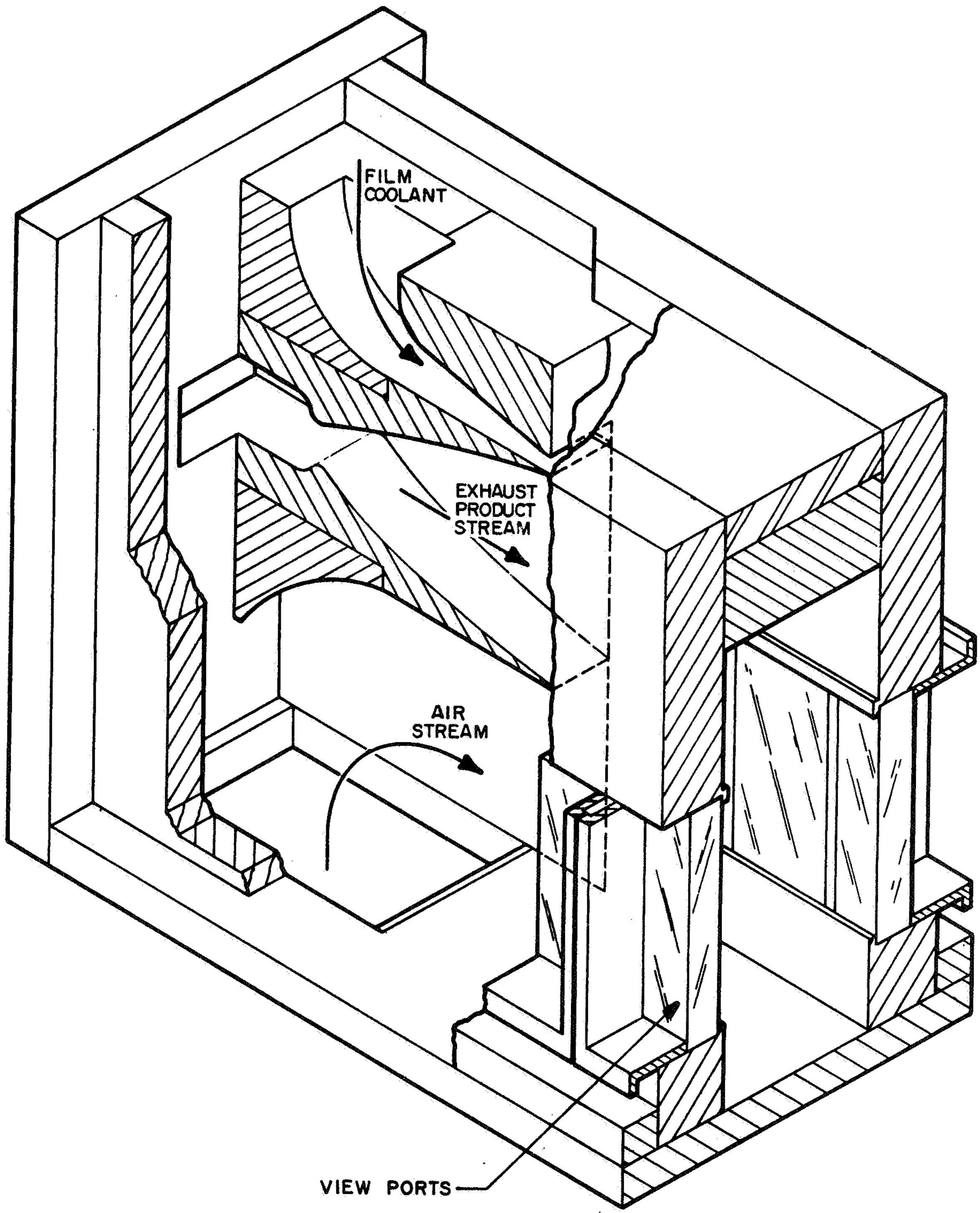

Figure 7. Combustor Exhaust Nozzle and Test Section Schematic

TABLE 1

SUMMARY OF COMBUSTOR AND CEN/TS NOMINAL PARAMETERS AND DIMENSIONS*

Combustor

Chamber Pressure	= 402 psia
Flowrate at Mixture Ratio 5	= 6.5 lb/sec
Injector-to-Throat Length	= 11 inches
Height	= 2.03 inches
Width	= 3.54 inches

Exhaust Nozzle

Expansion Ratio	= 4.923
Throat Area	= 3.86 sq in.
Throat Height	= 1.090 inches
Exit Mach No.	= 2.70
Exit Pressure	= 13.7 psia

Air Nozzle

Height	= 5.88 inches
Throat Width	= 3.54 inches
Throat Mach No.	= 0.25
Throat Pressure	= 13.7 psia

Mixing Chamber

Height	= 11.982 inches
Width	= 4.46 inches
Chamber Pressure	= 13.7 psia

Film Coolant (Combustor Side Wall)

Slot Width	= 0.4 inch
Inlet Mach No.	= 1.0

(Combustor Top Wall)

Slot Width	= 3.54 inches
Slot Height	= 0.616 inch
Inlet Mach No.	= 1.0

(Air Side Wall)

Slot Width	= 0.4 inch
Inlet Velocity	= Air stream velocity

*Interface distance between all gas streams is 0.060 inch.

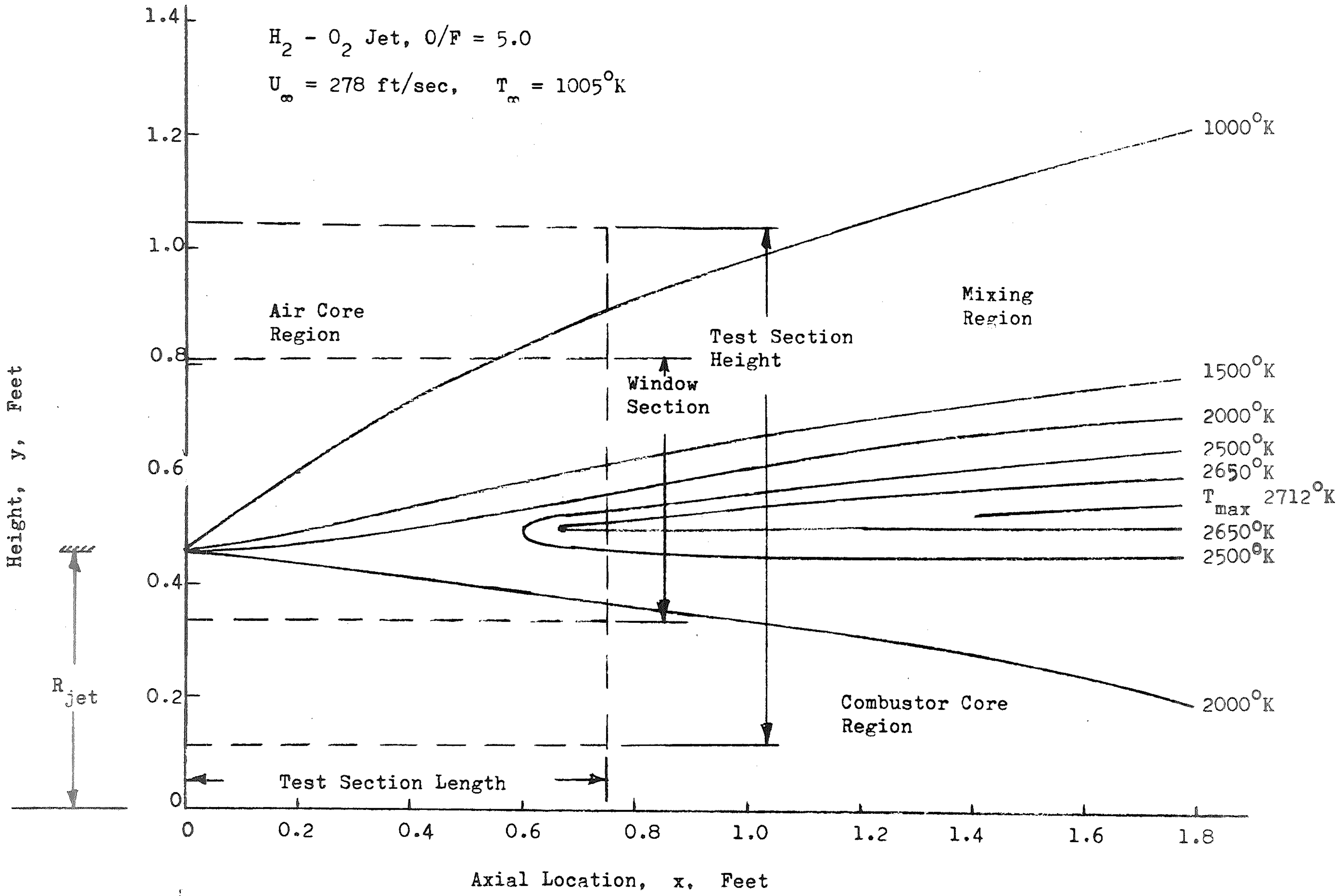

Figure 8. Calculated Mixing Layer Temperature Contours

calculated mixing region for an axial distance of 9 inches.

FLOW FACILITY

A specially designed flow facility was constructed at the Combustion and Heat Transfer Laboratory of the Rocketdyne Santa Susana Field Laboratory. The entire facility prior to instrumentation installation is illustrated in Fig. 9. It consists of a number of subsystems. These include: (1) LOX system, (2) GH_2 system, (3) hypergol triethylaluminum/triethylboron (TEAB) system, (4) H_2O system, (5) GN_2 system, and (6) the hot-air system. The control console for the various subsystems is illustrated schematically in Fig. 10.

The allowable engine thrust level for the thrust mount (rear view is shown in Fig. 11) is 7500 pounds which exceeds the maximum deliverable thrust by a factor of 3. The thrust mount provided for ease of engine installation and allowed removal of the injector without disassembly of the entire apparatus. The observed open area in Fig. 9, 10 feet deep on one side and 40 feet deep on the near side of the CEN/TS thrust mount, was reserved for the principle optical instrumentation, i.e., spectroradiometer, LASS (large aperture spectrometer/spectrograph), and photographic pyrometer.

LOX System

The LOX system is illustrated in Figs. 12 through 14. It consisted of a 43-gallon, 5000-psi, stainless-steel tank which was capable of supplying LOX at the test conditions for approximately six times the maximum run duration, i.e., 60 seconds. The tank was filled by attachment of a 300-gallon LOX trailer to the

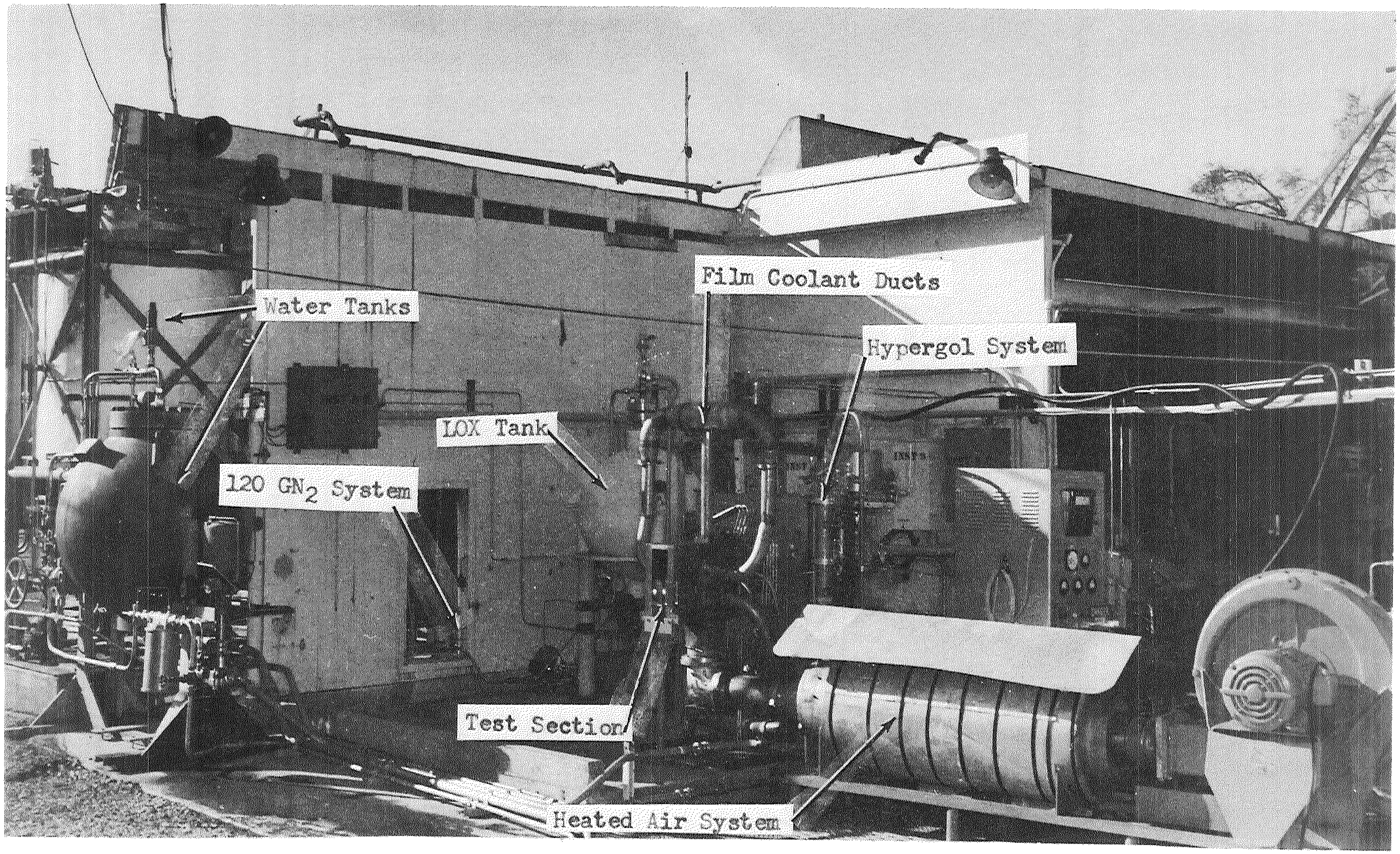

Figure 9. Flow Facility

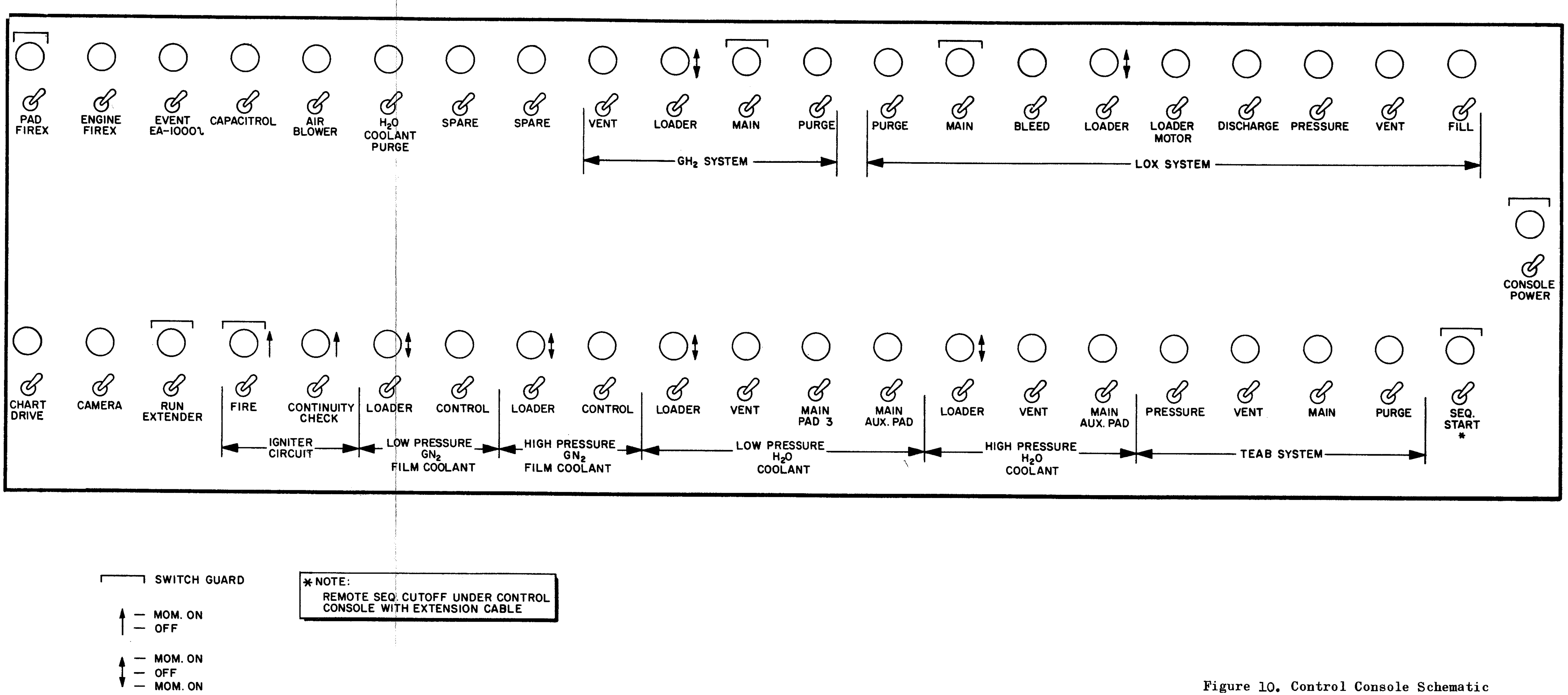

Figure 10. Control Console Schematic

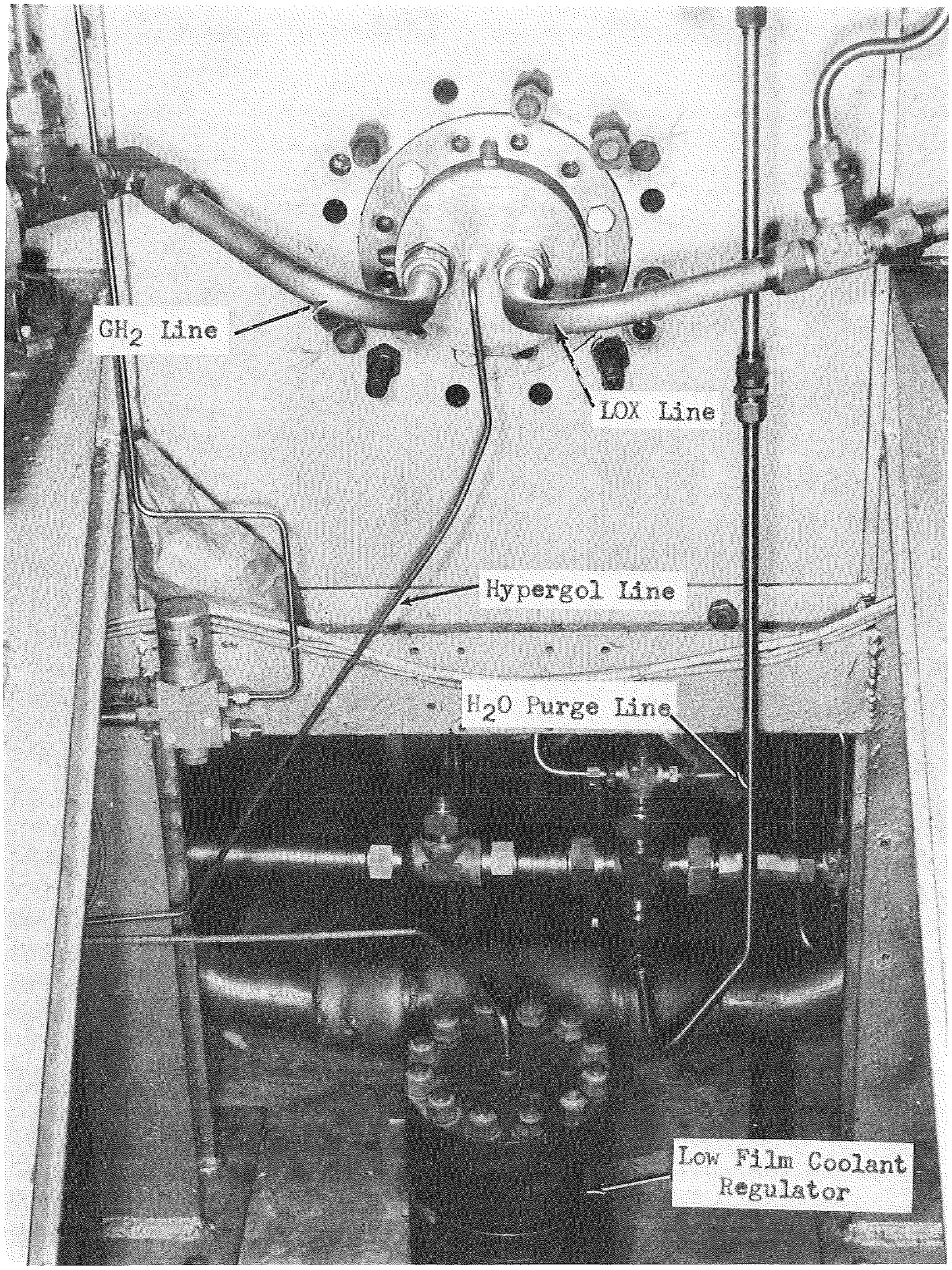

Figure 11. Thrust Mount (Rear View)

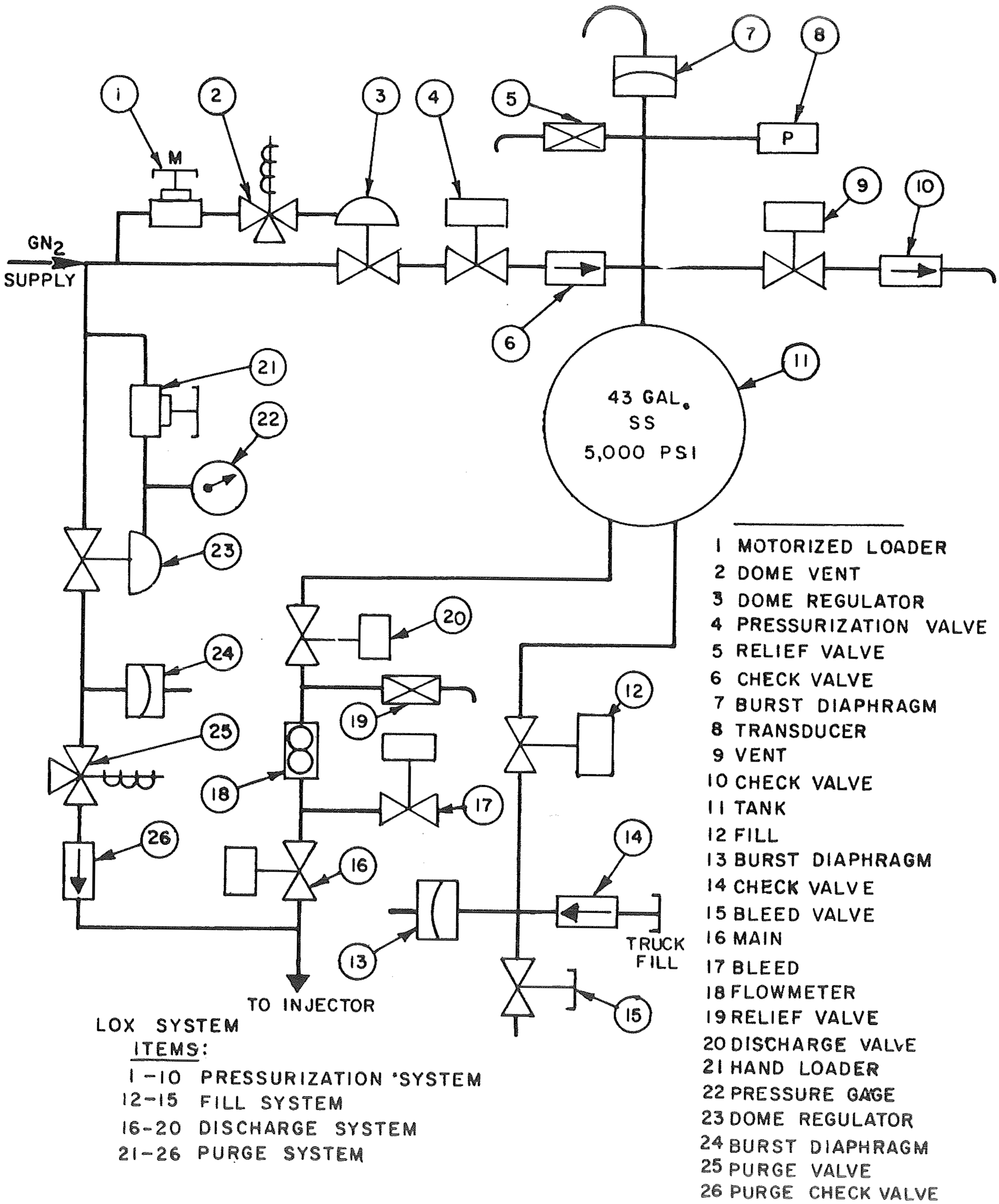

Figure 12. LOX System Schematic

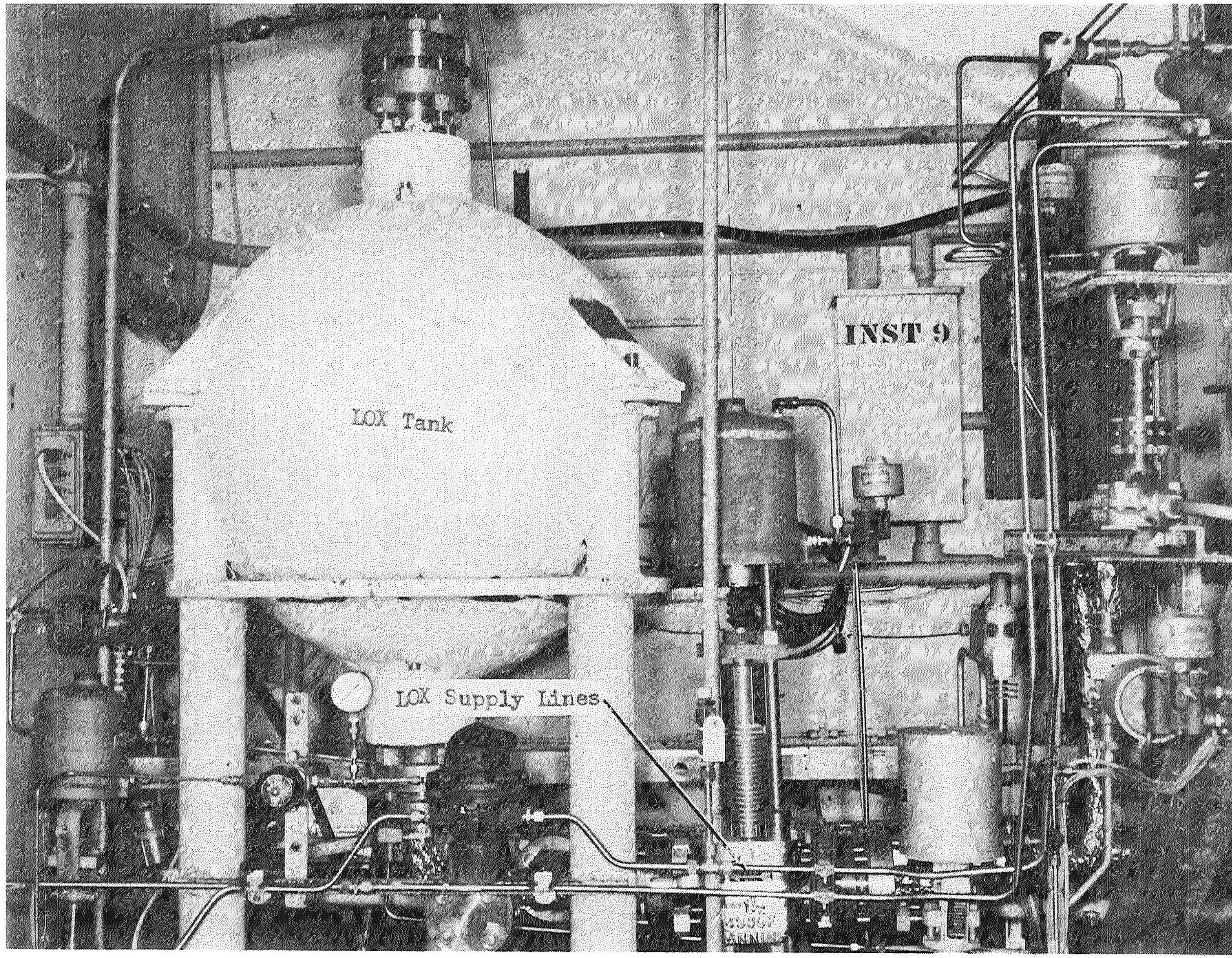

Figure 13. LOX System

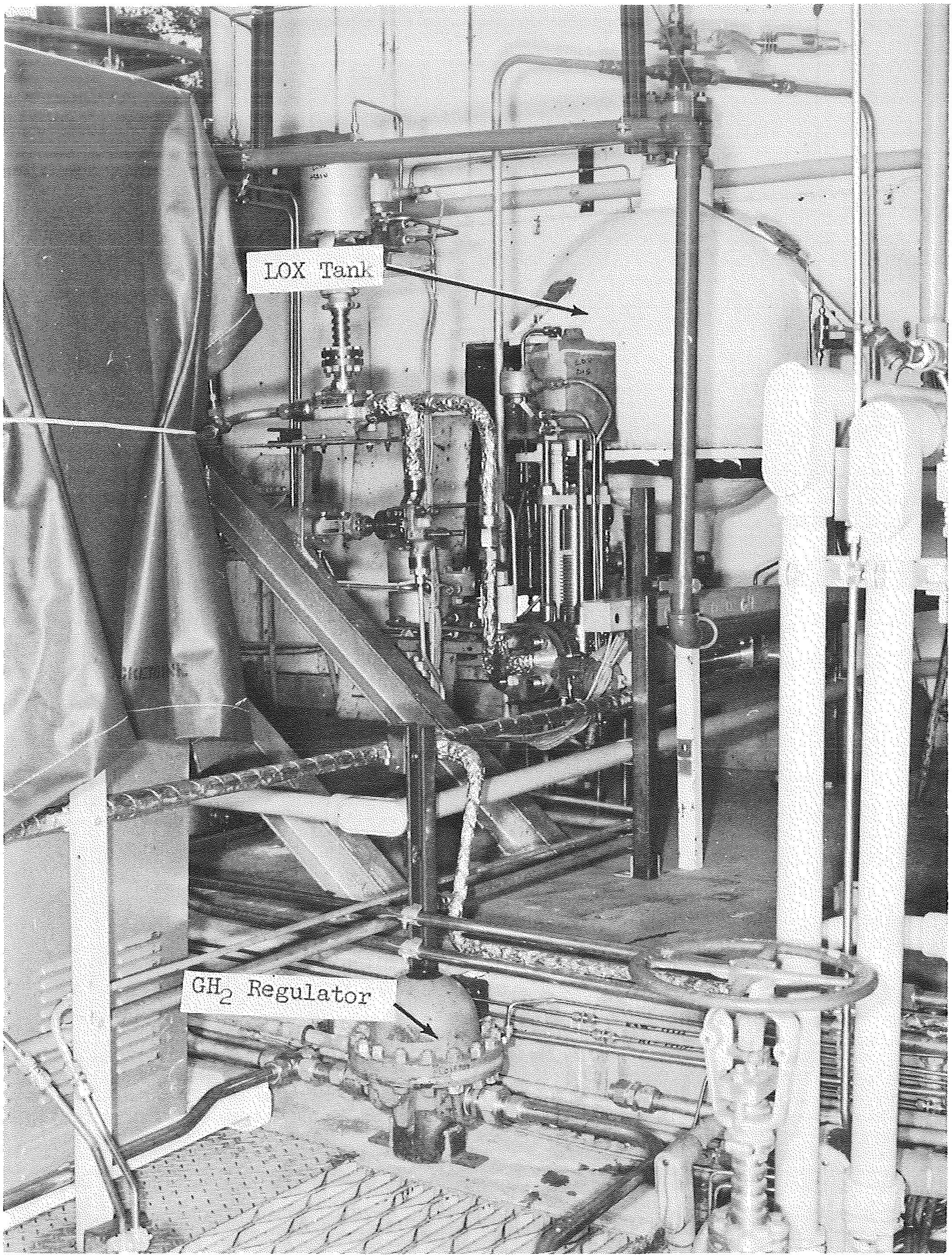

Figure 14. LOX and GH_2 System

truck fill tap. Gaseous nitrogen, appropriately regulated, was used for tank pressurization and the purge. The 700-psi tank pressure for the experimental firings was well below the coded value for the vessel. The discharge line size was 1 inch.

Gaseous Hydrogen System

The GH_2 system is illustrated in Figs. 14 and 15. A 600-cu.ft., 3000-psi bottle bank connected to the Santa Susana GH_2 network comprised the laboratory supply which was more than sufficient. A regulated 1-inch diameter run line connected to the 1-1/2-inch bottle bank outlet was located approximately 50 feet from the pad. The hydrogen pressure delivered at the supply outlet was approximately 2600 psi. Therefore, since the combustor operating pressure was nominally 402 psia, pressure drop through the relatively small run line was not a problem. Gaseous nitrogen fed from the regulator output of the hypergol purge served as the fuel purge.

Hypergol System

The TEAB hypergol system is illustrated in Figs. 16 and 17. It consisted of a 2-quart, 5000-psi, stainless-steel tank which was capable of supplying sufficient hypergol for approximately 30 tests.

The regulated GN_2 supply used for tank pressurization also served for the hypergol, H_2O, and GH_2 purges. The 300-psi working pressure of the hypergol system was well below the pressure rating of the tank. The discharge line size was 1/4 inch.

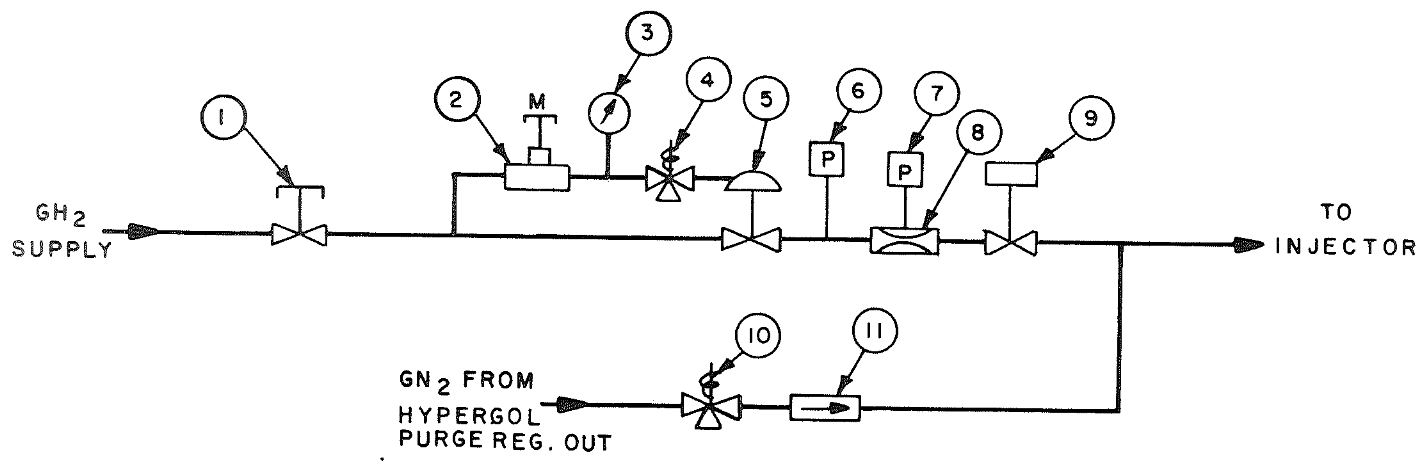

1. SHUT-OFF
2. MOTORIZED LOADER
3. PRESSURE GAGE
4. DOME VENT
5. DOME REGULATOR
6. TRANSDUCER
7. TRANSDUCER
8. VENTURI
9. MAIN
10. PURGE VALVE
11. PURGE CHECK VALVE

GH_2 SYSTEM
ITEMS:
1–6 PRESSURIZATION SYSTEM
7–9 DISCHARGE SYSTEM
10–11 PURGE SYSTEM

Figure 15. GH_2 System Schematic

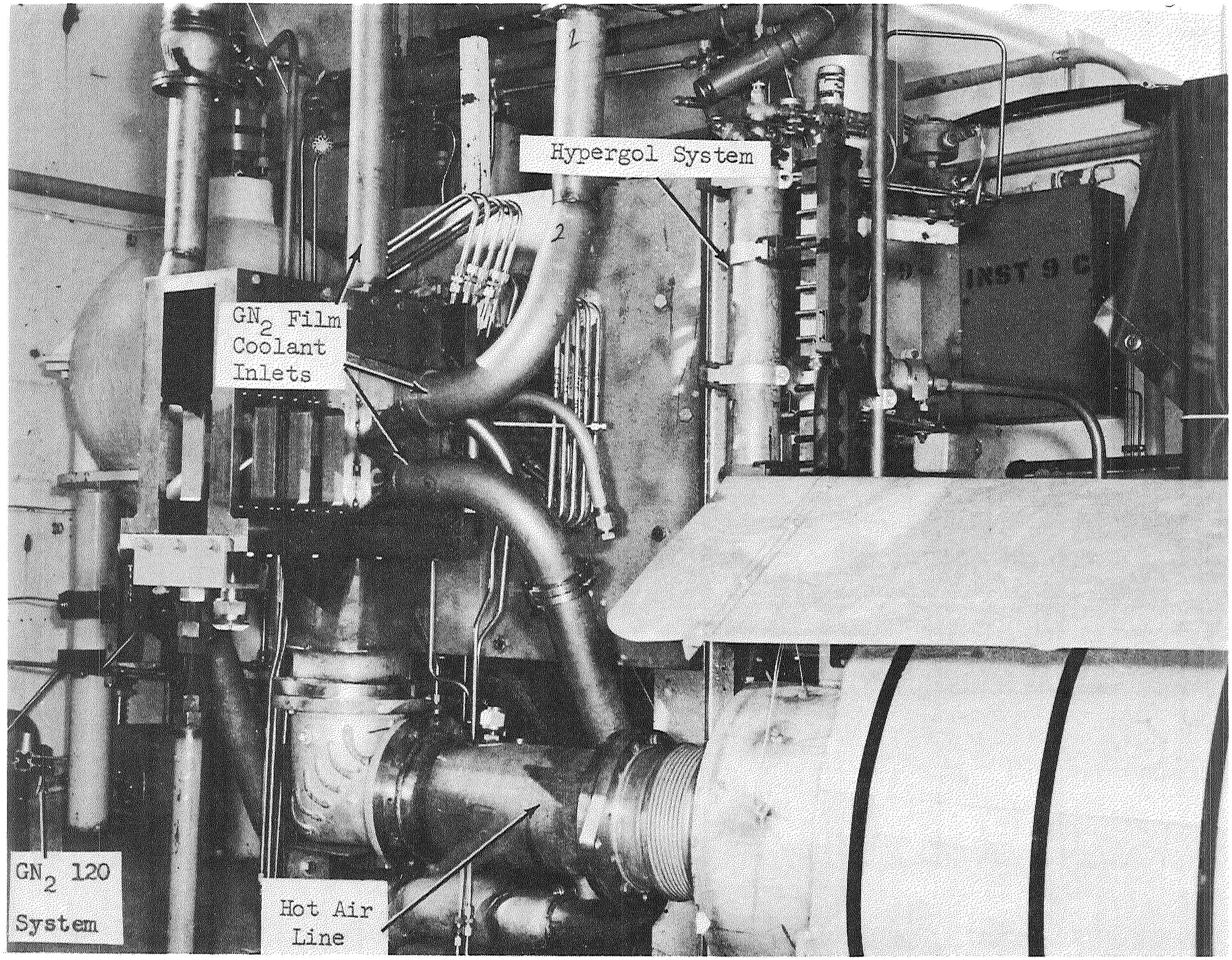

Figure 16. Heated Air, GN_2 and Hypergol Systems

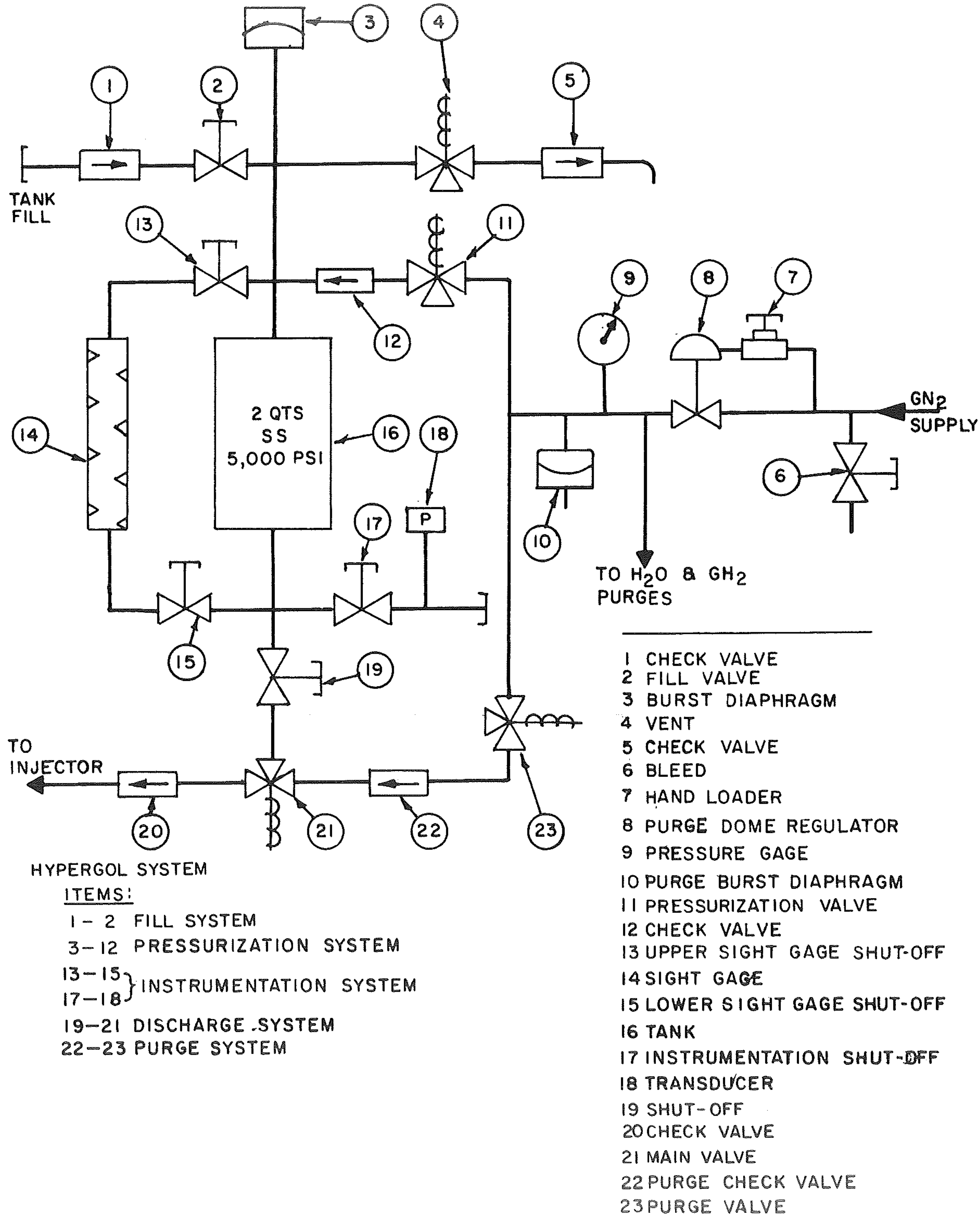

Figure 17. Hypergol System Schematic

TEAB was selected over ClF_3 or F_2 as the ignition agent because it is less corrosive and easier to handle. In addition, tanking was done on-site rather than at a special area.

Water System

The water system (Fig. 18) consisted of two steel tanks (200 gallon, 1500 psi; and 600 gallon, 1500 psi) capable of supplying coolant water for approximately 150 seconds, i.e., fifteen times the maximum test duration. This large supply of water permitted relatively long pre- and post-test cooling of the hardware. The tanks were filled from a soft water supply which was filtered before entering the tanks. A schematic of the entire system is presented in Fig. 19 and attachment of the coolant water to the combustor and the CEN/TS is illustrated in Fig. 20. Gaseous nitrogen fed from the regulator output of the hypergol purge served as the water purge. A separate, regulated, GN_2 supply was used for tank pressurization. The run pressure of 1100 psi for both water tanks was well below the coded values for the vessels. Both discharge lines were 1-1/2 inch.

Gaseous Nitrogen System

The distribution of the gaseous nitrogen (GN_2) system is illustrated schematically in Fig. 21. The low-pressure film coolant regulator is shown in Fig. 11. The other regulator (not shown) was located on the top of the thrust mount. The attachment of the film coolant ducting can be seen in Figs. 16 and 20. Also shown on Fig. 16 is the 120-psi pneumatic system for the operation of all control valves. The remaining GN_2 plumbing for purges and pressurization is displayed

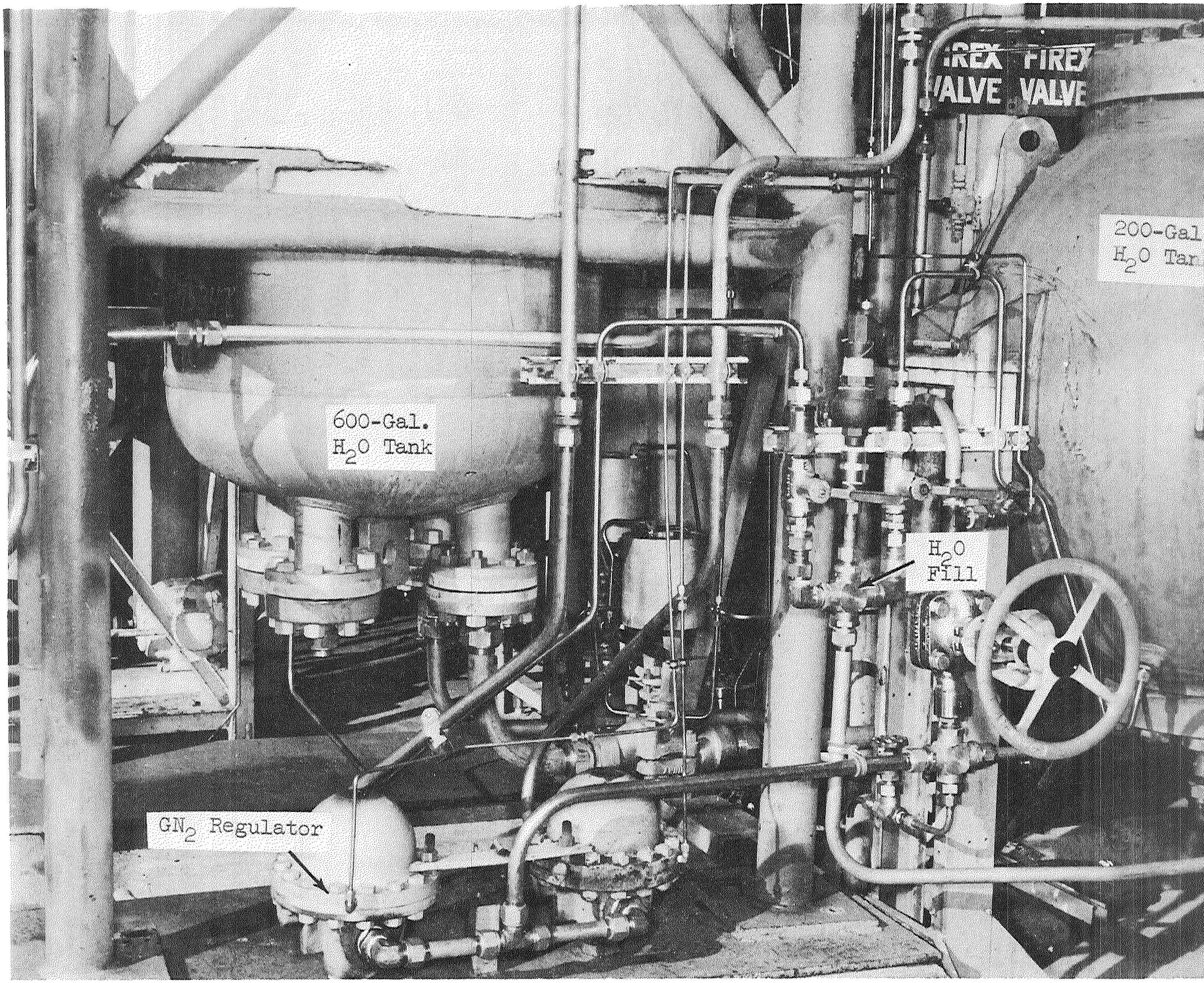

Figure 18. H_2O System

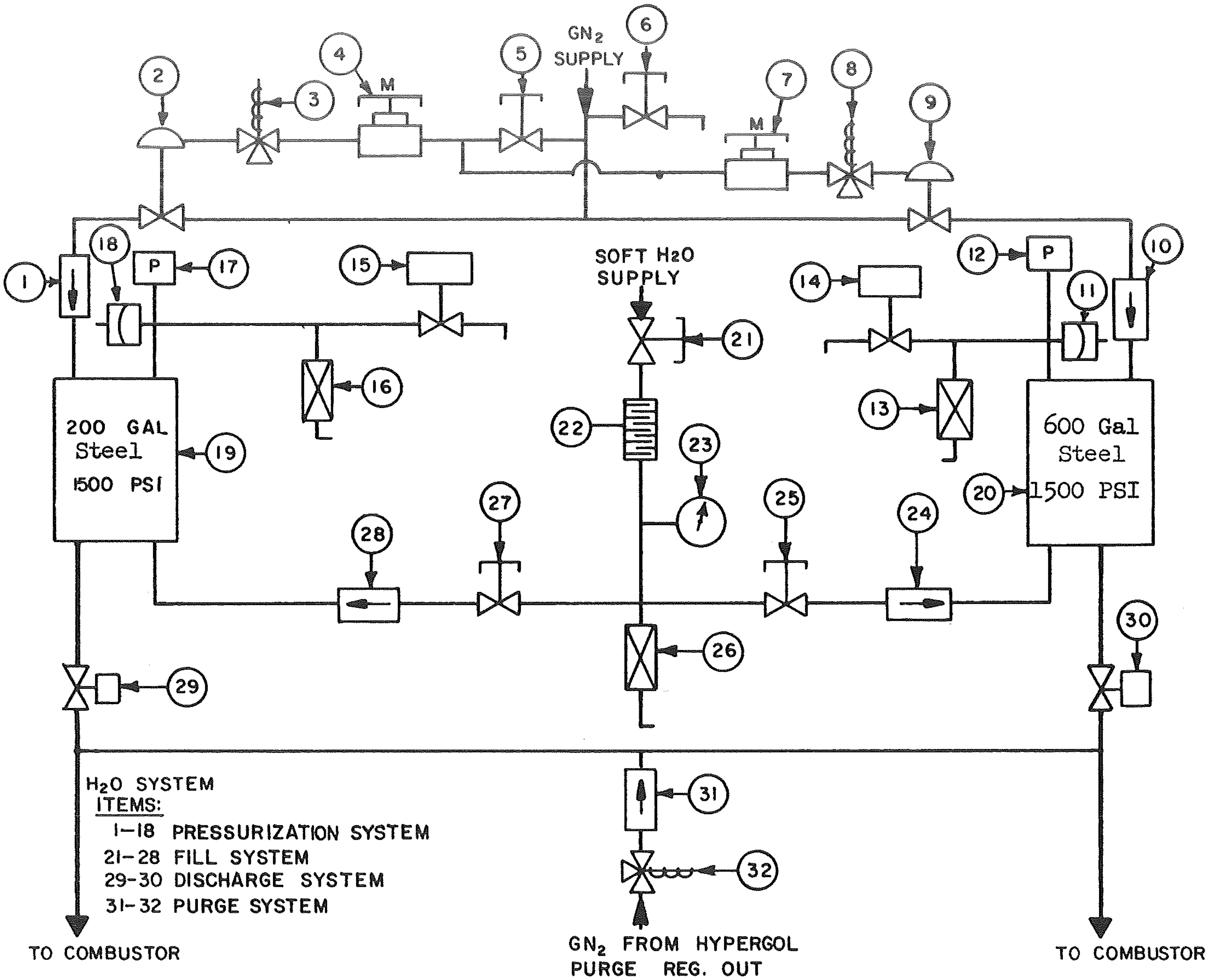

1. CHECK VALVE
2. DOME REGULATOR
3. DOME VENT
4. MOTORIZED LOADER
5. SHUT-OFF
6. VENT
7. MOTORIZED LOADER
8. DOME VENT
9. DOME REGULATOR
10. CHECK VALVE
11. BURST DIAPHRAGM
12. TRANSDUCER
13. RELIEF VALVE
14. VENT
15. VENT
16. RELIEF VALVE
17. TRANSDUCER
18. BURST DIAPHRAGM
19. TANK
20. TANK
21. SHUT-OFF
22. FILTER
23. PRESSURE GAGE
24. CHECK VALVE
25. FILL
26. RELIEF VALVE
27. FILL
28. CHECK VALVE
29. MAIN
30. MAIN
31. PURGE CHECK VALVE
32. PURGE VALVE

Figure 19. H_2O System Schematic

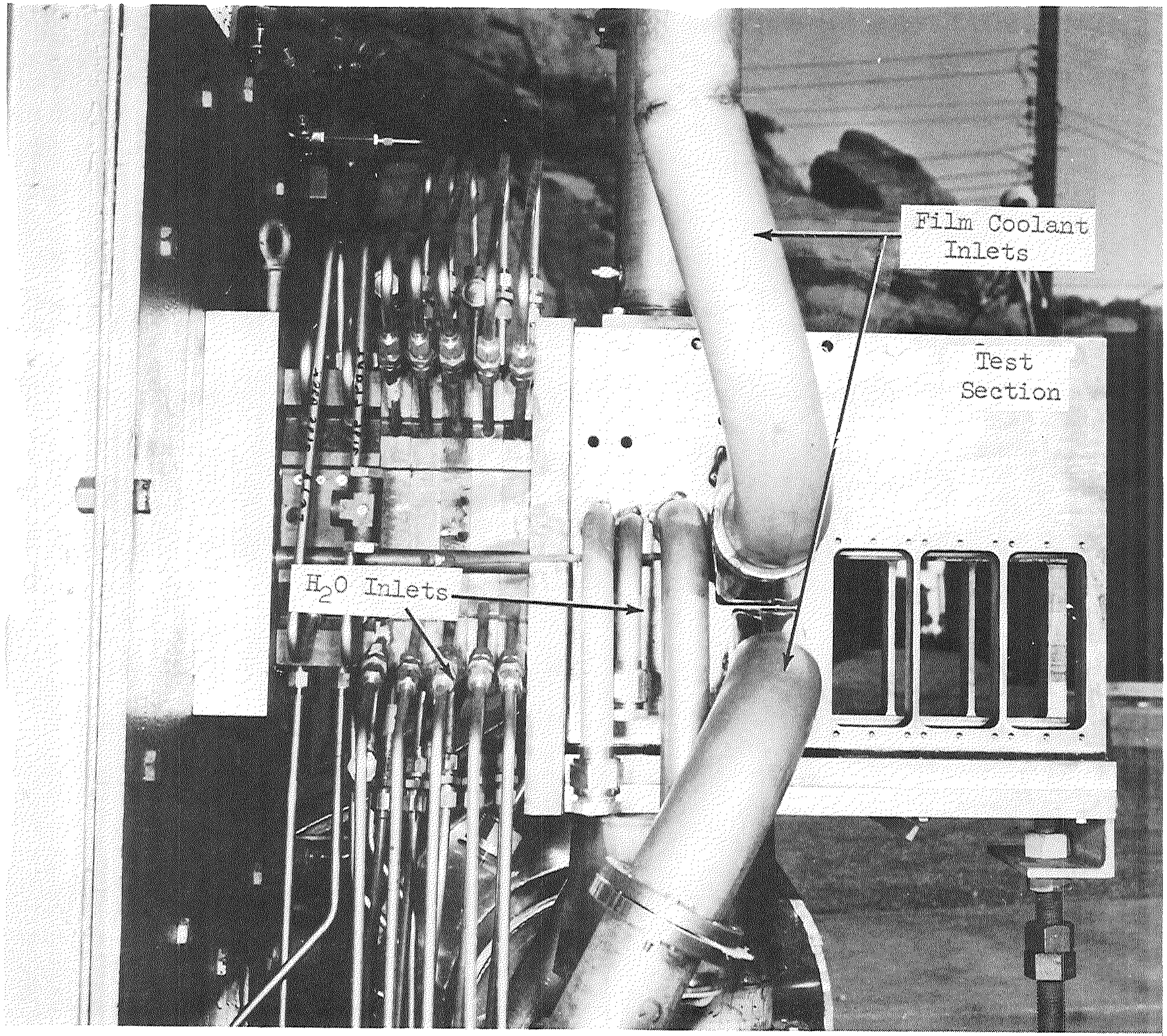

Figure 20. Attachment of H_2O and GN_2 to the CEN/TS

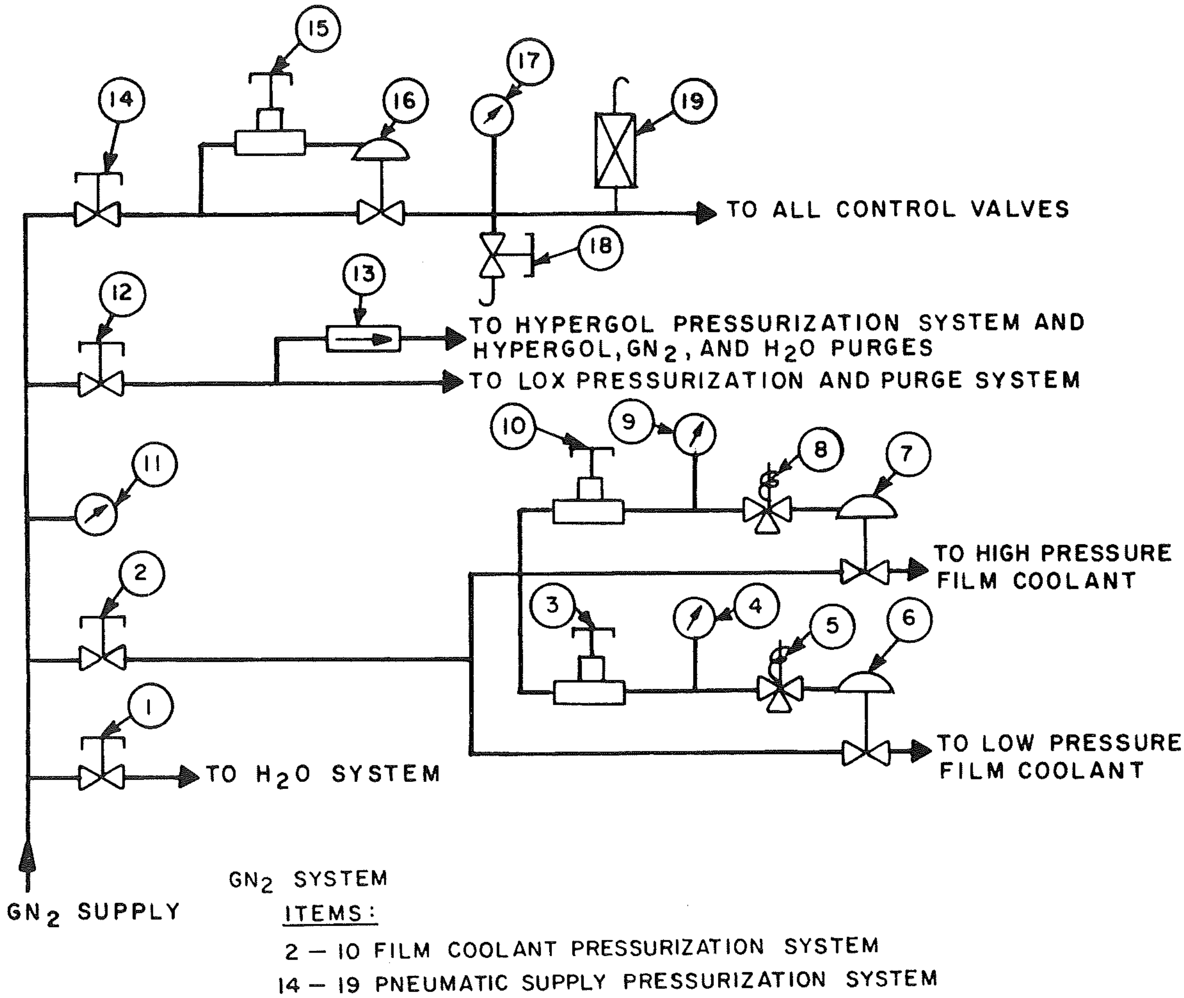

1. SHUT-OFF
2. SHUT-OFF
3. HAND LOADER
4. PRESSURE GAGE
5. DOME VENT
6. DOME REGULATOR
7. DOME REGULATOR
8. DOME VENT
9. PRESSURE GAGE
10. HAND LOADER
11. PRESSURE GAGE
12. SHUT-OFF
13. CHECK VALVE
14. SHUT OFF
15. HAND LOADER
16. DOME REGULATOR
17. PRESSURE GAGE
18. VENT
19. RELIEF VALVE

Figure 21. GN_2 System Schematic

with each particular subsystem. The 2350-psi GN_2 bottle bank laboratory supply was connected to the Santa Susana 3000-psi GN_2 network. This created essentially an unlimited nitrogen supply.

Hot Air System

The entire steady-state hot air system (blower, heater, and heater power supply) is shown in Fig. 9. The method of attainment of the air ducting to the CEN/TS is illustrated in Fig. 16. The air blower, shown in Fig. 22, produced a 1-psi head and an air flowrate of 2 lb/sec. Flowrate control was achieved by restricting the blower inlet. The 8-inch-square outlet was close-coupled to the air heater. Diffusion screens at the heater inlet aided in expanding the flow to the 16-inch external diameter of the packed tube bundle heater. The electrical power supply and the 28-volt dc control wiring for the air blower are shown schematically in Fig. 23.

The air heater, shown during assembly in Fig. 24 consisted of a 6.75-foot, 16-inch by 0.375-inch wall, electrically heated, stainless-steel shell. This shell was packed with approximately 1200 pounds of 0.5-inch by 0.065-inch wall stainless-steel tubing. The shells were closed by welded ASME flanges. The packed tube bundle was held in place fore and aft by diffusion screens tack welded to the chamber body (Fig. 25). Both heater inlet and outlet were 8 inches in diameter. Prior to final assembly, a flow diverter was placed in the heater inlet to prevent channeling of the flow. Twelve rod type heaters requiring 24 kilovolt-amperes were imbedded in the tube bundle matrix. These resistance elements heated the entire assembly by conduction. The outer case was insulated to a 4-inch radial

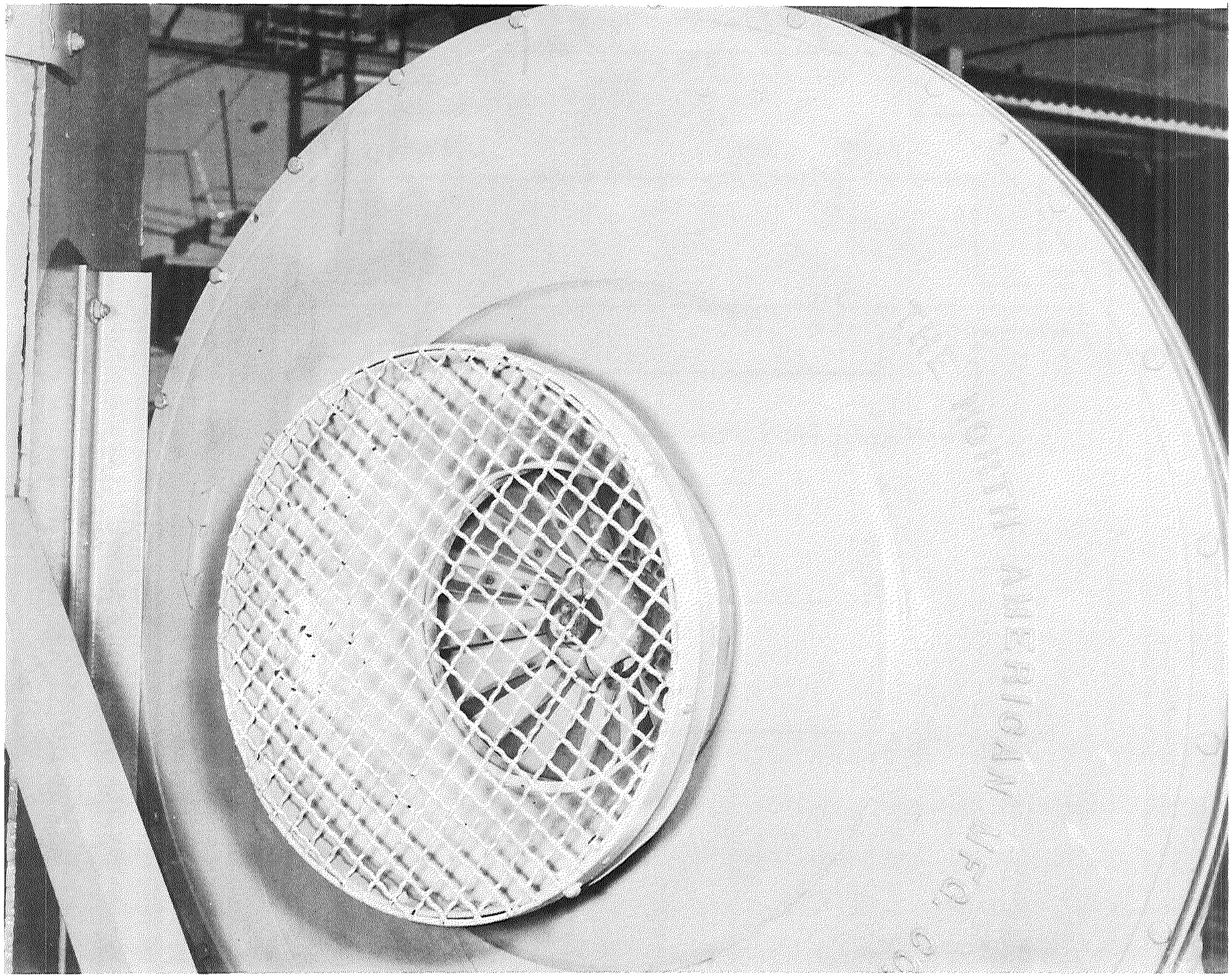

Figure 22. Air Blower Inlet

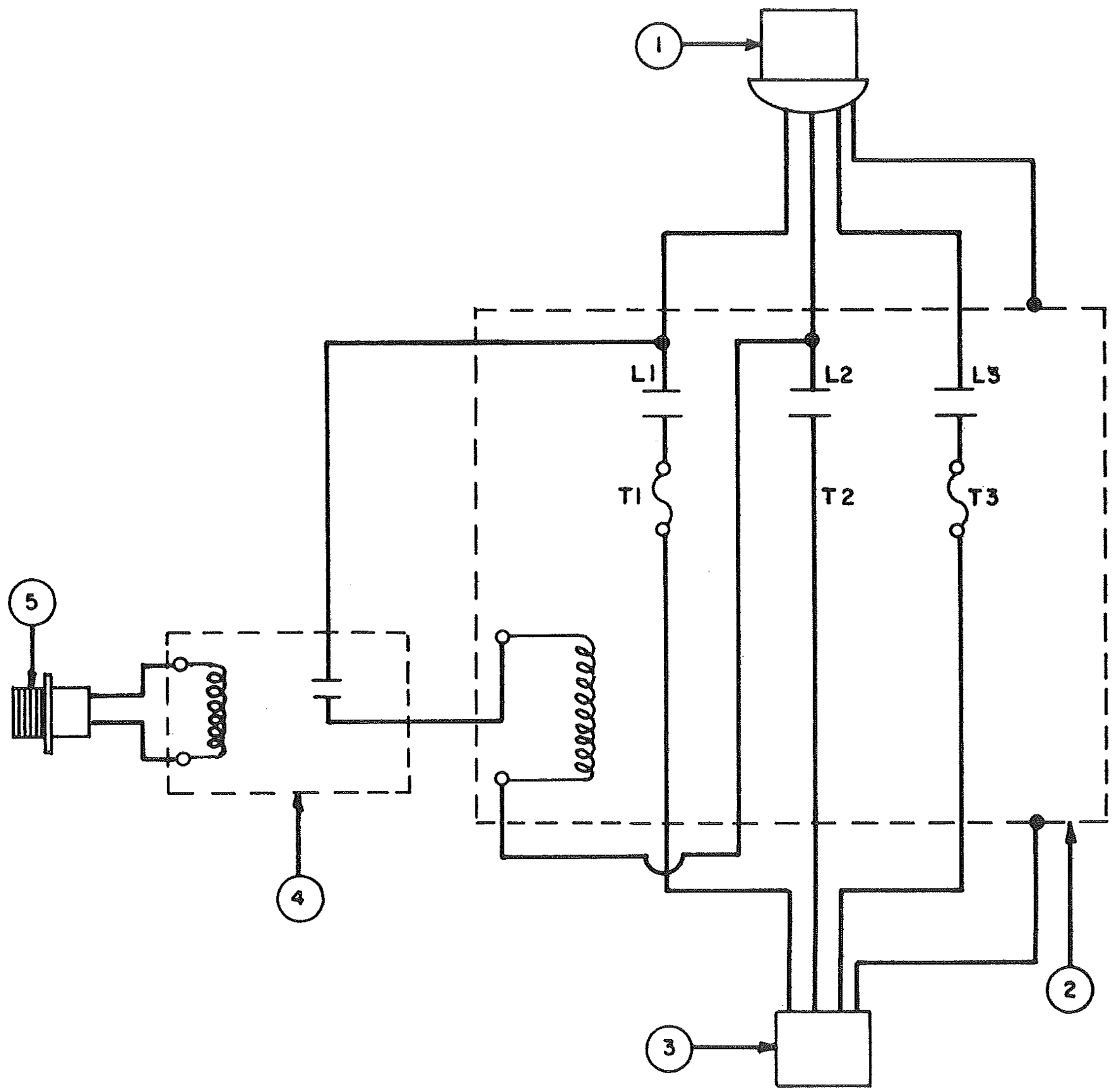

1 440 VAC, 60 AMP, 4 WIRE PLUG

2 440 VAC, 50 AMP, 3 POLE MAGNETIC CONTRACTOR

3 440 VAC, 60 AMP, 4 WIRE RECEPTACLE

4 28 VDC, 50 AMP, LEACH RELAY

5 28 VDC, 2 PIN, CANNON RECEPTACLE

Figure 23. Blower Power Schematic

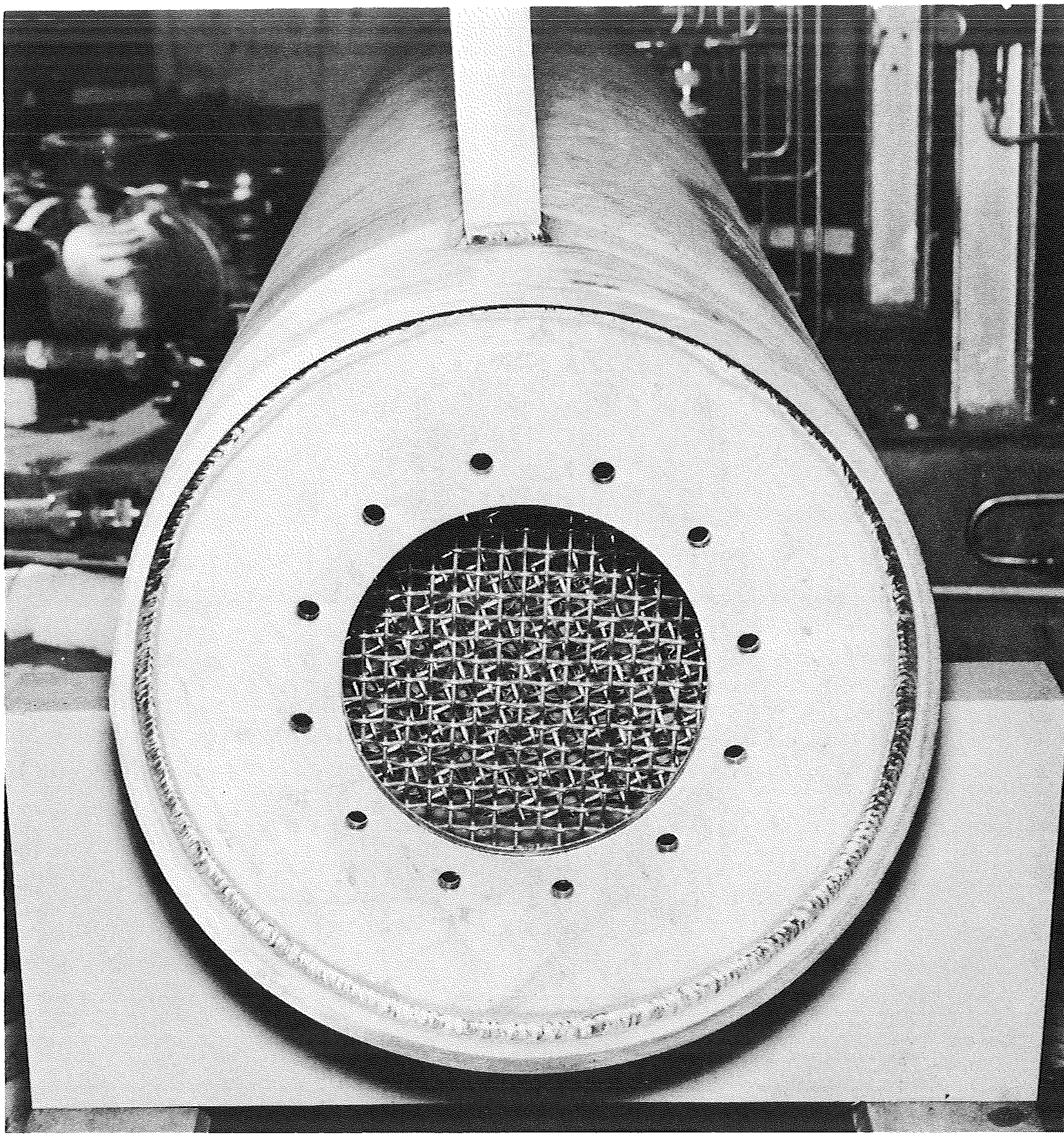

Figure 24. Air Heater During Assembly

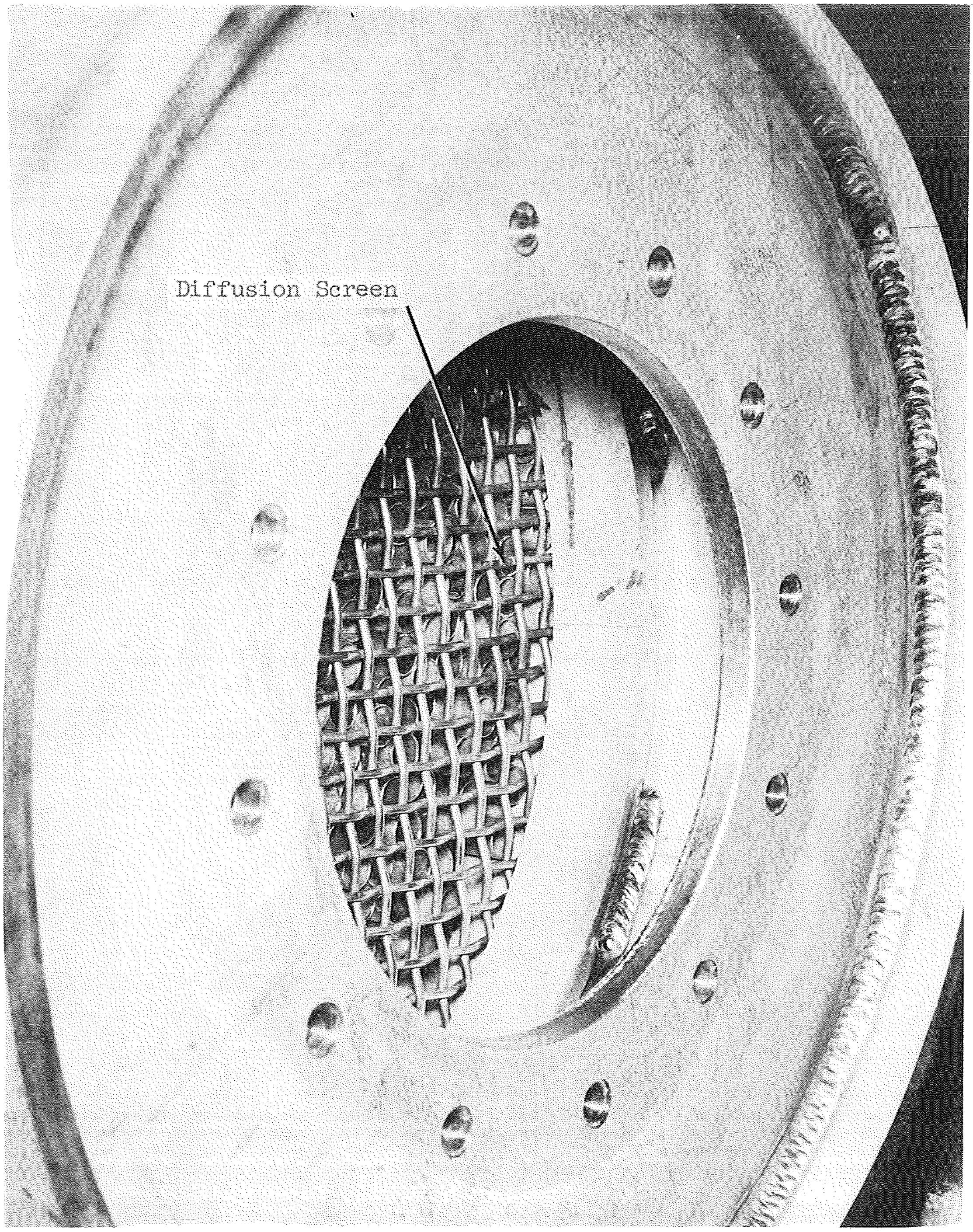

Figure 25. Aft-End Heater Diffusion Screen

thickness with rock wool with an overwrap of aluminum foil. The heater capacity was sufficient to warm a 2 lb/sec flow of air to 1000 F for 2 minutes.

The 25-kilovolt-ampere heater power supply and its 28-volt dc control wiring are shown schematically in Fig. 26. The electrical power was supplied from a 440-volt ac three-phase, four-wire distribution system. Variable heating power was obtained from a three-gang, three-phase motorized powerstat connected in a Y configuration. The heaters were operated as balanced loads on three single-phase circuits. A platinum/platinum 13-percent rhodium thermocouple (0.020-inch diameter wires) was mounted on the external heater metal shell to serve as an overall temperature protection device. This thermocouple and a Barber-Coleman Capacitrol controlled the energizing circuit of the three-pole magnetic contact, allowing remote and/or untended heater operation. The power supply was located near the 440-volt ac outlet on the test stand.

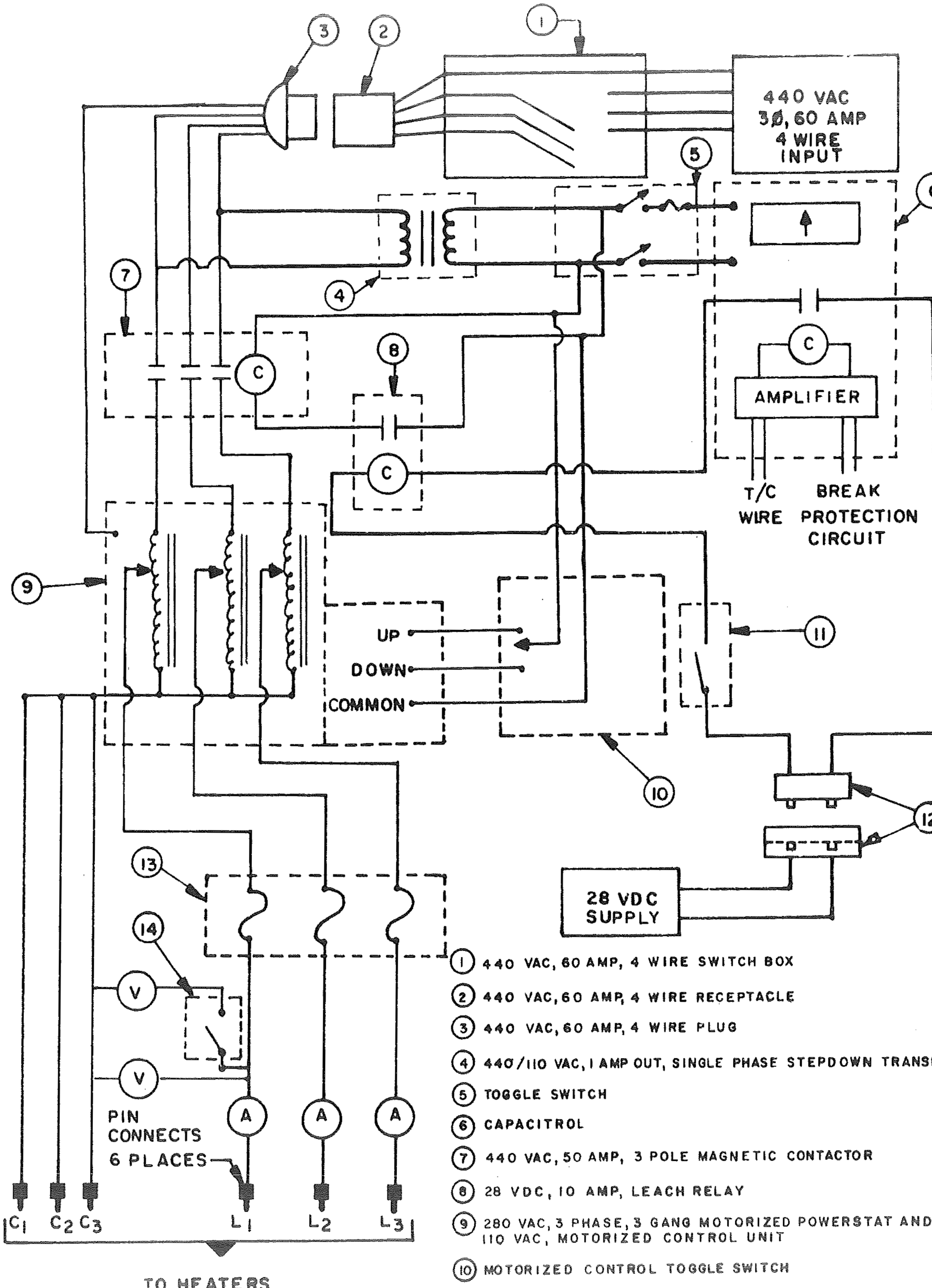

1. 440 VAC, 60 AMP, 4 WIRE SWITCH BOX
2. 440 VAC, 60 AMP, 4 WIRE RECEPTACLE
3. 440 VAC, 60 AMP, 4 WIRE PLUG
4. 440/110 VAC, 1 AMP OUT, SINGLE PHASE STEPDOWN TRANSFORMER
5. TOGGLE SWITCH
6. CAPACITROL
7. 440 VAC, 50 AMP, 3 POLE MAGNETIC CONTACTOR
8. 28 VDC, 10 AMP, LEACH RELAY
9. 280 VAC, 3 PHASE, 3 GANG MOTORIZED POWERSTAT AND 110 VAC, MOTORIZED CONTROL UNIT
10. MOTORIZED CONTROL TOGGLE SWITCH
11. MICROSWITCH SAFETY DEVICE
12. 28 VDC CANNON PLUG
13. 35 AMP CIRCUIT BREAKERS
14. MOMENTARY ON TOGGLE SWITCH FOR LOW RANGE VOLTMETER

Figure 26. Heater Power Supply Schematic

INSTRUMENTATION

A number of specialized instrumentation systems were utilized in this program. A discussion of these devices is given in the following paragraphs.

ZONE RADIOMETER

The zone radiometer system, developed to study rocket exhaust radiative processes under Contract NAS8-11261 (Ref. 5), was used to determine the temperature and partial pressure profiles of the H_2O molecule from measurements of the spectral emissivity and spectral radiance for various lines of sight.

The zone radiometer spectroscopy system is shown schematically in Fig. 27. The greybody source and spectroradiometer are described in complete detail in Ref. 5, and will therefore be discussed only briefly here. Special care was taken in the installation of this instrument to minimize the transmission of engine vibration to the optical components.

The greybody source consisted of a 6-inch long, 3/8-inch diameter, electrically heated graphite rod mounted in a water-cooled, argon-purged housing. Greybody radiation was optically chopped with a cylindrical "squirrel-cage" chopper to produce an AC signal for absorption measurements. The housing was equipped with a shutter.

With reference to Fig. 27, flat mirror M_1 and an 8-inch diameter spherical mirror M_2 form a 1:1 image of the greybody source across a vertical plane perpendicular

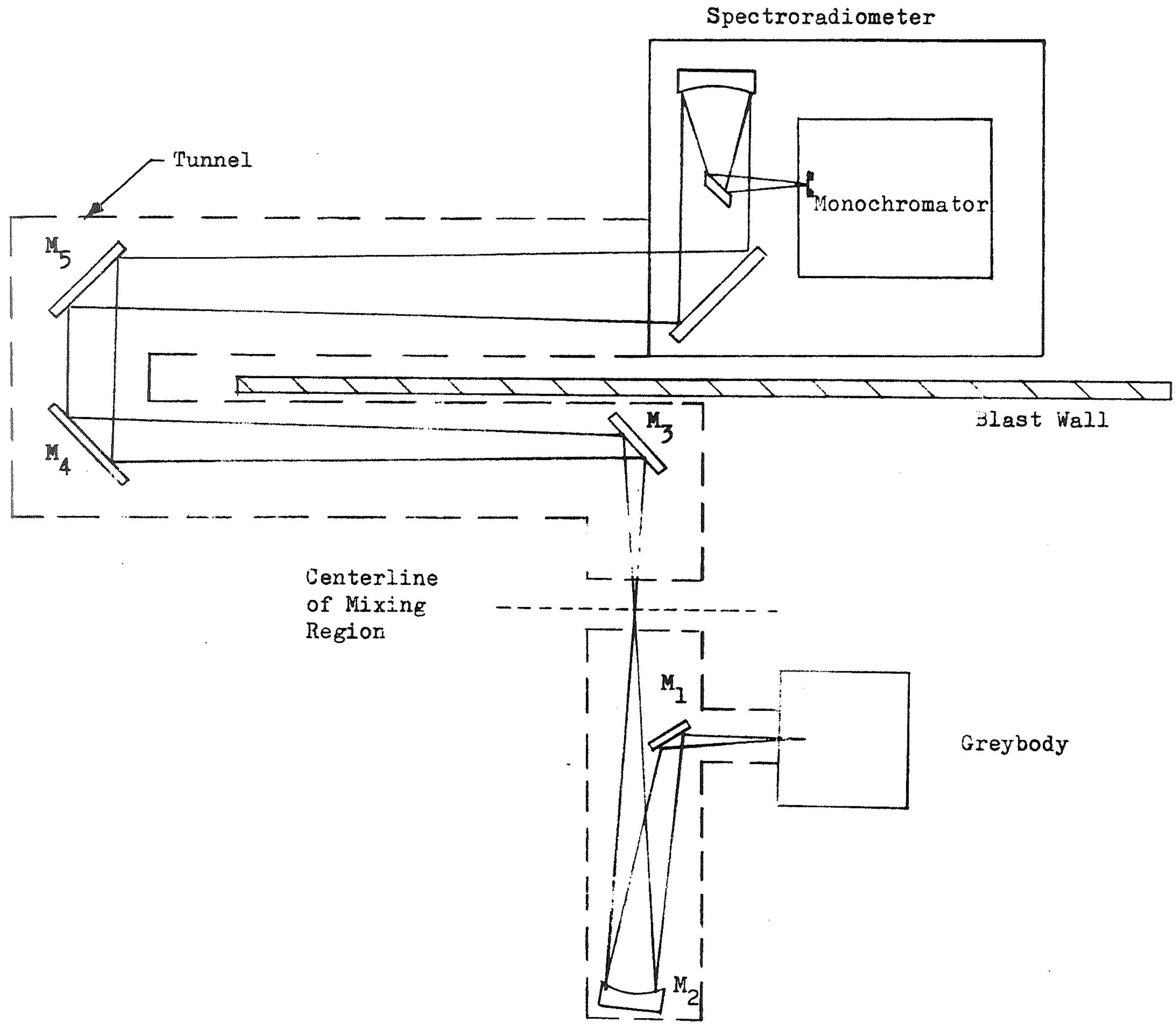

Figure 27. Zone Radiometry Schematic

to the flow axis in the mixing region. The greybody housing was actually mounted above the horizontal optical plane of the system so that it would not obscure a view of the mixing region from other instrumentation. The greybody source optics and flat mirror M_3 were moved parallel to the flow axis to change the horizontal field of view of the system. Flat mirrors M_4 and M_5 relayed radiation from the part of the mixing region under study to the spectroradiometer.

An optical diagram of the spectroradiometer is shown in Fig. 28 and Fig. 29 is a photograph of the instrument. The optical path, which was enclosed and purged with dry nitrogen, to eliminate atmospheric water vapor in the line of sight, was of such a length that a 10:1 reduced image of a portion of the mixing region was formed at the monochromator entrance slit by the telescope objective mirror. The field of view of the spectroradiometer at the mixing region was rectangular in cross section (on the order of 3 x 3 millimeters) and perpendicular to the flow axis. The width of this field of view was 10 times the width of the entrance slit. The height of the field of view was determined by an adjustable aperture at the entrance slit. During a test this cam driven aperture scanned different zones of the mixing region in the vertical direction. The cross sectional size of the field of view was determined from a trade-off between desired spectral and spatial resolution and available energy.

For emission measurements, the greybody shutter was closed and radiation from the mixing region was optically chopped at the monochromator exit slit. (This chopper was not used during absorption measurements.)

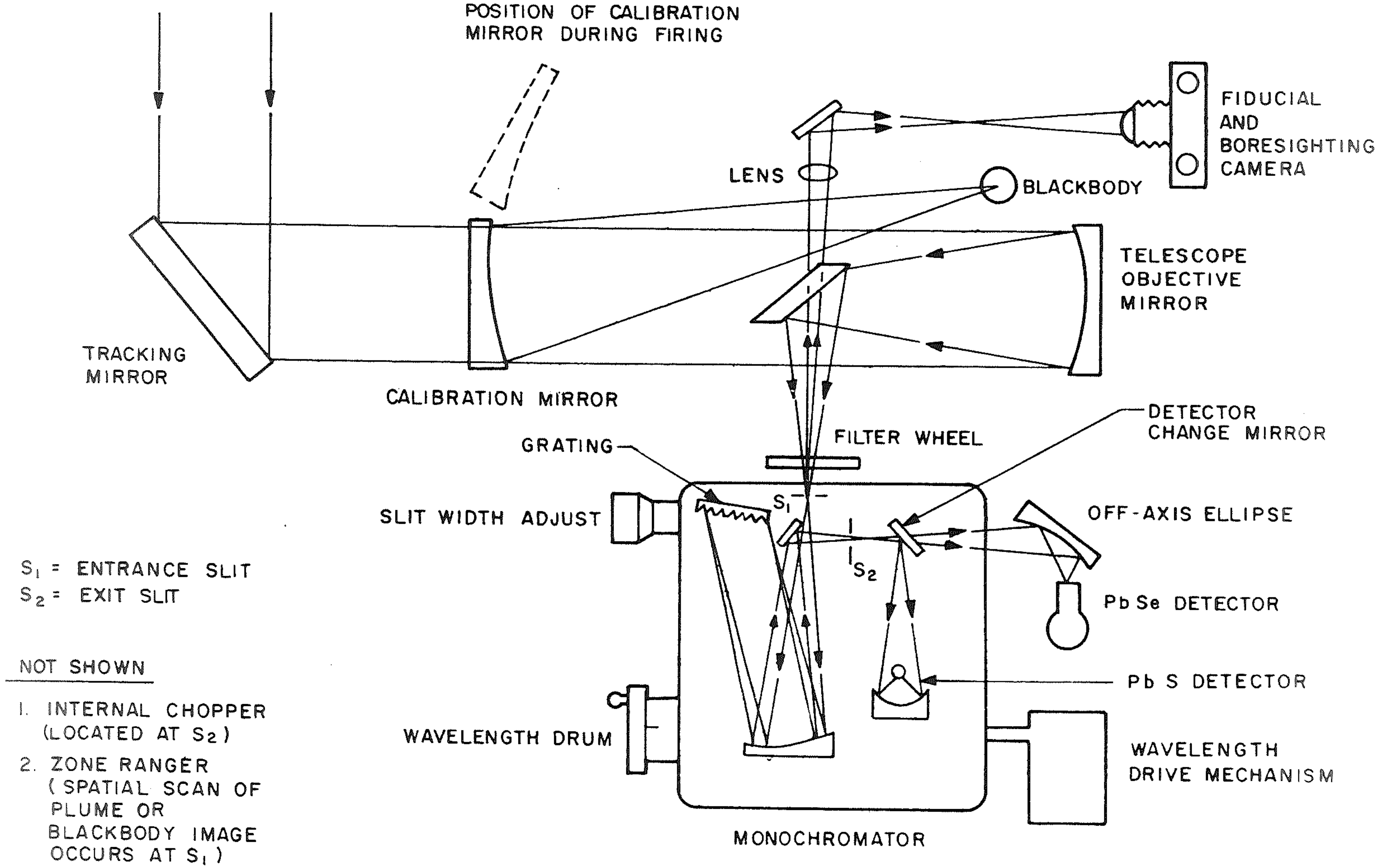

Figure 28. Optical Diagram of the Spectroradiometer

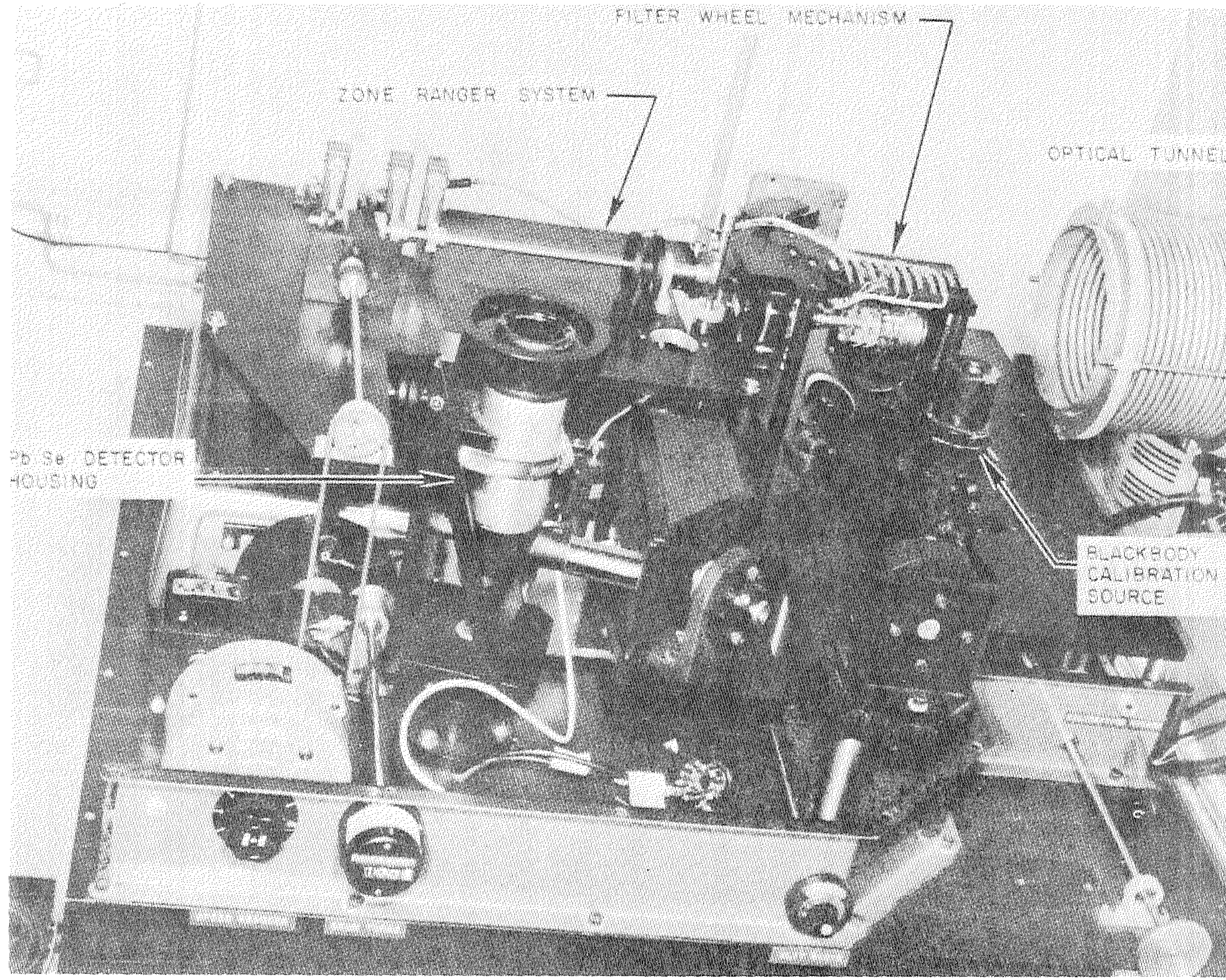

Figure 29. Infrared Spectroradiometer

The Perkin-Elmer Model 98-G monochromator was equipped with a 240-groves-per-millimeter grating blazed at 3.75 microns and used in first order. Overlapping orders were eliminated by a germanium filter. An uncooled PbS detector was used. The AC output from the detector was amplified, synchronously rectified, and displayed on a strip chart recorder.

An additional flat mirror relay system was assembled so that the spectroradiometer could view the mixing region outside the combustor from above, rather than horizontally. This system was used to assist in checking the two-dimensionality of the flow field.

PHOTOGRAPHIC MEASUREMENTS

A number of photographic measurements were utilized to provide visual information supplementary to the optical data collection. These measurements included schlieren, ultra-violet, infrared, color, and photopyrometry photography. A brief discussion of these techniques follows.

Schlieren Photography

Schlieren photography was used to determine the boundaries of the mixing region. This technique provided a cross reference with the data gathered with the zone radiometer and furnished a visual picture of the phenomena of interest. Simple, efficient operation was achieved through the use of a specially-designed schlieren lens attachment for a 16-millimeter Fastax camera and a portable parabolic mirror. A high intensity pulsed light source was provided by an

EG&G, Inc., Model 501 high-speed stroboscope. The test set-up is shown schematically in Fig. 30. For these experiments the knife edge was oriented horizontally to accentuate vertical density gradients. A detailed discussion of the theory of operation of a schlieren system can be found in Refs. 6 and 7.

Motion Picture Photography

The photographic coverage incorporated an array of three cameras to record radiation from the following spectral regions:

1. 2850 - 3150 A - corresponding to the (0,0) OH band, the region where OH radiates most intensely;

2. infrared from 7000-8500A - corresponding to weak water emission bands which have been recorded in previous work at Rocketdyne;

3. visible from 3500-6300 A - includes some of the blue continuum and impurities which may be present.

The basis for selection of these particular spectral regions for photographic coverage evolved from the experience gained under NAS7-521.

Table 2 presents the spectral regions recorded, the possible emitter species, and types of lens, filters, and films utilized. The film records were evaluated for their information content and only those that yielded specifically useful information are discussed in Appendix 4.

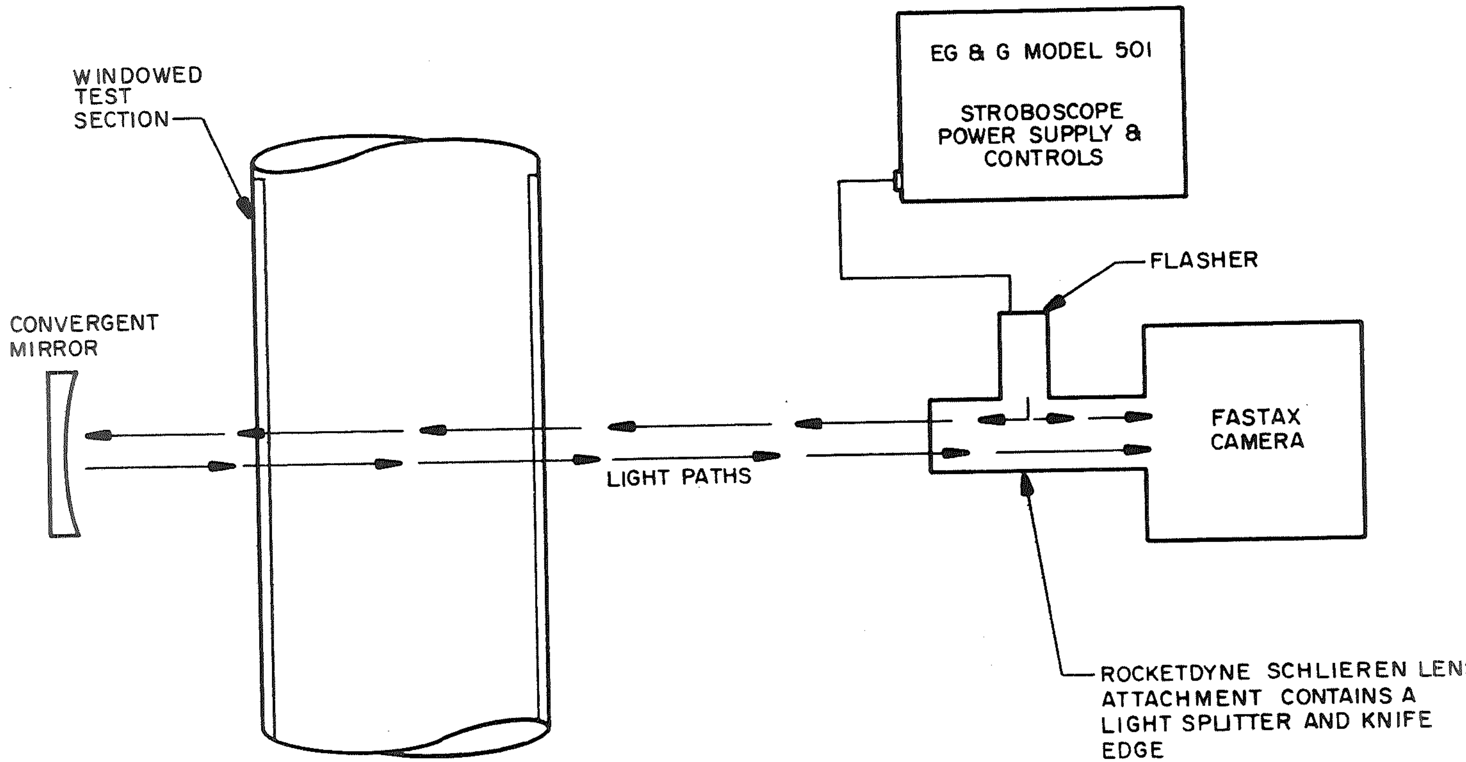

Figure 30. Schematic of Schlieren Apparatus

TABLE 2

PHOTOGRAPHIC SPECIFICATIONS

Spectral Region (A)	Chief Emitter	Lens Type	Filter	Film
2850-3150	OH	Quartz, Ultra-violet transmitting	OCLI	2498 RAR
7000-8500	H_2O	Glass	Wratten 89B	IR
3500-6300	H_2O, $O + OH$ Recombination, Impurities	Glass	None	Ektachrome EF Daylight

The UV and IR cameras were located approximately 10 feet from the engine with a direct line of sight perpendicular to the windows. Initially, Fastax cameras capable of framing rates up to 8000 frames per second were utilized; however, emission was too weak to be recorded at these high framing rates. Subsequently, Bell and Howell cameras were employed. Motion picture coverage determined the spatial distribution of emission from the principal emitting species and provided a visual analog to the spectroscopic data.

Photopyrometry

The photopyrometer consisted of a Nikon F 35 mm camera equipped with an automatic rewind motor, an ultraviolet transmitting lens, optical interference filters to isolate a narrow band of radiation in the desired spectral region, a tungsten ribbon filament lamp, and an optical calibration system consisting of mirrors and an attenuating step filter. These components are shown schematically in Fig. 31.

The ultraviolet photopyrometer records the radiation from the OH radical photographically for the determination of a contour map of the OH brigntness temperature. The map assists in defining the spatial extent of combustion. A tungsten lamp ribbon filament of known spectral radiance which is also imaged on the film record serves as the calibration source. The ribbon filament was attenuated by a step filter of known attenuation and thus provided a calibration scale for data reduction. The flow field was mapped through utilization of an automatic-scanning microdensitometer which produced an isodensity contour map of the gas flow image and a density measurement of each zone of the step filtered lamp

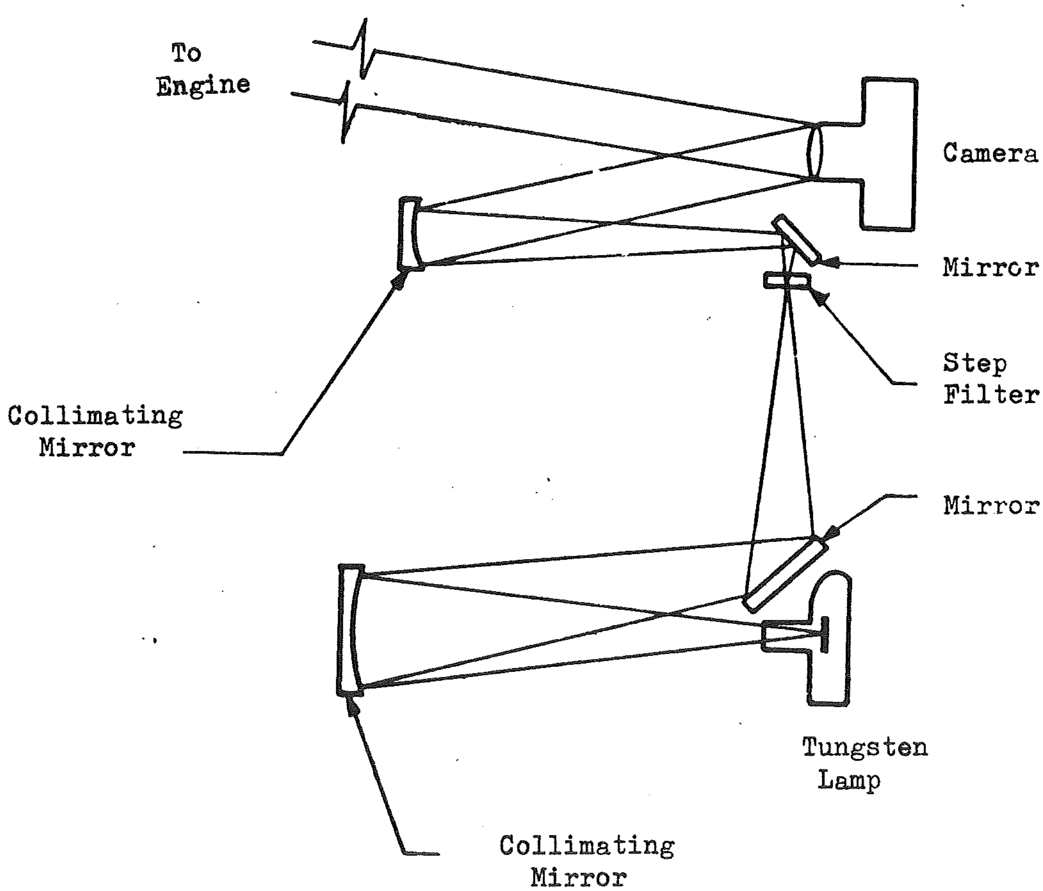

Figure 31. Optical Diagram of Photographic Pyrometer

image. The film response was determined by plotting the film density of each zone as a function of the logarithm of radiance. A value of radiance or its equivalent brightness temperature can then be assigned to each isodensity contour in the flow field.

The OH brightness temperature at a given point in the flow field is a function of both OH concentration and the electronic excitation temperature, which may be equal to or greater than the gas translational temperature. Complete interpretation of the photopyrograms requires correlation with ultraviolet spectroscopic data.

OTHER INSTRUMENTATION

Manometer Bank

A 50-tube manometer bank for mapping the test-section static pressure was procured and installed adjacent to the test pit (Fig. 32). A total of 30 static pressure taps were located on the four test-section walls. The manometer bank was also used to monitor the pressure in the air heater transfer ducting. The physical location of the static pressure taps is given in Table 3. Manometer bank data is presented in Appendix 1.

Ancillary Instrumentation

A series of difficulties precluded the collection of data from some of the instruments planned for use on this program. These instruments included the

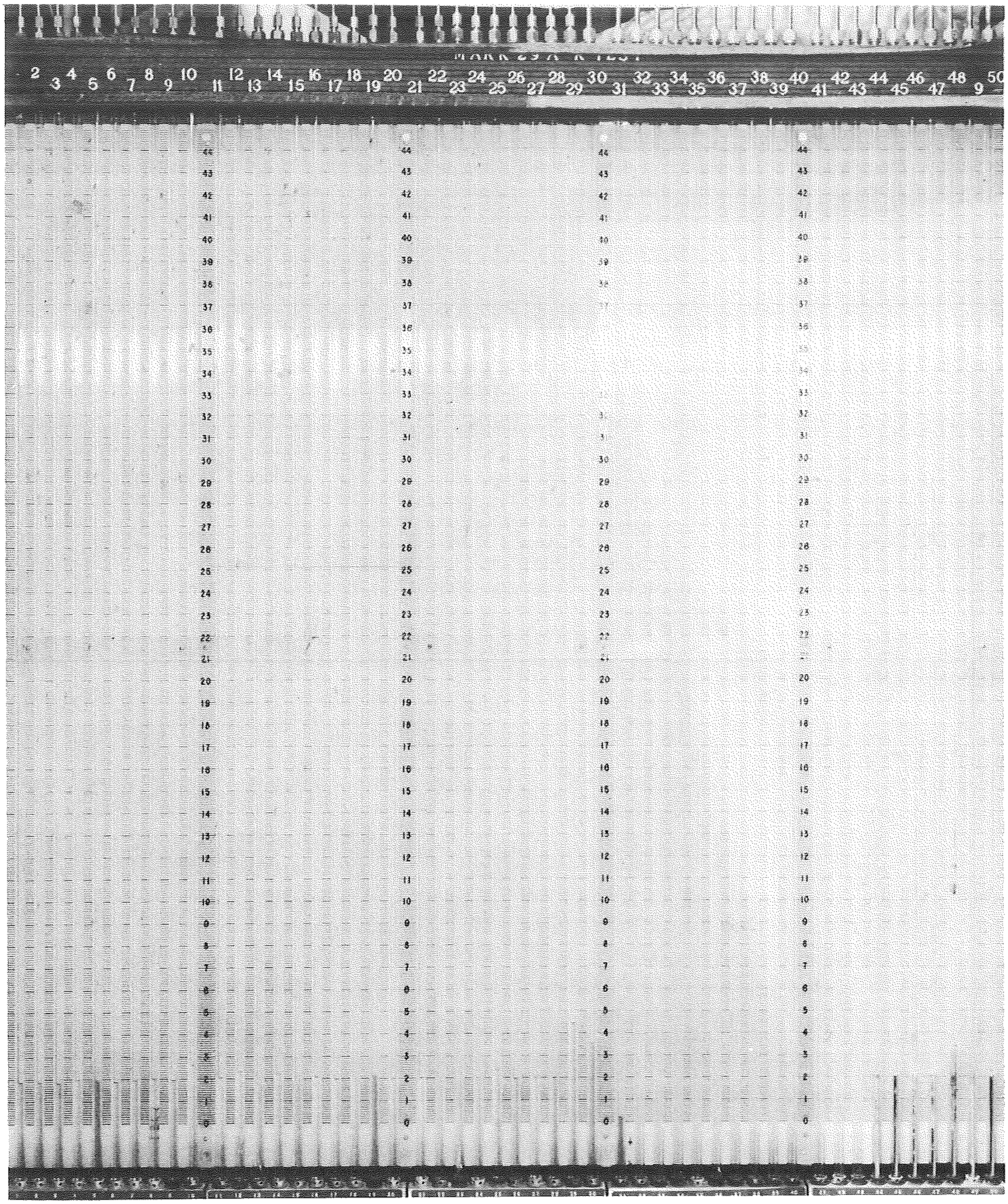

Figure 32. 50-Tube Manometer Bank

TABLE 3

STATIC PRESSURE TAP LOCATIONS

Pressure Tap	X, in	Y, in	Z, in
1	8.625	11.982	2.23
2	5.585	11.982	2.23
3	5.585	11.306	4.46
4	8.625	9.306	4.46
5	-.078	11.306	4.46
6	5.585	11.982	1.34
7	5.585	11.982	3.12
8	5.585	9.306	4.46
9	2.875	9.306	4.46
10	-.078	9.306	4.46
11	8.625	0	3.12
12	8.625	0	1.34
13	5.585	11.306	0
14	2.875	9.306	0
15	-.078	11.306	0
16	8.625	0	.45
17	8.625	9.306	0
18	5.585	9.306	0
19	-.078	9.306	0
20	2.875	11.982	2.23
21	5.585	0	.45
22	2.875	0	.45
23	5.585	0	4.01
24	-.078	0	4.01
25	-.078	0	3.12
26	-.078	0	.45
27	8.625	0	4.01
28	2.875	0	4.01
29	-.078	0	1.34
30	-.078	0	2.23

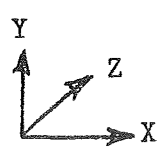

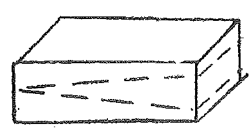

LASS (larger aperture spectrometer/spectrograph), greyrad probe, and hot wire anemometer. Concurrance with the technical monitor always preceded elimination of these devices from the test program.

DATA REDUCTION

ZONE RADIOMETRY

Measurements

Because of the two-dimensionality of the flow field, the data reduction procedure was much simpler than described in Ref. 5. The data reduction procedure for each line-of-sight (LOS) is that used for a uniform gas.

The two quantities , the spectral radiance (N_{LOS}), and the emissivity (ϵ_{LOS}) are indirectly measured by the spectroradiometer. N_{LOS} is determined from point-by-point comparison of spatial scans of flow field emission to emission from a blackbody as corrected for mirror losses, i.e.,

$$N_{LOS} = \frac{1.42\ D_f}{D_{BB}} \tag{1}$$

when D_f = flame emission

D_{BB} = blackbody emission

and 1.42 is the window loss correction factor.

Point by point comparison of spatial scans of greybody radiation as attenuated by the flow field during a test allowed preparation of graphs of fractional transmission (τ_{LOS}) or emissivity ($\epsilon_{LOS} = 1 - \tau_{LOS}$) as a function of line of sight, i.e.,

$$\tau = \frac{D_{f-g}}{D_g} \qquad (2)$$

where D_{f-g} = intensity of attenuated greybody radiation

D_g = intensity of greybody radiation

and

$$\epsilon = 1 - \tau.$$

Plots of these initial spectroradiometer measurements N_{LOS} and ϵ_{LOS} are given in Appendix 3.

From the fundamental measurements described above, line-of-sight (LOS) temperature and H_2O partial pressure can be derived.

The line-of-sight temperature is defined by the relation

$$\frac{N_{LOS}}{\epsilon_{LOS}} = N_{BB}\,(T_{LOS}) \qquad (3)$$

where $N_{BB}\,(T_{LOS})$ is the spectral radiance of a blackbody at temperature T_{LOS} and at the wave length at which the measurement was carried out. In this case the temperature **was derived by reference to a standard blackbody** table for the wave length of 2.49 microns, the wave length utilized in these experiments.

H_2O partial pressure (P_{LOS}) is determined from the simple Lambert-Beer Law expression

$$\tau_{LOS} = e^{-KL\ P_{LOS}} \tag{4}$$

where L is the path length of the flow field along the line-of-sight and K is the value of the spectral absorption coefficient of H_2O at the temperature and measurement wave length. The absorption coefficient was obtained from Ref. 11 as a function of temperature. The wave length utilized for measurement was 2.49μ. As discussed in the following paragraphs the simple expression above is not precisely correct, primarily due to pressure broadening of the spectral lines. However, the error in applying equation 4 can be acceptably small depending upon the wave length selected for measurement (i.e., in the wings of the band K_V x constant) and the overall accuracy of the data. It was estimated that the maximum error in applying equation 4 at a wave length of 2.49 μ was 15% in water vapor partial pressure. Plots of these derived data, T_{LOS} and $P_{H_2O_{LOS}}$, are given in Appendix 3.

A discussion of the method utilized for the determination of H_2O partial pressure is presented in the following paragraphs.

Lambert-Beer's Law, Eq. 4, can be easily derived assuming that the absorption of each molecule is independent of every other molecule. However, since (1) monochromatic light is difficult to achieve, (2) the collision of molecules cause variation in the absorption, and (3) all absorption lines are of finite width, deviations in the Lambert-Beer Law occur.

In fact, many cases of deviations in the Lambert-Beer Law have been measured and documented in the literature.

A more general form of the absorption law is:

$$\tau = \frac{\int_0^\infty S_v \exp(-K_v\, pl)\, f(|v - v_i|, a)\, dv}{\int_0^\infty S_v f(|v - v_i|, a)\, dv} \qquad (5)$$

where S_v = energy distribution in the radiation of the incident light

$f(|v-v_i|, a)$ = the spectrometer transmission function

K_v = $\sum_m \alpha_m\, \delta/\pi \left[(v-v_m)^2 + \delta^2\right]$, Lorentz collision damping function

v = wave length frequency

α_m = $\int_0^\infty K_{vm}\, d_v$

δ = damping constant

a = slot width

m = center of band

Equation (5) has been solved for several specific conditions by Elsasser and Plass. When applicable, application of one of these models allows the theoretical determination of the absorption for a given path length, and partial pressure at selected frequencies; if the transmission and path length are known from experimental measurements, then the corresponding partial pressure can be determined. The various solutions of equation (5) all result in two dimensionless parameters: one involving the total pressure of the gases and the other the product of partial pressure of the absorbing gas and the path length. An example of one set of solutions is presented in Fig. 33 (taken from Ref. 9). Note that significant deviations from the Lambert-Beer Law occur as the optical path becomes thick. Also note that the total pressure of the gases produces a broadening effect on the absorbing gas.

The non-Lambert-Beer Law behavior has been measured numerous times for water vapor which is of interest in this program. Some typical results are shown in Fig. 34 (taken from Ref. 10). Excellent agreement was found with the results taken at $\lambda = 2.845\mu$ with the Statistical Model described by Plass. Ferriso et al (Ref. 11) empirically determined the absorption coefficients of H_2O from 300 to 3000°K. The assumption in their work is that for optically thick gases the curve growth is also given by the Statistical Model. They tabulated their results as a function of wave length and temperature. For a wave length of 2.49μ their results are plotted in Fig. 35.

Comparison of these calculated results with the measurements made by several other investigators showed good agreement. These results suggest that the Statistical Model can be utilized to determine absorption characteristics for water vapor in the presence of other gases. It is important to note that the Statistical Model describes absorption characteristics which deviated from standard Lambert-Beer Law behavior.

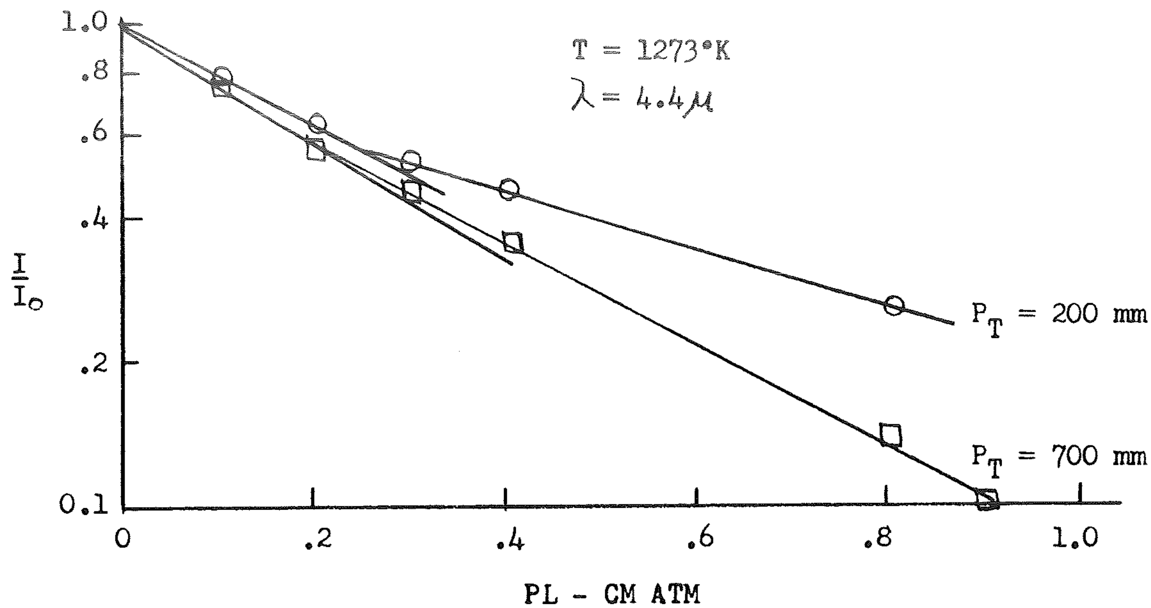

Figure 33. Effect of Optical Path Length on CO_2 Transmittance with N_2 as Broadener

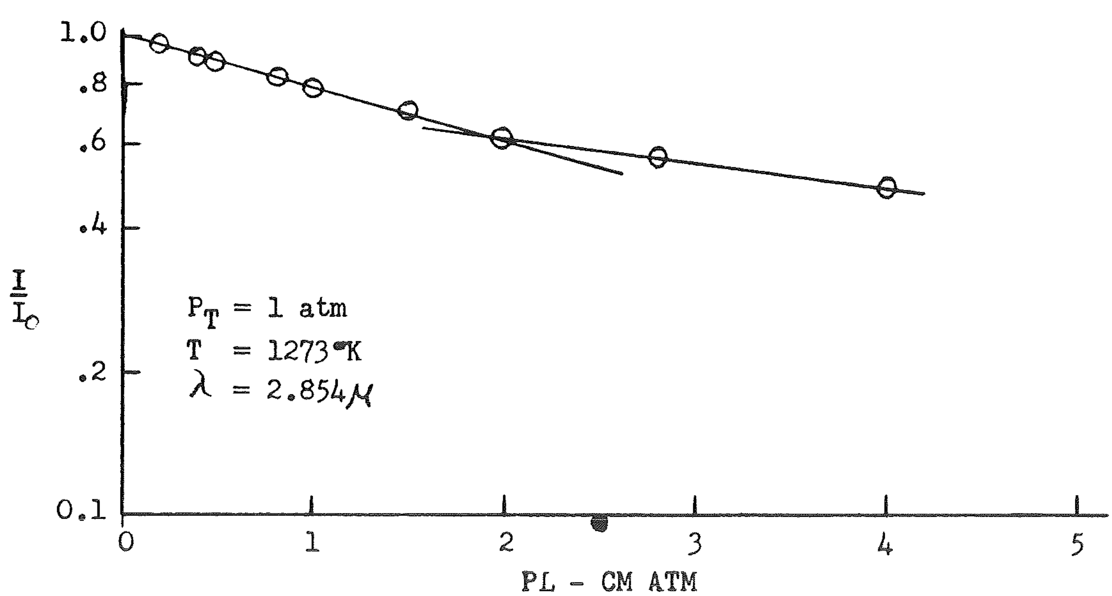

Figure 34. Effect of Optical Path Length on H_2O Transmittance with N_2 as Broadener.

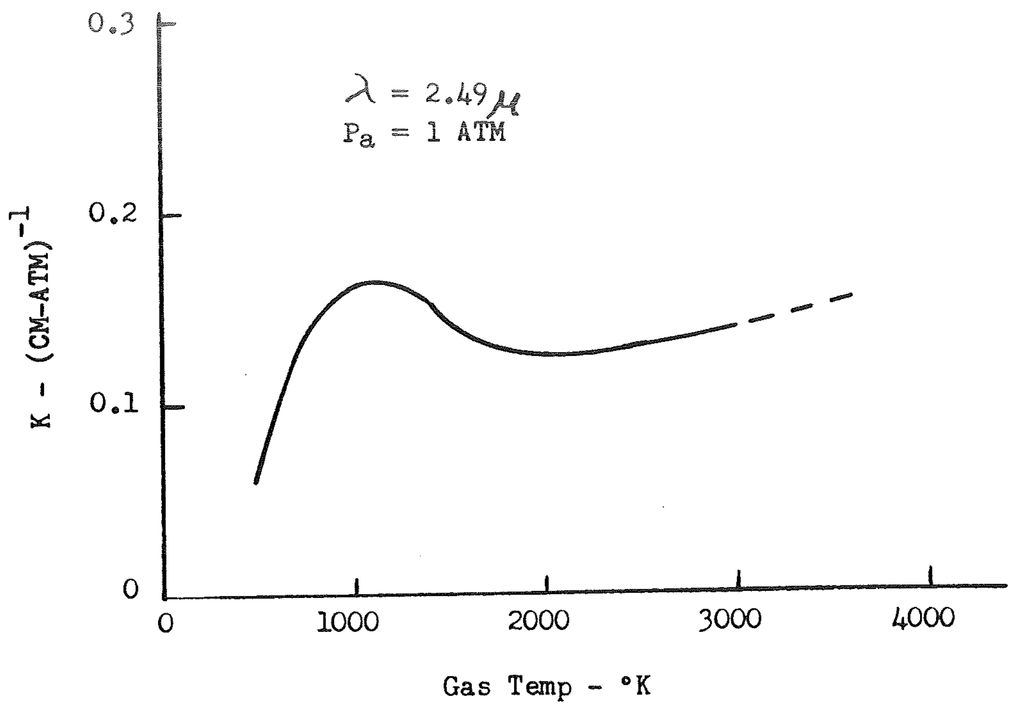

Figure 35. Absorption Coefficient as a Function of Temperature for Water Vapor

Many investigators have overcome the difficulty of integrating the absorption equation by simply developing "working calibration curves". This is accomplished by measuring the absorptance as a function of both known partial pressures and path length. The working curve is then used directly to determine the unknown partial pressure of the gas mixture, however, due to the high combustion temperatures encountered on this program this could not be readily accomplished. Therefore, Fig. 35 was utilized for data reduction.

Instrument Calibration

Wave length calibration of the spectroradiometer was conducted by recording atmospheric absorption spectra. Intensity calibration for emission data was made with a blackbody radiation source. Corrections were applied to include the losses caused by the various mirrors and windows in the optical path.

The background spectra for absorption measurements was obtained by scanning the greybody prior to a test. Spatial calibration of the spectrometer field of view was obtained by using the travelling aperture to scan the images of small light sources placed at known positions with respect to the test chamber.

Mode of Operation

The spectroradiometer initially was used in a conventional spectral scan mode with a fixed line-of-sight through the mixing region. This furnished data for the selection of the optimum wave length, slit width, and electronic amplification values for the zone radiometry measurements.

On all subsequent test firings, zone radiometry was conducted for emission and absorption measurements at a selected wave length (2.49μ) across a single plane (perpendicular to the flow axis) of the test chamber. Different planes were measured on different tests. During the first half of a test the travelling aperture scanned the mixing region image for emission measurements and radiation intensity was recorded as a function of spatial position. During the second half of the test the internal chopper was turned off, and the greybody shutter was opened. Chopped greybody radiation attenuated by combustion products was recorded as a function of spatial position. Before and after a test the blackbody and the greybody were similarly scanned for calibration purposes.

PRESSURE AND TEMPERATURE INSTRUMENTATION

The large quantity of pressure and temperature instrumentation utilized to monitor the operation of the facility necessitated computerized data reduction. Appropriate data reduction equations were assembled and a computational sequence was formulated. These procedures and the computer programs are presented in Appendix 7.

PHOTOGRAPHIC MEASUREMENTS

The large volume of photographic information gathered necessitated a two-step data reduction process. The films were initially screened to eliminate obviously poor films (poor field of view or redundancy). Then a compulation of film records that were representative of the experiments was assembled and enlargements that depicted the available information were made. The spatial location of the momentum boundary layer (displayed in the schlieren prints) and chemical reaction zones (displayed on the UV and IR prints) were recorded and analyzed for gross data trends. Analysis of these data is given in Appendix 4.

A similar procedure was applied to the photopyrograms; however, due to the relatively high cost of reducing these data to isodensity maps and ultimately to relative brightness temperature maps, greater care was given to the selection of the frames to be reduced. The analysis of the available data (discussed in detail in Appendix 4) indicated that no significant changes occurred in the plume as a function of the test variables; therefore, only those frames that typified the high air temperature and medium air temperature tests were reduced. The data reduction procedure was as discussed previously.

RESULTS AND DISCUSSION

The large quantity of experimental data obtained would usually be presented in this section, however, due to its bulk and to provide a less congested flow of information, data from this program are included in the Appendices. Appropriate discussion, when applicable, is also presented. The Appendices include:

- Appendix 1 - Manometer Bank Data (Test section static pressure)
- Appendix 2 - Transient Data
- Appendix 3 - Zone Radiometer Data
- Appendix 4 - Photographic Data
- Appendix 5 - Velocity Profiles
- Appendix 6 - Test Firing Data
- Appendix 7 - Data Reduction Computer Programs

A brief discussion of the hot fire tests is given below, after which a discussion of the data is presented. Data analysis, in its usual interpretation, was not a part of this program. Correlation of these test data with theory and reduction to turbulent transport properties was beyond the scope of the present effort.

HOT FIRE TESTS

A total of 36 hot fire tests were conducted on this program. The test matrix and associated principal instrumentation locations are given in Table 4. For comparison purposes the data were grouped according to the following:

TABLE 4

TEST MATRIX

Test No.	Date	Type	Instrumentation & Location
1	11/19/69	Instrumentation Checkout (Ta = 1000°F)	ZR-H-8-SPECT-E LASS-2-SPECT-E, PYRO SCH-H-2
2	11/19/69	Instrumentation Checkout (Ta = 1000°F)	ZR-H-8-SPECT-E LASS-2-SPECT-E, PYRO SCH-H-2
4	11/26-69	Instrumentation Checkout (Ta = 1000°F)	ZR-H-1-SPAT-E, PYRO SCH-V-10, LASS-5-SPECT-E
021	1/13/70	Flow Characterization (Ta = 1000°F)	ZR-H-8-SPAT-EA, PYRO LASS-Vibration Test
041	1/13/70	Instrumentation Checkout Ta = 1000°F)	ZR-H-1-SPECT-E, PYRO LASS - Internal Scan
5	1/13/70	Flow Characterization and 2D Determination (Ta = 1000°F)	ZR-H-1-SPECT-EA LASS-SPECT, PYRO SCH-V-10
10	5/26/70	Film Coolant and 2D Determination (Ta = 1000°F)	ZR-H-8-SPAT-EA, SCH-V-10
11	5/26/70	Flow Characterization (Ta = 1000°F)	ZR-H-3-SPAT-EA, SCH-V-10
12	5/26/70	Flow Characterization (Ta = 1000°F)	ZR-H-6-SPAT-EA
13	5/28/70	Flow Characterization (Ta = 1000°F)	ZR-H-4-SPAT-EA, SCH-H-10
14	5/28/70	Flow Characterization (Ta = 1000°F)	ZR-H-5-SPAT-EA, HW-6-M-B
16	6/9/70	Film Coolant and 2D Determination (Ta = 1000°F)	ZR-V-10-SPAT-E
17	6/9/70	Flow Characterization (Ta = 1000°F)	ZR-H-1-SPAT-EA, HW-9-M-B

TABLE 4 (Cont'd)

Test No.	Date	Type	Instrumentation & Location
18	6/9/70	Flow Characterization (Ta = 1000°F)	ZR-H-2-SPAT-EA
19	6/10/70	Flow Characterization (Ta = 700°F)	ZR-H-10-SPAT-EA, SCH-H-5,PYRO
20	6/10/70	Flow Characterization (Ta = 700°F)	ZR-H-2-SPAT-EA
21	6/10/70	Flow Characterization (Ta = 700°F)	ZR-H-3-SPAT-EA
22	6/24/70	Flow Characterization (Ta = 700°F)	ZR-H-8-1/2-SPAT-EA, SCH-H-2
23	6/24/70	Flow Characterization (Ta = 700°F)	ZR-H-5-SPAT-EA
24	6/24/70	Flow Characterization (Ta = 700°F)	ZR-H-6-SPAT-EA, PYRO
25	6/24/70	Flow Characterization (Ta = 700°F)	ZR-H-7-SPAT-EA
26	6/25/70	Flow Characterization (Ta = 700°F)	ZR-H-1-SPAT-EA, SCH-H-10
27	6/25/70	Flow Characterization (Ta = 700°F)	ZR-H-5-SPAT-EA
28	6/25/70	Flow Characterization (Ta = 700°F)	ZR-H-8-SPAT-EA
29	6/25/70	Scan at no H_2O Absorption (Ta = 700°F)	ZR-H-8-SPAT-EA
30	6/25/70	Flow Characterization (Ta = 1000°F)	ZR-H-7-SPAT-EA
31	6/25/70	Flow Characterization (Ta = 1000°F)	ZR-H-10-SPAT-EA
32	6/26/70	Velocity Ratio - Blower Wide Open (Ta = 1000°F)	ZR-H-8-SPAT-EA, PYRO, SCH-H-3

TABLE 4 (Cont'd)

Test No.	Date	Type	Instrumentation & Location
33	6/26/70	Velocity Ratio - Blower Inlet Restricted (Ta=1000°F)	ZR-H-8-SPAT-EA, PYRO, SCH-H-3
34	6/26/70	Air Temperature (Ta = 100°F)	ZR-H-8-SPAT-EA, PYRO, SCH-H-3
35	7/1/70	Air Turbulence-1/2-inch Screen Grid (Ta = 1000°F)	ZR-H-8-SPAT-EA,SCH-H-3, PYRO
36	7/1/70	Velocity Ratio-Blower Inlet Restricted (Ta=1000°F)	ZR-H-8-SPAT-EA,SCH-H-3,PYRO
37	7/1/70	Velocity Ratio-Blower Inlet Restricted (Ta=1000°F)	ZR-H-8-SPAT-EA,SCH-H-3,PYRO
38	7/1/70	Air Turbulence-1/8-inch Screen Grid (Ta=1000°F)	ZR-H-8-SPAT-EA,SCH-H-3,PYRO
39	7/1/70	Flow Characterization (Ta = 1000°F)	ZR-H-9-SPAT-EA,SCH-H-3,PYRO
40	7/1/70	Air Turbulence-1/2-inch Dem (Ta = 1000°F)	ZR-H-8-SPAT-EA,SCH-H-3,PYRO

High Temperature Air	Runs 10*, 11*, 12, 13, 14, 16*, 17, 18, 30, 31, 39
Medium Temperature Air	Runs 19, 20, 21, 22, 23, 24, 25, 26, 27, 28, 29
Low Temperature Air	Run 34
High Velocity Air	Run 32
Low Velocity Air	Runs 33, 36, 37
1/2-inch Screen	Run 35
1/8-inch Screen	Run 38
1/2-inch Dam	Run 40
Check-out Runs**	Runs 1, 2, 4, 021, 041, 5*

Setting the various utilities on a given test day consisted of a number of calculations referenced to the local atmospheric pressure and empirical data gathered during sub-system checkouts. A typical test set-up is summarized below. The various working equations group all "fixed" variables and are unique.

a) Water System: Fixed conditions based upon check-out tests. Set tank 1 pressure to 1140 psig and tank 2 pressure to 1110 psig.

b) Air System: $P_{Duct} = 1.026\ P_{atm}$. Select proper blower inlet restriction from empirical plot of $P_{Duct}-P_a$ versus percentage inlet restriction.

*These tests also included film coolant and 2-D studies.
**The data were run at conditions similar to high temperature air tests.

c) Film Coolants: The low pressure film coolant upstream duct pressure is selected from a generated plot of P_{Duct} versus T_{atm} with P_{atm} as a parameter. The high pressure film coolant upstream duct pressure is determined from $P_{Duct} = 1.87\ P_{atm}$.

d) Propellant Flows: $P_c = 29.35\ P_{atm}$. Assuming an $\eta_{c*} = 96.6$, $\dot{w}_{LOX} = .409\ P_{atm}$ and P_{Tank} is derived from an empirical plot of P_{Tank} versus $\dot{w}_{LOX}$. Hydrogen flowrate = $.0818\ P_{atm}$ and P_{Tank} is derived from an empirical curve of P_{Tank} versus $\dot{w}_{GH_2}$ as a function of T_{GH_2}.

After pre-chilling the injector with LN_2, the various utilities are loaded to their respective pre-test values. The oxidizer lines are chilled with LOX and the countdown is initiated. A typical sequence of events is presented in Table 5. The calculated test firing data for the 36 conducted experiments is given in Appendix 6. A summary of the averaged test firing data for the principal parameters conforming to the aforementioned experiment groupings is given in Table 6. These data also include calculation of the variance and standard deviation when more than one run was made to characterize a given condition.

In general, testing went smoothly and transient behavior was not a problem (see Appendix 2). With the exception of Run 15 where ignition did not occur and Run 17 where the LOX regulator did not maintain a constant LOX tank pressure, all sub-systems performed normally. The air system and the

TABLE 5

TYPICAL SEQUENCE - RUN 22

	Seconds
Start, #1 H_2O On, #2 H_2O On	0.000
Camera ON	4.555
LOX Power ON	5.420
LOX OPEN	5.520
LOX Full OPEN	5.560
TEB ON	5.665
GH_2 Power ON	5.665
GH_2 OPEN	5.985
GH_2 Full OPEN	6.150
TEB OFF	6.335
GH_2 Power OFF	15.900
LOX Power OFF	16.025
LOX OFF	16.060
LOX Full OFF	16.085
GH_2 OFF	16.158
GH_2 Full OFF	16.320
Camera OFF	16.475
#1 H_2O, #2 H_2O OFF	19.960
Sequence OFF	20.210
Duration - GH_2 Full OPEN to LOX OFF	9.910

TABLE 6

AVERAGED DATA FOR THE VARIOUS EXPERIMENTS

Parameter	High Temperature Flow Characterization $\bar{X}$, average	High Temperature Flow Characterization σ^2, variance	High Temperature Flow Characterization σ, standard duration	Medium Temperature Flow Characterization $\bar{X}$, average	Medium Temperature Flow Characterization σ^2, variance	Medium Temperature Flow Characterization σ, standard deviation	Low Temperature Air Test	High Velocity Air Test	Low Velocity Air Tests $\bar{X}$, average	Low Velocity Air Tests σ^2, variance	Low Velocity Air Tests σ, standard deviation	1/2" Screen Test	1/8" Screen Test	1/2" Dam Test
Air System														
Flowrate, lb/sec	2.33	0.01251	0.145	2.43	0.0033	0.058	2.71	2.24	1.23	0.0004	0.020	1.23	1.17	1.91
Inlet Pressure, psig	0.0005	88×10^{-8}	0.0009	0.0014	88×10^{-8}	0.0009	0.002	0.002	0.001	-	0	0.621	0.641	0.182
Inlet Temp, °F	829	2589	50.9	612	1662	40.8	278	850	902	1190	34.5	849	950	928
Inlet Density, lb/ft^3	0.0292	1.8×10^{-6}	0.0013	0.0350	98×10^{-8}	0.0010	0.0505	0.0285	0.0275	43×10^{-8}	0.0007	0.0298	0.0278	0.0273
Inlet Velocity, ft/sec	563	741	27.2	487	237	15.4	376	549	313	25	5.0	287	294	491
Mach. No.	0.319	1.77×10^{-4}	0.013	0.304	61×10^{-6}	0.0078	0.282	0.310	0.173	9×10^{-6}	0.003	0.162	0.160	0.269
Low GN_2 System														
Flowrate, lb/sec	1.10	0.0036	0.060	1.11	0.0071	0.084	1.04	1.04	1.00	0.0022	0.047	0.90	1.03	1.02
Inlet Pressure, psig	0.09	1.5×10^{-4}	0.012	0.093	2.36×10^{-4}	0.015	0.082	0.082	0.073	38×10^{-6}	0.0062	0.424	0.313	0.579
Inlet Temperature, °F	10	408	20.2	23	224	15.0	42	42	40	54	7.35	29	42	42
Inlet Density, lb/ft^3	0.0777	1×10^{-5}	0.0032	0.0745	3.47×10^{-6}	0.0019	0.0723	0.0723	0.0727	1.34×10^{-6}	0.0012	0.761	0.0737	0.0751
Inlet Velocity, ft/sec	480	512	22.6	503	784	22.5	488	487	462	187	13.7	401	474	459
Mach. No.	0.444	4.5×10^{-4}	0.0222	0.455	6.29×10^{-4}	0.025	0.473	0.436	0.414	2.28×10^{-4}	0.015	0.364	0.424	0.411
High GN_2 System														
Flowrate, lb/sec	4.51	0.0093	0.0965	4.42	0.0073	0.086	4.35	4.34	4.31	0.0070	0.084	4.43	4.35	4.38
Inlet Pressure, psig	1.50	0.0329	0.181	1.51	0.0694	0.264	1.49	1.46	1.51	0.0258	0.161	1.46	1.46	1.51
Inlet Temp. °F	-61	268	16.4	-45	93	9.65	-36	-35	-38	26	5.10	-50	-35	-38
Inlet Density, lb/ft^3	0.1007	15.7×10^{-6}	0.004	0.0969	6.84×10^{-6}	0.0026	0.0943	0.0940	0.0950	4.73×10^{-6}	0.0022	0.0976	0.0941	0.0950
Inlet Velocity, ft/sec	997	387	19.7	1016	140	11.8	1027	1028	1025	36	6.0	1010	1028	1025
Engine														
LOX Flowrate, lb/sec	5.98	0.116	0.341	5.80	0.0255	0.160	5.70	5.66	5.74	0.0065	0.081	5.79	5.82	5.66
Injection Temp., °F	-289	47.5	6.90	-283	40	6.33	-291	-287	-282	3	1.74	-291	-286	-288
GH_2 Flowrate, lb/sec	1.14	0.0002	0.014	1.14	0.0002	0.014	1.12	1.07	1.13	0.0001	0.010	1.13	1.12	1.14
Injection Temp., °F	76	200	14.1	95	123	11.1	107	106	100	92	9.6	83	106	98
Chamber Pressure, psig	395	120	11.0	384	86	9.28	382	383	386	28	5.30	384	391	382
Mixture Ratio	5.23	0.0838	0.289	5.09	0.0273	0.165	5.08	5.30	5.08	0.0021	0.046	5.10	5.21	4.97
C* Efficiency, η_{c*}	95.1	3.01	1.74	94.5	3.30	1.82	95.7	98.1	95.8	0.241	0.49	94.9	96.6	95.6
Atmospheric Press., psia	13.91	0.0015	0.0388	13.88	0.0018	0.042	13.82	13.82	13.84	0.0002	0.014	13.85	13.85	13.85

GN_2 film coolant systems deviated slightly from the theoretically derived operating or pre-set conditions. These deviations were caused by the flows adjusting to the actual conditions within the mixing chamber upon the onset of supersonic flow. The ejector characteristics of this stream cause a moderate increase, over the design value, of the GN_2 film coolants and air streams. This behavior was noted during the checkout firings, but, since the increases noted were only approximately 10% and did not significantly alter the flow field under investigation, modification to these sub-systems were deemed unnecessary.

Examination of Table 6 together with the individual results given in Appendix 6 indicate that the experiments were quite reproducible, therefore, side by side comparisons can be made. The groupings of the experiments given at the beginning of this section include both characterization experiments, high temperature and medium temperature air tests, and diagnostic information, i.e., 2-Dimensionality, film coolant effects, low temperature air, air velocity, and air turbulence level. A discussion of this information will be given in the following paragraphs.

Among the checkout runs were some to ascertain if stable combustion was attained.

The basic combustor utilized as the generator for the supersonic fuel-rich combustion products did not have a history of any detectable instabilities; however, the changes made to that engine raised the possibility that instabilities might have been present in the configuration utilized. The initial measurement attempt utilized a streak camera focused at the exit plane of the combustor. Due to the relatively low intensity level in the plume, exposures could not be recorded at the framing rates required. The next attempt utilized an AC radiometer as the measurement device. Measurements were made on three test firings and the data were reduced. No indication of any mode of instability was evident, only noise which is a characteristic of typical rocket engine behavior.

DATA COMPARISONS

Data Cross Plots

A major portion of the zone radiometer data is presented in Figs. 36 to 39. They include temperature and H_2O partial pressure maps for the two with characterized cases of high temperature (829 F) and medium temperature (612 F) air. The reference case for all data comparisons is the 829 F air tests. All diagnostic information was gathered utilizing this nominal air stream temperature.

The boundaries of the apparatus and the theoretical mixing axis are superimposed on these figures. The actual data points for the various zone radiometer positions are connected by solid lines. Attempts to smooth these data are superimposed with coded lines representing a particular isotherm or isobar. The code for the smoothing curves is referenced to the code for the data points. An identification key is given in the figures.

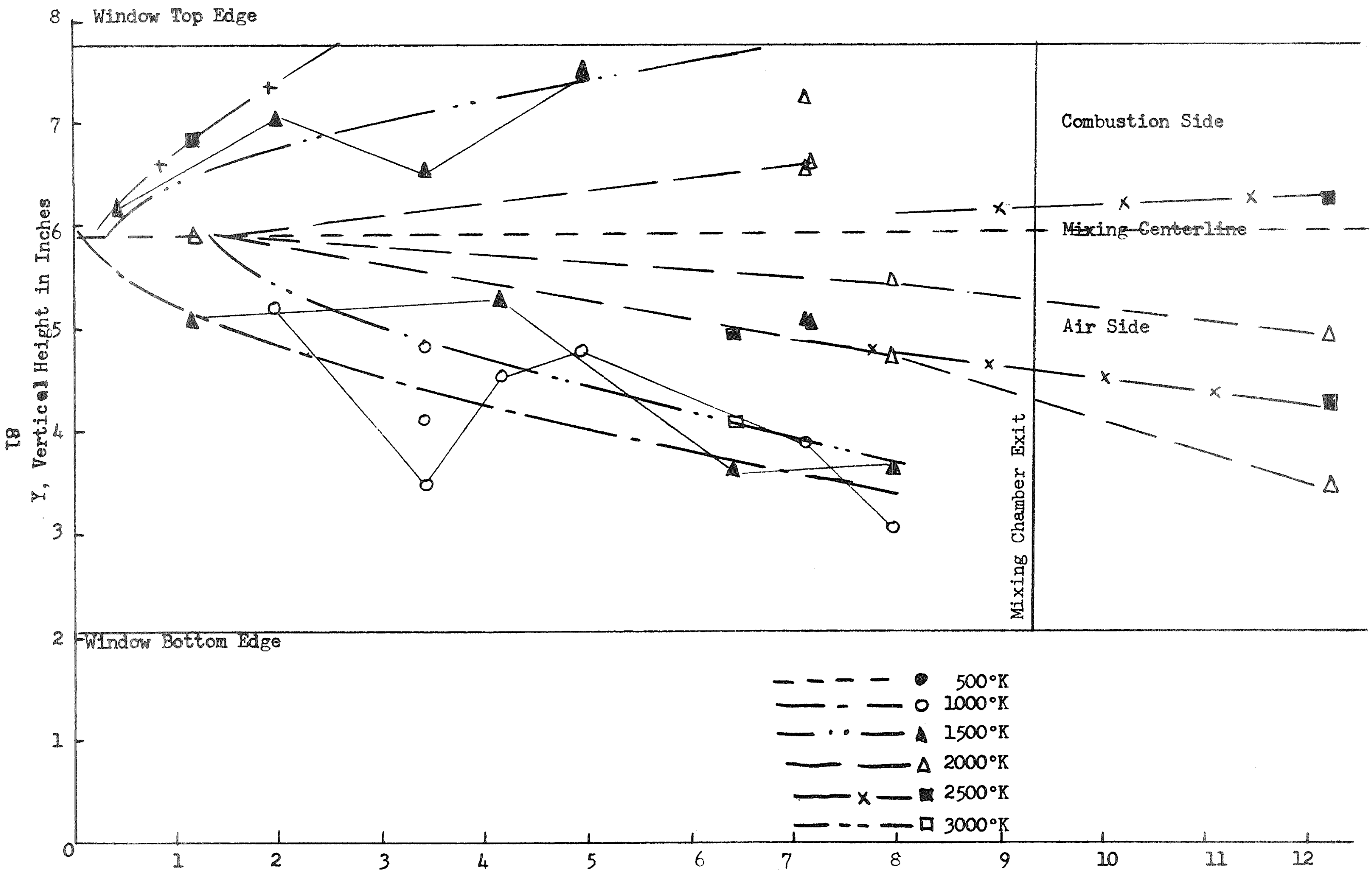

Figure 36. Temperature Map--829°F Air

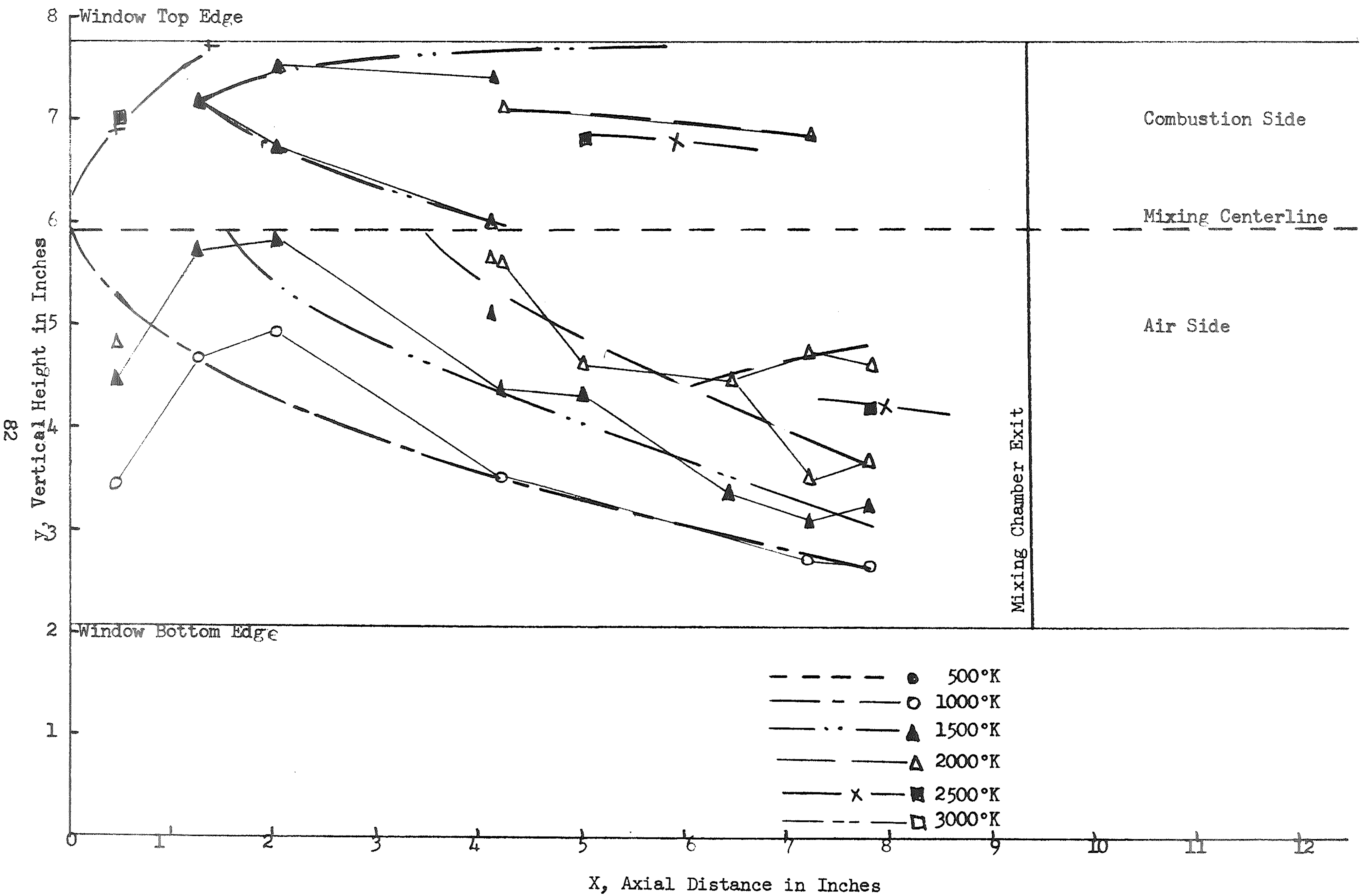

Figure 37. Temperature Map--612°F Air

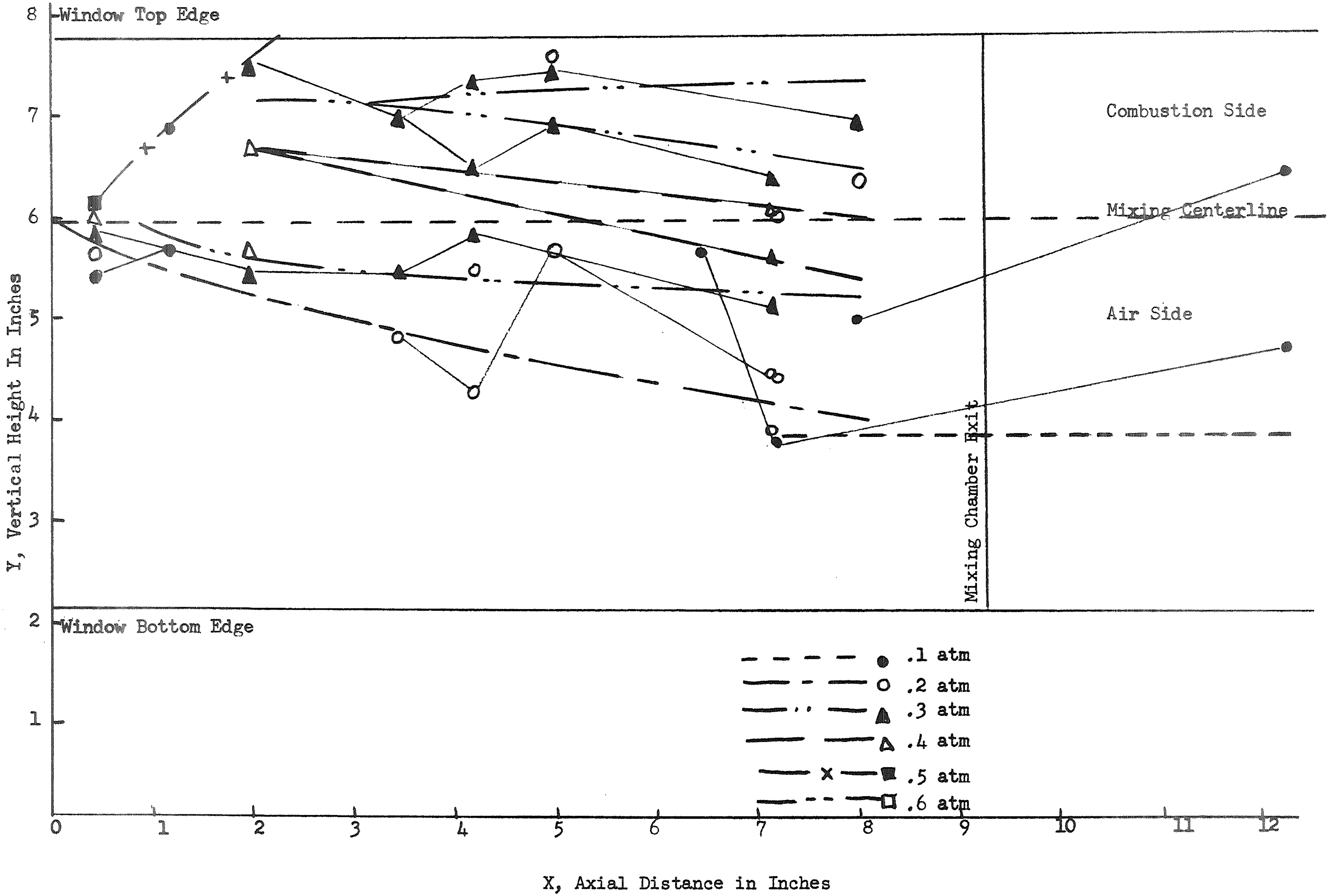

Figure 38. H_2O Partial Pressure Map - 829°F Air

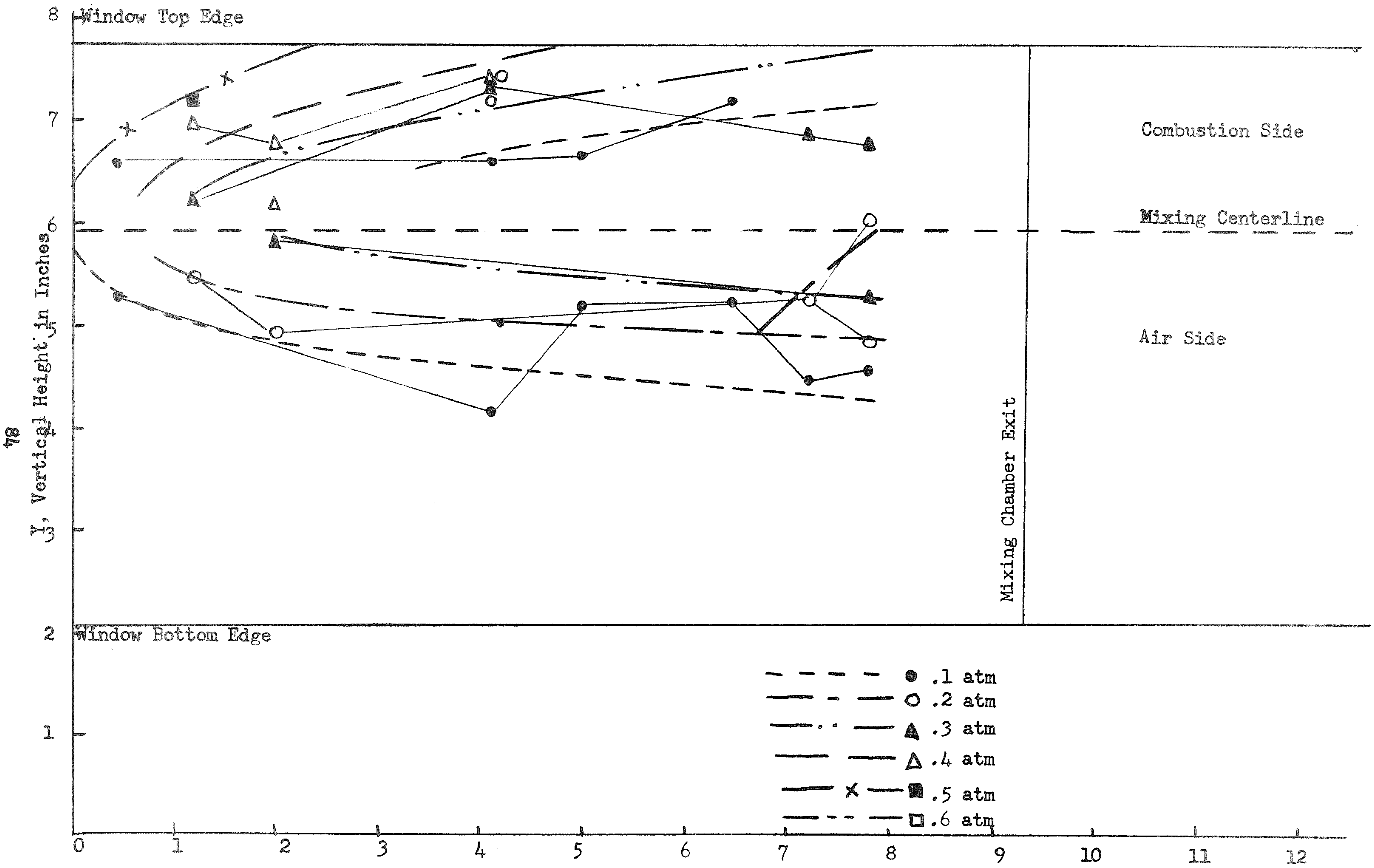

Figure 39. H_2O Partial Pressure Map - 612°F Air

Comparison of the smoothed data curves (idealized data) to the actual data curves as the mixing layer penetrates the air stream indicates non-monotonic behavior. At the onset of mixing, variable mixing rates are observed and no similarity between actual and idealized behavior is apparent. However, similarity is obtained farther downstream. Abramovitch, Ref. 12, gives some justification for this behavior. His experiments indicate that as the velocity ratio goes to infinity the maintenance of constant pressure mixing can only be accomplished if a vortex exists near the entrance to the mixing chamber. This hypothesized vortex appears to be present in this experiment, see infrared photograph, Fig. 4-13. Therefore, the "washing-out" of the data in the near field appears due to this vortex.

The vortex affects the temperature data to the greatest extent. This indicates that it is relatively weak and only recirculates a small quantity of combustion products from the very edge of the mixing region; if it were strong the actual temperature data would not converge to the smoothed data near the mixing chamber exit. In addition, it would have a much greater effect on the concentration data. It should be noted that every individual little jog in the data defies explanation. The data presented represent only one run at each location; therefore, a host of reasons could be brought to bear.

Data reliability was checked by two sets of runs made at identical conditions (Runs 021 and 10 for 829 F air and Runs 23 and 27 for 612 F air) and are included in Figs. 36 and 37. Agreement is reasonable; however, it is not within the precision that would yield great confidence in the data obtained. However, this does not compromise the data obtained, it does indicate that a much larger quantity of data is necessary before concrete arguments can be presented in support or disagreement with available theories. Although an Edisonian approach would have been desirable from a statistical standpoint, i.e., 3 to 4 tests at each condition, the objectives and the available funding precluded this.

The measured temperatures and H_2O partial pressures were compared to theoretical values. The results of this calculation which utilized mixture ratio as a parameter is presented in Fig. 40. Comparison of the zone radiometer measurement maximums taken in the unmixed core of MR 5.0 at the initiation of mixing to these data show fairly good agreement ($\pm 15\%$). The measured maximum H_2O partial pressure was 0.5 atmospheres and the theoretical value was 0.61 atmospheres while the recovery temperature maximum was 2500°K and the theoretical value was 2130°K.

Two-Dimensionality and Film Coolant Experiments

A series of runs, 5, 10, 11, and 16 were conducted to determine if the flow was indeed two-dimensional and what effect the film coolants had on the mixing process. Both zone radiometric and photographic data were gathered.

Direct color photographs, Figs. 41 (a side view) and 42 (a rear view) indicated that the flow was indeed two-dimensional. Additional data, to reaffirm this fact, were gathered with schlieren photography and zone radiometry measurements viewing the test section from the top, aft of the exit. The

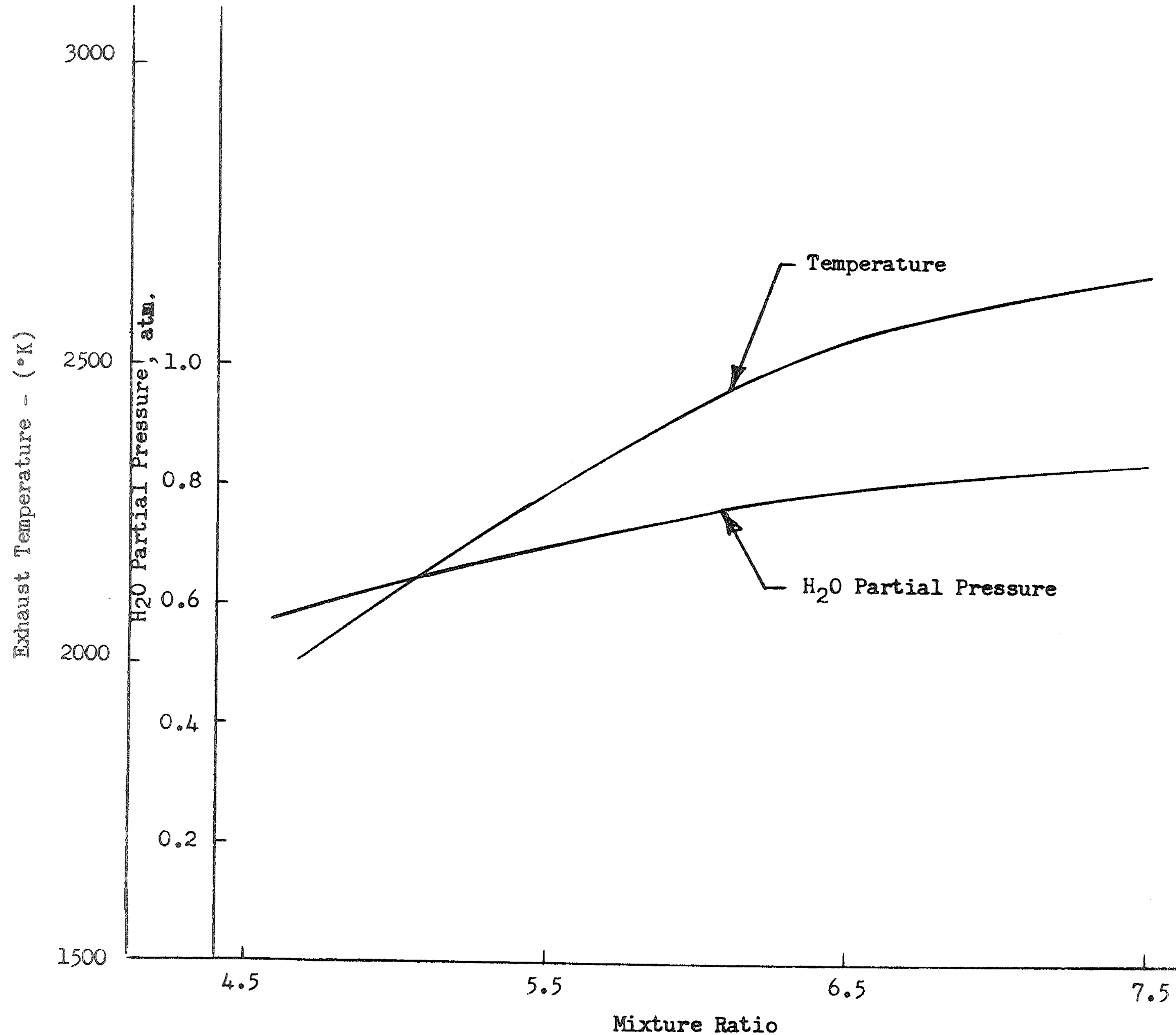

Figure 40. Theoretical Exhaust Temperature and H_2O Partial Pressure as a Function of Mixture Ratio

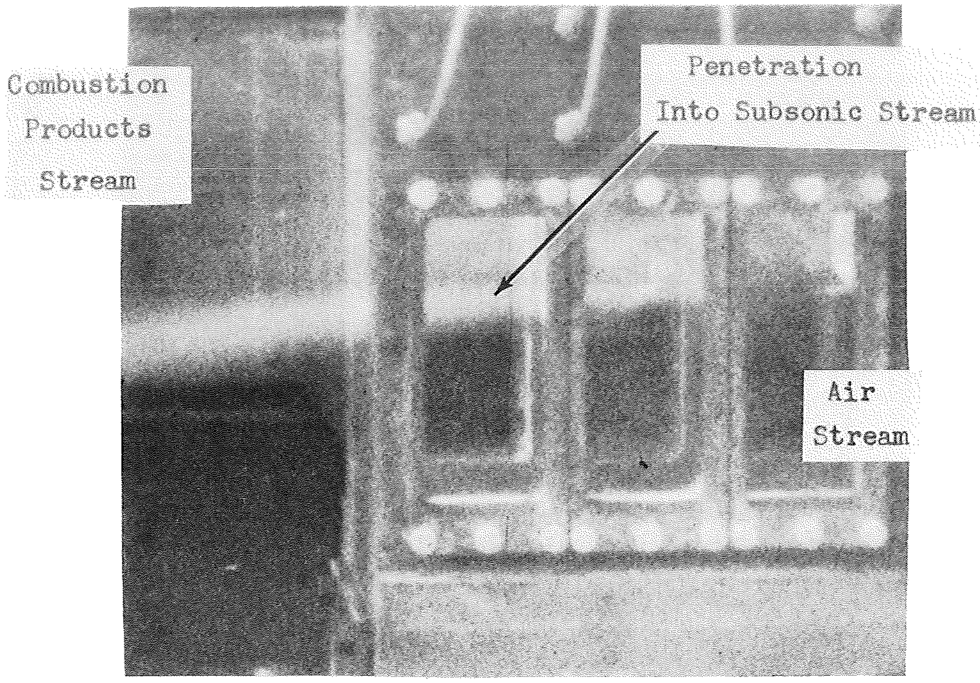

Figure 41. Side View of Test Section

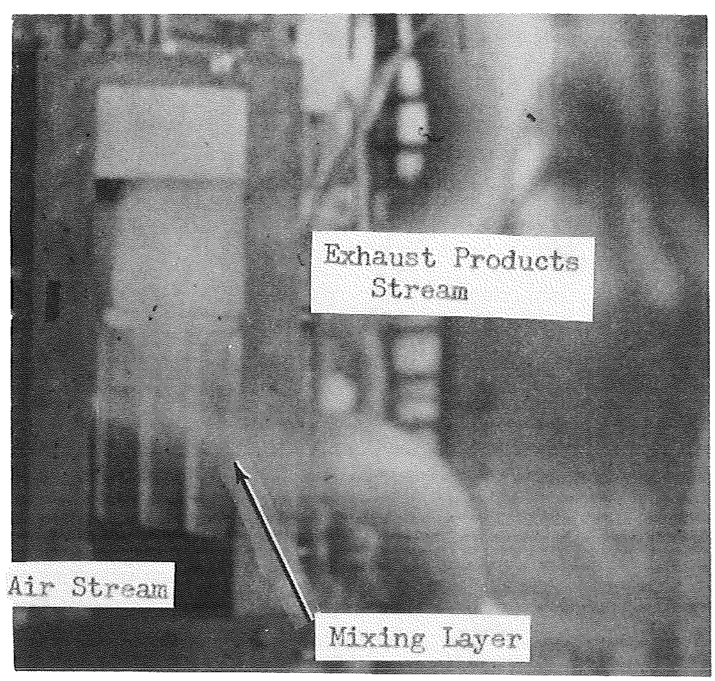

Figure 42. Aft End View of Test Section

Schlieren photographs are shown in Figs. 4-1 and 4-2. Figure 4-2 was taken in the middle of the stream and indicates a uniformly mixed highly turbulent flow field. Figure 4-2 is a similar view; however, the Schlieren apparatus was relocated to have the mixing between the ambient environment and the exhaust stream in its field of view. Again, a uniformly mixed highly turbulent flow field was evident; however, it is of particular interest to note that a distinct boundary between the film coolant stream and the exhaust products stream is not evident. This indicates that the film coolant stream has mixed into the supersonic stream. Therefore, zone radiometry measurements should indicate a reduction in temperature at the boundaries of the flow. This prediction was confirmed in Fig. 3-7. This figure shows a plot of the flame radiance as a function of position. If the emissivity was constant, this plot would be directly related to temperature*; however, the figures does indicate that nitrogen dilution takes place along a given horizontal line of sight. In summary, experimental evidence indicates that the flow is two-dimensional with some nitrogen dilution near the vertical walls. A calculation was made to determine the maximum temperature drop in the combustion products and air stream at the exit of the mixing chamber assuming that all of the film coolant was completely mixed with the streams of interest. It was determined that a maximum of a 400 F drop could occur in the combustion products stream and approximately a 200 F drop in the hot air stream. It should be noted that these calculated temperature drops are a maximum value.

*Due to the great difficulty and cost of locating the greybody for the data taken from the top, only emission measurements were made and, therefore, actual temperatures cannot be calculated.

No other deleterious effects were noted that could be attributable to the film coolants. During two experiments the film coolants were turned off for approximately 2 seconds. Visual observation confirmed by the photographic coverage indicated that the plume adjusted its position to fill the voids in the mixing chamber caused by the lack of film coolants; however, no change in the location of the mixing line was apparent.

Temperature Effects

The effect of air temperature on the mixing is indicated in Figs. 36 to 39 and Fig. 43. Figure 43 is a representation of the diagnostic (screening) experiments taken at position number 8. Only the air temperature data (Run 34) from that figure are utilized in this discussion. Data comparisons for identical run conditions except for a variable air temperature indicated that thermal penetration increases and concentration (H_2O partial pressure) penetration decreases with decreasing air temperature. The behavior observed for the indicated trend of the thermal penetration or mixing is contrary to theory.

It has been established by Ferri, et al, Ref. 13, that mixing is proportional to $\Delta \rho u$. The values of ρu for the air stream were 16.5, 17.0, and 19.0 for the respective air temperatures of 829, 612, and 278 F. The ρu of the combustion products stream was constant at a value of approximately 55.6. Therefore, on this basis, the charge in mixing should be small (about 10%), but, a slight trend of decreased thermal mixing with decreasing air temperature should have been evident.

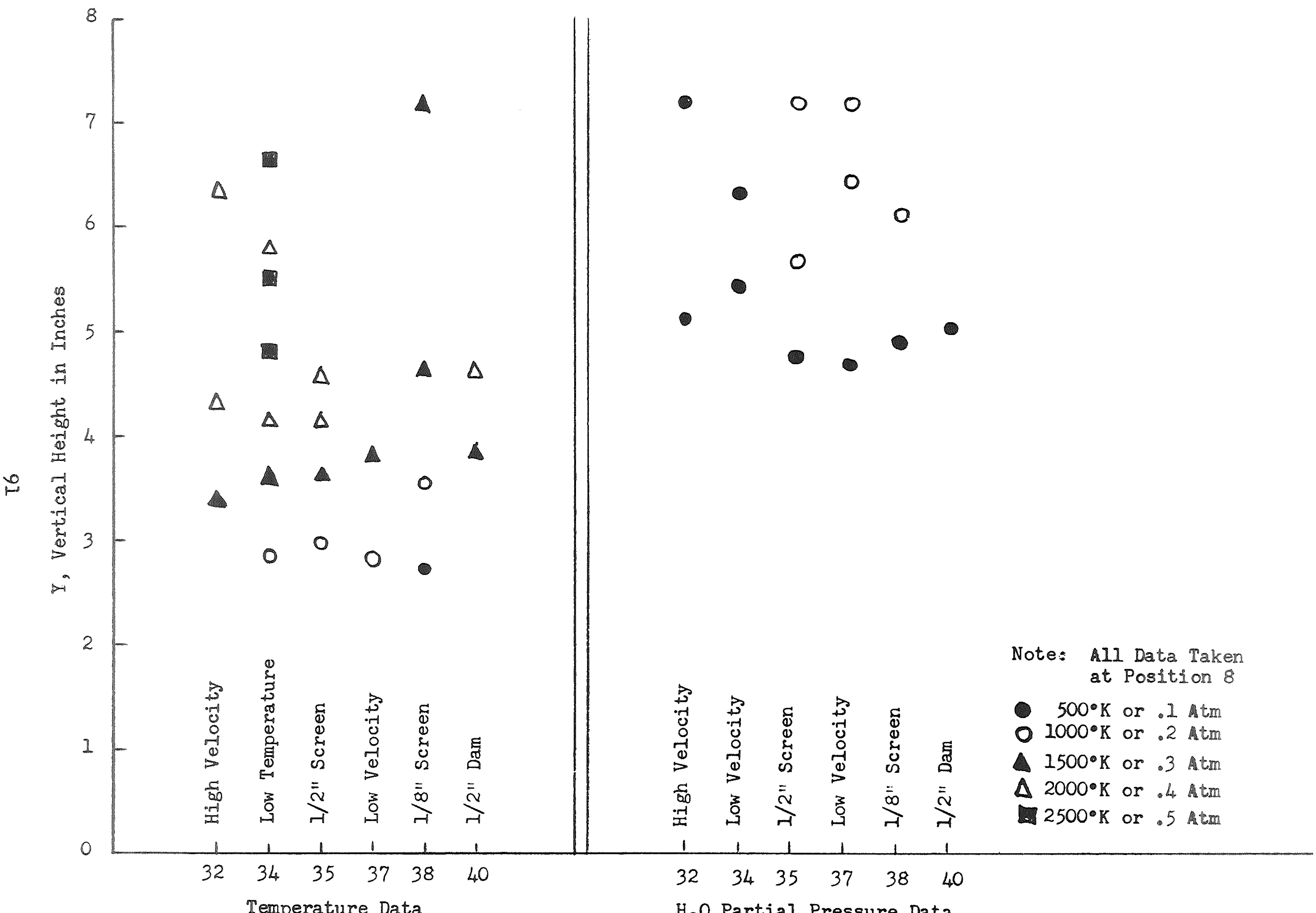

Figure 43. Temperature and H_2O Partial Pressure Data for Diagnostic Experiments

The contrary trend indicated by the temperature data possibly suggests that thermal mixing is controlled by a different mechanism than momentum exchange, i.e., Ferri's correlation. It should be noted that it is not being suggested that momentum exchange has no effect upon thermal mixing, but rather, momentum exchange and an additional mechanisms influence thermal mixing. If one postulates correlation of the basis of $\rho C_p T$, the enthalpy of the flows, it follows that the greater the difference in enthalpy between the two flows, the greater the mixing. This correlates, both quantitatively and qualitatively, the thermal mixing described above.

Another possible reason for this behavior may be a result of the apparent vortex observed near the onset of mixing. This vortex was described as relatively weak and not interfering with the visible mixing line; however, according to Ref. 12, it does have sufficient strength to alter the stream lines. Therefore, the low pressure region caused by the vortex causes the flow to expand ever increasingly as the temperature is lowered, thereby indicating an increase in thermal mixing as temperature is lowered. Additionally, this effect does not significantly affect the concentration profiles because the vortex recirculates air which is at too low a temperature to induce significant chemical reaction.

Velocity Effects

The diagnostic data discussed in the following two sections were all taken at one line of sight and consisted of one test only. These tests were only screening in nature. The effect of velocity is represented in Fig. 43. The velocity for the high velocity case was not appreciably greater than that for the characterization experiments for 829 F air; therefore, comparison will only be made between the two tests indicated on the figure. The trends indicated show thermal mixing decreases slightly as the air velocity decreases and the concentration profiles make a greater penetration into the air stream as the velocity decreases. This latter result is consistent with the arguments presented above; however, the thermal mixing again is contrary to anticipated behavior. Rationalization of this apparent inconsistency would require additional experimentation.

Turbulence Effects

Alteration of the turbulence level of the air stream was accomplished by the insertion of screens (1/2-inch and 1/8-inch mesh) and a 1/2-inch dam. With reference to Fig. 43, the thermal mixing decreased as the screen mesh size decreased and approached the thermal mixing characterized in Fig. 36. The decrease in mixing as one goes to a finer mesh size indicates that gross increases in turbulence scale will increase mixing while decreasing the scale tends to laminarize the flow and create a situation identical to that which existed without the presence of induced turbulence. Thermal data gathered for the 1/2-inch dam were practically coincident with the 1/2-inch mesh screen. All of these devices indicated that thermal mixing was enhanced if the physical character of the flow was significantly altered; however, this was not the case for the concentration profiles. All of them were similar and portrayed a decrease in mixing (when compared to Fig. 37) with augmentation of the inlet characteristics. It is well known from the literature, Ref. 14, that alterations of the inlet conditions delay the intimate contact of the streams to be mixed and cause a displacement of mixing by the length of the potential core of any deadwater region that retards stream contact, i.e., retards mixing. However, this deadwater region is in itself a vortex and may give rise to additional vortices in the stream of insufficient thermal content to cause additional chemical reaction, but having sufficient heat to warm the flow. This supposition permits explanation of the contrary trends observed.

CONCLUSIONS AND RECOMMENDATIONS

The mixing flow field of a supersonic fuel-rich hydrogen/oxygen two-dimensional jet and a subsonic heated air stream was mapped in temperature and H_2O concentration. Two reference cases of 829 and 612 degree F air streams in addition to several single runs at varying conditions of temperature, velocity, and temperature level were evaluated. In the following paragraphs a number of conclusions and recommendations are given.

1. The concentration measurements and trends in this data are consistent with existing mixing theories. Mixing increases as air temperature is increased, air velocity is decreased, and inlet conditions are streamlined.

2. Correlation of the temperature measurements could not be made within the confines of available theories.

3. The experiments were indeed two-dimensional and the use of film coolants did not alter the mixing process; however, the film coolants did slightly reduce the temperature of the streams of interest.

4. Zone radiometry is a useful tool for the measurement of flow properties, however, to establish a valid confidence level for zone radiometric measurements a statistical data sample (approximately 3 to 4 measurements) at each data location should be gathered.

5. The flow facility performed excellently and appears capable of performing a large number of additional tests.

6. The vortex that possibly appeared in the flow was relatively weak and did not appear to affect the concentration measurements.

It is recommended that the apparatus be utilized for a more comprehensive experimental program. This program would provide well controlled precise experimental data for the determination of the effects of temperature ratio, turbulence level, velocity ratio, and changes in ambient conditions upon the mixing. The characterization of the mixing region should include a mapping of temperature, velocity, pressure, concentration, enthalpy, and turbulence intensity. Recommended experiments that will help to gather the required data are as follows:

1. A complete set of diagnostic experiments to accurately determine the two dimensionality of the flow field and the effect of film cooling on the mixing region (approximately 20 tests).

2. A mixing study that includes a more precise mapping of the mixing region for the basic case, then a determination of the effects upon the mixing layer produced by changes in the air turbulence level, air temperature, inlet geometry, and velocity ratio (approximately 120 tests).

3. Tests with a CO_2 seeded air stream. The use of this tracer enables further elucidation of the penetration of the air stream into the combustion products stream (approximately 10 tests).

4. Testing, which would require additional hardware, over a more complete range of experimental variables. These would include different mixture ratios, a wide range of combustion product-air stream velocity ratios, and elevated test section pressures (approximately 150 tests).

REFERENCES

1. Wrubel, J. A.: Performance Analysis of Composite Propulsion Systems, Phase I Final Report, Contract NAS7-521, Rocketdyne, a Division of North American Rockwell Corporation, Canoga Park, California, January 1968.

2. Wrubel, J. A.: Performance Analysis of Composite Propulsion Systems, Phase II Final Report, Contract NAS7-521, Rocketdyne, a Division of North American Rockwell Corporation, Canoga Park, California, April 1969.

3. Goldstein, R. J., E. R. G. Eckert, F. K. Tsou, and A. Haji-Sheikh, "Film Cooling with Air and Helium Injection Through a Rearword-Facing Slot into a Supersonic Air Flow," AIAA Journal Vol. 4, No. 6, pp 981-985, June 1966.

4. McGimsey, L. R., "Mixing Analysis for Rocketdyne Two-Dimensional Hydrogen/Oxygen Combustion Experiments," Huntsville Research and Engineering Center, Lockheed Missiles and Space Company, TDR 54/20-78, 5 August 1967.

5. Rocketdyne, An Instrumentation System to Study Plume Radiative Processes, Final Report, NAS8-11261, August 1965.

6. Shapiro, A. H.: The Dynamics and Thermodynamics of Compressible Fluid Flow, The Ronald Press Company, New York, 65-67, 1963.

7. Keagy, W. R., Jr., and H. H. Ellis: "The Application of the Schlieren Method to the Quantitative Measurement of Mixing Gases and Jets," Third Symposium on Combustion, Flame, and Explosion Phenomena, Williams & Wilkins Co., Baltimore, Md., 1959.

8. Shapiro, A. H., The Dynamics and Thermodynamics of Compressible Fluid Flow, Vol. I, Ronald Press Co., New York, 1953.

9. Penzias, G. S., et al, Infrared Analysis of High Temperature Gases in Situ, Final Report, NASA-CRL, October 1962.

10. Penzias, G. S., and J. Maclay, Analysis of High Temperature Gases in Situ by Means of Infrared Band Models, NASA CR-34002, December 1963.

11. Ferriso, C., Ludwig, C., and A. Thorson, Empirically Determined Absorption Coefficients, Journal of Quantitative Spectroscopy and Radiative Transfer, Vol. 6, 1966, pp. 241-275.

12. Abramovich, G. N., "The Theory of Turbulent Jets," MIT Press, Cambridge, Massachussetts, 1963, p. 173.

13. Ferri, R., Libby, P. A. and V. Zakkay, "Theoretical and Experimental Investigation of Supersonic Combustion," Polytechnic Institute of Brooklyn, ARL-62-467, September 1962.

14. Korst, H. H. and W. L. Chow, "Non-Isoenergetic Turbulent (Pr = 1) Jet Mixing Between Two Compressible Streams at Constant Pressure," University of Illinois, Urbana, Ill., Grant No. NsG-13-59, NASA CR-419, April 1966.

NOMENCLATURE

B - 1 Inch Above Base

E - Emission

EA - Emission and Absorption Measurement

H - Horizontal

HW - Hot Wire Aneometer

LASS - Large Aperture Spectrometer/Spectrograph

M - Vertical Flow Axis

PYRO - Optical Pyrometer

SCH - Schlieren System

SPAT - Spatial Scan

SPECT - Spectral Scan

V - Vertical

VS - Vertical Scan

ZR - Zone Radiometer

APPENDIX 1

MANOMETER BANK DATA

A summary of manometer bank data is presented in Table 1-1. The location of the static pressure ports is given in Fig. 1-1 (Ref. Fig. 3-57 for orientation to the test apparatus). The display of static pressure data for the individual runs is given in Figs. 1-2 to 1-36.

For comparison purposes the data were grouped according to the following:

High Temperature Air	Runs 10*, 11, 12, 13, 14, 16*, 17, 18, 30, 31, 39
Medium Temperature Air	Runs 19, 20, 21, 22, 23, 24, 25, 26, 27, 28, 29
Low Temperature Air	Run 34
High Velocity Air	Run 32
Low Velocity Air	Runs 33, 36, 37
1/2" Screen	Run 35
1/8" Screen	Run 38
1/2" Dam	Run 40
Checkout Runs**	Runs 1, 2, 4, 021, 041, 5

*These tests also included film coolant and 2-D studies.

**These data were run at conditions similar to high temperature air tests.

TABLE 1-1

MANOMETER BANK DATA*

Tube No.	Run Number 1	2	4	021	041	5	10	11	12	13
1	1.36	1.36	1.36	1.36	1.36	1.36	.15	3.4	ND	.16
2	1.36						.38	4.92		.29
3	1.36						.45	4.52		.44
4	1.21						.01	2.42		.17
5	.29		1.2	1.28	1.28	1.28	.01	.01		.01
6	1.36		1.36	1.36	1.36	1.36	.47	4.67		.44
7	1.36			1.36		1.36	.35	4.92		.34
8	1.12			1.32		1.32	-	.03		-
9	1.36			1.36		1.36	-.36	3.32		-.27
10	-.01	.00	-.01	.02	.02	.02	-	-		-
11	.05	.11	.09	.03	.02	.03	-.01	-.18		-.01
12	.03	.08	.06	.09	.08	.76	-.01	-.09		-.01
13	1.36	1.36	1.36	1.36	1.36	1.36	.26	4.92		.26
14	1.11	1.36	1.36	1.36	1.34	1.36	.06	.06		.06
15	1.09	.09	.10	.07	.07	.07	-	3.6		-
16	.04	.10	.07	.13	.10	.11	.01	.12		.01
17	1.20	1.36	1.36	1.36	1.34	1.36	.05	.05		.05
18	1.28	1.36	1.36	1.36	1.34	1.34	0	0		0
19	.06	-.06	-.13	.14	.10	.10	-	-		-
20	1.36	1.36	1.36	1.36	1.36	1.36	.15	4.92		.16
21	.11	.23	.18	.33	.27	.27	-.03	.33		-.04
22	.15	.33	.25	.40	.38	.38	-	.415		-
23	.10	.23	.18	.35	.30	.30	-.05	.34		-.09
24	-.11	.20	.13	.28	.24	.24	-	.33		-
25	-.24	-.187	.24	.09	.10	.10	-	-.07		-
26	-.14	.01	.24	.10	.15	.13	0	0		0
27	.04	.10	.09	.14	.14	.12	-.01	.15		-.01
28	.17	.35	.28	.43	.40	.39	-	.44		-
29	-.05	.08	.02	.16	.14	.10	-	.16		-
30	-.14	-.14	.01	.06	.01	.06	-	-.02		-
31	.433	.668	.563	.758	.758	.679	.750	.762	.750	.750

*All pressures are in psig

TABLE 1-1 (CONT'D)

Tube No.	Run Number									
	14	16	17	18	19	20	21	22	23	24
1	.42	3.15	4.06	3.66	3.98	3.79	3.5	3.64	3.63	3.76
2	.70	4.58	4.92	4.56	4.92	4.92	4.57	4.39	4.68	4.62
3	.87	4.07	4.92	4.12	4.92	4.46	4.92	3.92	4.45	4.48
4	.27	.76	.76	.76	.78	.77	.82	.71	.73	.71
5	.01	.01	.01	.01	.07	.07	.08	-.00	-.01	-.00
6	.72	4.36	4.92	4.45	4.92	4.92	4.69	4.22	4.63	4.63
7	.76	4.54	4.92	4.92	4.92	4.92	4.92	4.44	4.48	4.48
8	.49	.40	.44	.40	.48	.52	.52	.39	.42	.39
9	.13	3.19	4.47	2.86	4.13	3.39	3.24	2.75	3.33	3.39
10	-	-	-	-	-	-	-	.16	.16	.10
11	.01	.34	.43	.18	.23	.18	.19	.12	.18	.19
12	-.01	.50	.60	.11	.14	.11	.13	.09	.10	.12
13	.80	4.92	4.92	4.92	4.92	4.92	4.92	4.40	4.40	4.40
14	.06	.05	.09	.05	.07	.07	.07	.05	.06	.07
15	-	.25	1.38	0	.72	.39	.36	.06	.06	.06
16	-.01	.55	.66	.13	.18	.14	.14	.12	.13	.14
17	.05	.05	0	0	0	0	.05	.04	.03	.04
18	0	.01	0	0	0	0	0	-.01	.01	-.00
19	-	.17	.29	.17	.19	.18	.18	.18	.05	.20
20	.44	4.92	4.92	4.23	4.92	4.92	4.92	4.08	4.48	4.48
21	-.03	.55	.66	.31	.39	.32	.32	.28	.31	.32
22	.08	.57	.70	.33	.45	.37	.38	.32	.36	.37
23	-.05	.54	.68	.33	.41	.32	.35	.31	.34	.35
24	-	.49	.65	.26	.36	.36	.27	.22	.26	.28
25	-	.17	.42	-.02	-.02	0	-.05	.02	.02	.03
26	0	-.01	0	-.01	0	0	0	-.01	-.01	-.00
27	-.01	.30	.39	.16	.21	.16	.17	.14	.16	.17
28	.11	.62	.75	.41	.52	.41	.44	.39	.42	.44
29	-	.39	.55	.10	.22	.15	.14	.06	.12	.13
30	-	.26	.46	-.01	.10	.05	0	-.01	-.01	.00
31	.755	.814	.885	.702	.737	.706	.698	.640	.666	.674

TABLE 1-1 (CONT'D)

Tube No.	Run Number									
	25	26	27	28	29	30	31	32	33	34
1	3.64	3.63	3.62	3.64	3.83	3.74	3.71	3.81	3.49	3.81
2	4.62	4.62	4.69	4.62	4.62	4.62	4.62	4.62	4.66	4.62
3	4.39	4.16	4.18	4.31	4.48	4.42	4.40	4.41	4.06	4.35
4	.72	.62	.63	.70	.70	.72	.70	.74	.72	.70
5	-.01	-.00	-.00	-.01	-.00	-.00	-.01	-.02	-.01	-.02
6	4.63	4.56	4.55	4.64	4.64	4.64	4.64	4.65	4.53	4.65
7	4.48	4.79	4.48	4.48	4.48	4.48	4.78	4.48	4.48	4.48
8	.42	.36	.38	.39	.38	.42	.37	.51	.50	.49
9	3.23	3.13	3.02	3.24	3.46	3.33	3.39	3.38	2.92	3.16
10	.07	.14	.28	.24	.16	.13	.09	.13	.11	.08
11	.17	.17	.17	.14	.17	.16	.17	.17	.04	.17
12	.10	.10	.11	.08	.09	.09	.09	.09	.01	.10
13	4.40	4.67	4.67	4.67	4.67	4.67	4.67	4.62	4.62	4.62
14	.05	.08	.05	.04	.05	.06	.05	.06	.06	.05
15	.06	.06	.06	.06	.05	.06	.05	.05	.06	.05
16	.12	.13	.13	.11	.12	.12	.12	.11	.01	.13
17	.04	.04	.04	.04	.03	.04	.03	.03	.04	.03
18	-.00	.00	.00	.00	-.00	.00	-.00	-.01	-.00	-.01
19	.08	.11	.20	.10	.09	.21	.22	.06	.05	.11
20	4.48	4.47	4.52	4.47	4.47	4.47	4.47	4.48	4.51	4.48
21	.31	.31	.30	.77	.30	.29	.30	.30	.08	.31
22	.36	.36	.34	.32	.34	.34	.36	.36	.09	.34
23	.33	.34	.34	.27	.32	.30	.33	.32	.10	.33
24	.25	.26	.24	.19	.23	.22	.23	.23	.02	.24
25	-.02	.02	.03	.02	.02	.02	.02	.02	.03	.03
26	-.00	-.00	.00	-.00	-.00	-.00	.00	-.00	-.00	-.01
27	.16	.17	.17	.12	.15	.13	.15	.14	.03	.17
28	.41	.42	.42	.34	.40	.39	.41	.40	.13	.38
29	.12	.12	.10	.10	.12	.11	.12	.11	-.00	.50
30	-.00	-.00	-.00	-.00	-.00	-.00	-.00	-.01	-.00	.03
31	.670	.660	.640	.631	.630	.666	.667	.694	.208	.571

TABLE 1-1 (CONT'D)

Tube No.	Run Number					
	35	36	37	38	39	40
1	3.76	3.68	3.65	3.66	3.90	3.86
2	4.62	4.62	4.62	4.62	4.62	4.62
3	4.31	4.40	4.29	4.43	4.46	4.16
4	.83	.83	.86	.87	.85	.19
5	-.11	-.11	-.10	-.11	-.11	-.11
6	4.65	4.65	4.65	4.65	4.65	4.65
7	4.48	4.48	4.48	4.48	4.48	4.48
8	.49	.51	.48	.49	.52	.51
9	3.14	3.48	3.25	3.53	3.48	3.15
10	-.01	-.00	.00	-.02	.00	-.03
11	.11	.05	.04	.05	.17	.17
12	.06	.02	.01	.02	.10	.11
13	4.19	4.19	4.19	4.19	4.19	4.19
14	.06	.06	.05	.04	.06	.05
15	.06	.06	.06	.06	.06	.06
16	.05	.01	.00	.00	.11	.12
17	-.12	-.11	-.11	-.11	-.11	-.11
18	-.12	-.11	-.11	-.11	-.11	-.11
19	.07	.16	.08	.10	.20	.08
20	4.47	4.47	4.47	4.47	4.47	4.47
21	.15	.09	.08	.11	.29	.30
22	.17	.10	.09	.14	.35	.34
23	.18	.12	.11	.12	.31	.32
24	.06	.05	.04	.44	.22	.20
25	-.02	-.02	-.03	-.02	-.02	-.02
26	-.00	-.00	-.00	-.00	-.00	-.00
27	.10	.05	.04	.04	.14	.16
28	.12	.16	.15	.14	.40	.40
29	.00	-.00	-.00	-.00	.11	.05
30	.00	-.00	-.00	-.00	-.00	-.00
31	.813	.216	.206	.828	.677	.705

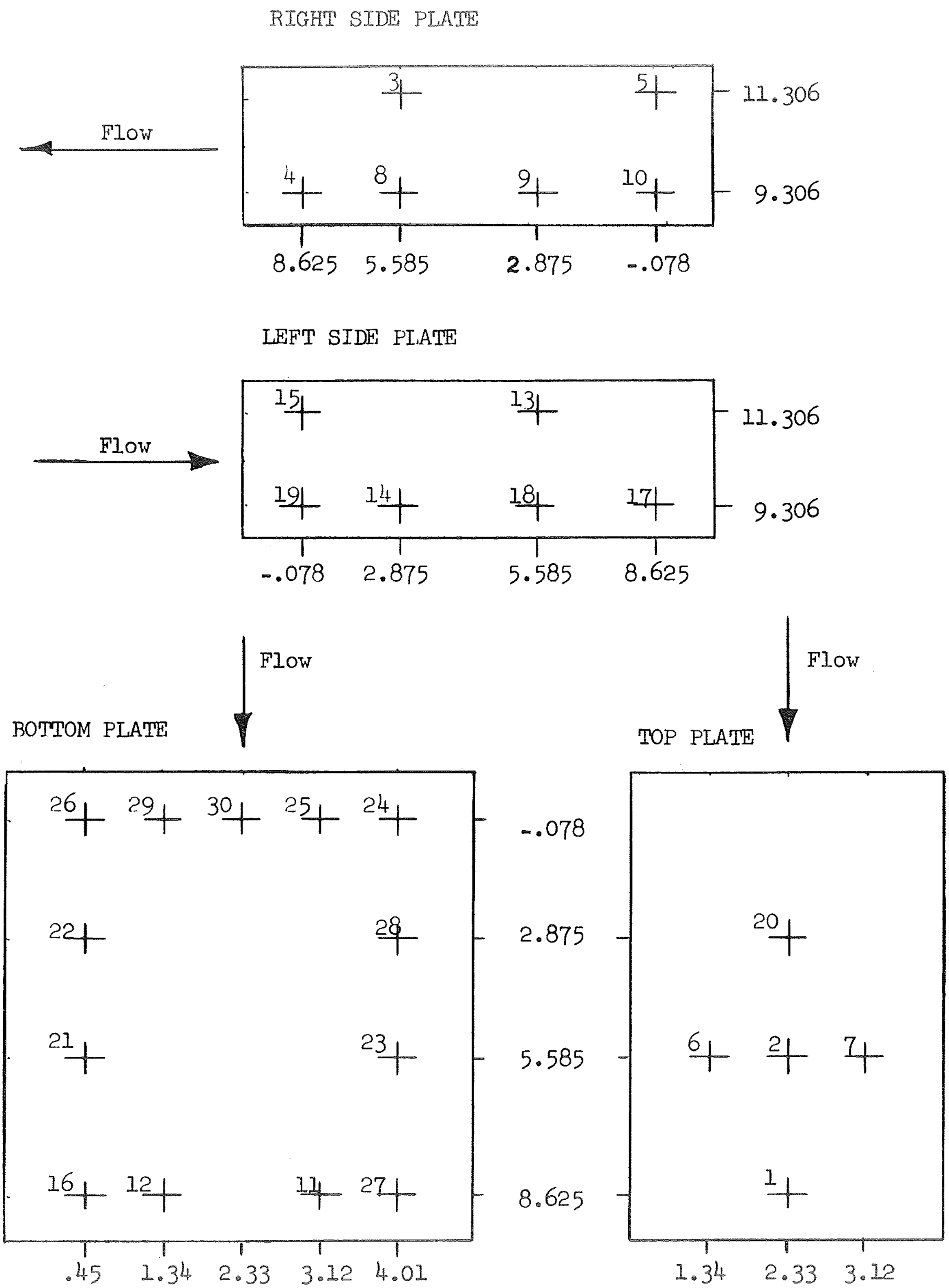

Figure 1-1. Static Pressure Tap Location

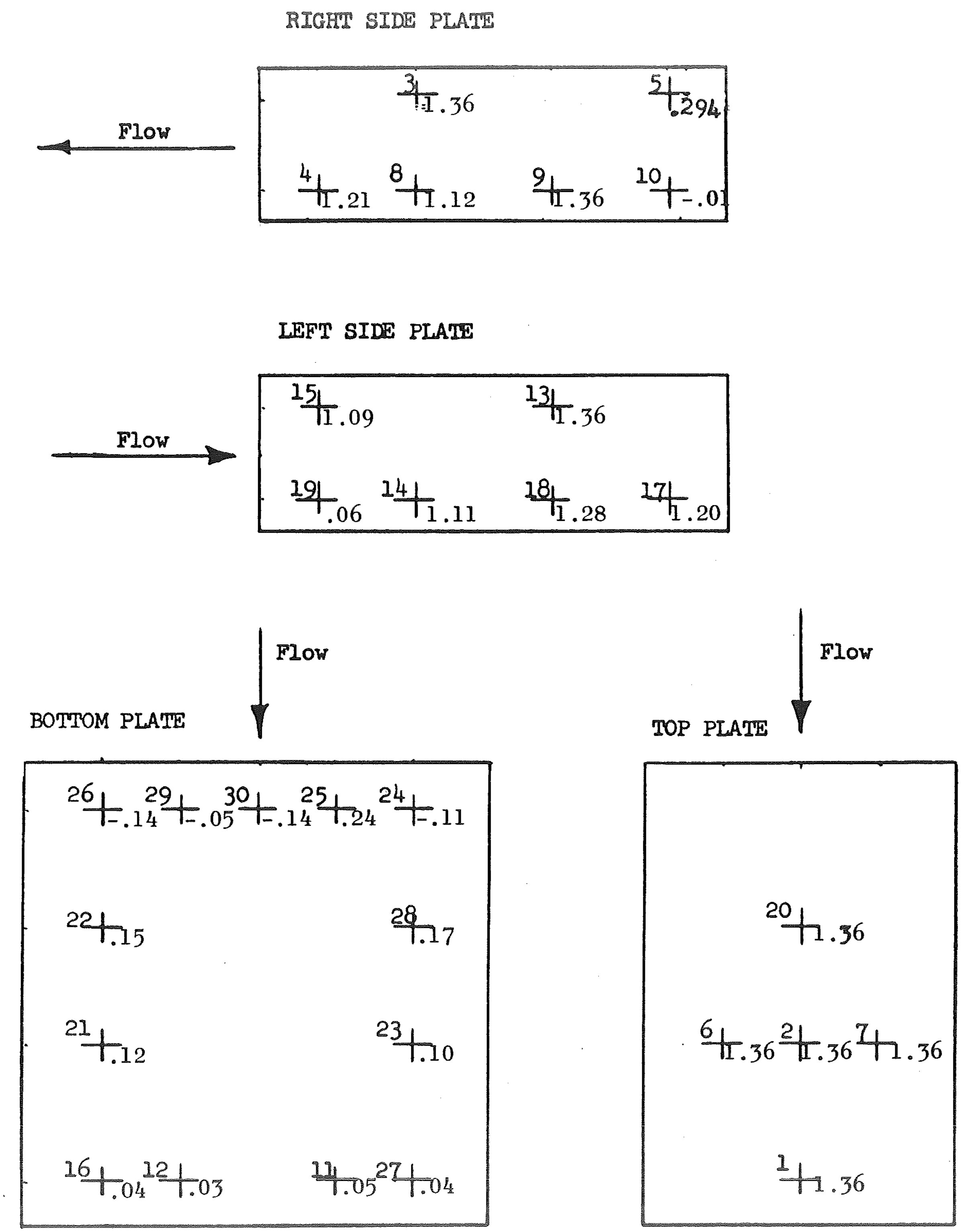

Figure 1-2 Static Pressure Data - Run 1

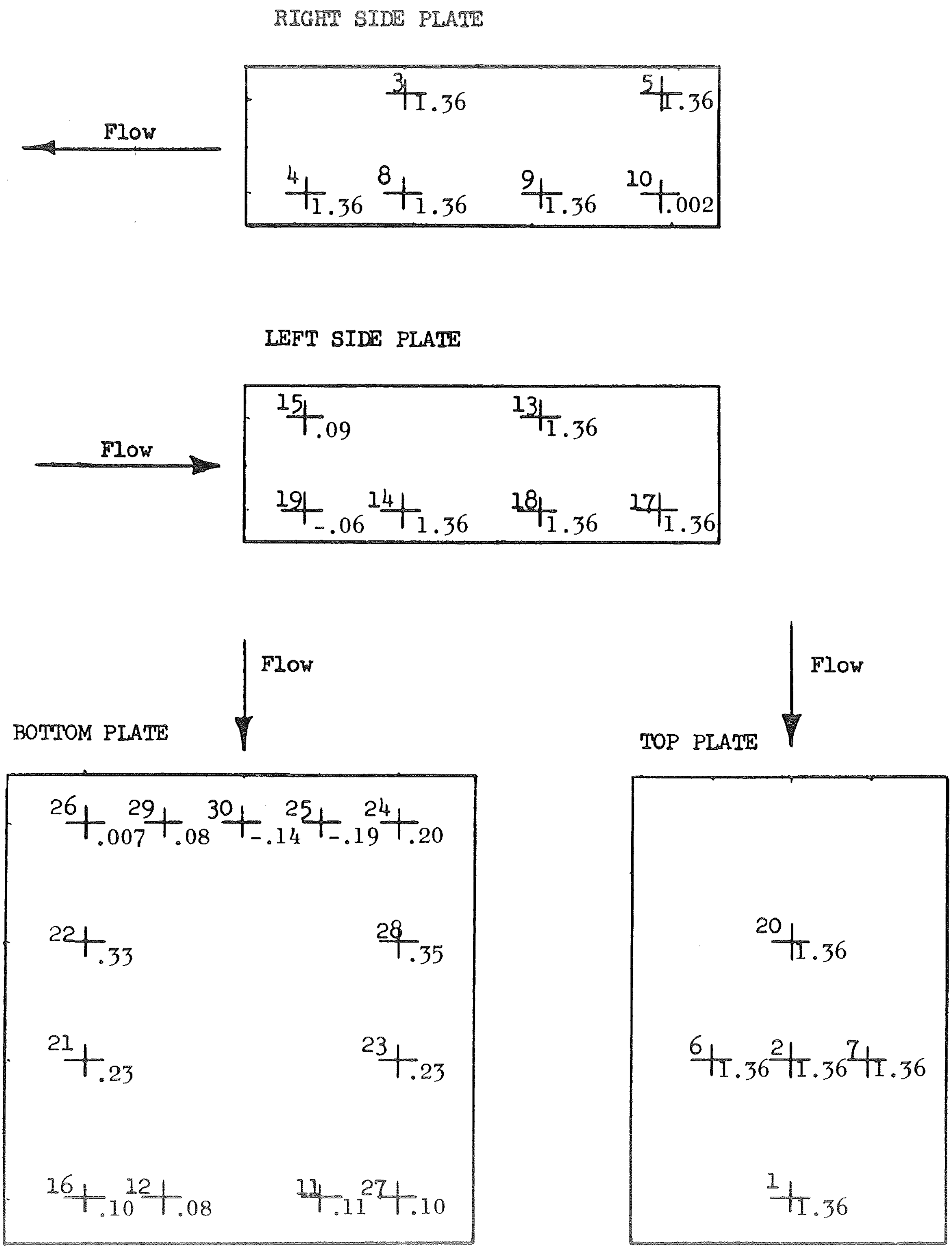

Figure 1-3 Static Pressure Data - Run 2

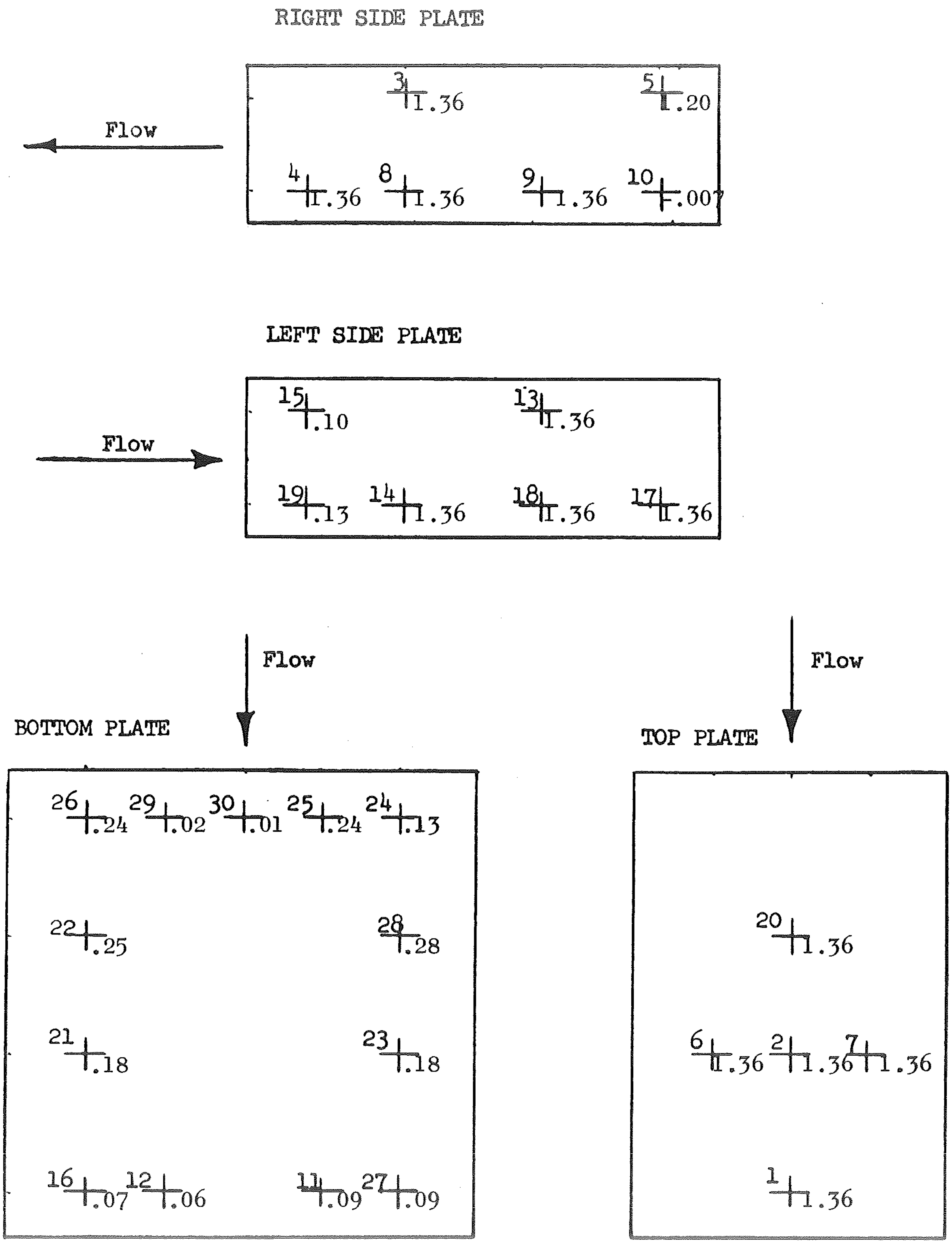

Figure 1-4 Static Pressure Data - Run 4

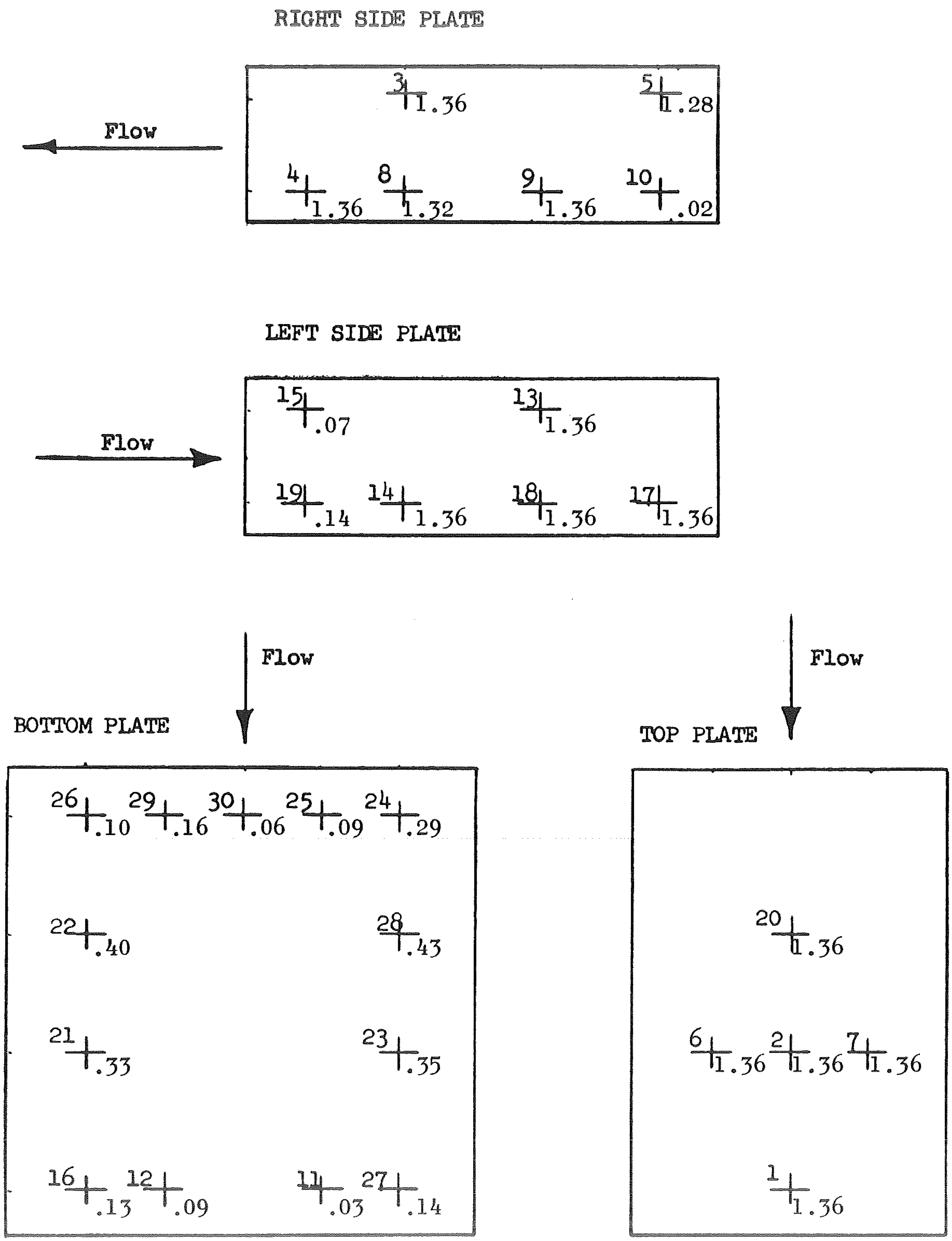

Figure 1-5 Static Pressure Data - Run 021

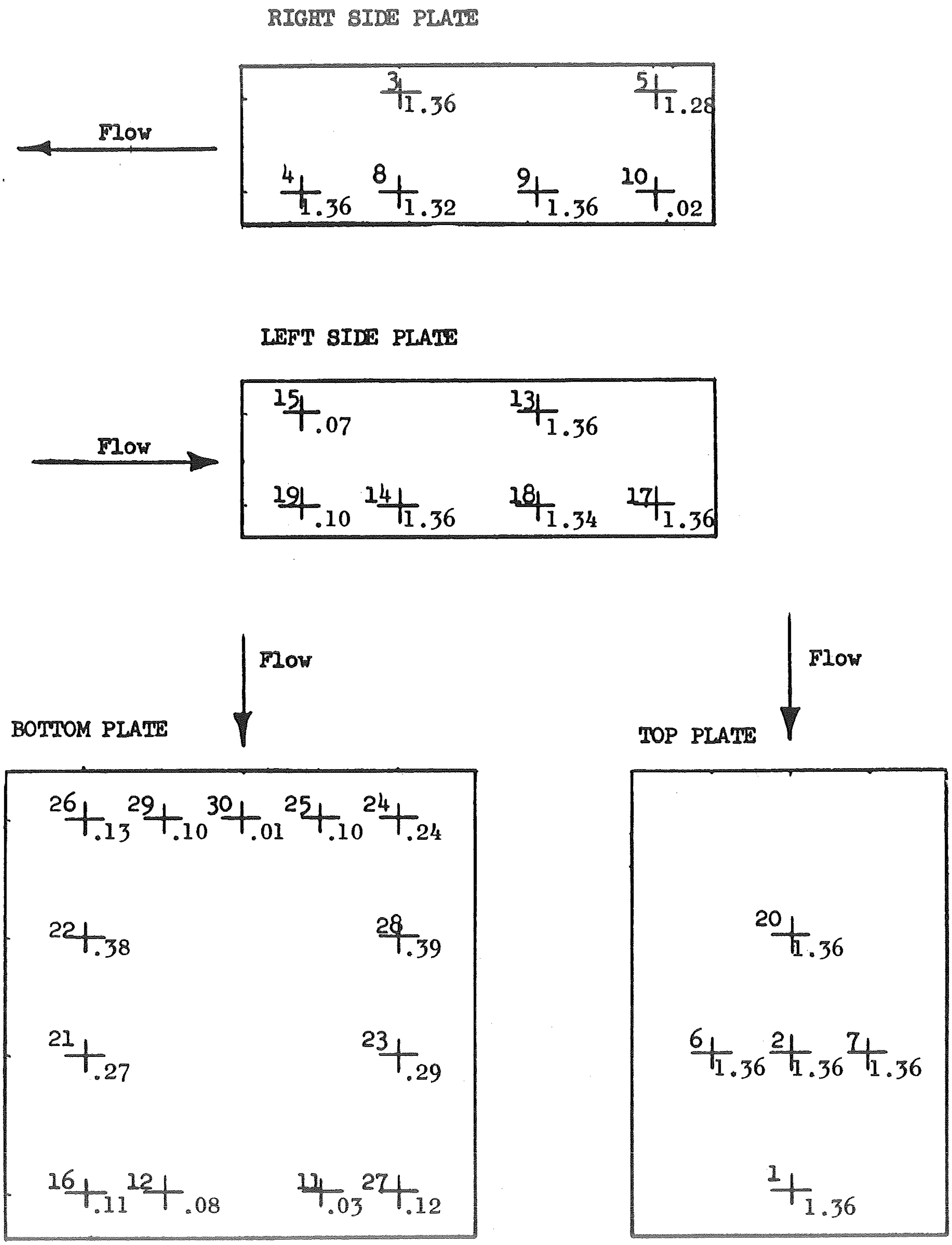

Figure 1-6 Static Pressure Data - Run 041

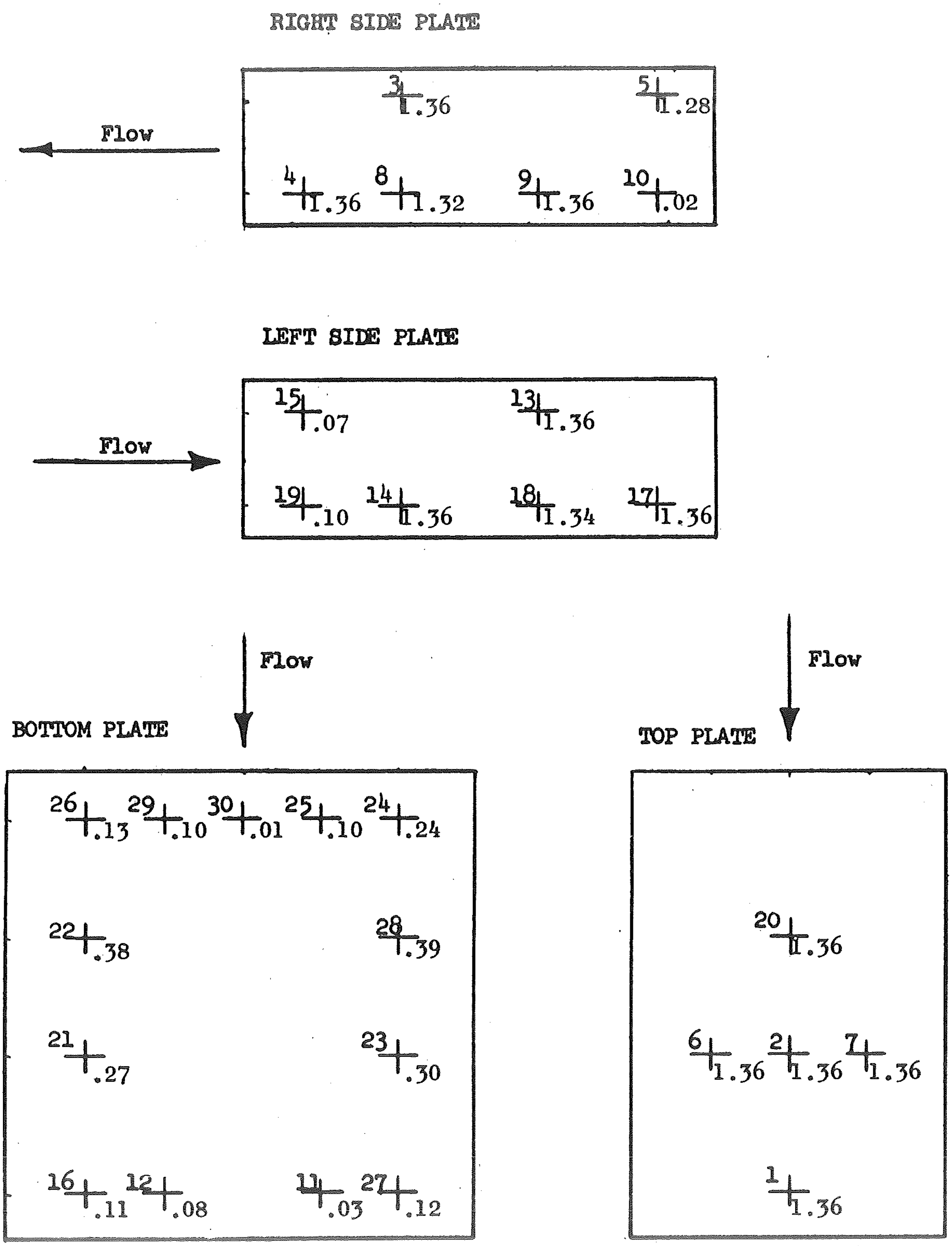

Figure 1-7 Static Pressure Data - Run 5

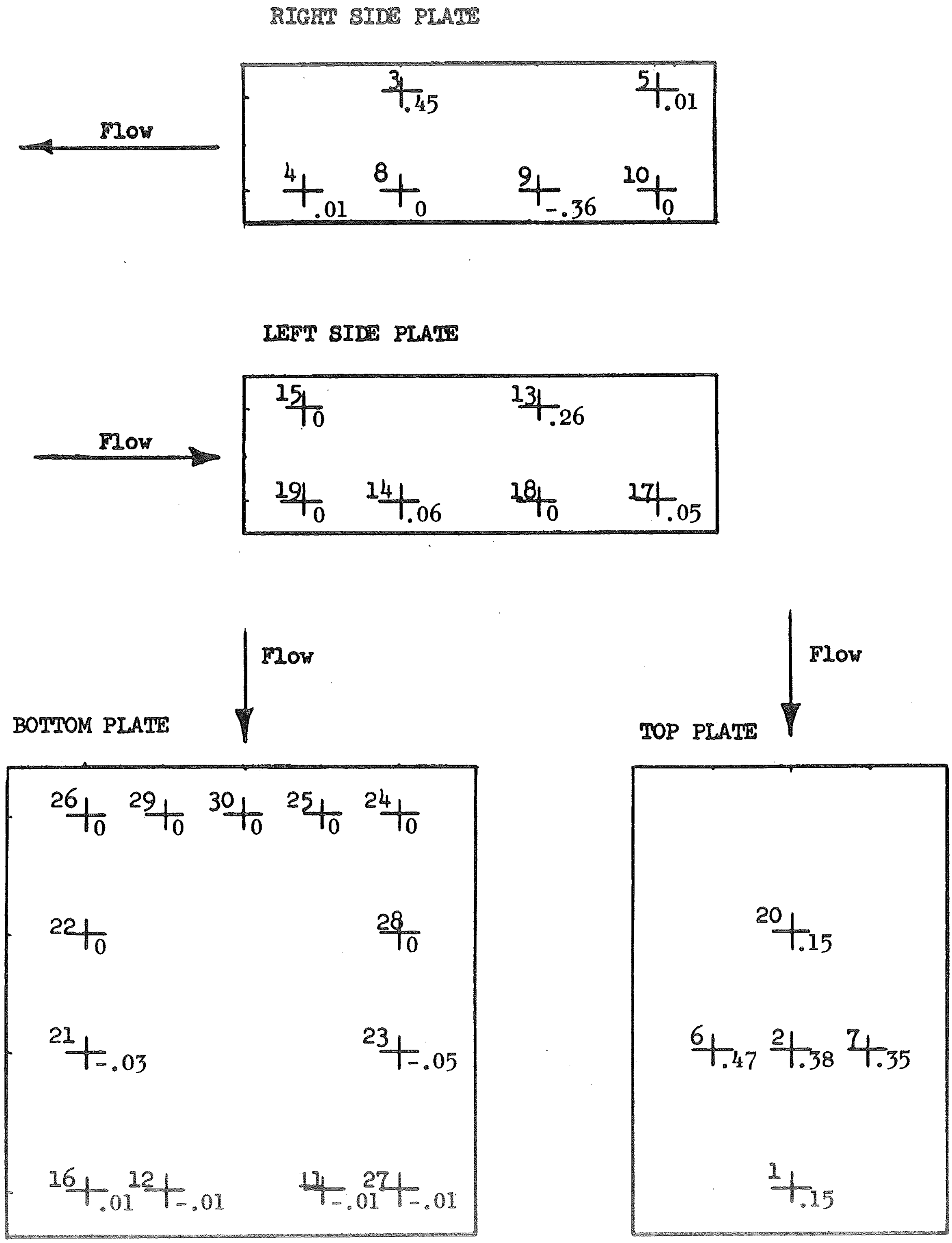

Figure 1-8 Static Pressure Data - Run 10

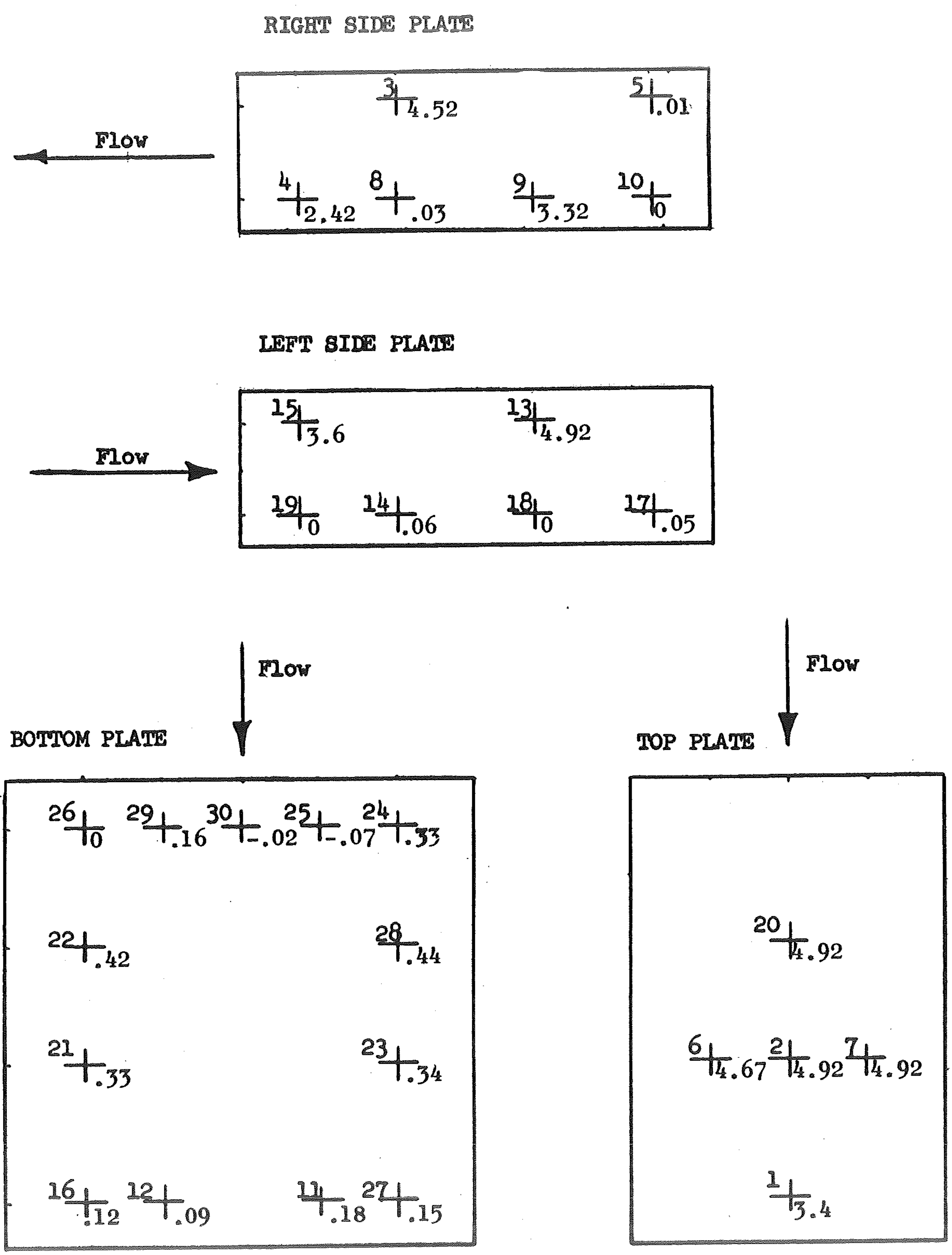

Figure 1-9 Static Pressure Data - Run 11

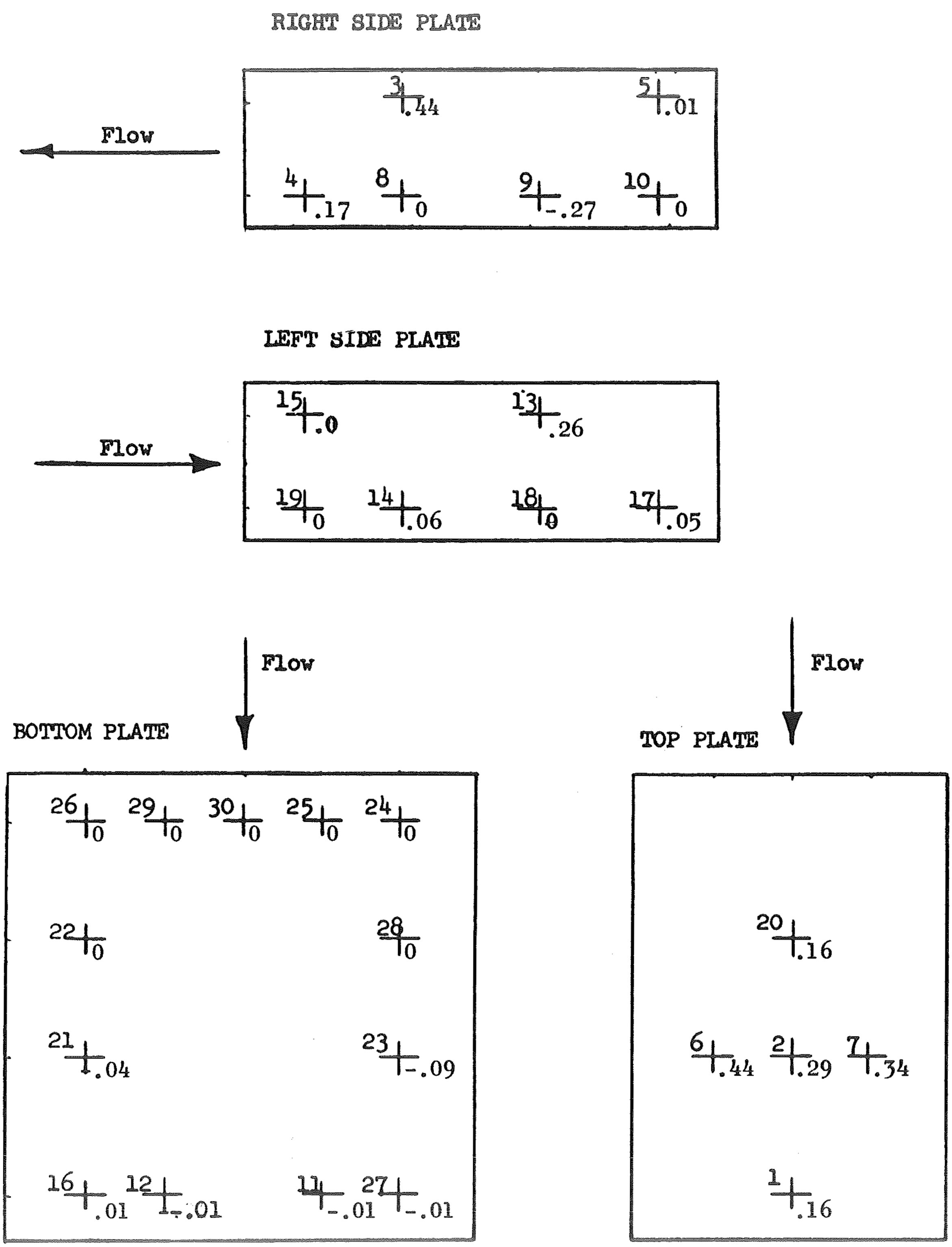

Figure 1-10 Static Pressure Data - Run 13

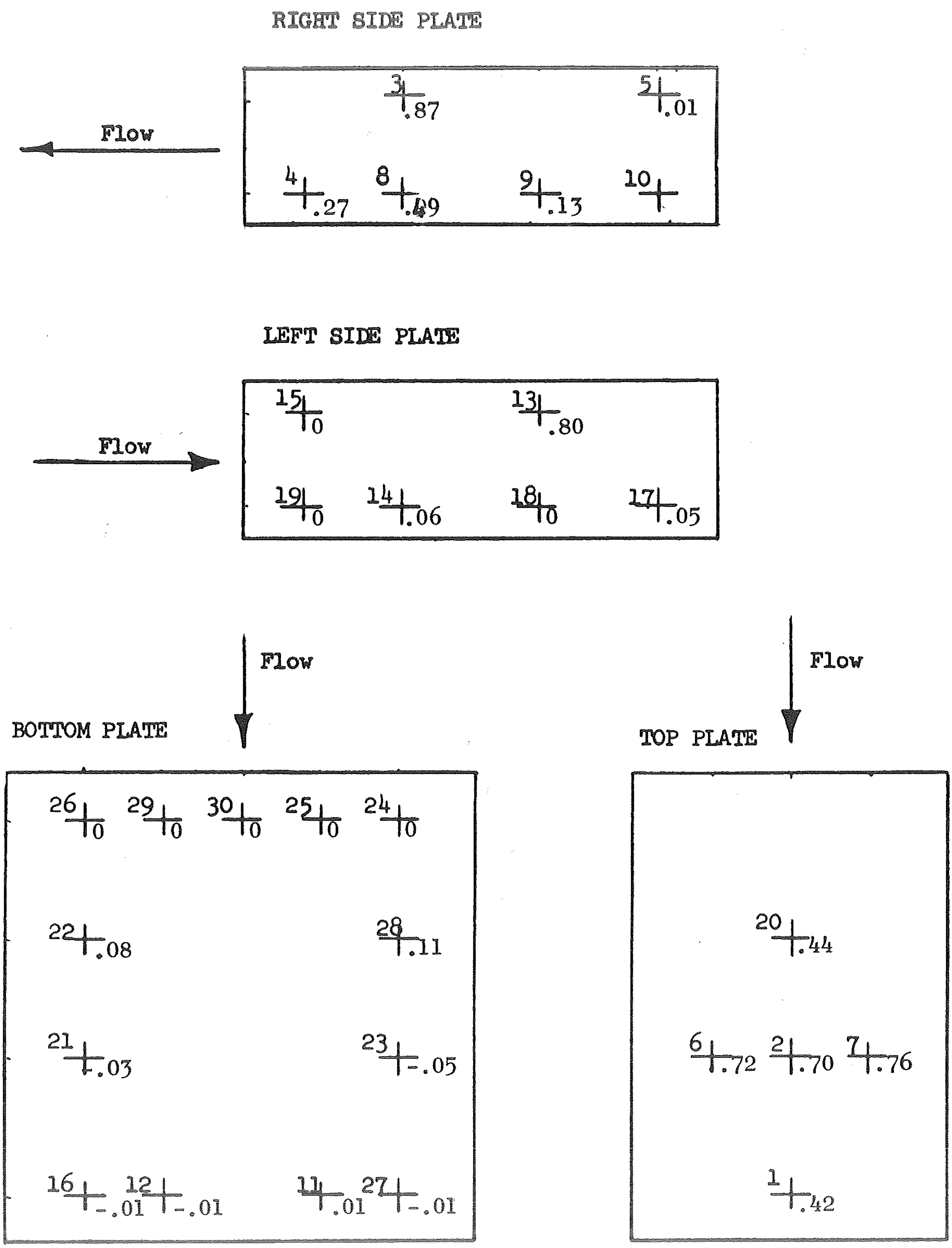

Figure 1-11 Static Pressure Data - Run 14

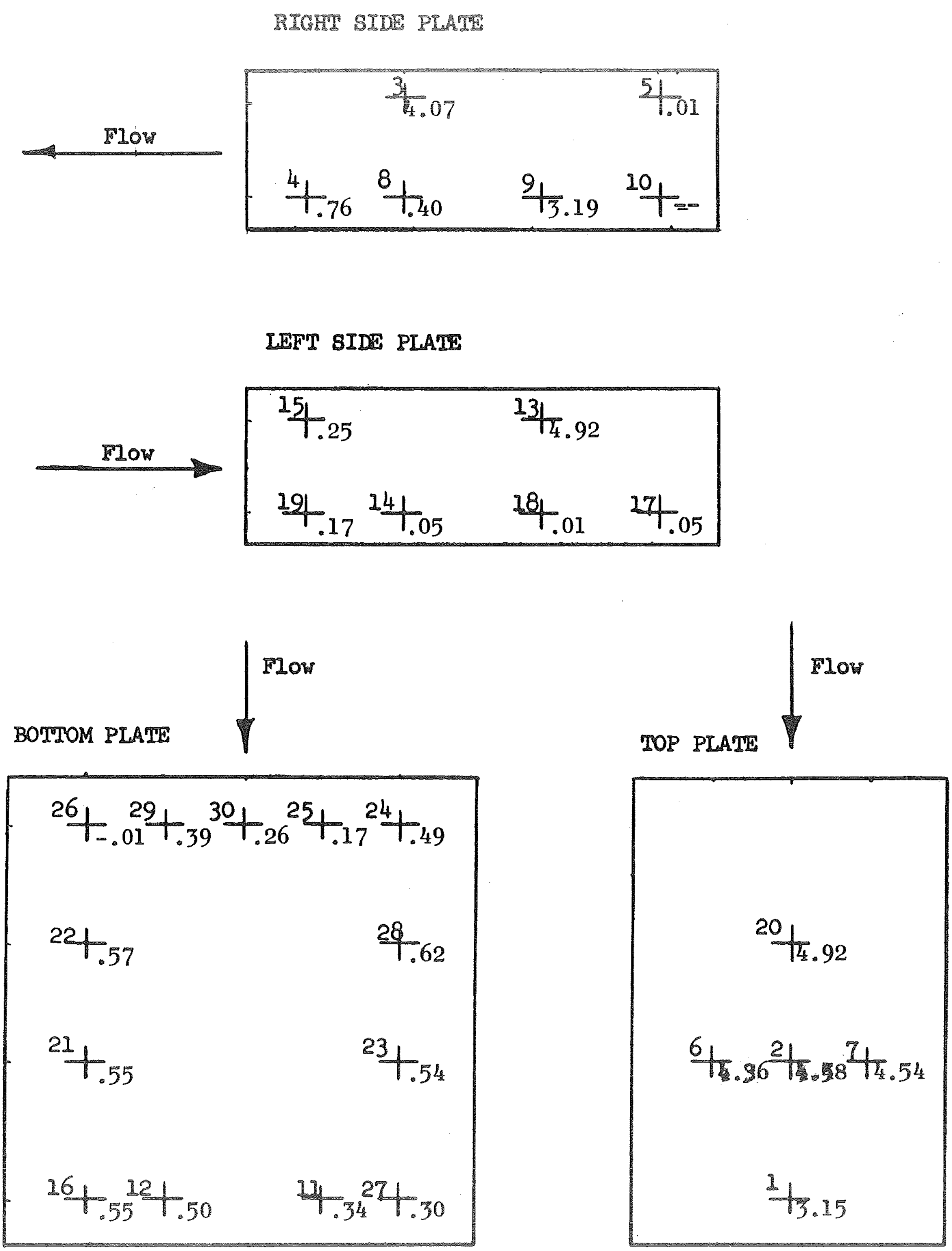

Figure 1-12 Static Pressure Data - Run 16

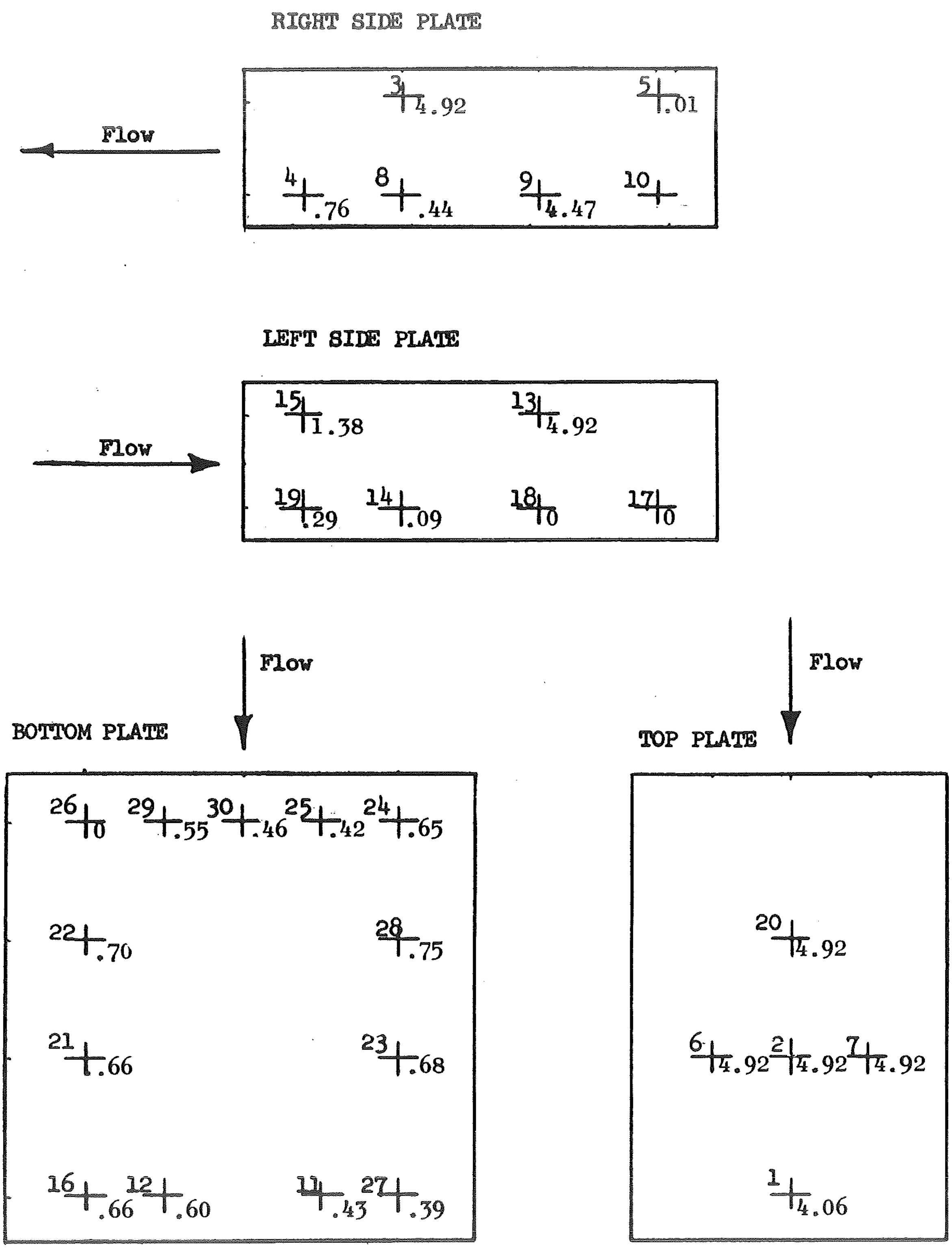

Figure 1-13 Static Pressure Data - Run 17

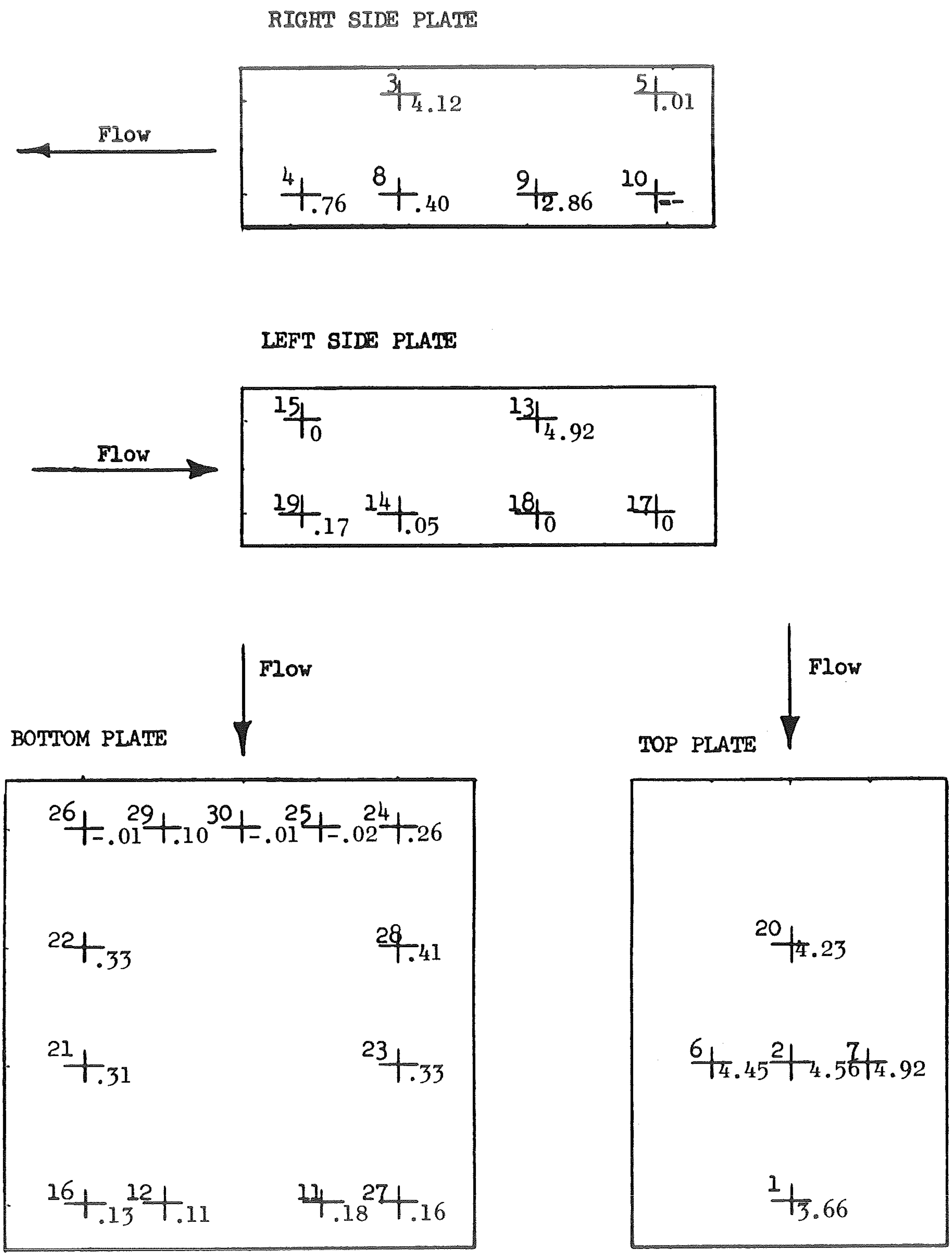

Figure 1-14 Static Pressure Data - Run 18

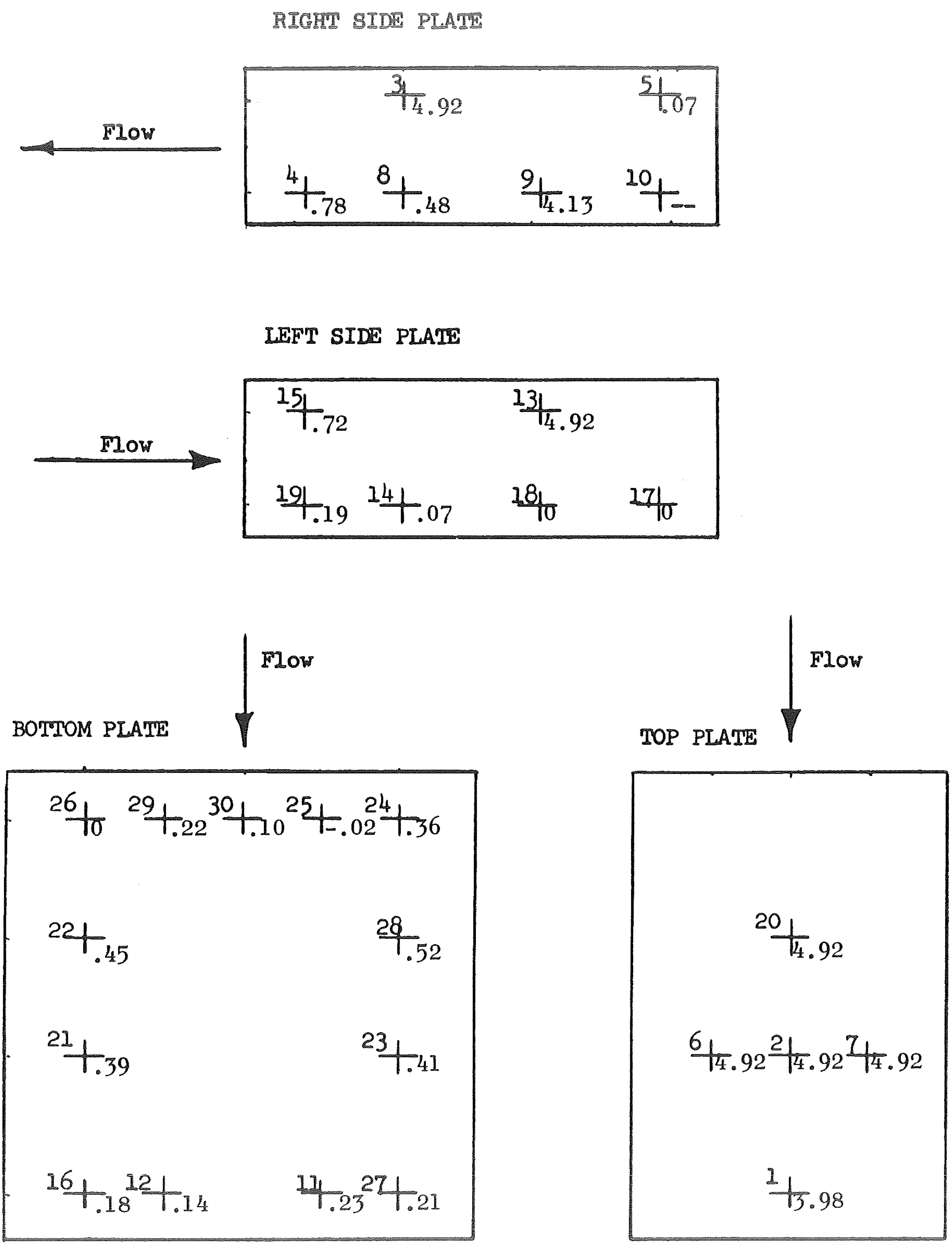

Figure 1-15 Static Pressure Data - Run 19

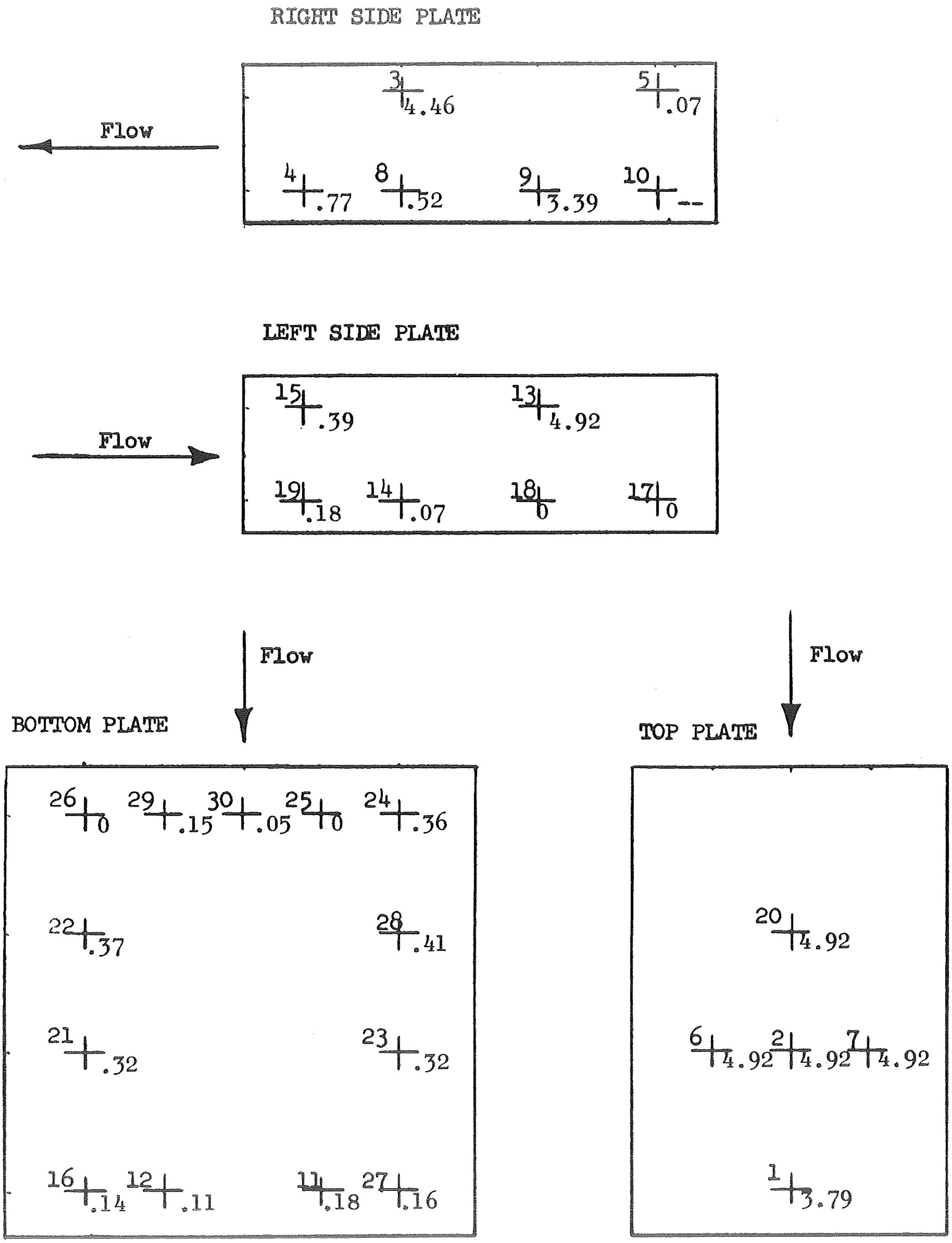

Figure 1-16 Static Pressure Data - Run 20

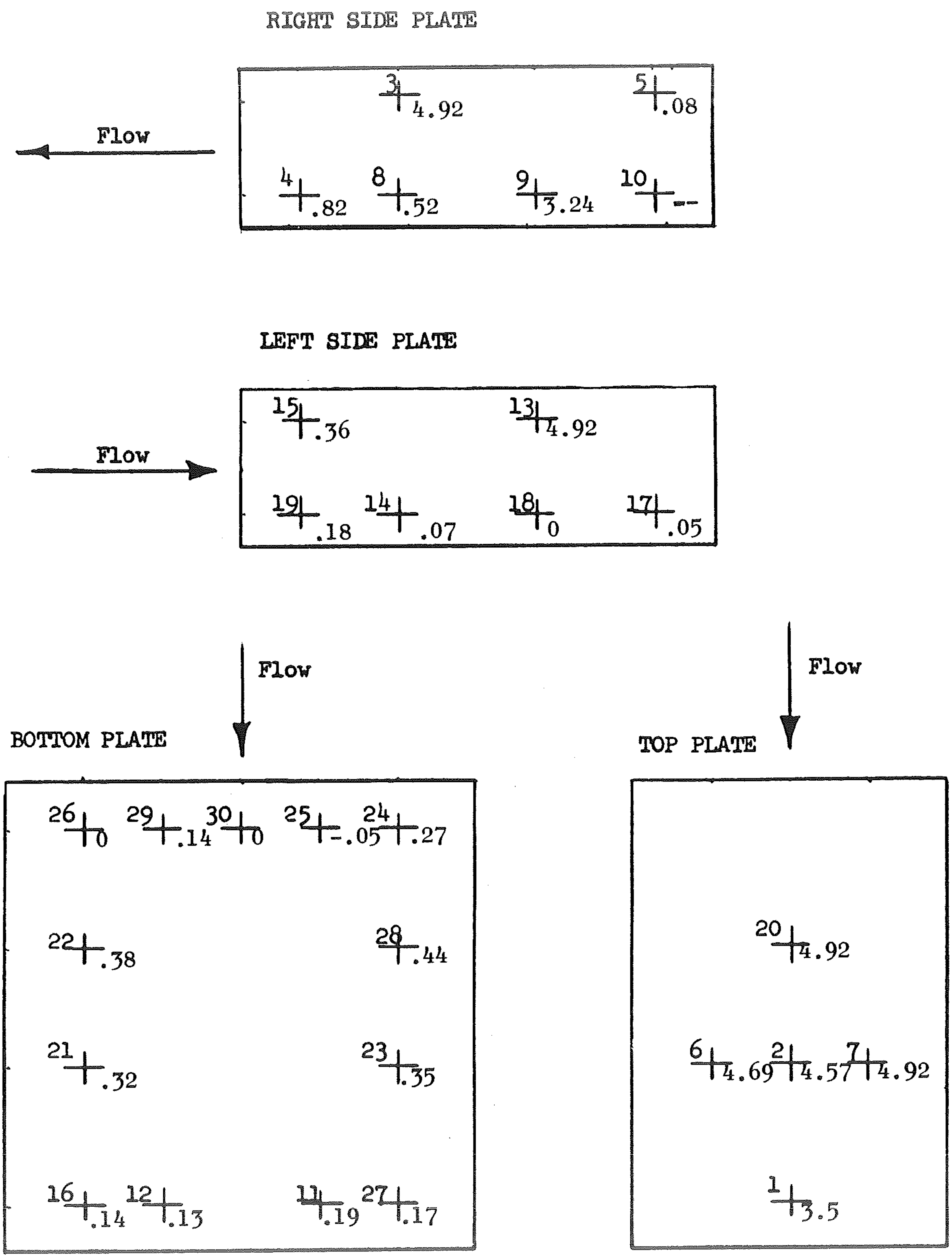

Figure 1-17 Static Pressure Data - Run 21

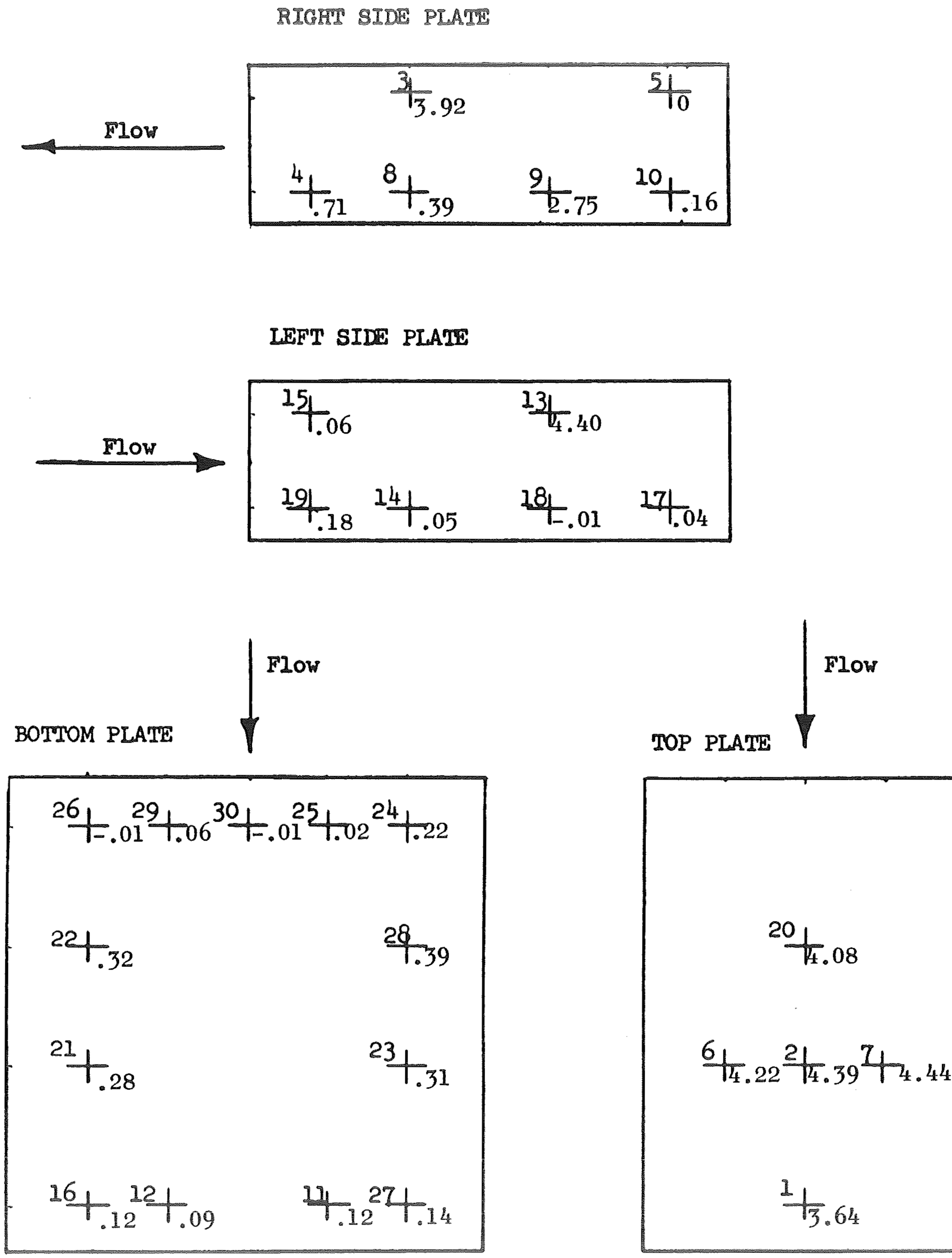

Figure 1-18 Static Pressure Data - Run 22

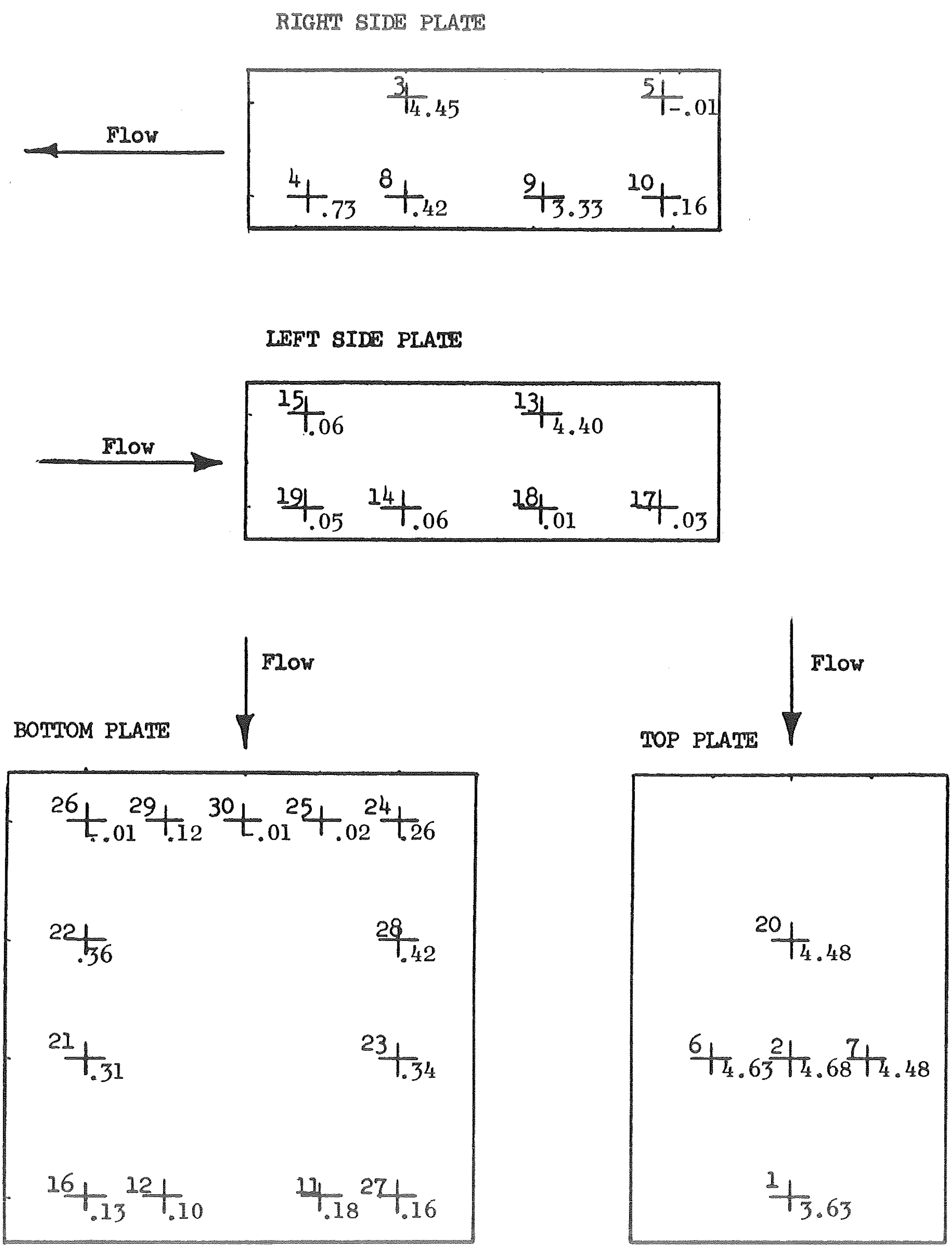

Figure 1-19 Static Pressure Data - Run 23

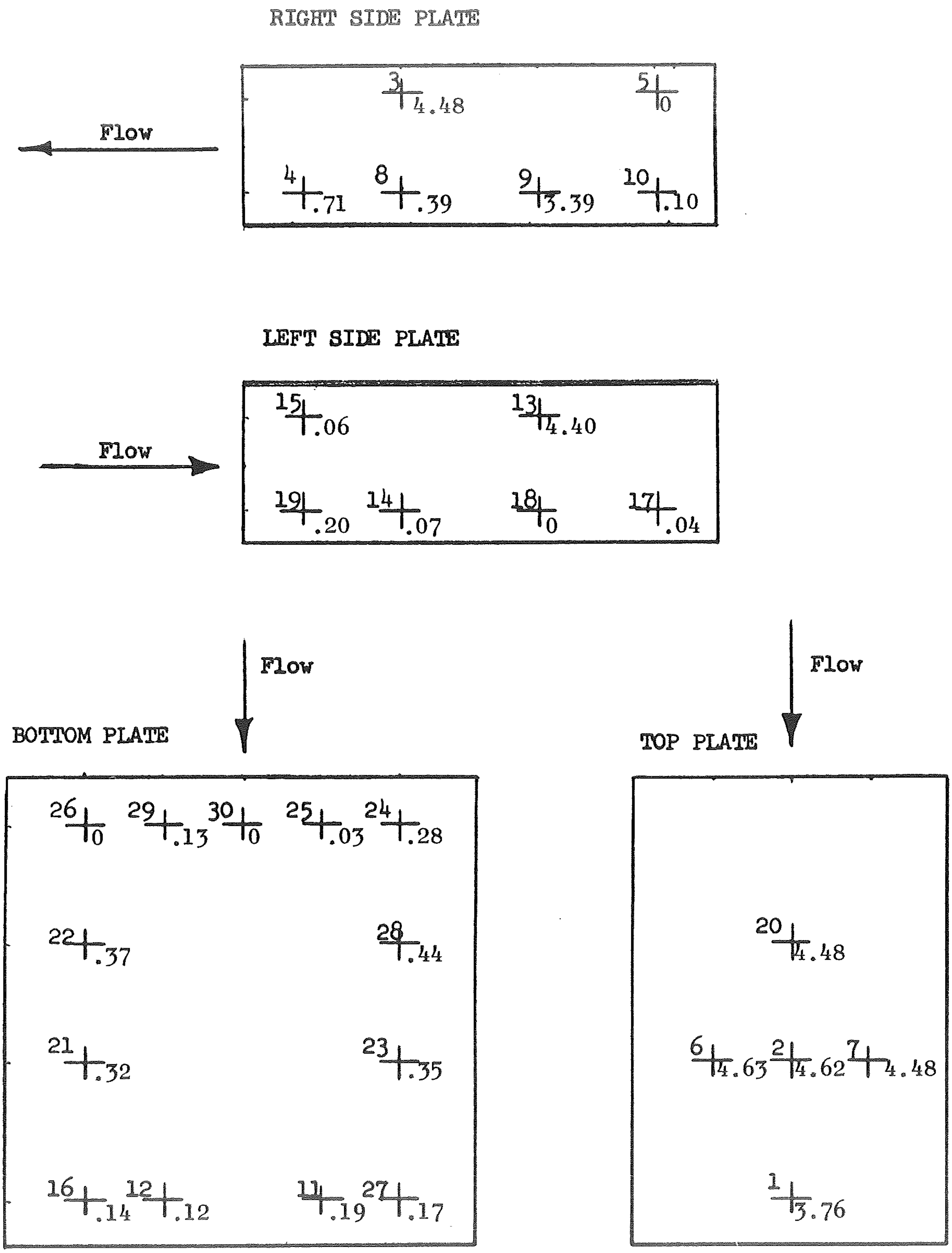

Figure 1-20 Static Pressure Data - Run 24

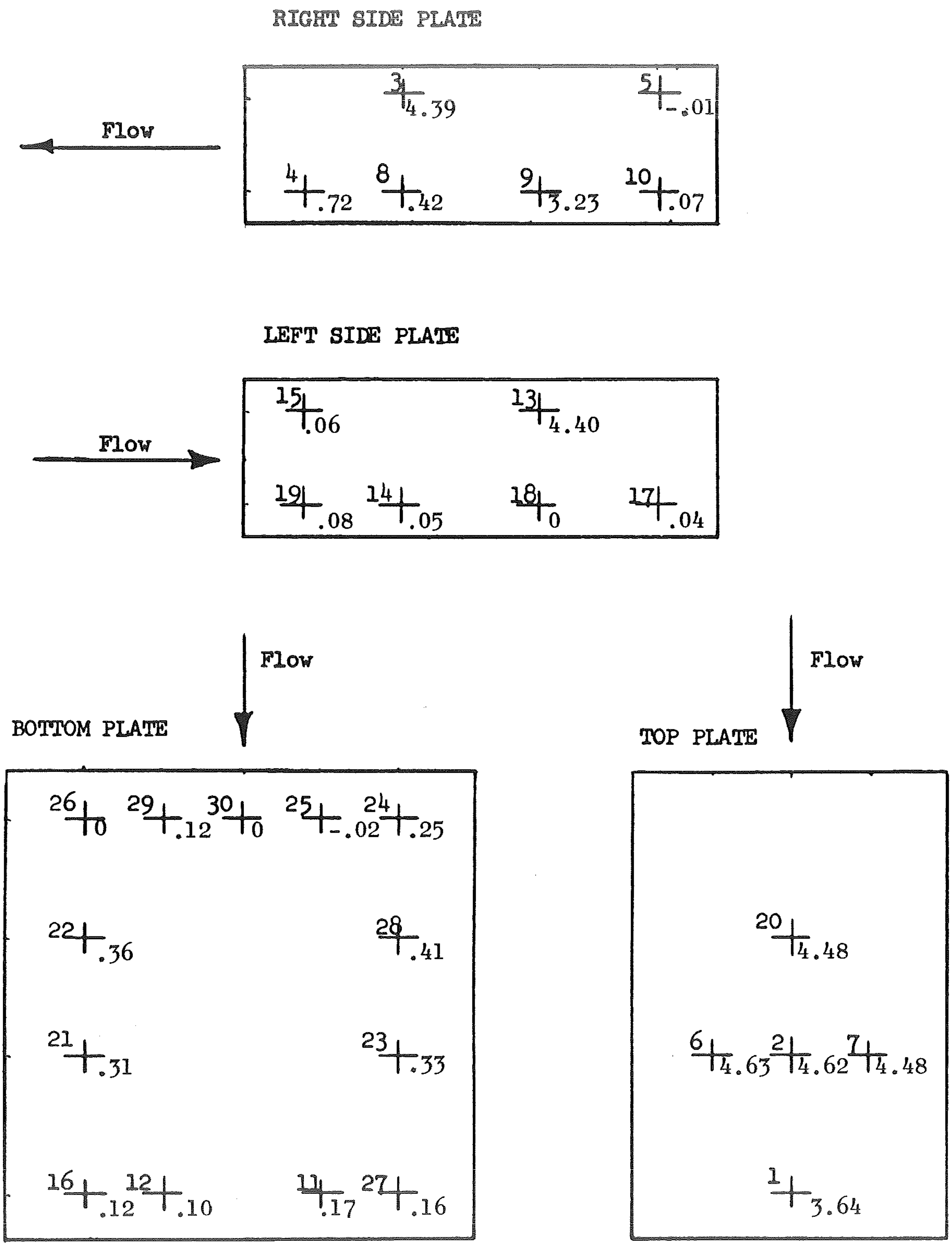

Figure 1-21 Static Pressure Data - Run 25

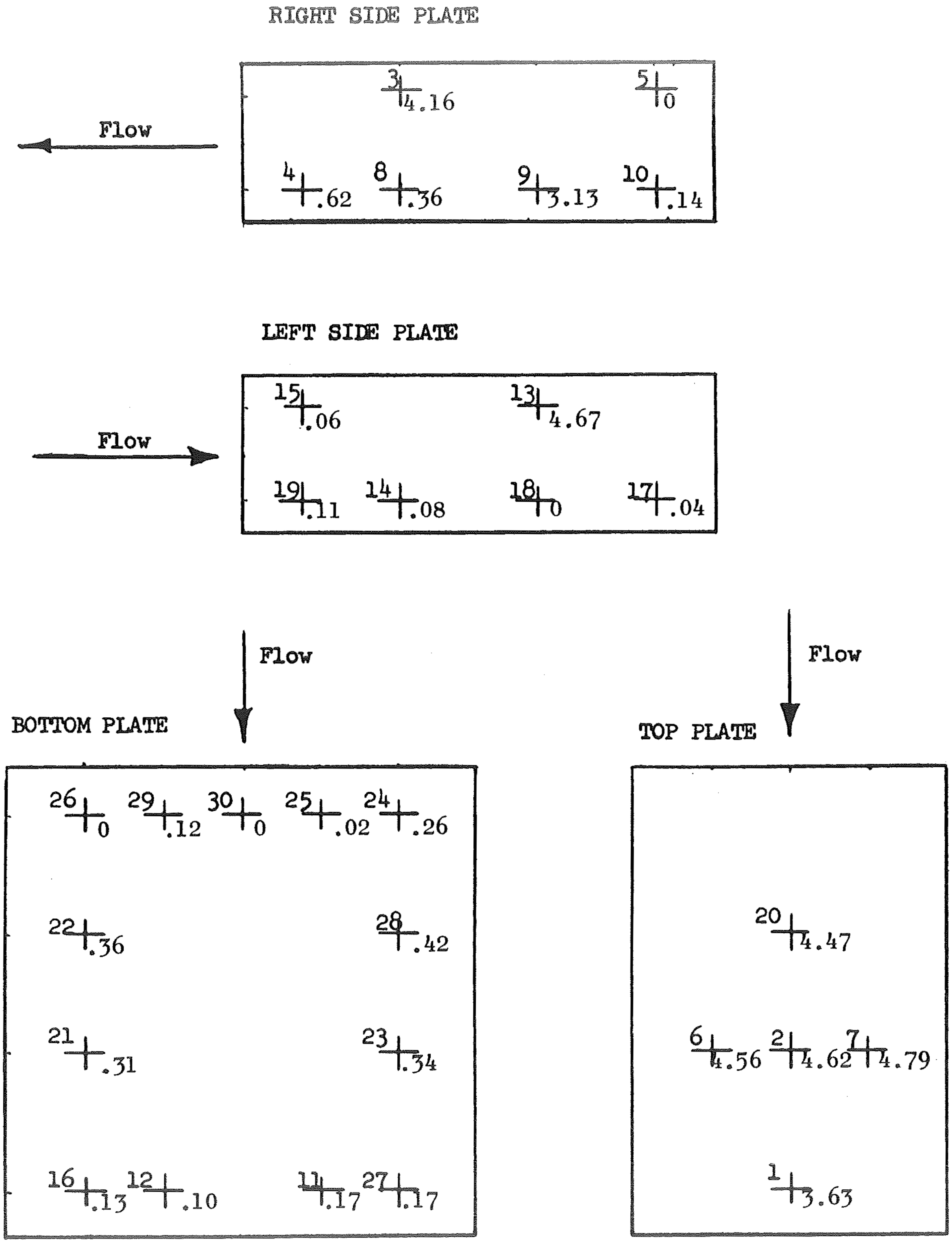

Figure 1-22 Static Pressure Data - Run 26

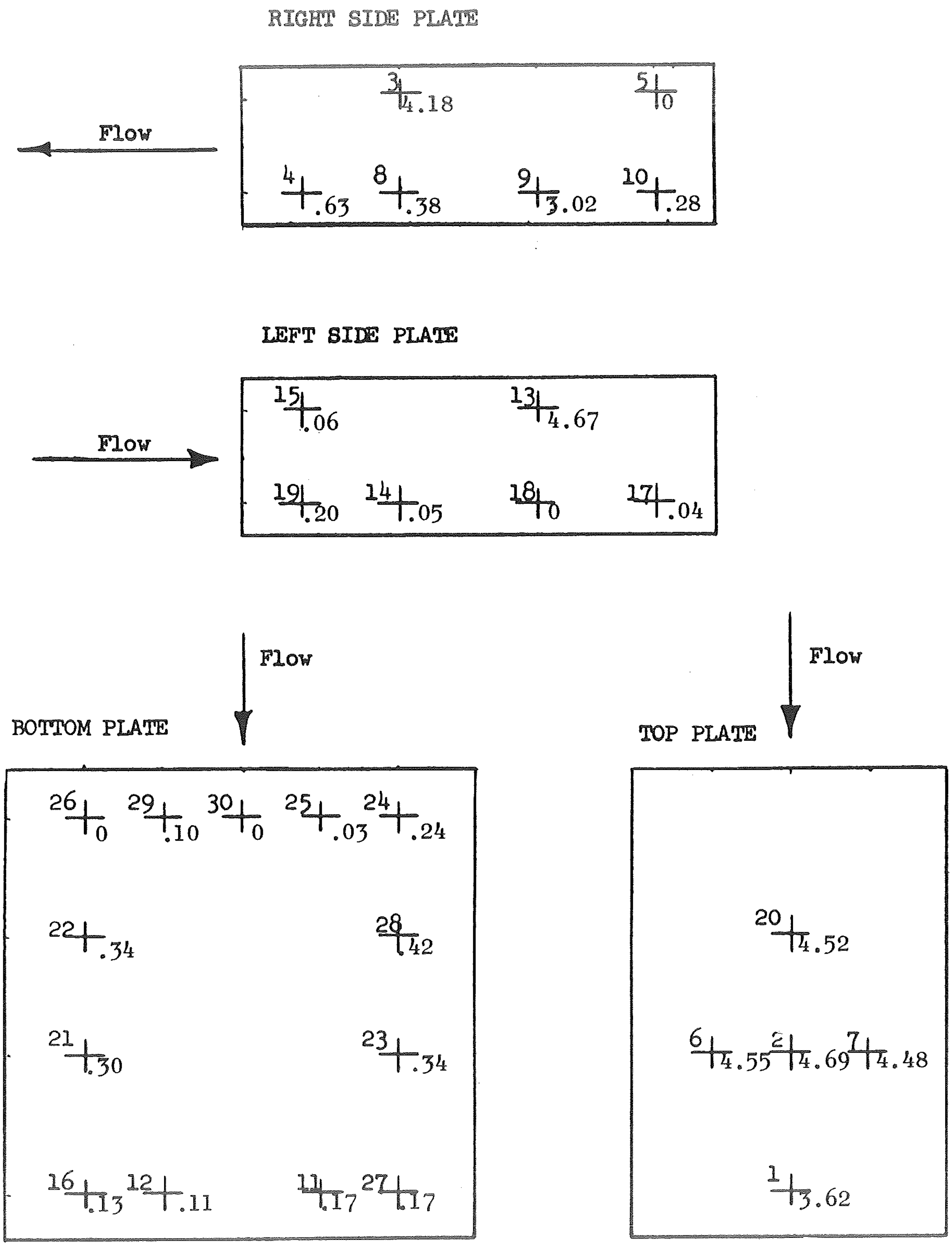

Figure 1-23 Static Pressure Data - Run 27

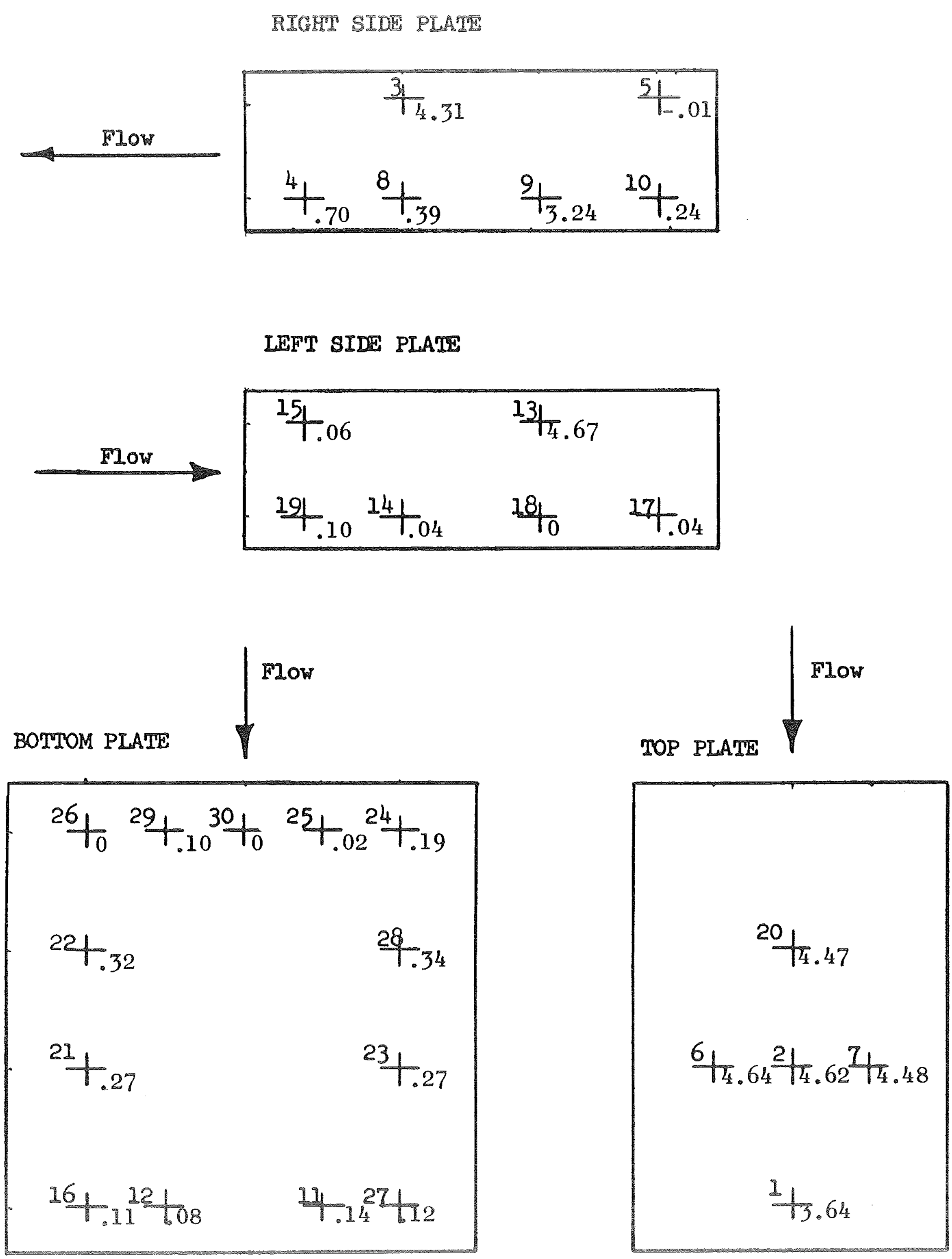

Figure 1-24 Static Pressure Data - Run 28

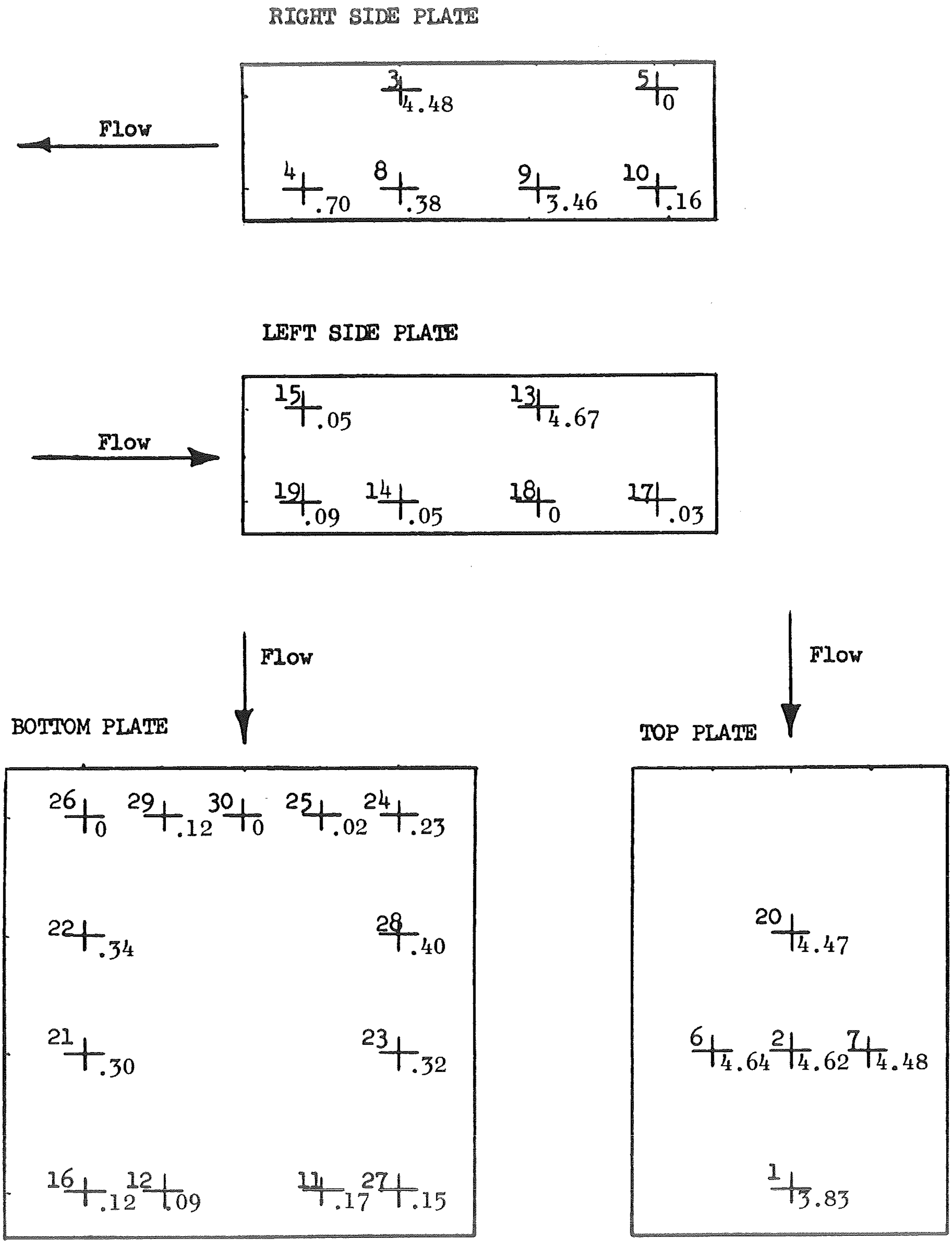

Figure 1-25 Static Pressure Data - Run 29

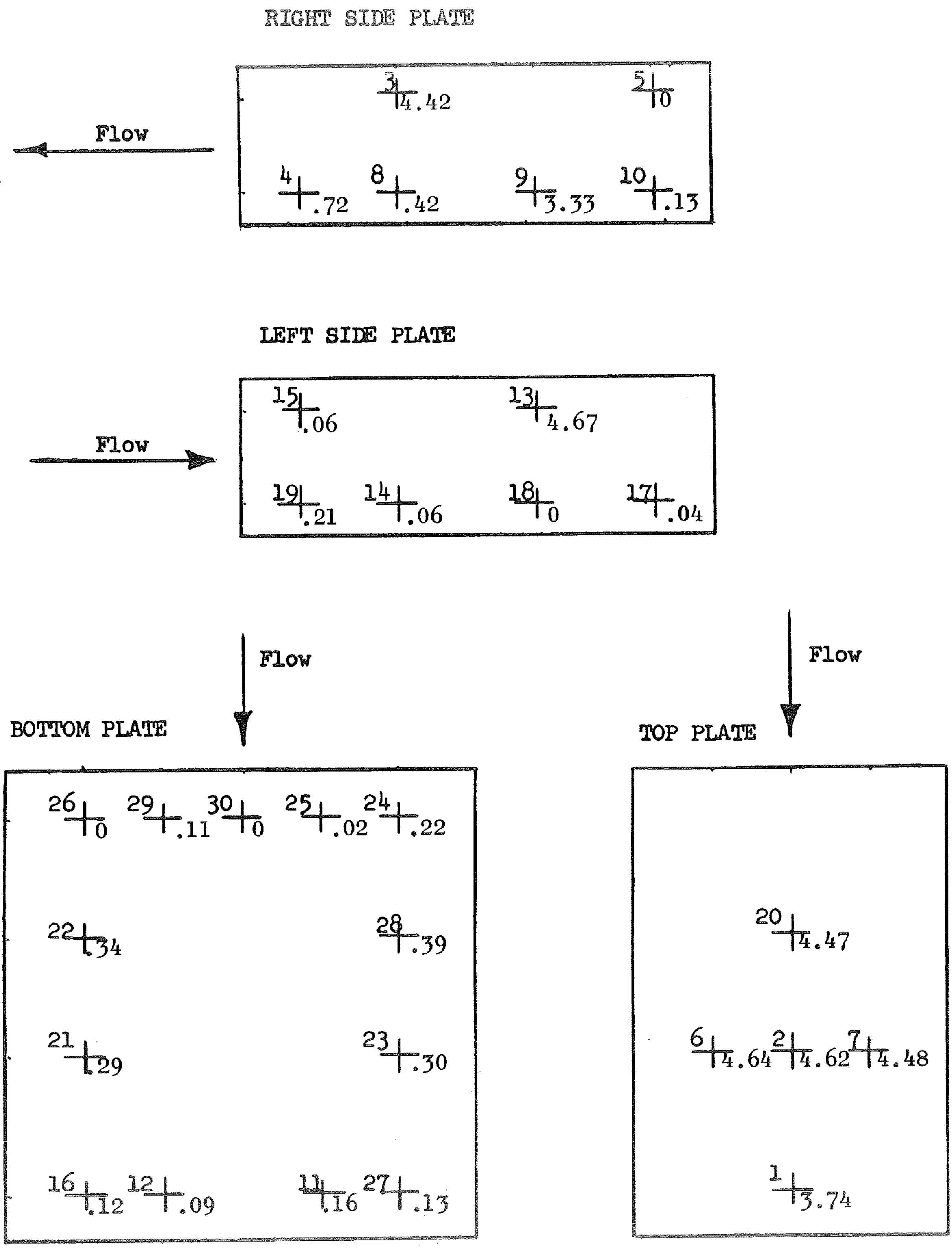

Figure 1-26 Static Pressure Data - Run 30

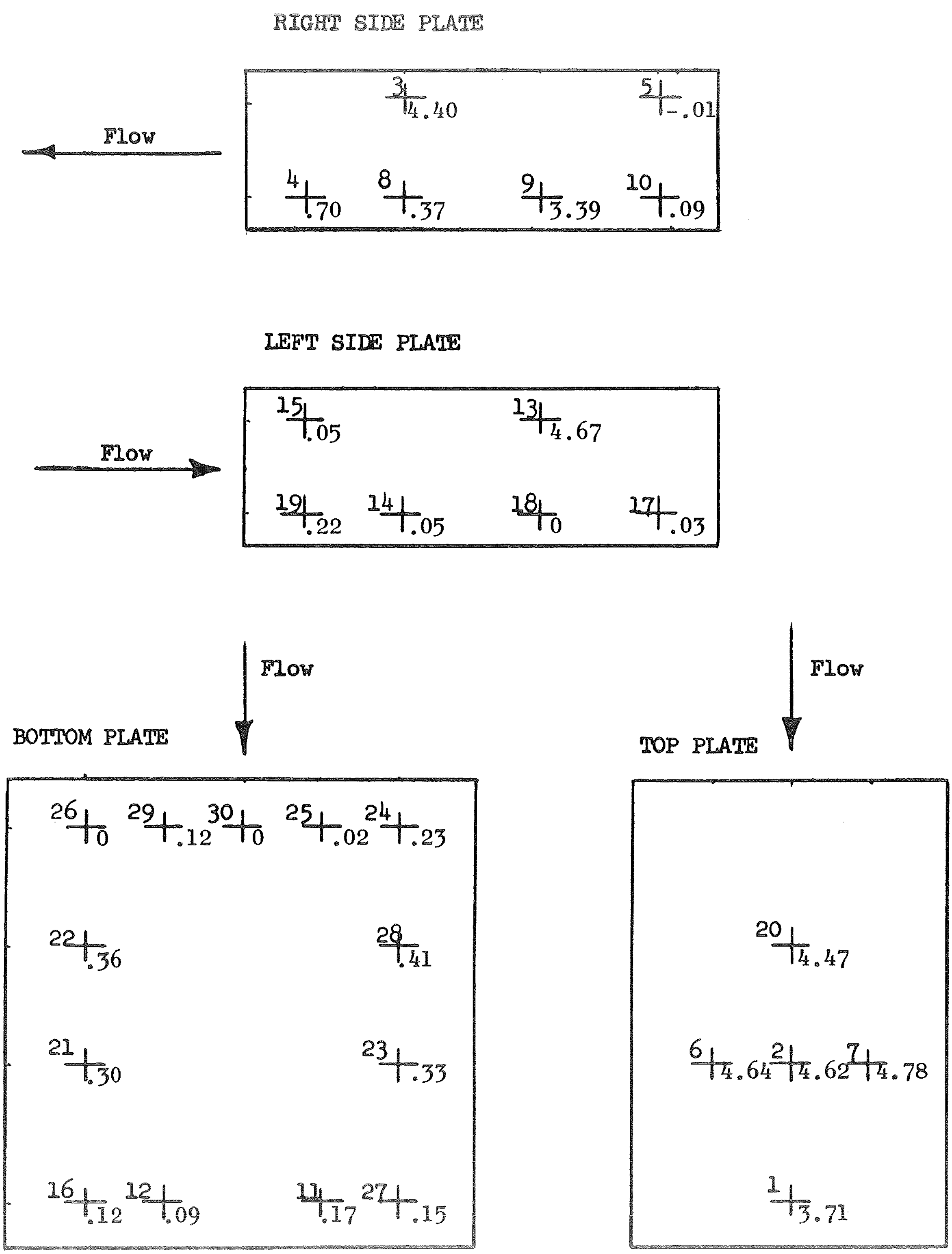

Figure 1-27 Static Pressure Data - Run 31

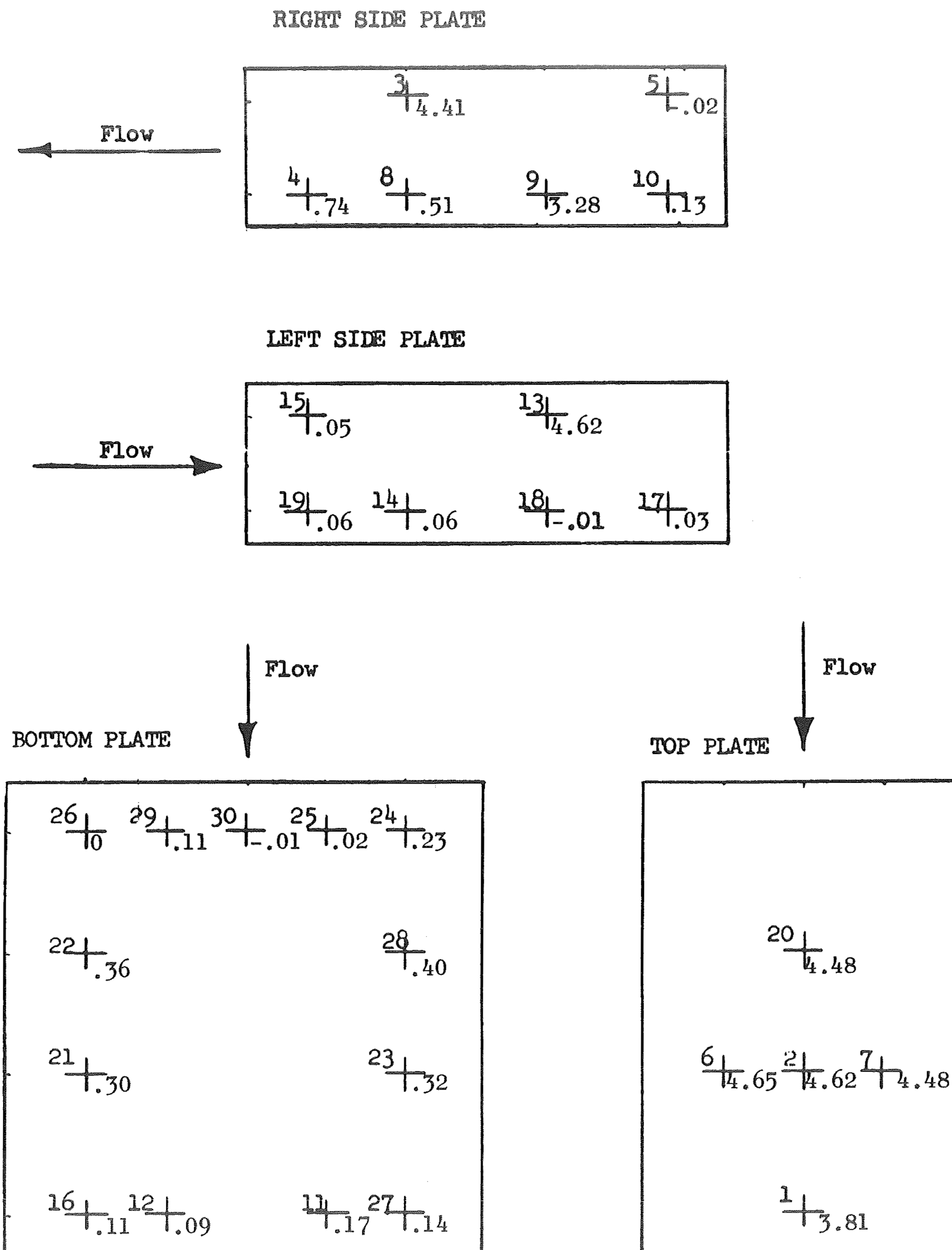

Figure 1-28 Static Pressure Data - Run 32

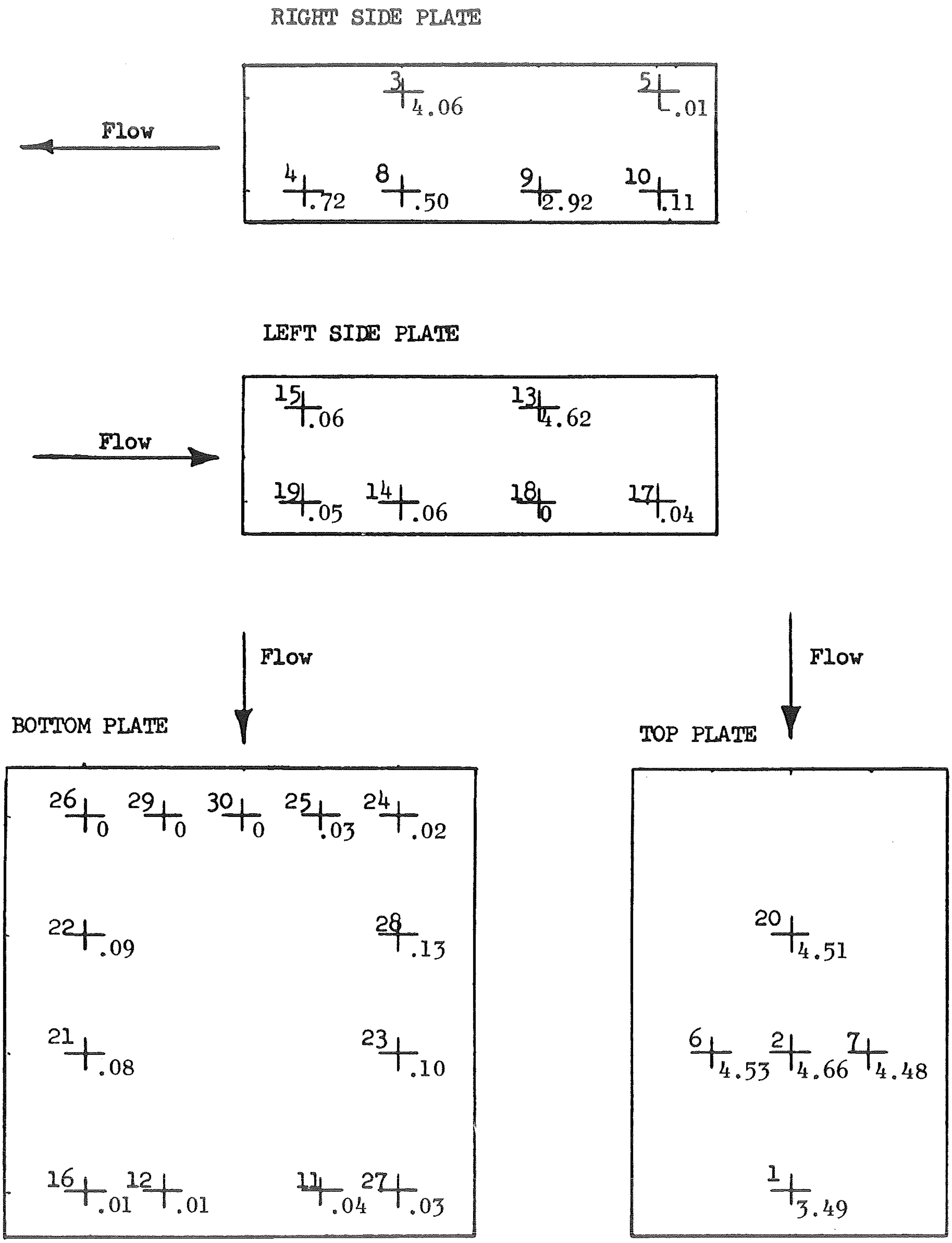

Figure 1-29 Static Pressure-Data Run 33

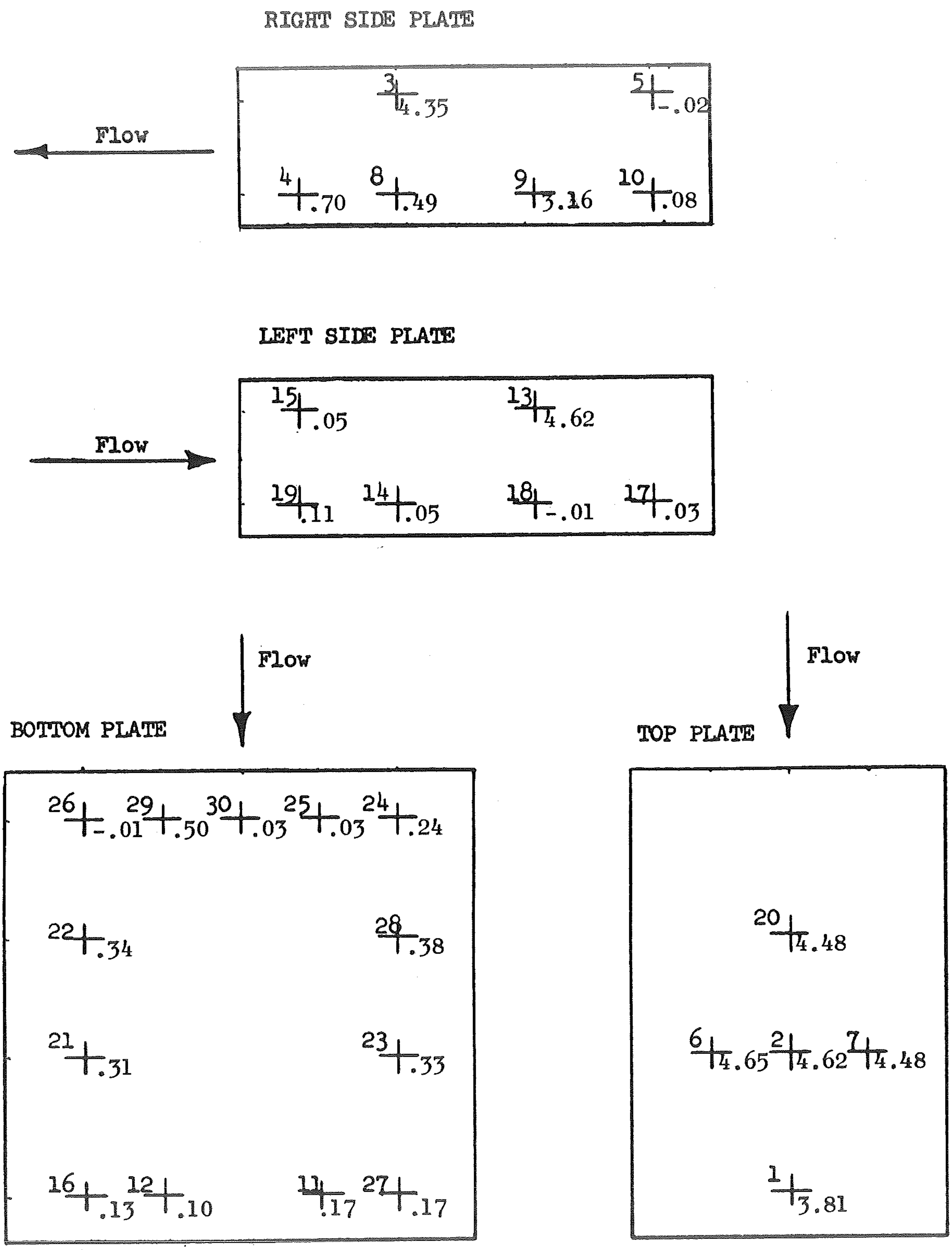

Figure 1-30 Static Pressure Data-Run 34

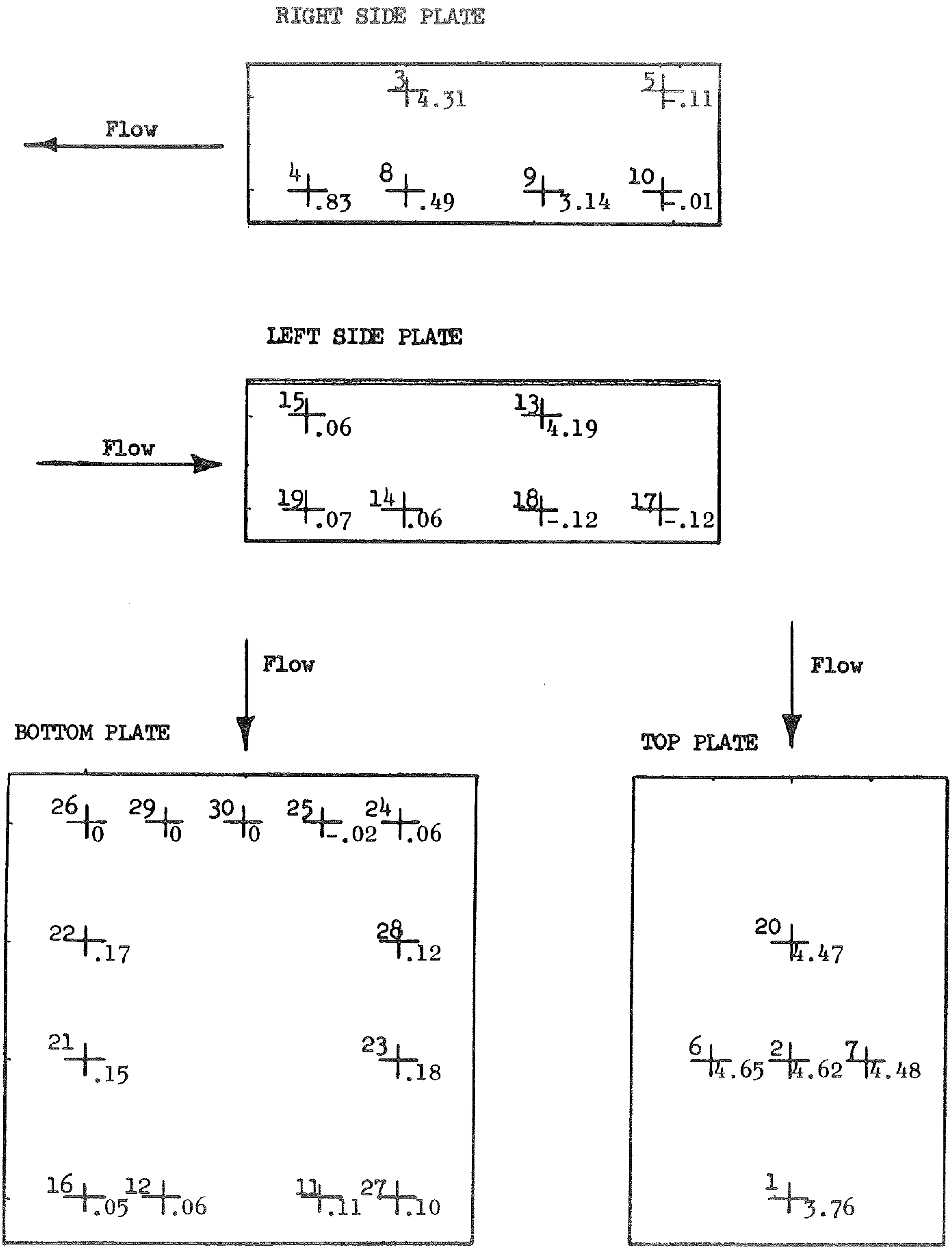

Figure 1-31 Static Pressure Data - Run 35

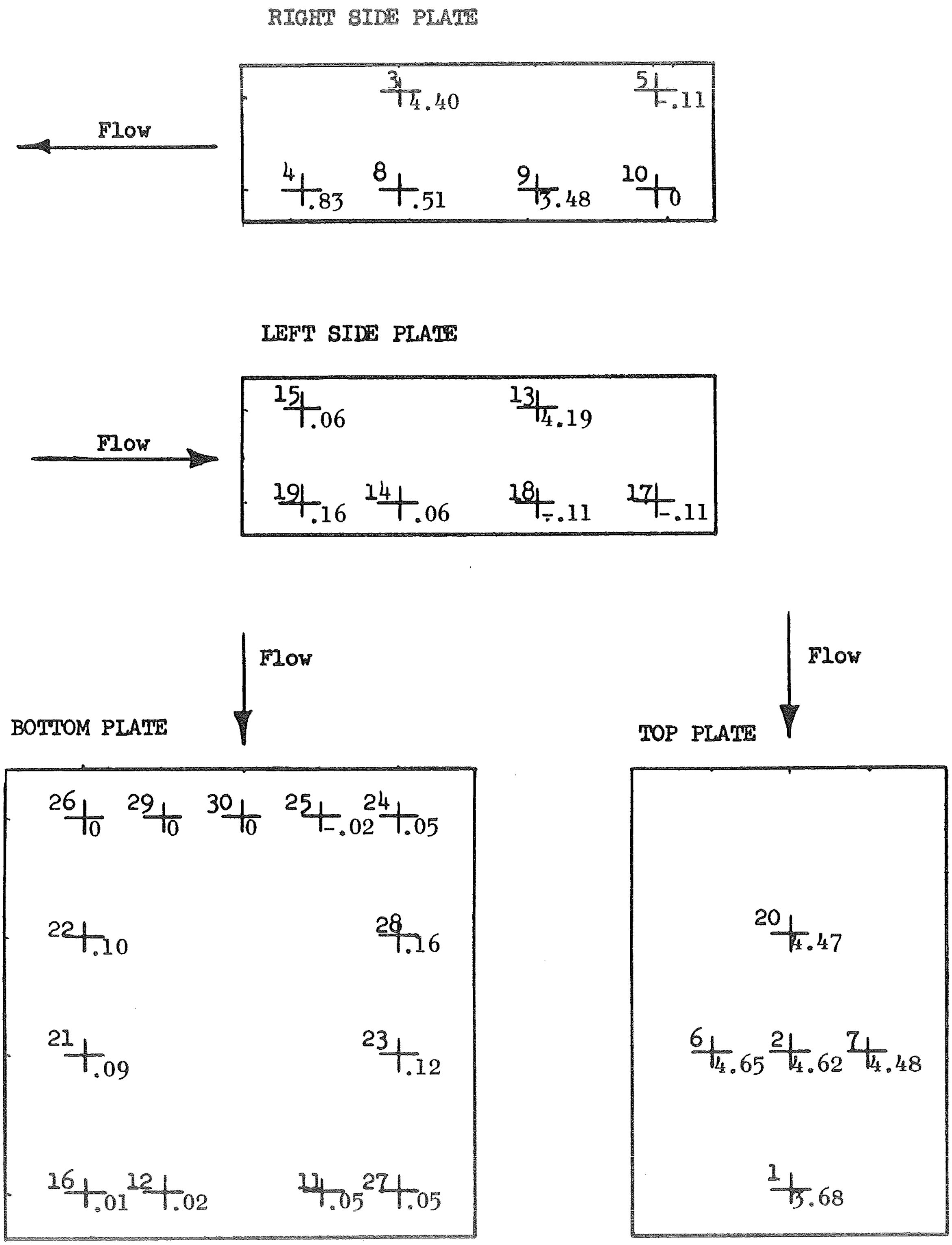

Figure 1-32 Static Pressure Data - Run 36

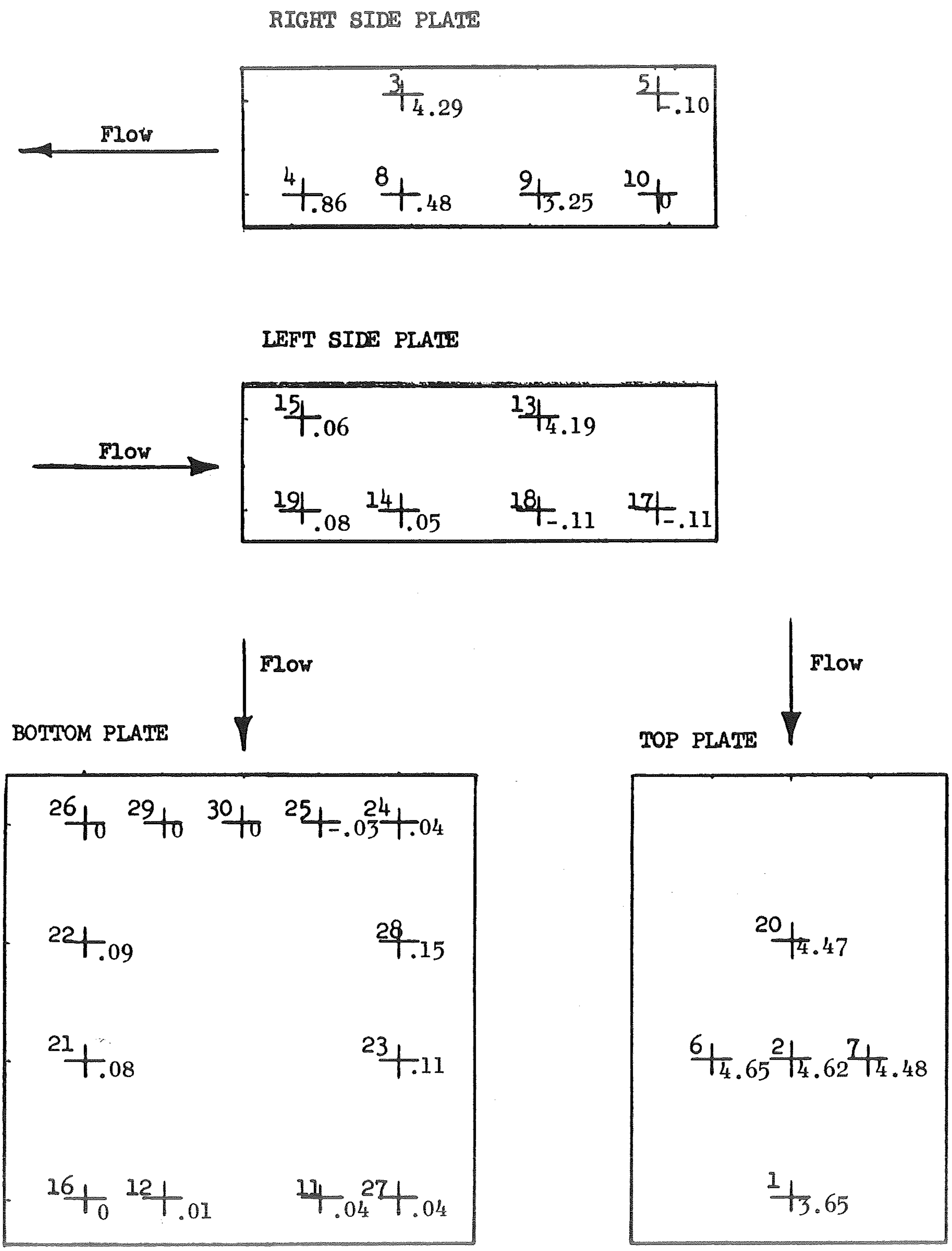

Figure 1-33 Static Pressure Data - Run 37

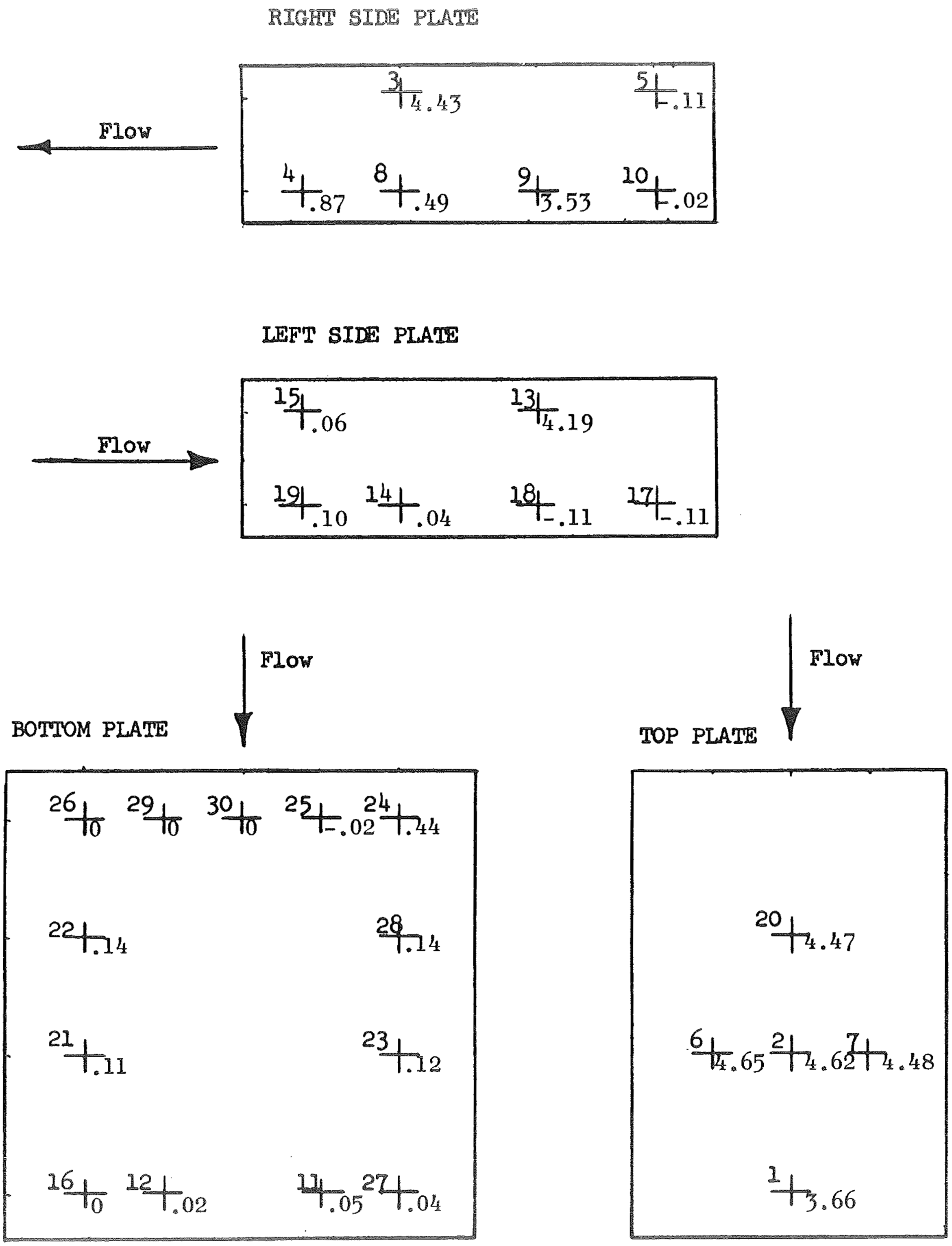

Figure 1-34 Static Pressure Data - Run 38

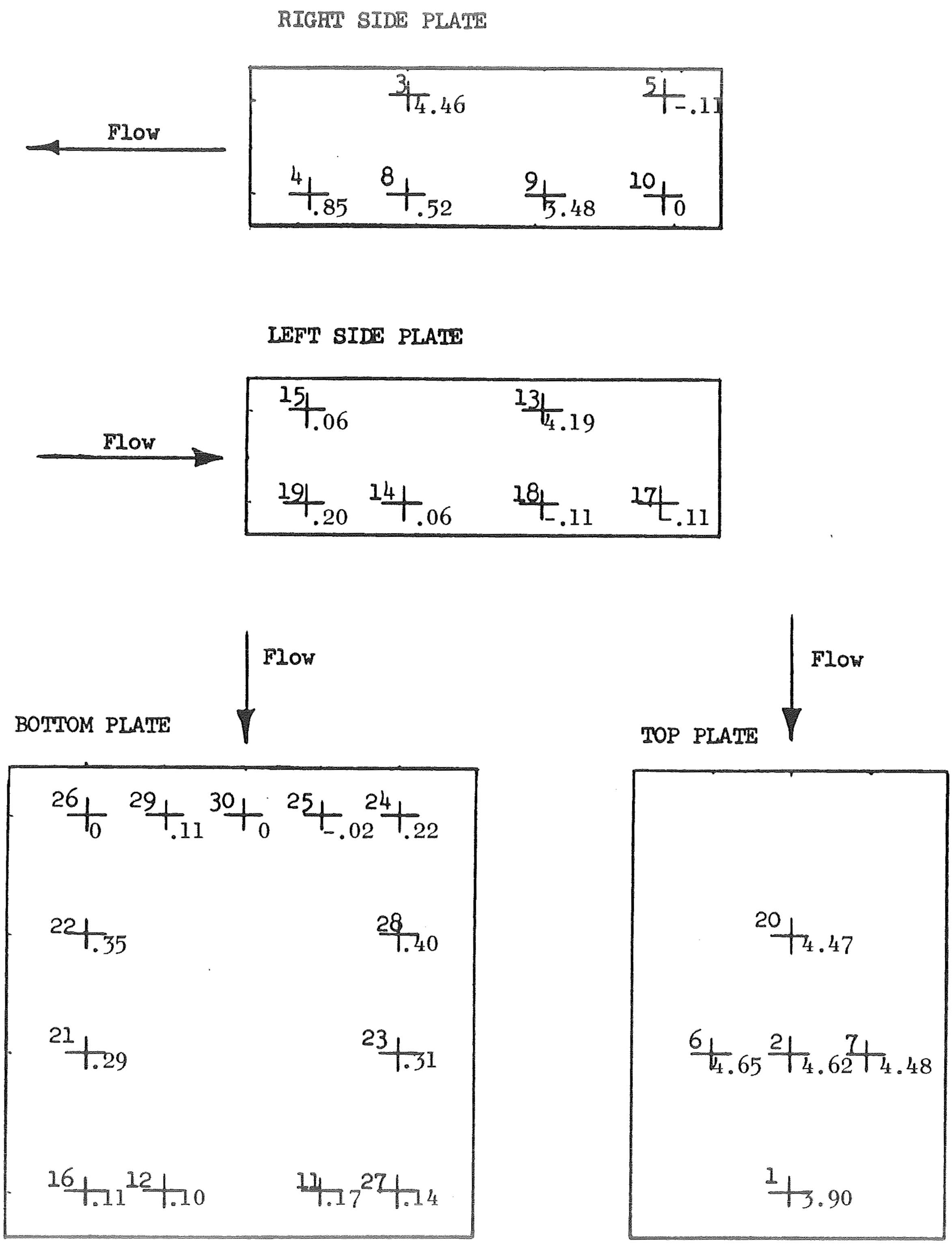

Figure 1-35 Static Pressure Data - Run 39

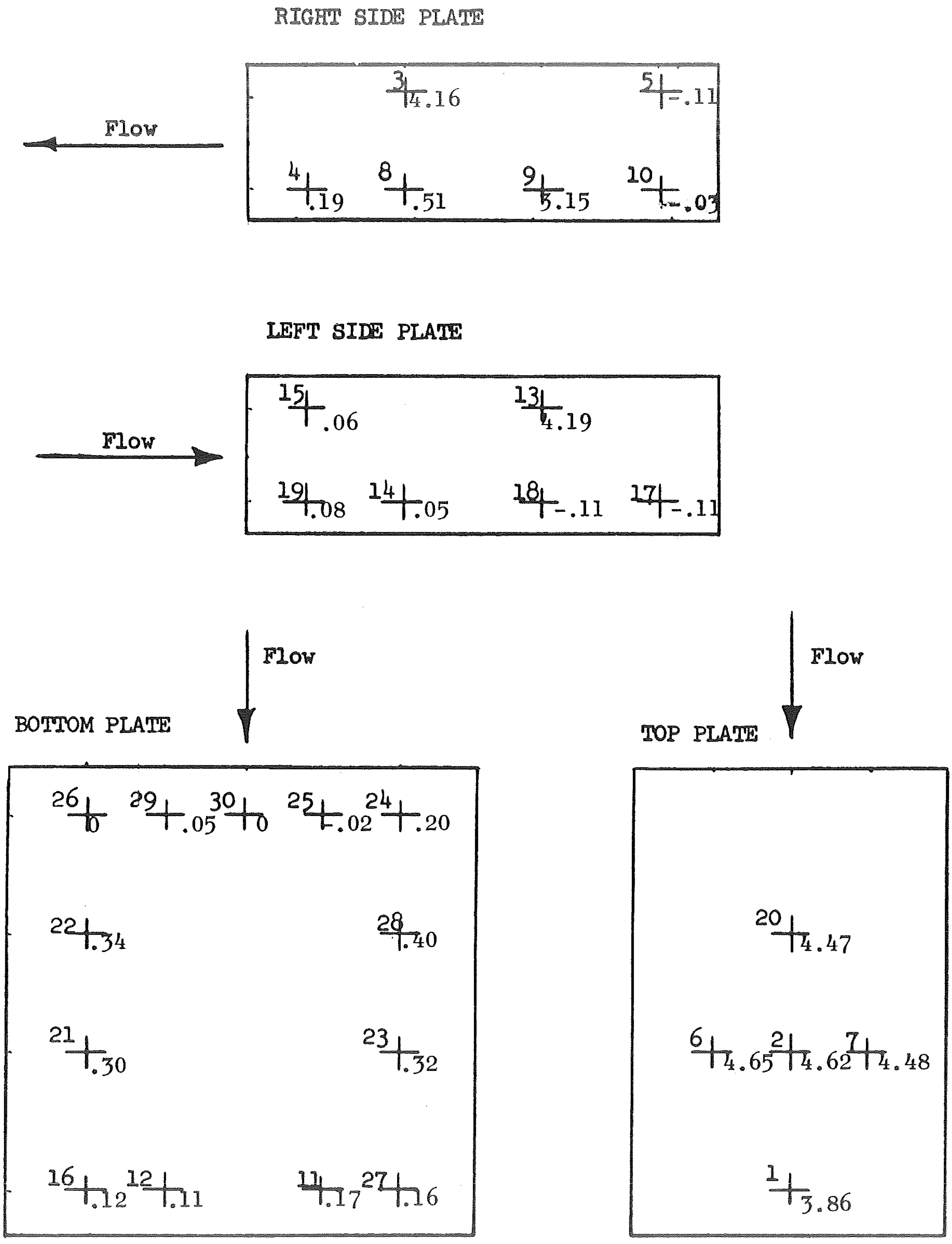

Figure 1-36 Static Pressure Data - Run 40

Table 1-2 presents the grouped data for the aforementioned tests; however, data for the checkout runs and tests 10-14 are not included in this data summary. The checkout run static pressure data were questionable due to frequent spill-over and bubble formation in a large number of the manometer bank tubes. Data for runs 10 to 14 only included information prior to engine start due to a malfunction of the data acquisition system. These data in general show that initially there is an approximate .5 psi positive pressure at the top of the mixing chamber and an approximately .02 psi negative pressure at the bottom of the mixing chamber. The averaged data are displayed in Figs. 1-37 to 1-39.

Analysis of the data presented in Table I-2 is summarized below:

(1) Pressure port numbers 1, 2, 3, 6, 7, 13, 20 were so located such that they reflected the static pressure of the high pressure film coolant streams and did not indicate the static pressure of the supersonic flow.

(2) Pressure port numbers 5, 10, 15, 19, 24, 25, 26, 29, 30 were located slightly upstream of the mixing chamber and reflected the entering conditions of the film coolants and air stream. It should be noted that these ports were in the region of separated flow as shown in the velocity survey, Appendix 5.

(3) Pressure ports 4, 8, 9, 11, 12, 14, 16, 18, 19, 21, 22, 23, 27, and 28 yielded a reading that could permit interpretations of the data as a function of test parameters; however, maximum static pressure variations were of the order of 0.3 psi, or less, which put the data

TABLE 1-2

GROUPED STATIC PRESSURE DATA, PSIG

Pressure Port No.	High Temp.	Medium Temp.	Low Temp.	High Velocity	Low Velocity	1/2" Screen	1/8" Screen	1/2" Dam
1	3.70	3.70	3.81	3.81	3.61	3.76	3.66	3.86
2	4.71	4.66	4.62	4.62	4.63	4.62	4.62	4.62
3	4.40	4.42	4.35	4.41	4.25	4.31	4.43	4.16
4	----	----	----	----	----	----	----	----
5	-.02	.02	-.02	-.02	-.07	-.11	-.11	-.11
6	4.61	4.64	4.65	4.65	4.61	4.65	4.65	4.65
7	4.69	4.62	4.48	4.48	4.48	4.48	4.48	4.48
8	.42	.42	.49	.51	.50	.49	.49	.51
9	3.45	3.30	3.16	3.28	3.22	3.14	3.53	3.15
10	----	----	----	----	----	----	----	----
11	.24	.17	.17	.17	.04	.11	.05	.17
12	.25	.11	.10	.09	.01	.06	.02	.11
13	4.72	4.64	4.62	4.62	4.33	4.19	4.19	4.19
14	.06	.06	.05	.06	.06	.06	.04	.05
15	.30	.18	.05	.05	.06	.06	.06	.06
16	.28	.13	.13	.11	.01	.05	0	.12
17	----	----	----	----	----	----	----	----
18	----	----	----	----	----	----	----	----
19	----	----	----	----	----	----	----	----
20	4.58	4.56	4.48	4.48	4.48	4.47	4.47	4.47
21	.40	.31	.31	.30	.08	.15	.11	.30
22	.44	.36	.34	.36	.09	.17	.14	.34
23	.42	.33	.33	.32	.11	.18	.12	.32
24	.34	.27	.24	.23	.04	.06	.44	.20
25	----	----	----	----	----	----	----	----
26	0	0	-.01	0	0	0	0	0
27	.21	.07	.17	.14	.04	.10	.04	.16
28	.50	.42	.38	.40	.15	.12	.14	.40
29	.23	.13	.50	.11	0	0	0	.05
30	.12	.01	.03	-.01	0	0	0	0

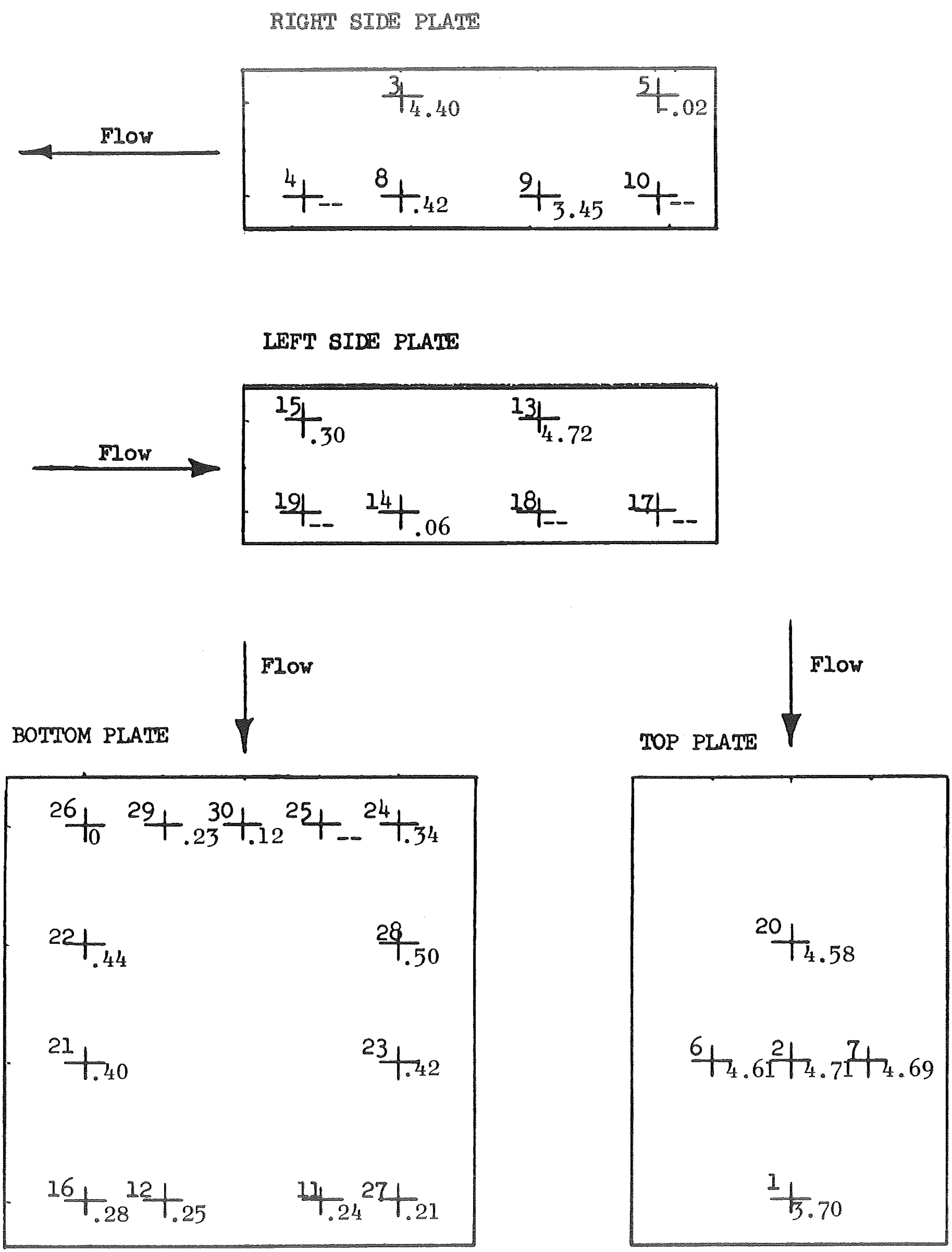

Figure 1-37 Average Static Pressure Data for High Temperature Air Tests

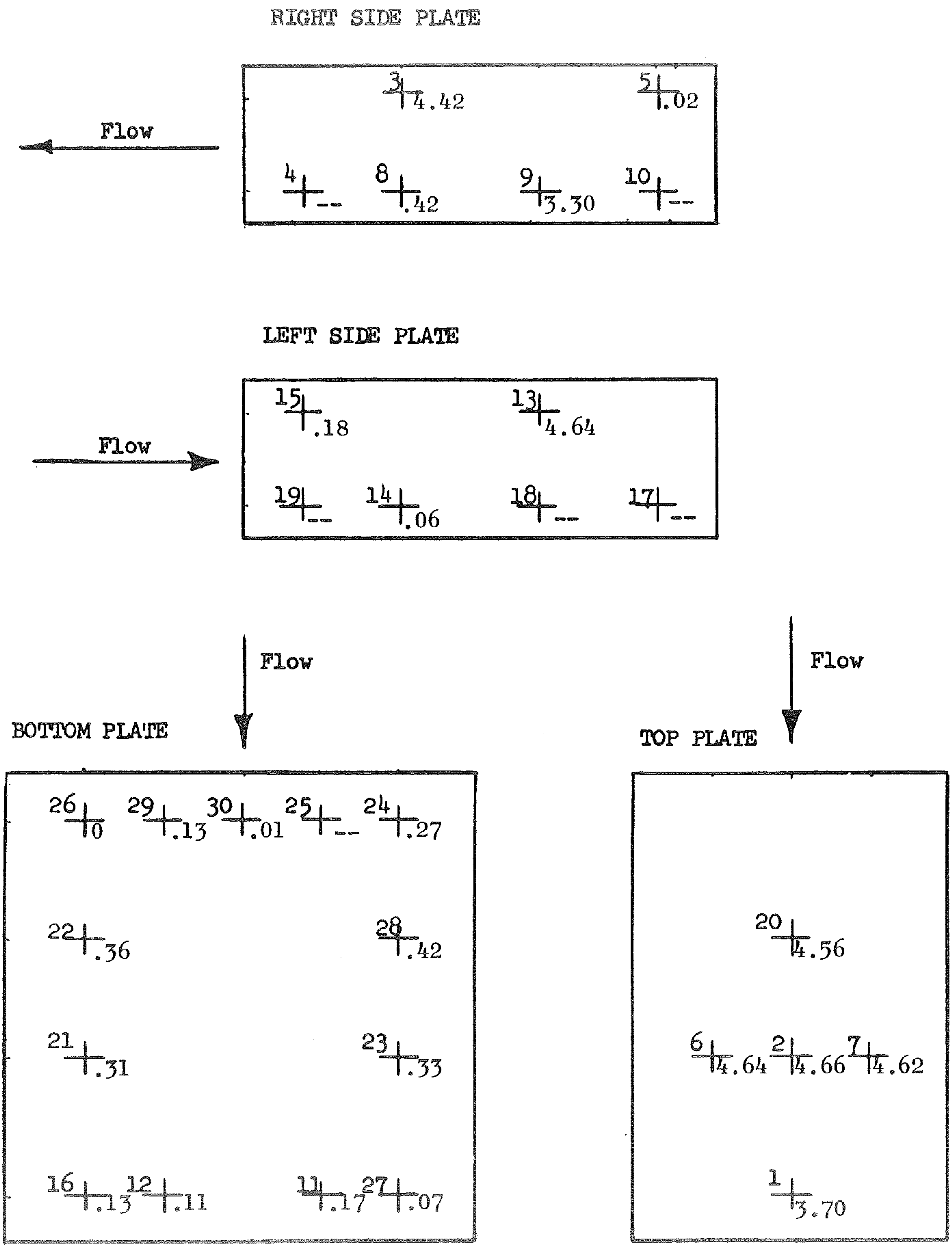

Figure 1-38 Average Static Pressure Data for Medium Temperature Air Tests

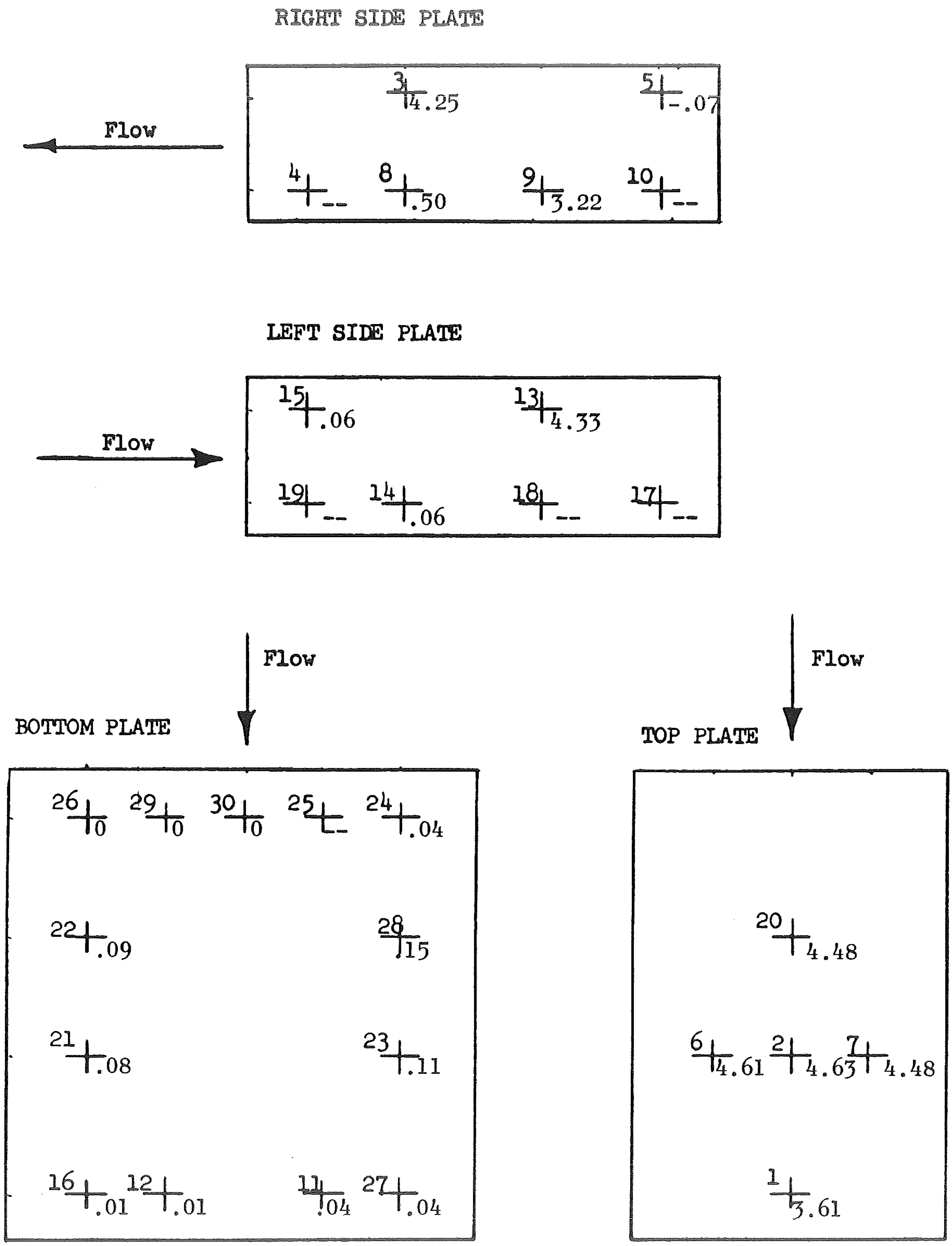

Figure 1-39 Average Static Pressure Data for Low Velocity Air Tests

within the range of experimental error. Therefore, no interpreation of the static data gathered will be given. The small variations measured for the different test cases did, however, indicate that the range of parameters investigated did not significantly alter the basic mixing process.

APPENDIX 2

TRANSIENT DATA

At the beginning of testing a detailed study of the system transient behavior was made. This included examination of all system pressures and temperatures. In general, during engine operation every parameter after the first second of engine operation indicated acceptable steady-state operation. Coolant water temperatures were well below the critical boiling point. All pressures and temperatures were constant with the exception of the heater bed temperatures and air inlet temperatures. Since air inlet temperature was a principal parameter, its transient behavior for Runs 10 to 40 is presented in Figs. 2-1 to 2-6. Slight variations in chamber pressure ($\pm$ 1.5 percent) were also noted. Due to its being a critical test parameter, it too is presented for Runs 10 to 40, Fig. 2-7 to 2-13.

Some flow adjustments in the non-choked film coolant and air supplies were evidenced at the beginning of each run. However, these adjustments occurred during the initial start-up period.

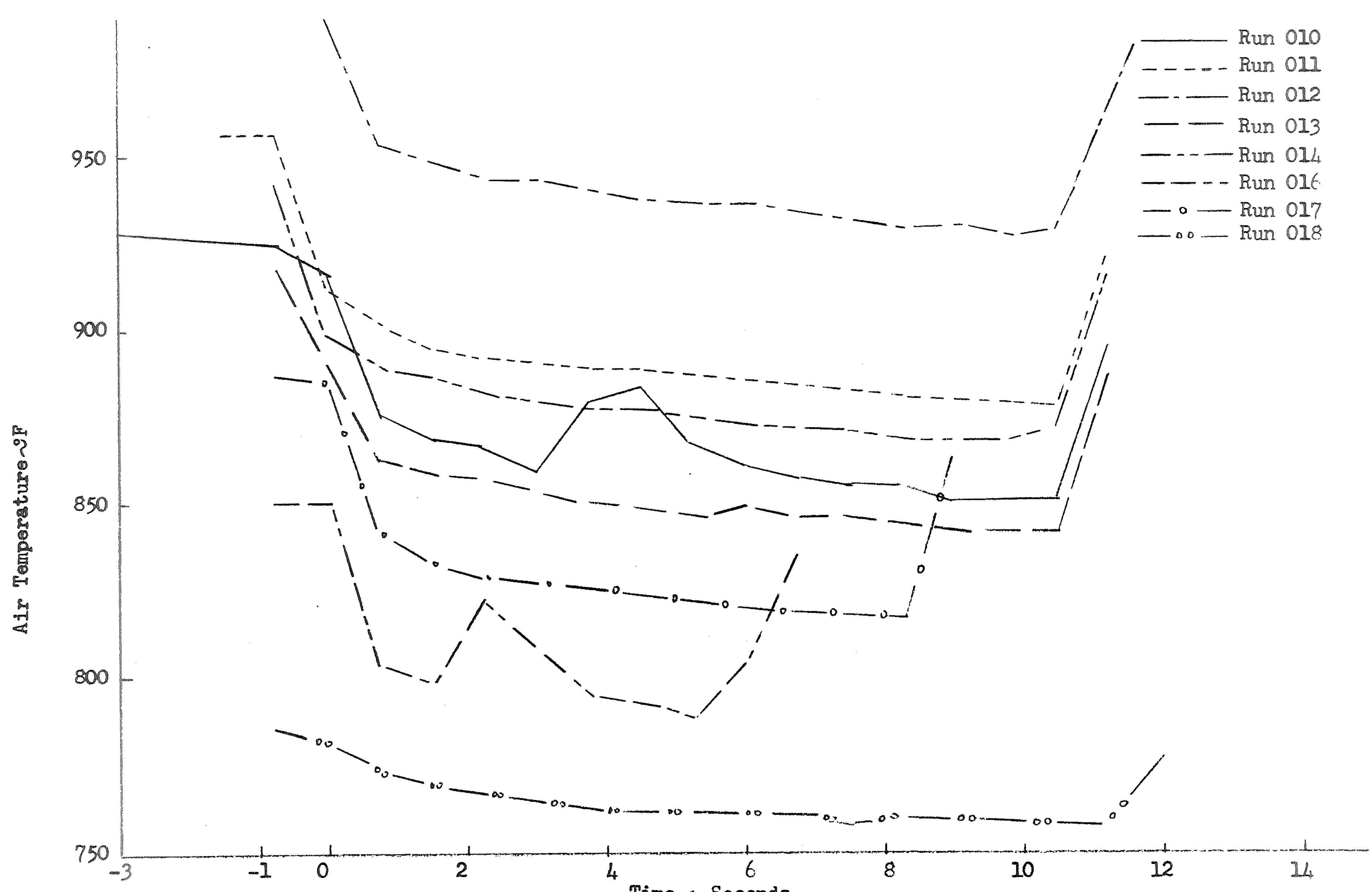

Figure 2-1. Air Inlet Temperature as a Function of Time - Runs 10 to 14 and 16 to 18

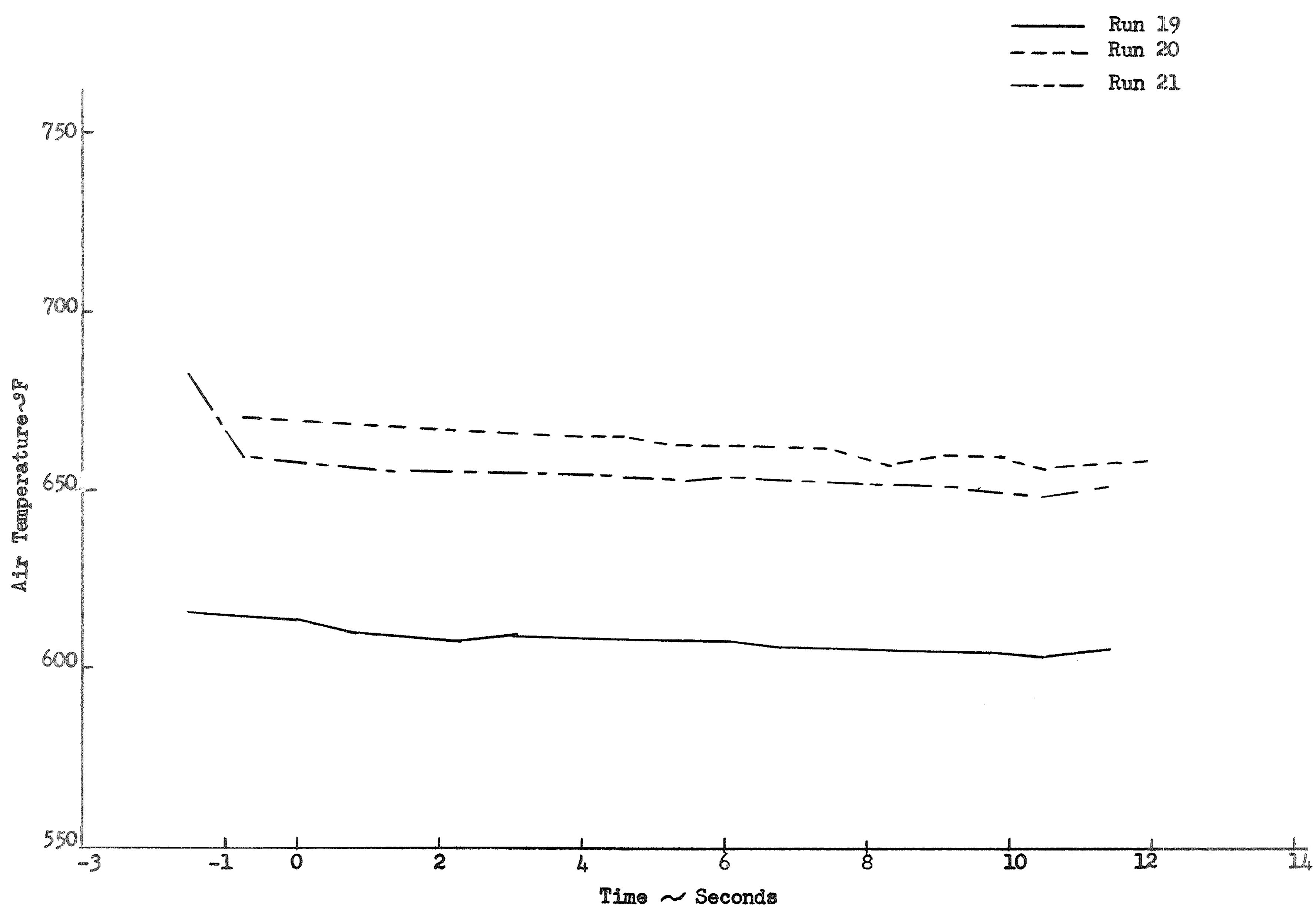

Figure 2-2. Air Inlet Temperature as a Function of Time - Runs 19 to 21

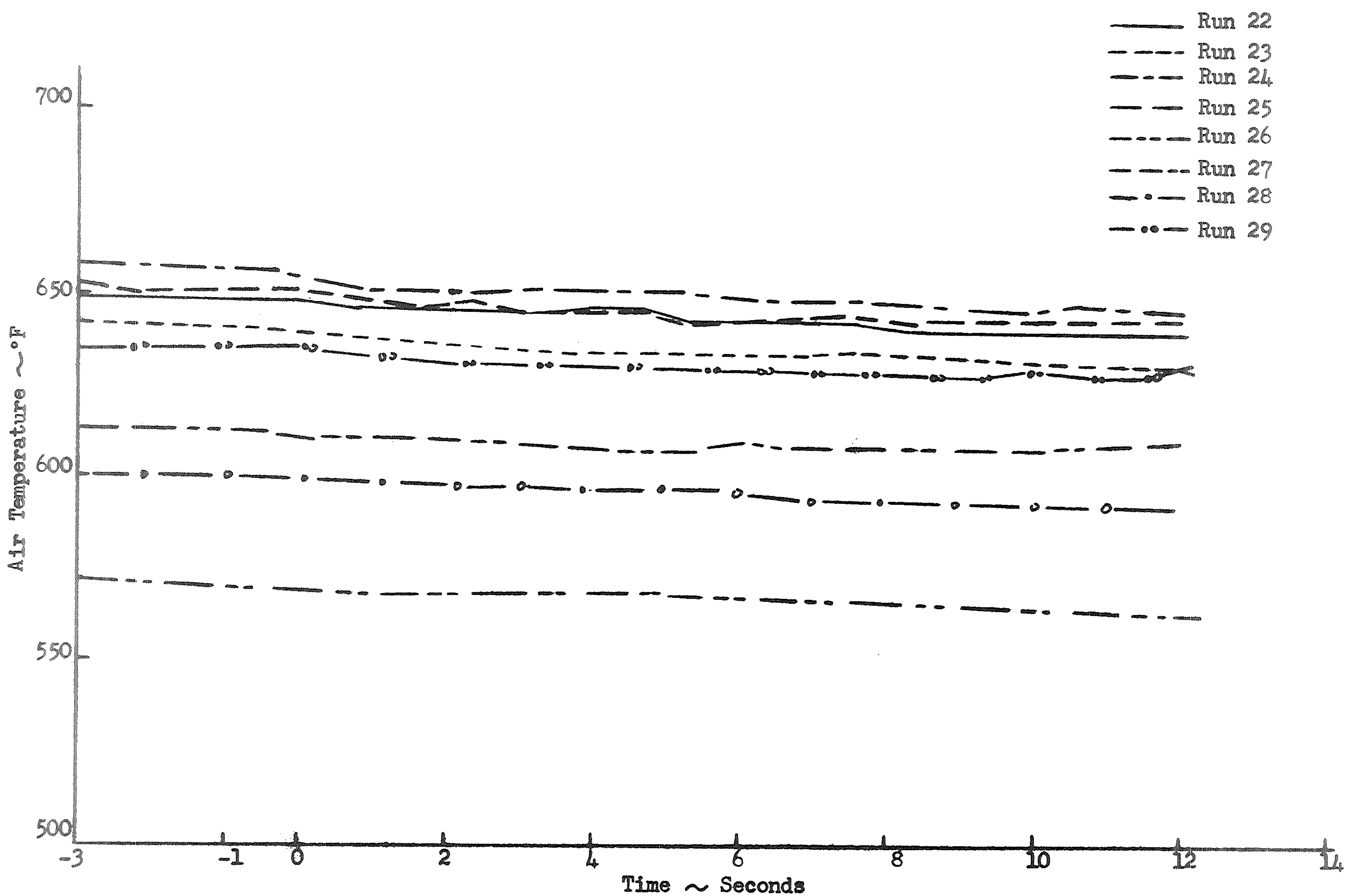

Figure 2-3. Air Inlet Temperature as a Function of Time - Runs 22 to 29

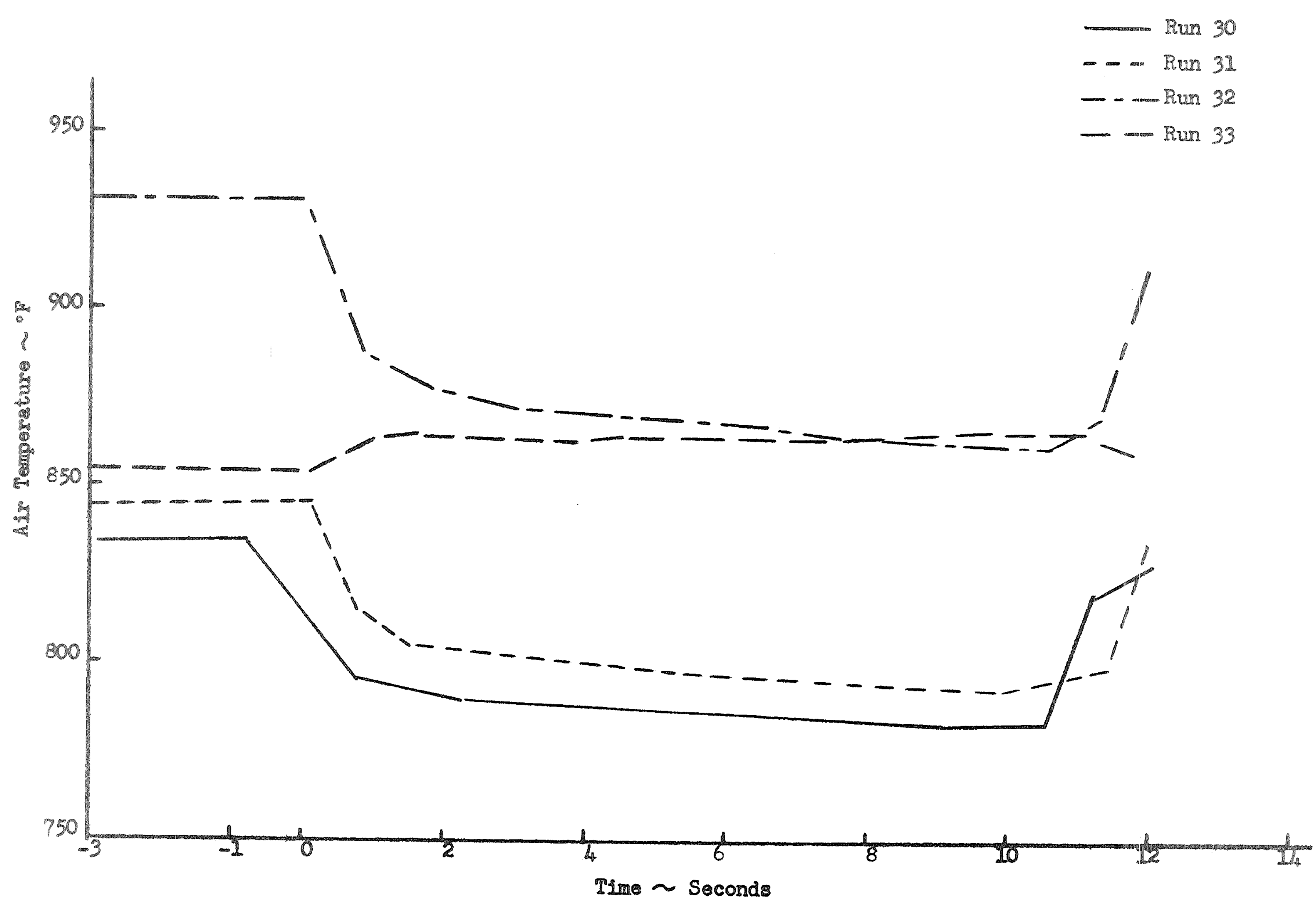

Figure 2-4. Air Inlet Temperature as a function of Time - Runs 30 to 33

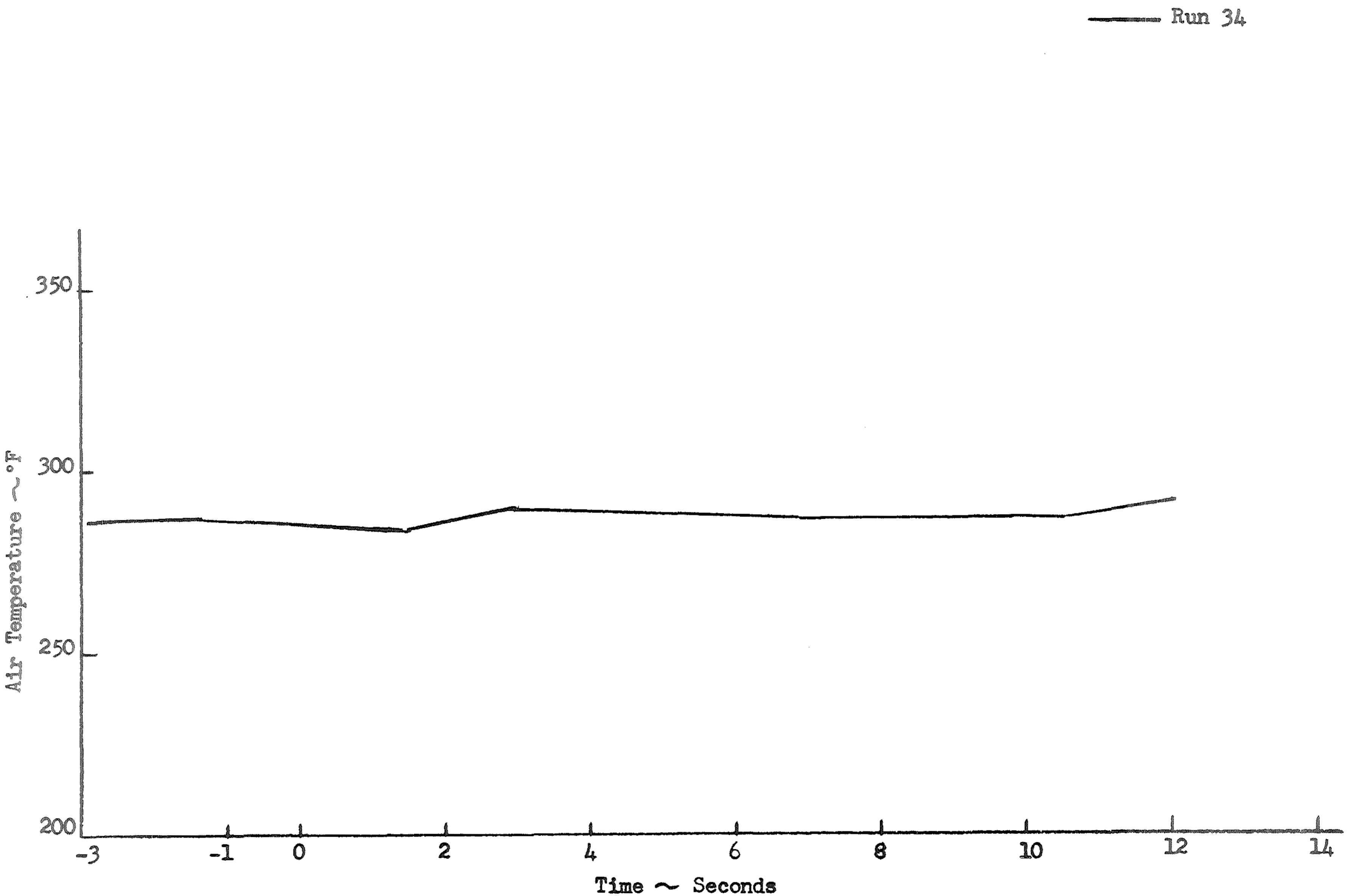

Figure 2-5. Air Inlet Temperature as a Function of Time - Run 34

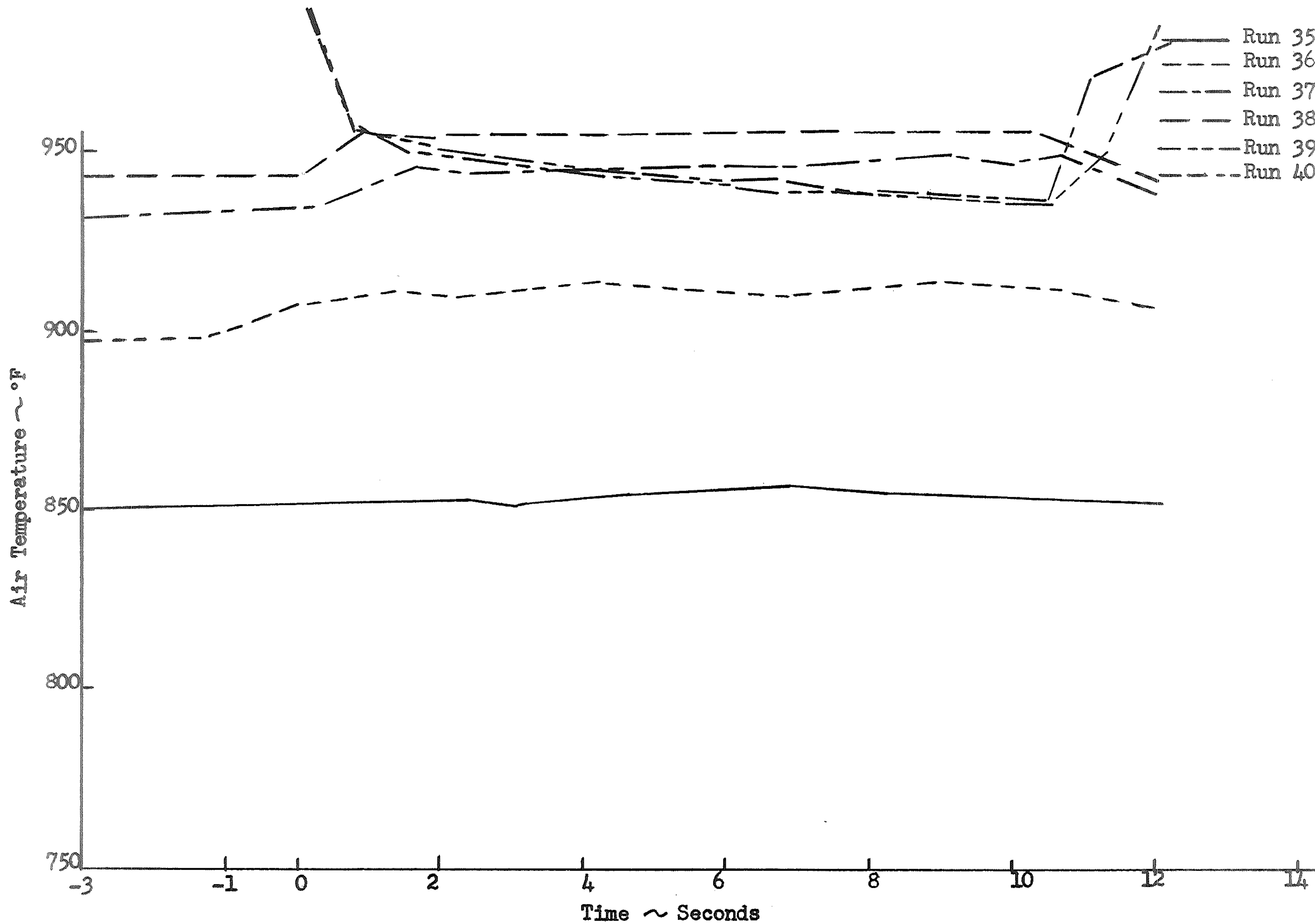

Figure 2-6. Air Inlet Temperature as a Function of Time - Runs 35 to 40

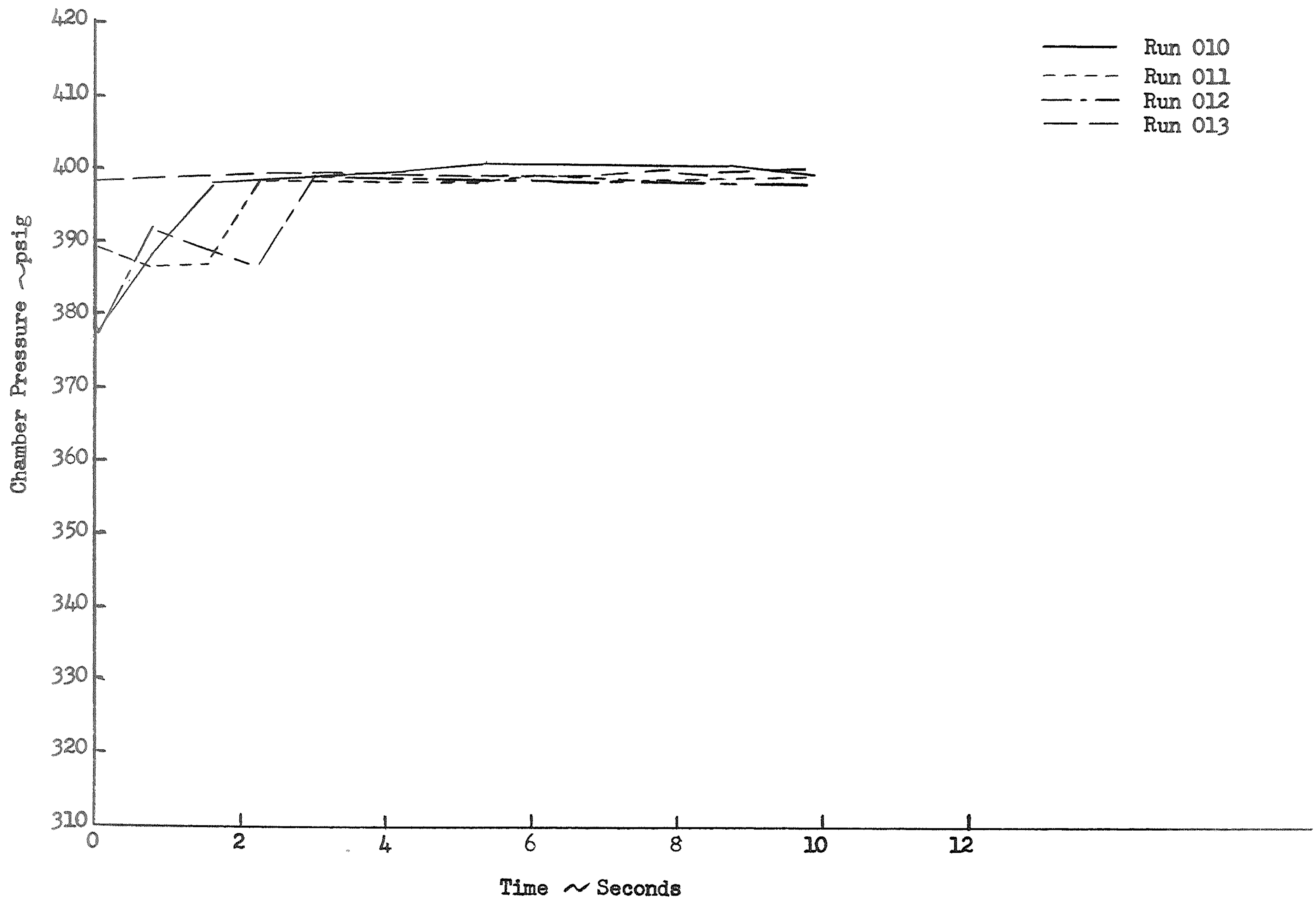

Figure 2-7. Chamber Pressure as a Function of Time - Runs 10 to 13

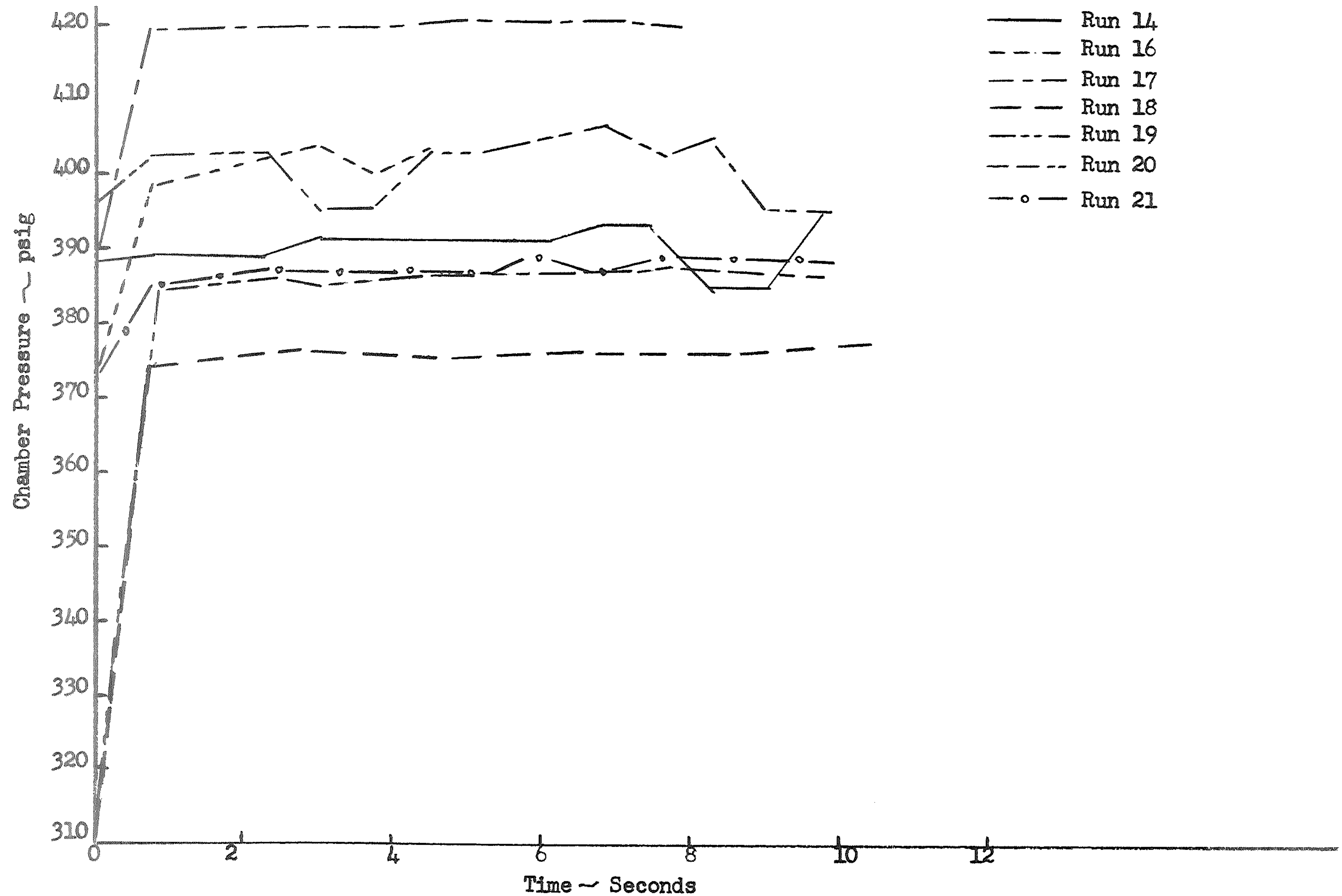

Figure 2-8. Chamber Pressure as a Function of Time - Runs 14 and 16 to 21

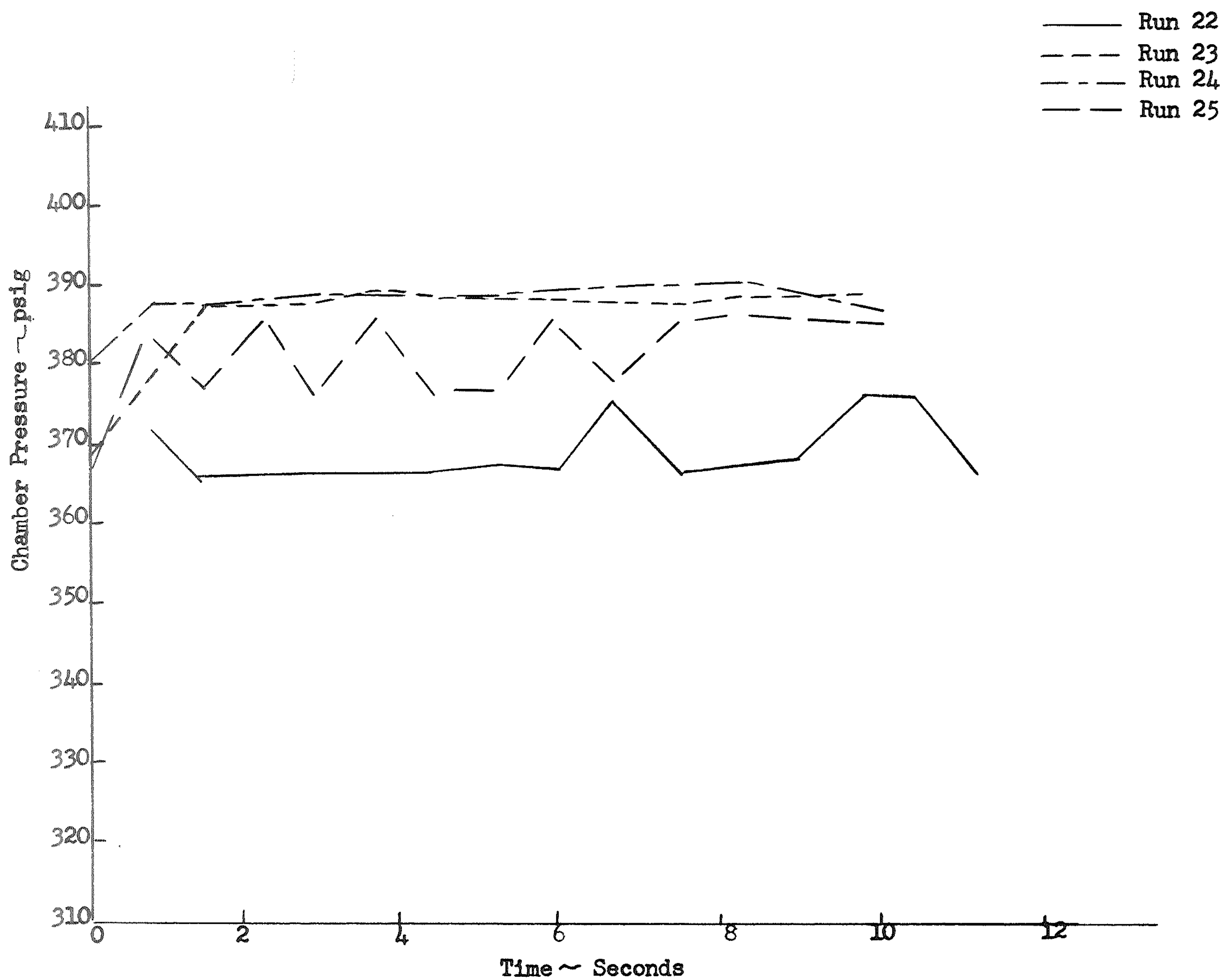

Figure 2-9. Chamber Pressure as a Function of Time - Runs 22 to 25

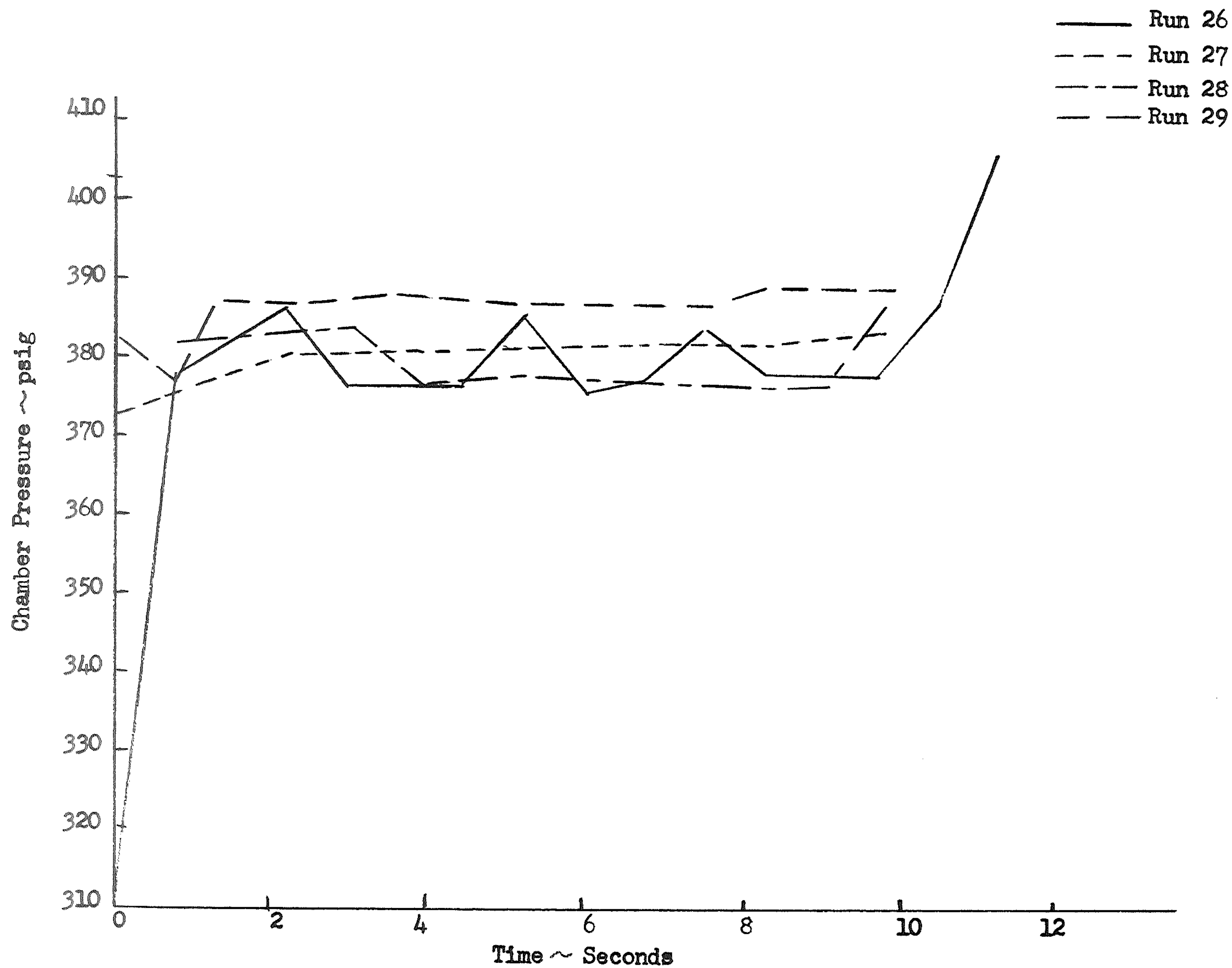

Figure 2-10. Chamber Pressure as a Function of Time - Runs 26 to 29

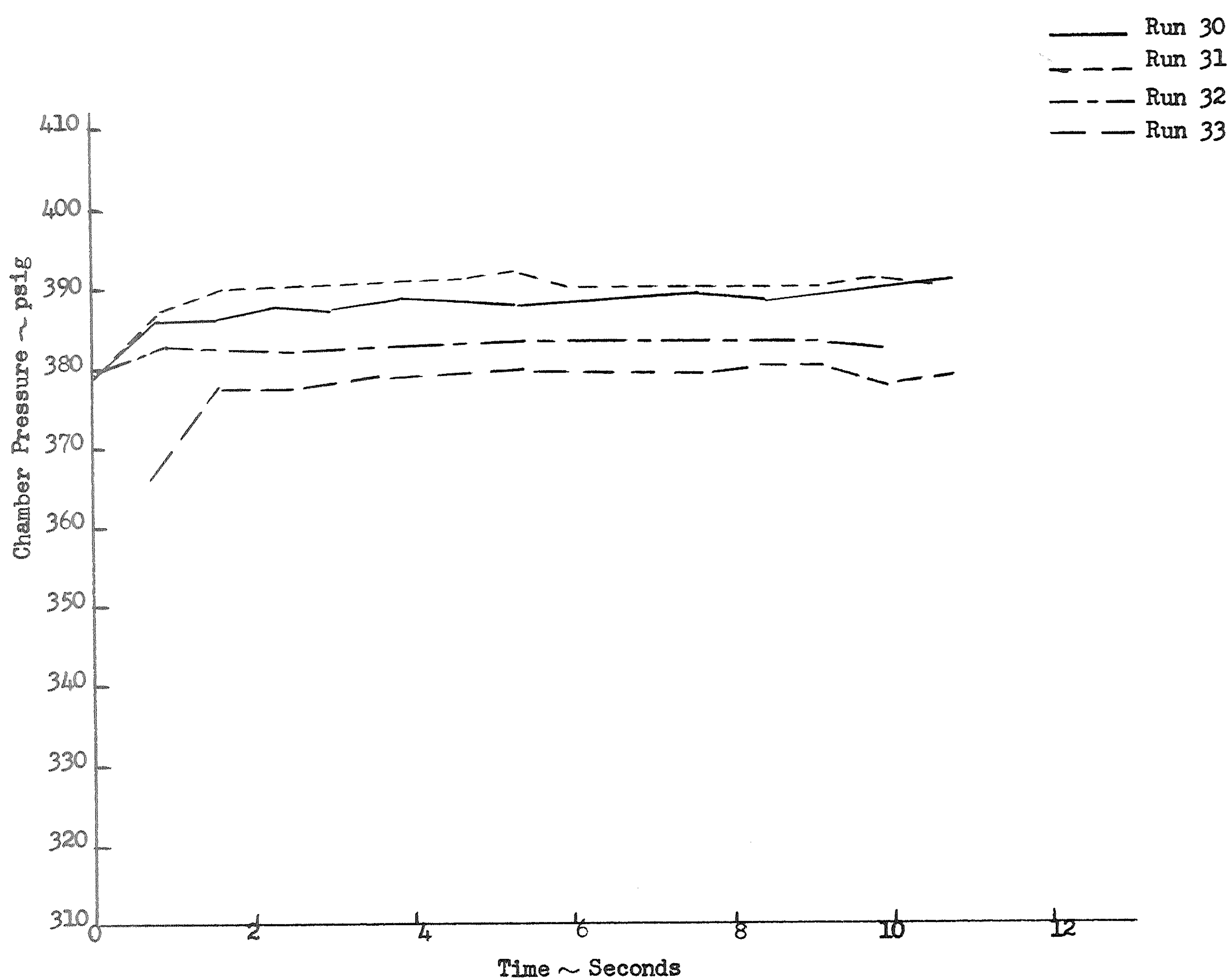

Figure 2-11. Chamber Pressure as a Function of Time - Runs 30 to 33

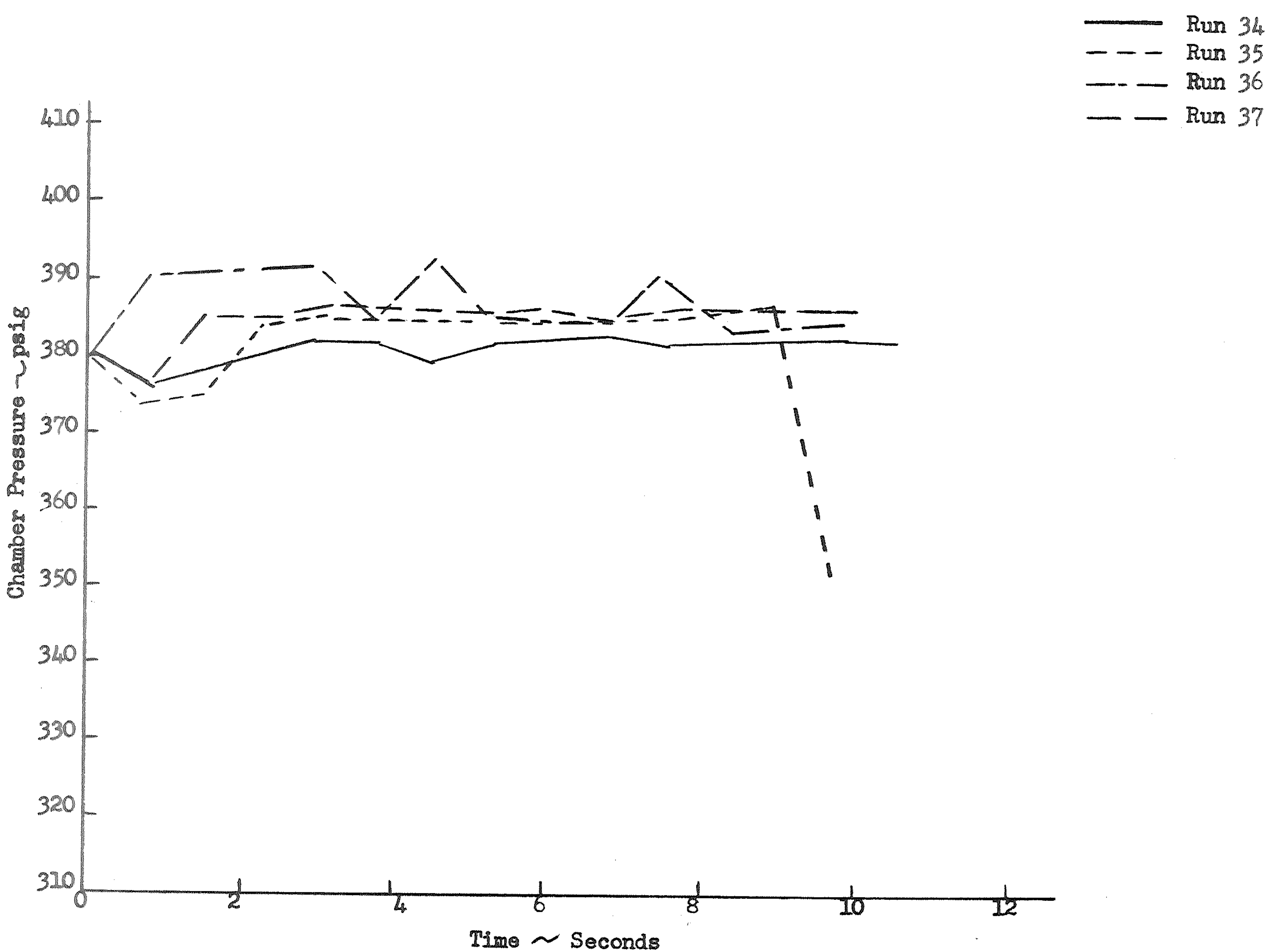

Figure 2-12. Chamber Pressure as a Function of Time - Runs 34 to 37

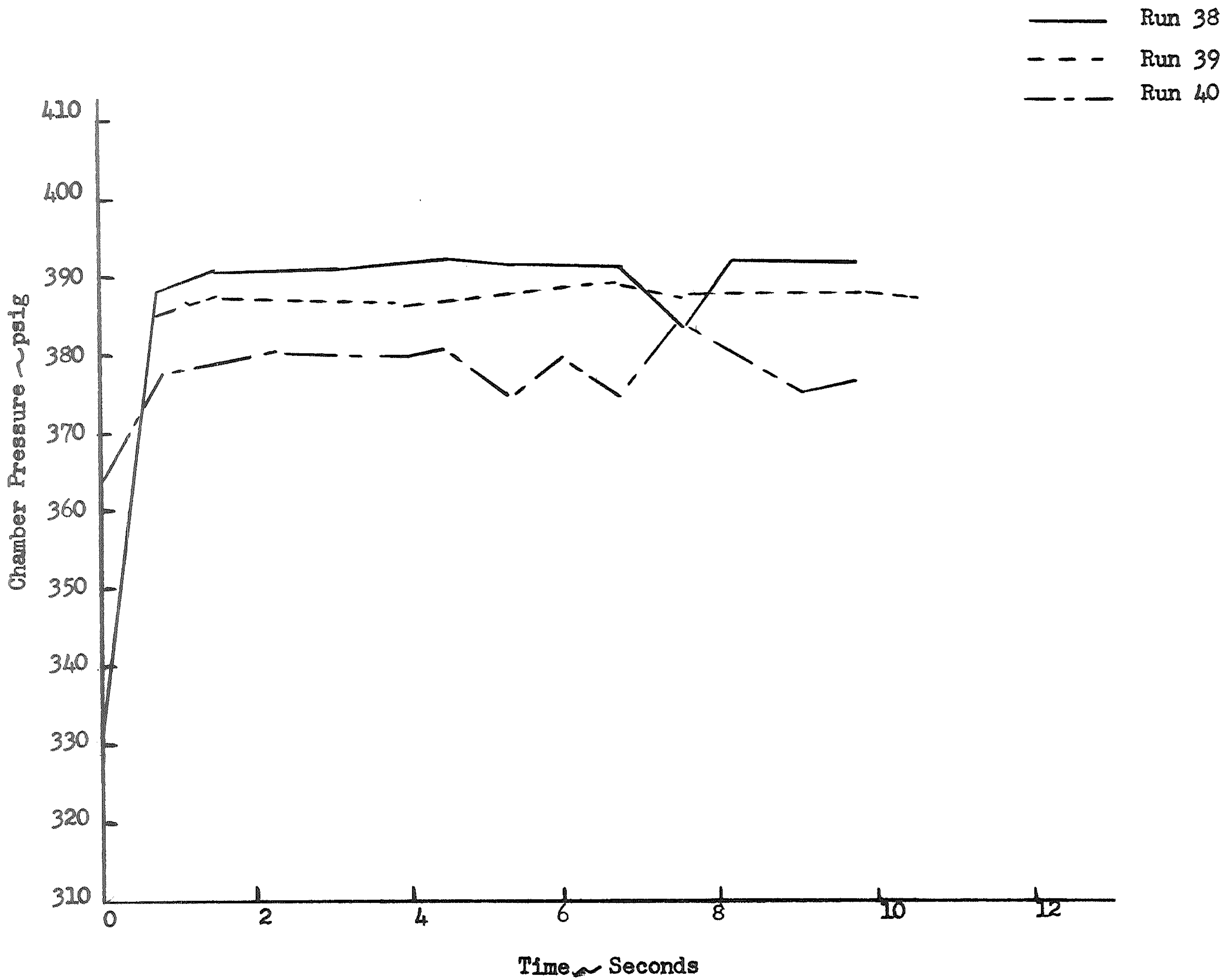

Figure 2-13. Chamber Pressure as a Function of Time - Runs 38 to 40

APPENDIX 3

ZONE RADIOMETRY DATA

Graphical representation of the zone radiometry data are presented in Figs. 3-1 to 3-55. For clarity, the data are presented in two groupings. Those data that are directly calculated from the spectrometer output, i.e., flame radiance, N, and emissivity, ϵ (Figs. 3-1 to 3-29) and those data that are derived from subsidiary calculations, i.e., plots of apparent flame temperature, T, and H_2O partial pressure, P (Figs. 3-30 to 3-55). The physical location of the instrumentation positions is illustrated in Fig. 3-56 and a schematic of the test section denoting principal dimensions is shown in Fig. 3-57. The conversion of line-of-sight (LOS) to the physical dimensions of the apparatus is given in Table 3-1. It should be noted that LOS refers to the vertical axis and the position numbers refer to the longitudinal or horizontal axis.

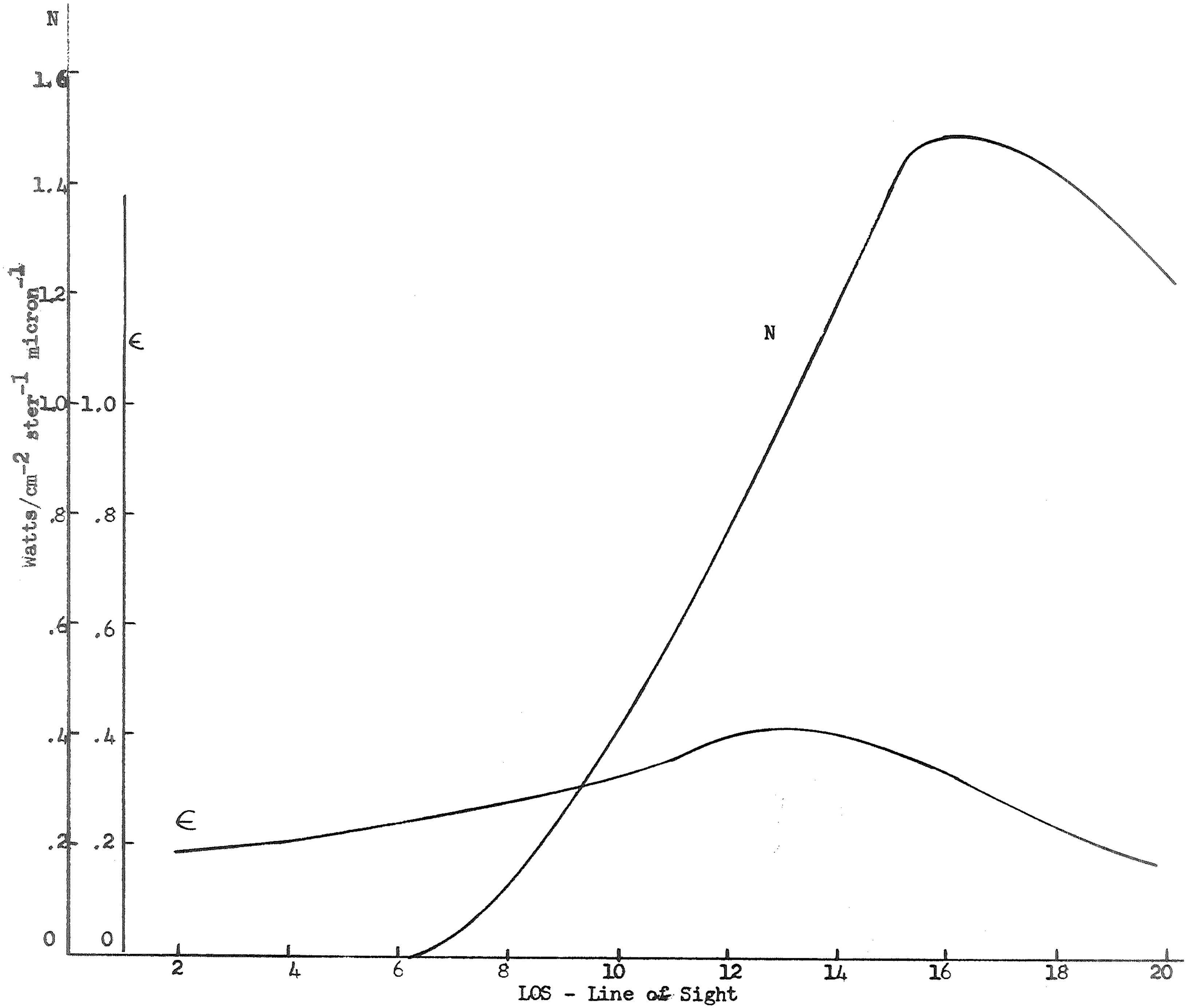

Figure 3-1 Flame Radiance and Emissivity - Run 021 Position 8

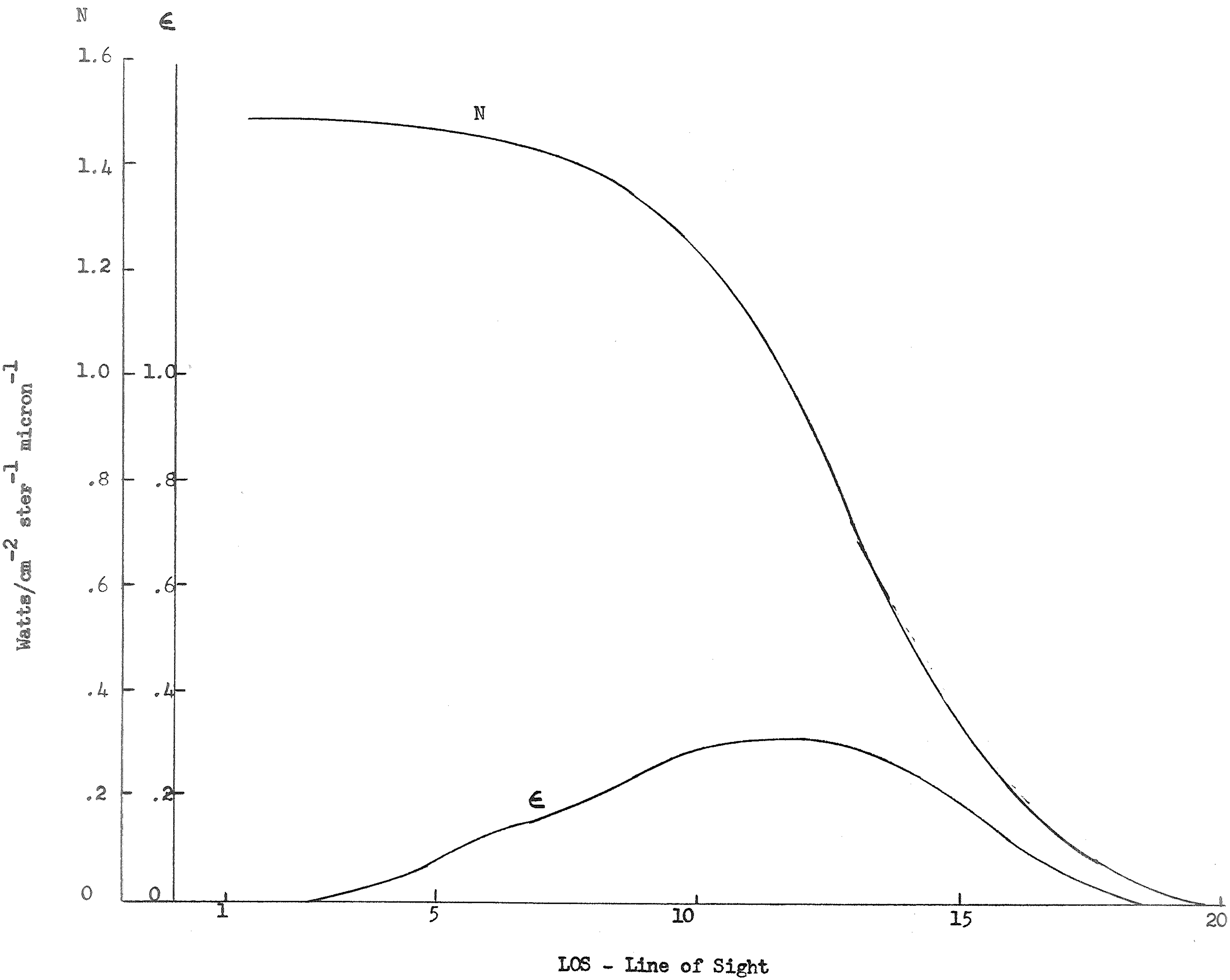

Figure 3-2 Flame Radiance and Emissivity - Run 10 Position 8

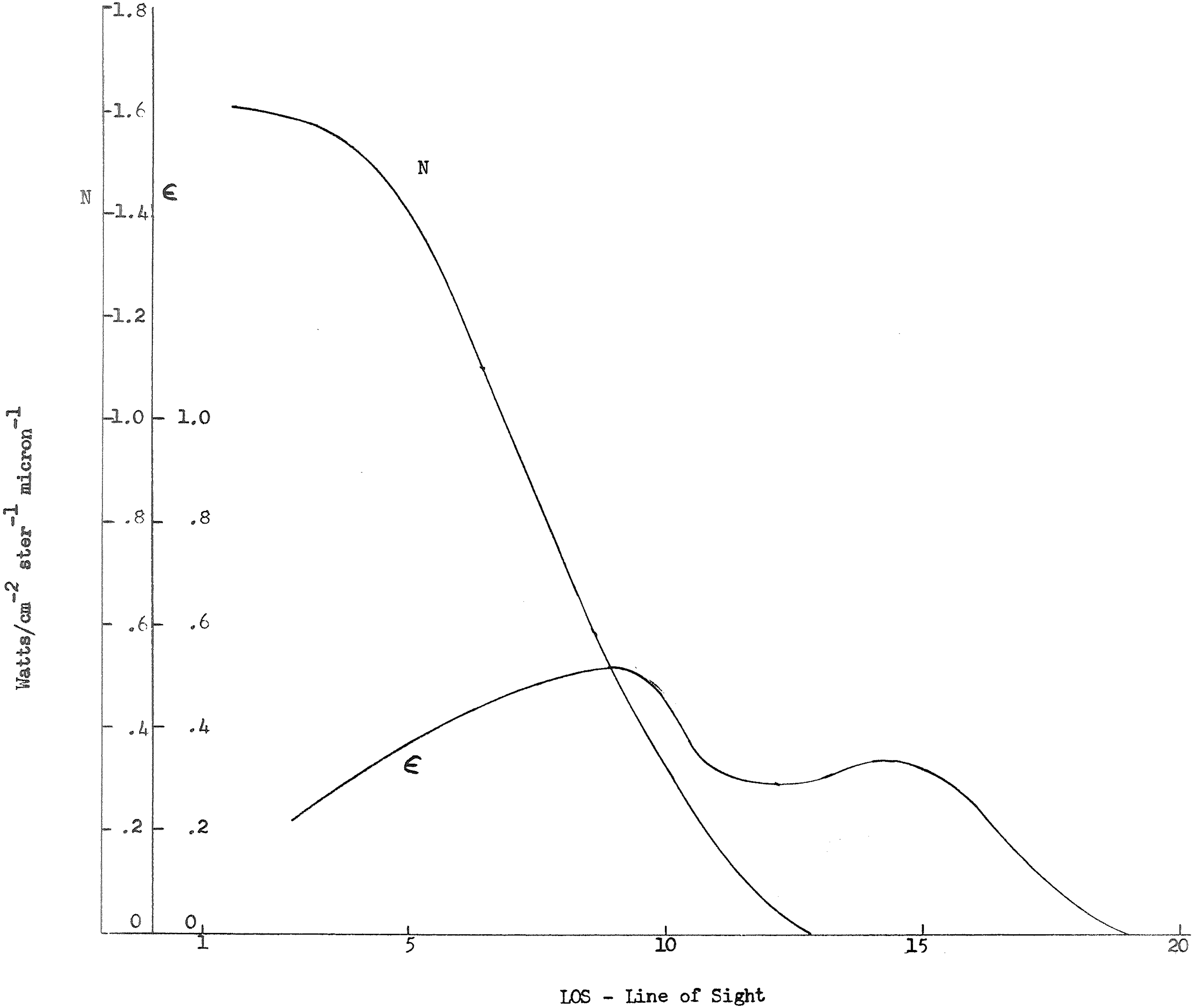

Figure 3-3 Flame radiance and emissivity - Run 11 Position 3

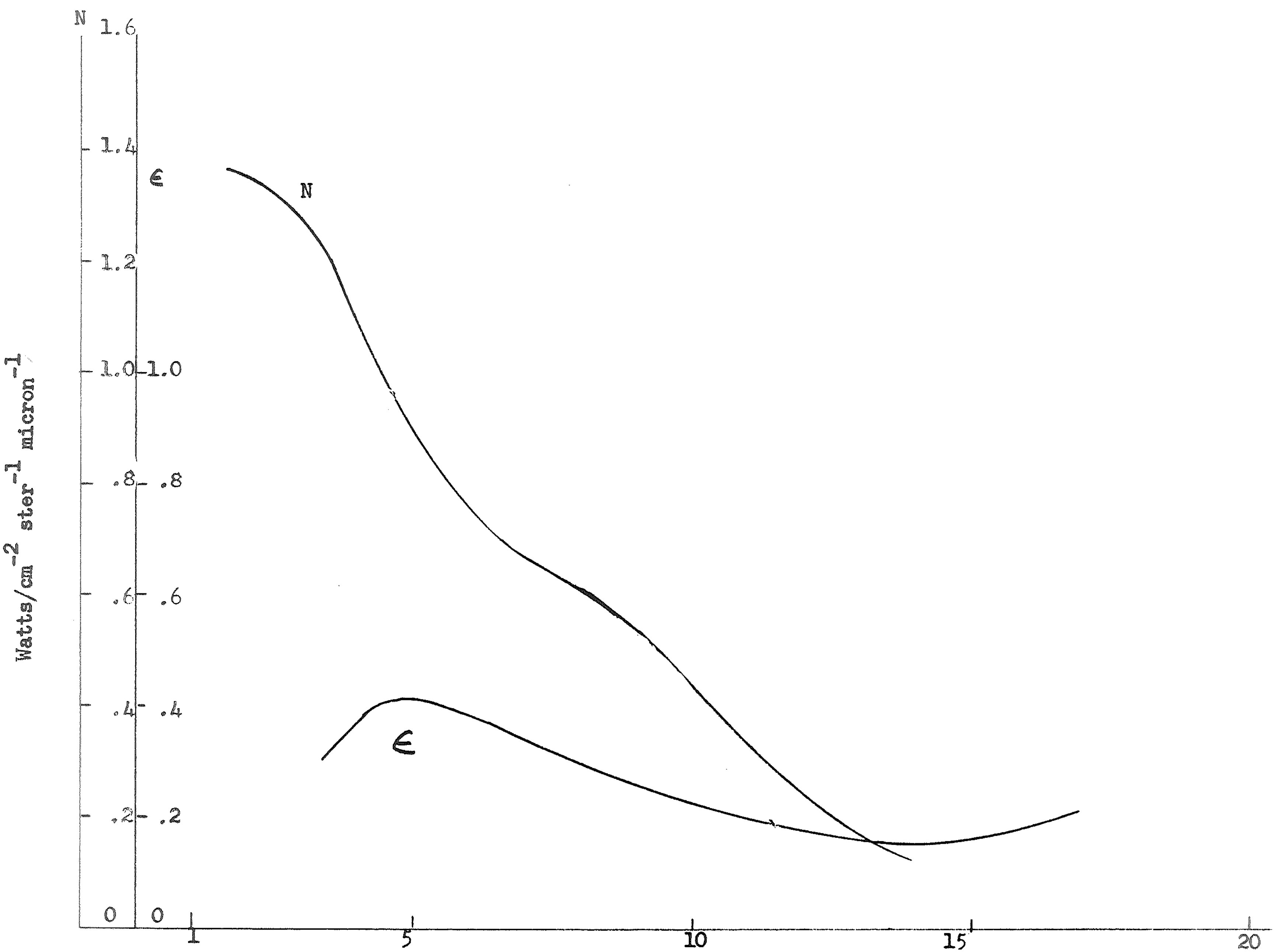

Figure 3-4 Flame radiance and emissivity - Run 12 Position 6

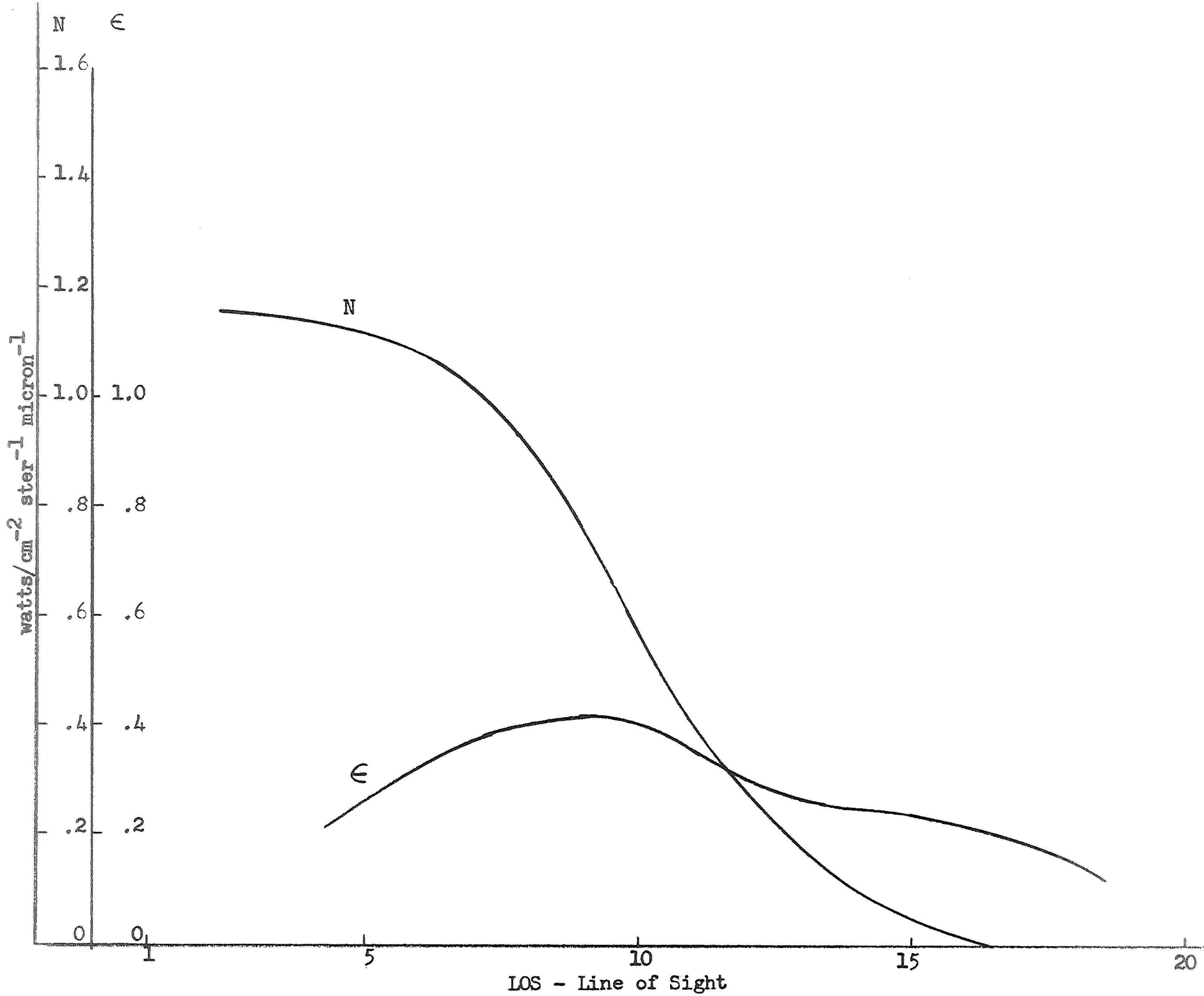

Figure 3-5 Flame radiance and emissivity - Run 13 Position 4

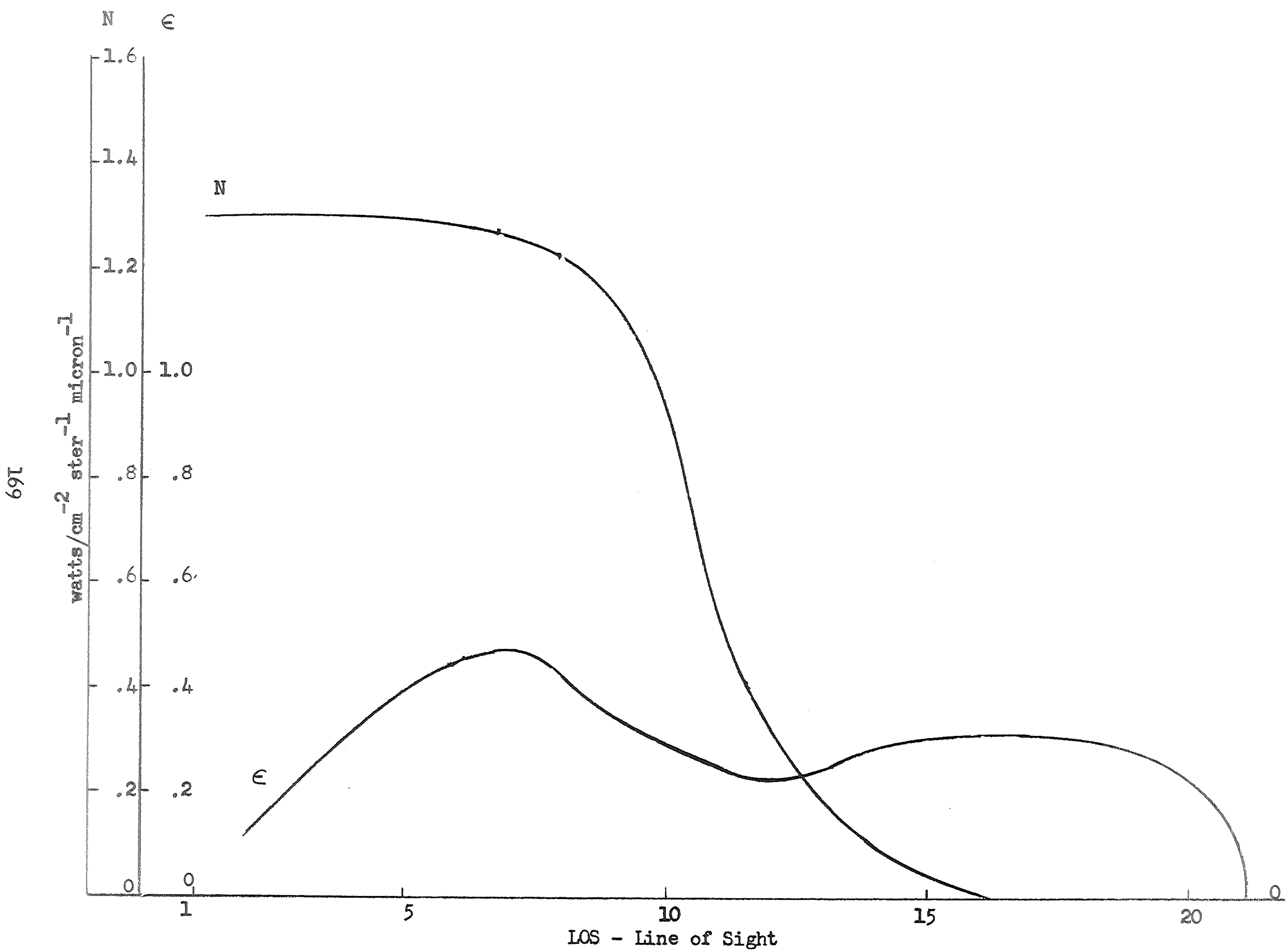

Figure 3-6 Flame radiance and emissivity - Run 14 Position 5

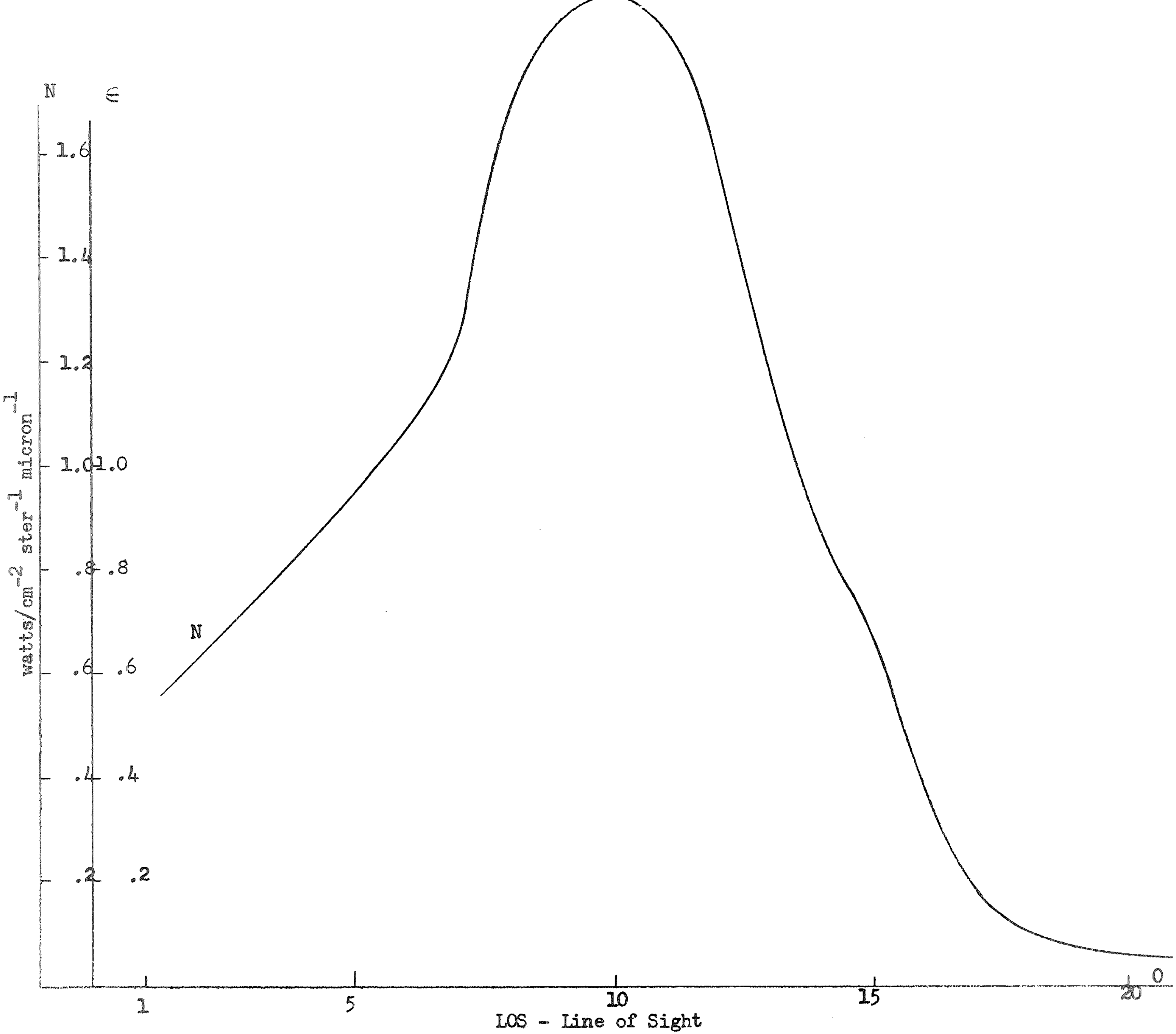

Figure 3-7 Flame radiance and emissivity - Run 16 Position 10 from top

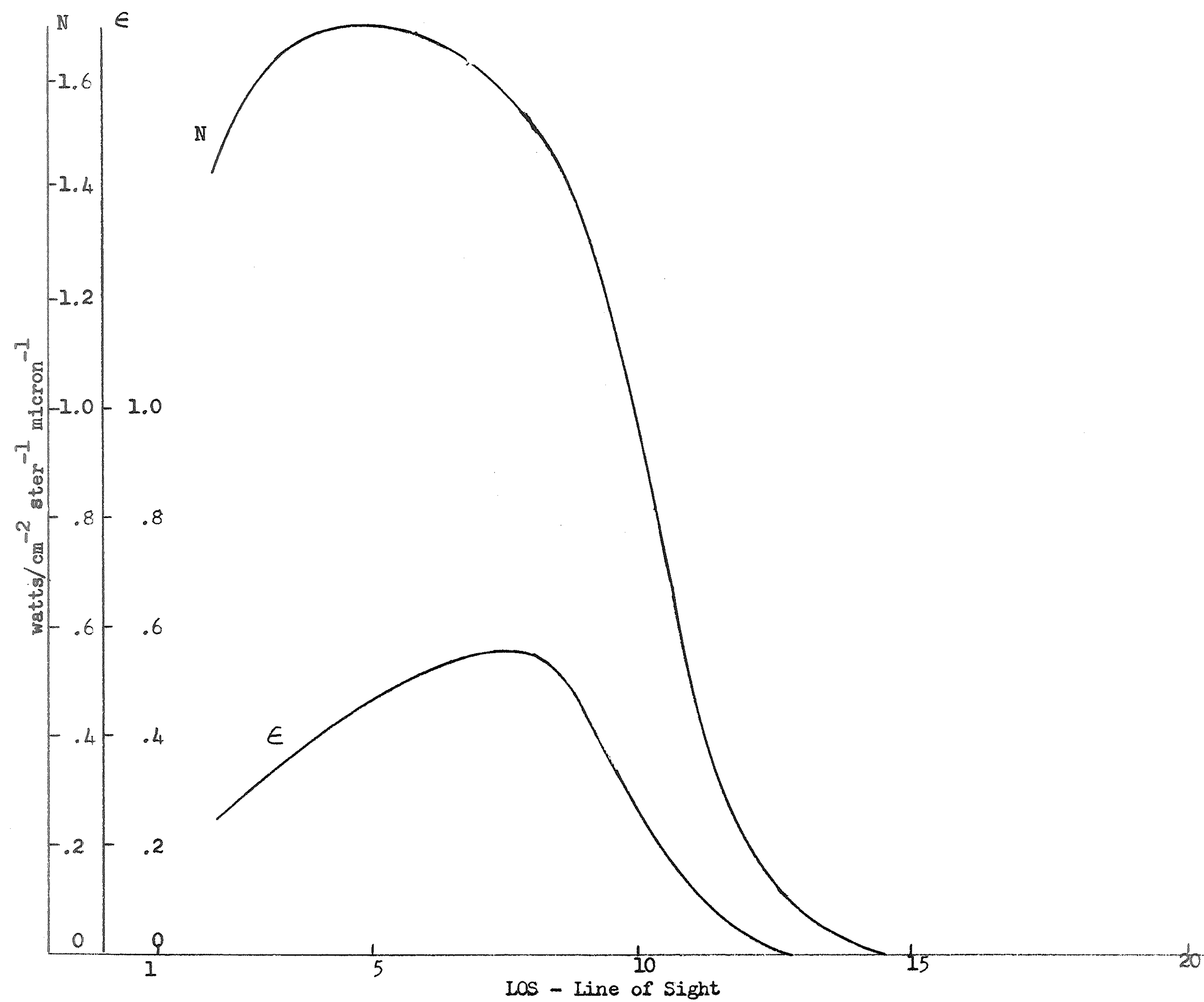

Figure 3-8 Flame radiance and emissivity - Run 17 Position 1

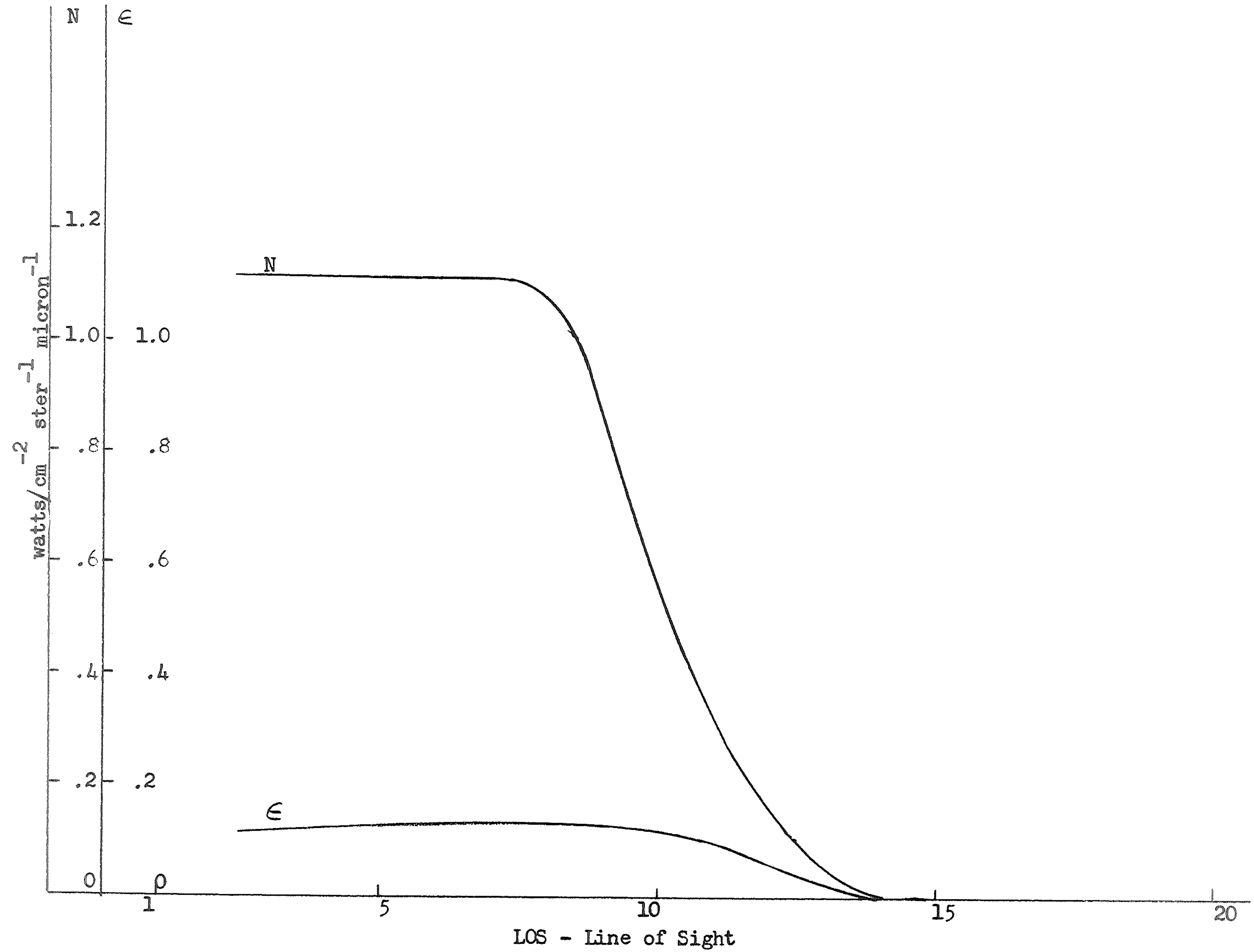

Figure 3-9 Flame radiance and emissivity - Run 18 Position 2

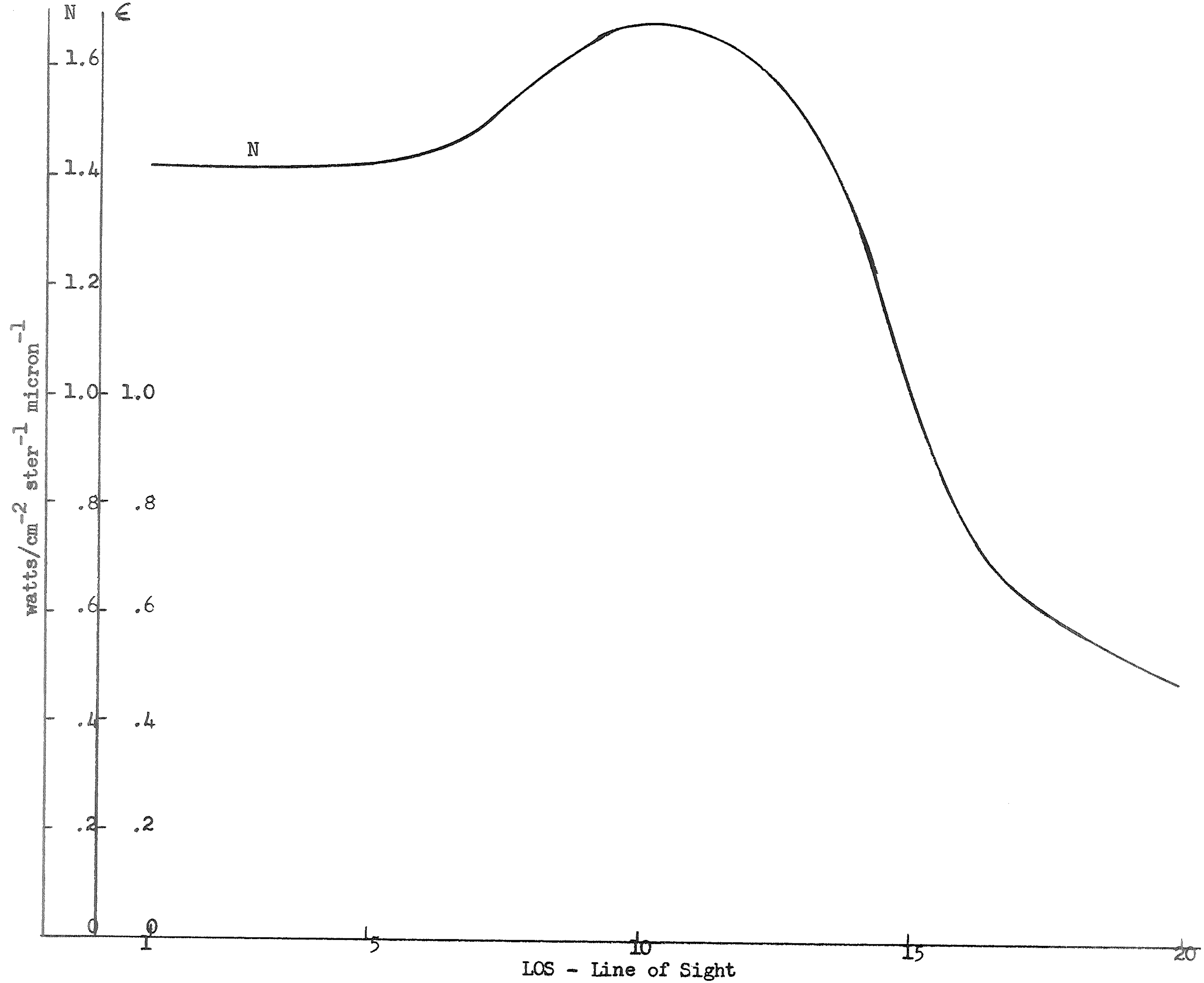

Figure 3-10 Flame radiance and emissivity - Run 19 Position 10

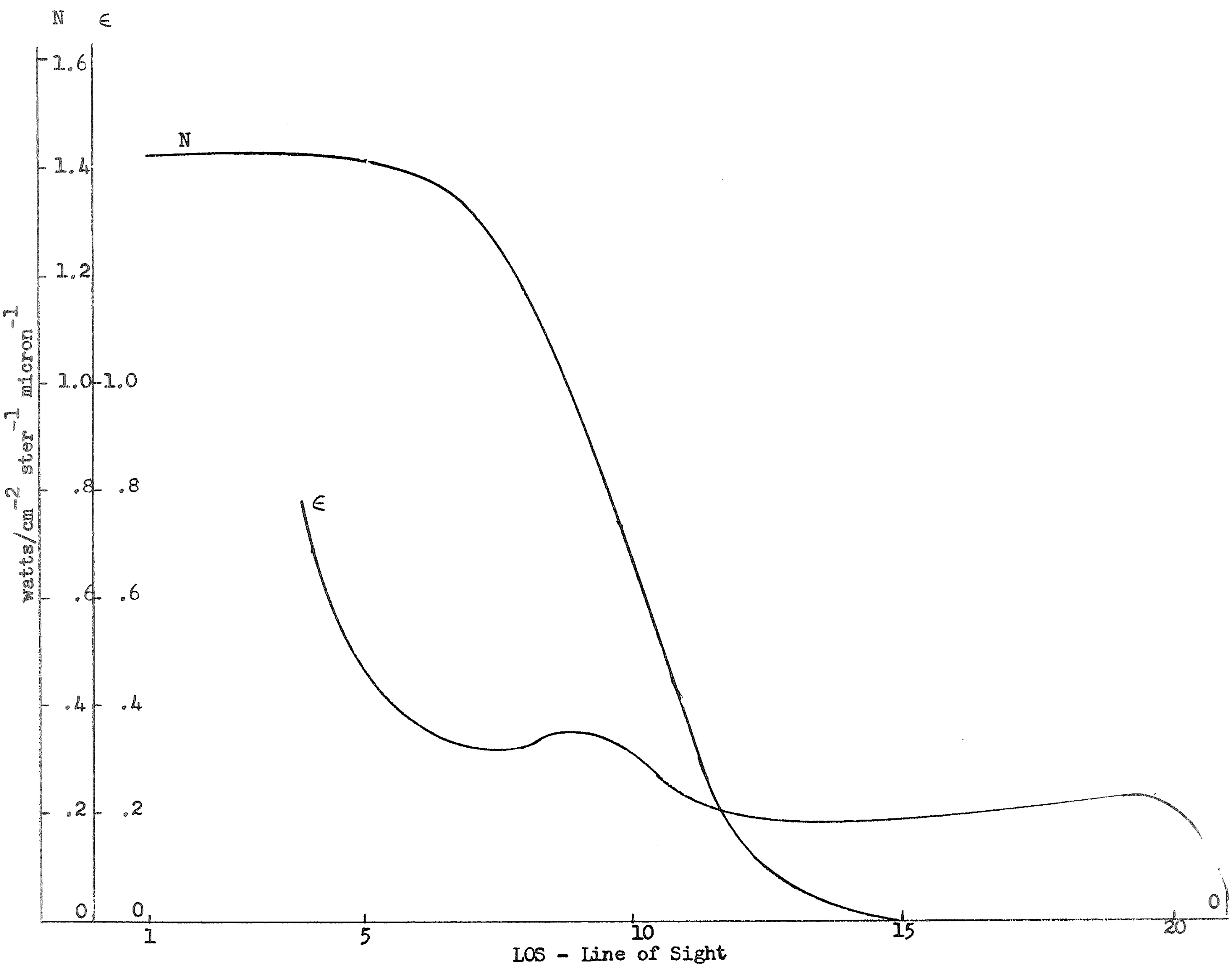

Figure 3-11 Flame radiance and emissivity - Run 20 Position 2

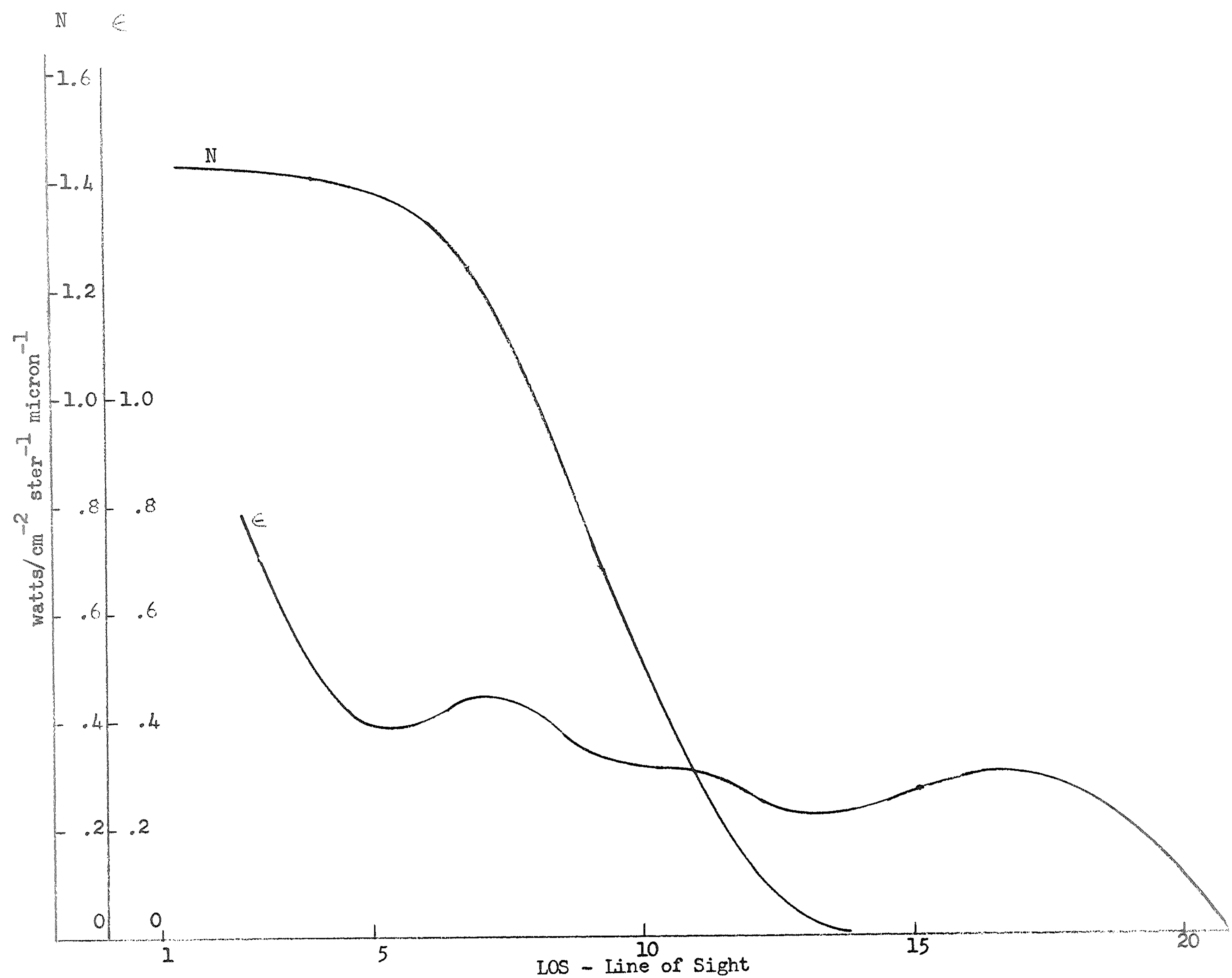

Figure 3-12 Flame radiance and emissivity - Run 21 Position 3

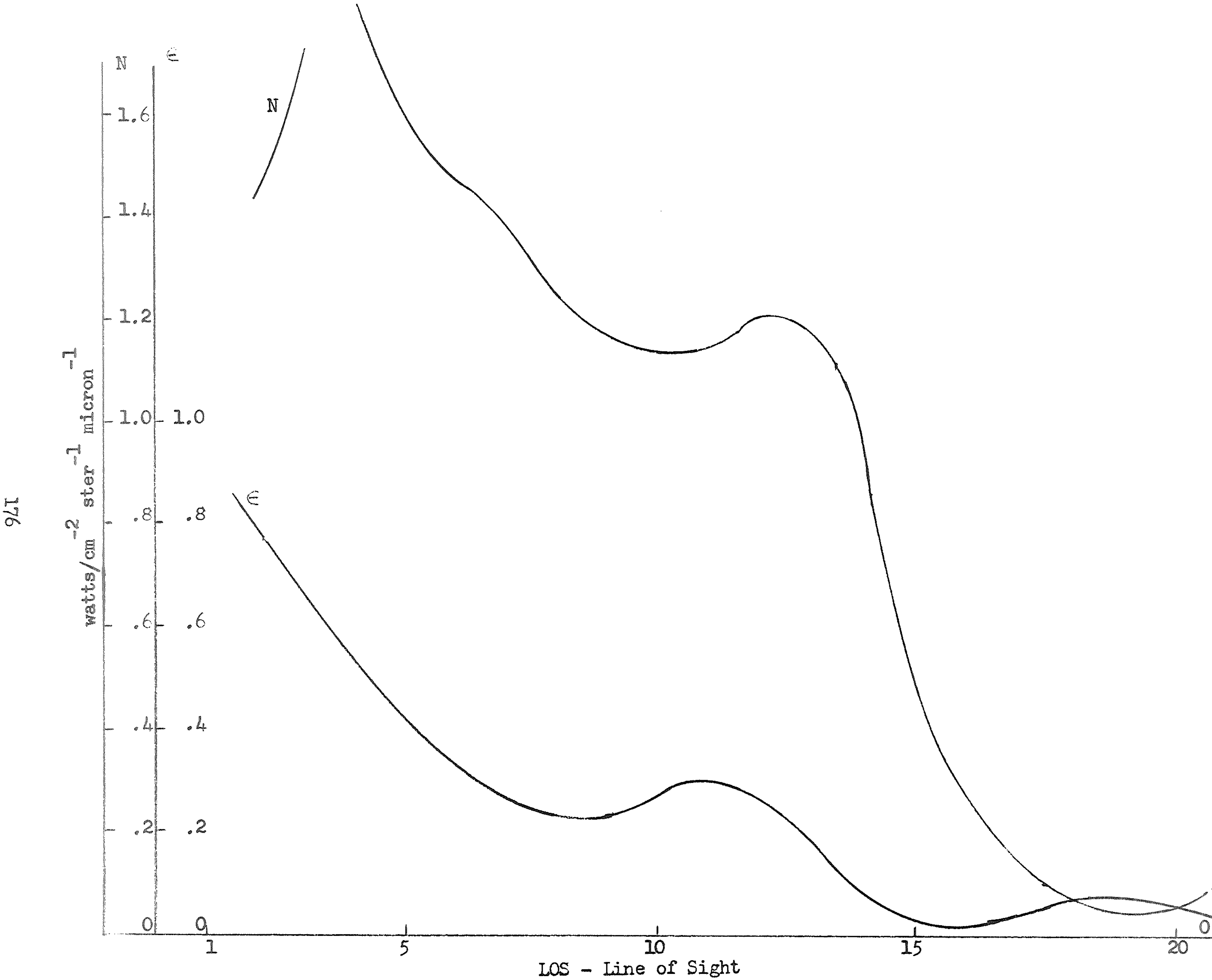

Figure 3-13 Flame radiance and emissivity - Run 22 Position 8 1/2

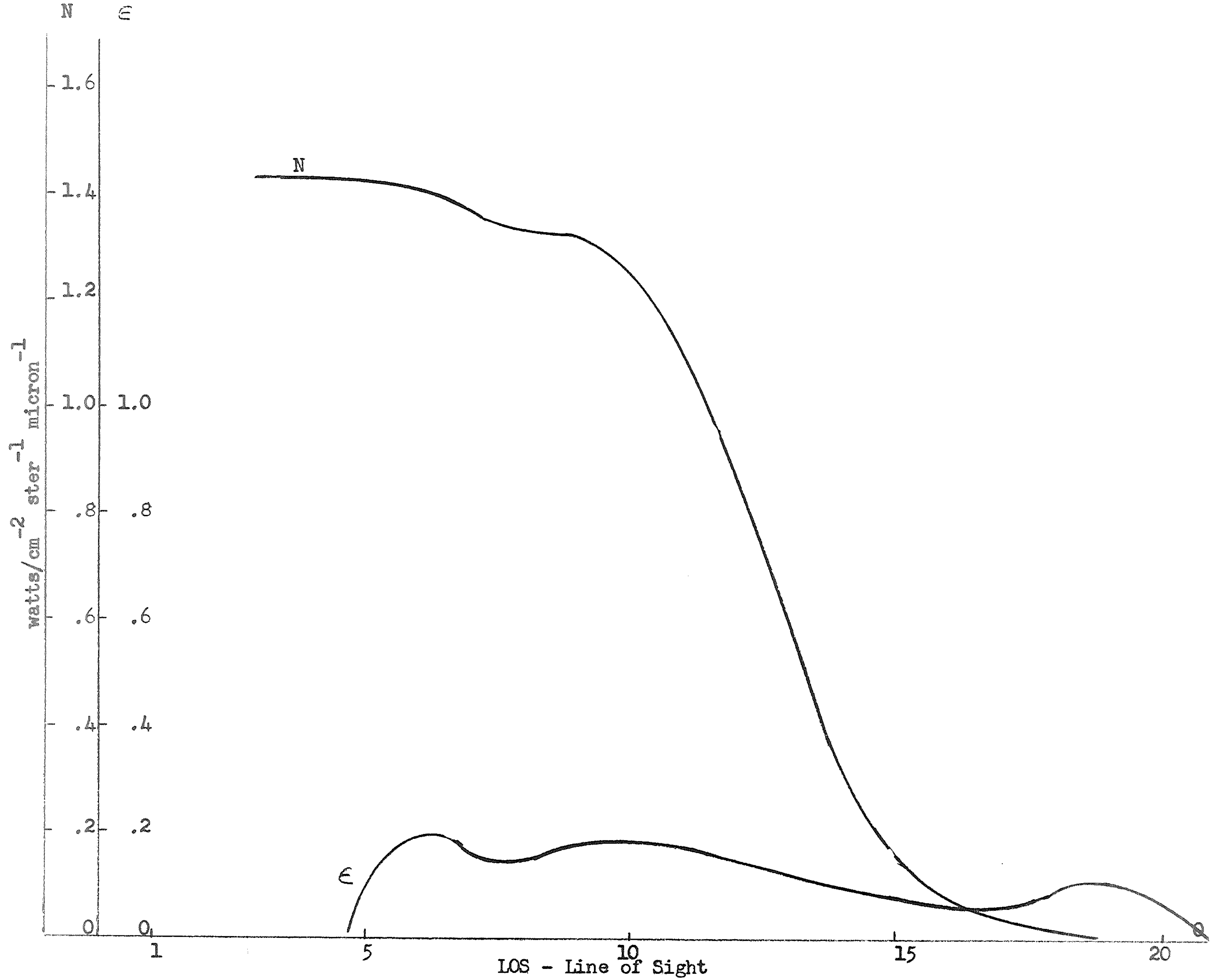

Figure 3-14 Flame radiance and emissivity - Run 23 Position 5

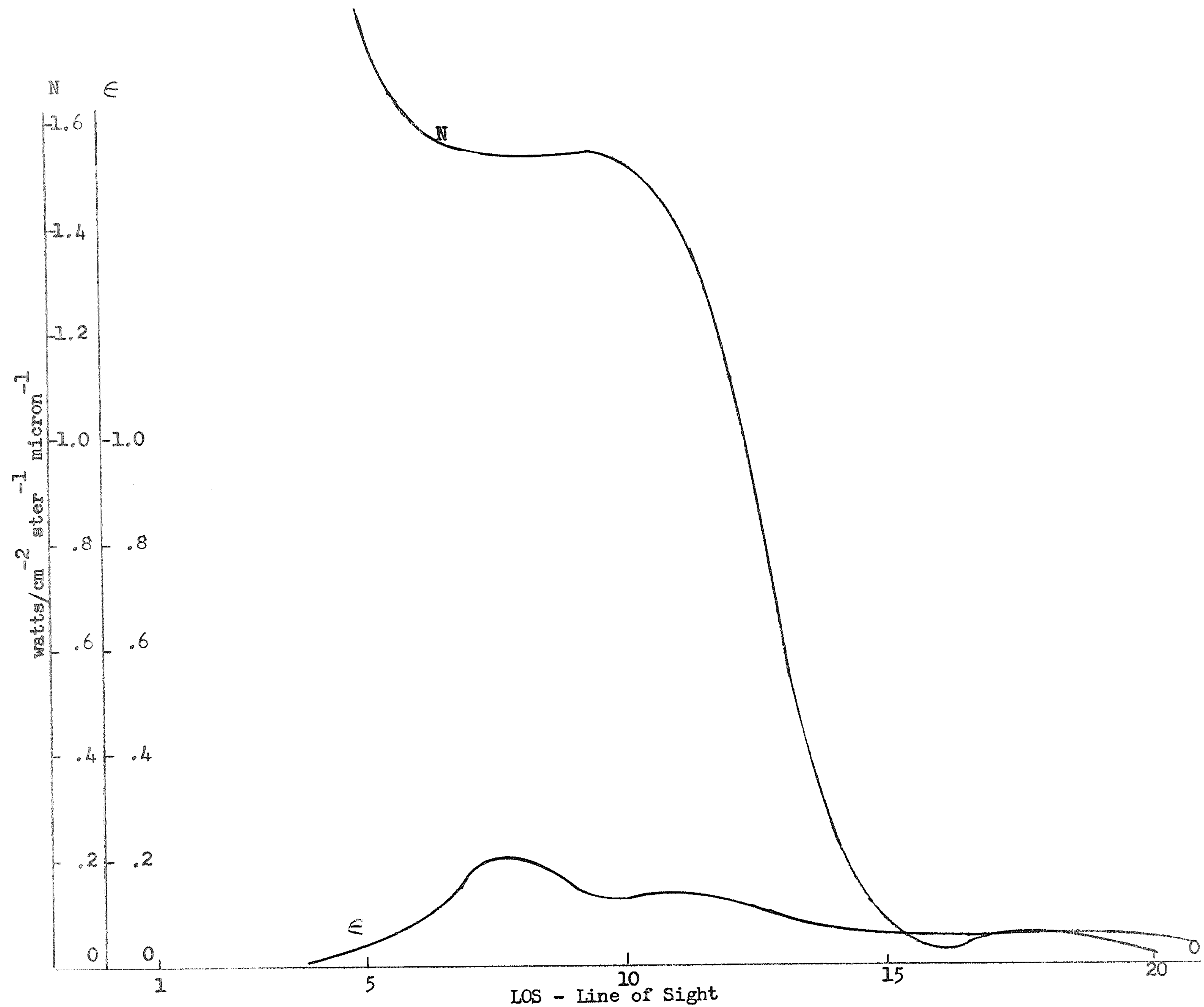

Figure 3-15 Flame radiance and emissivity - Run 24 Position 6

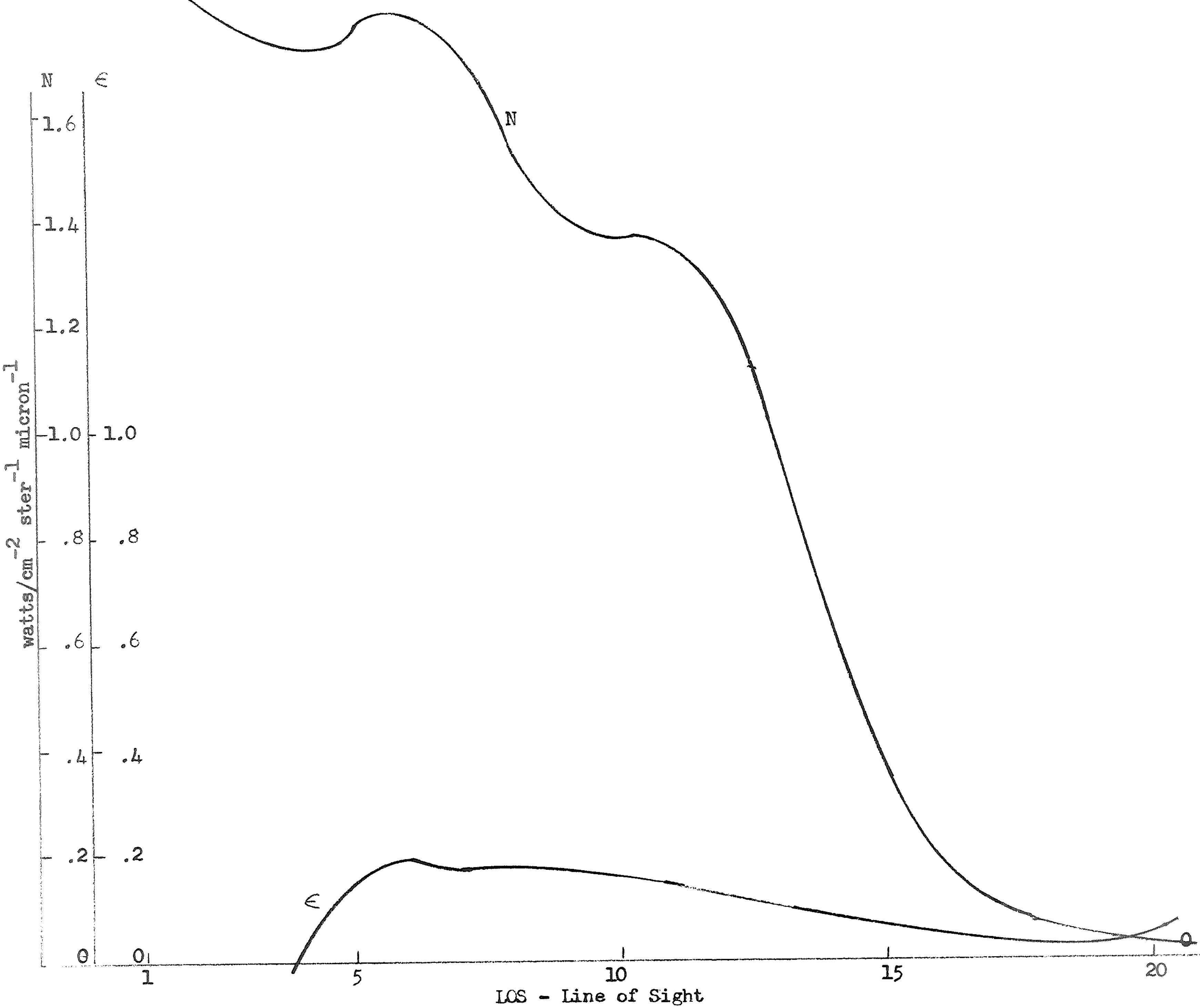

Figure 3-16 Flame radiance and emissivity - Run 25 Position 7

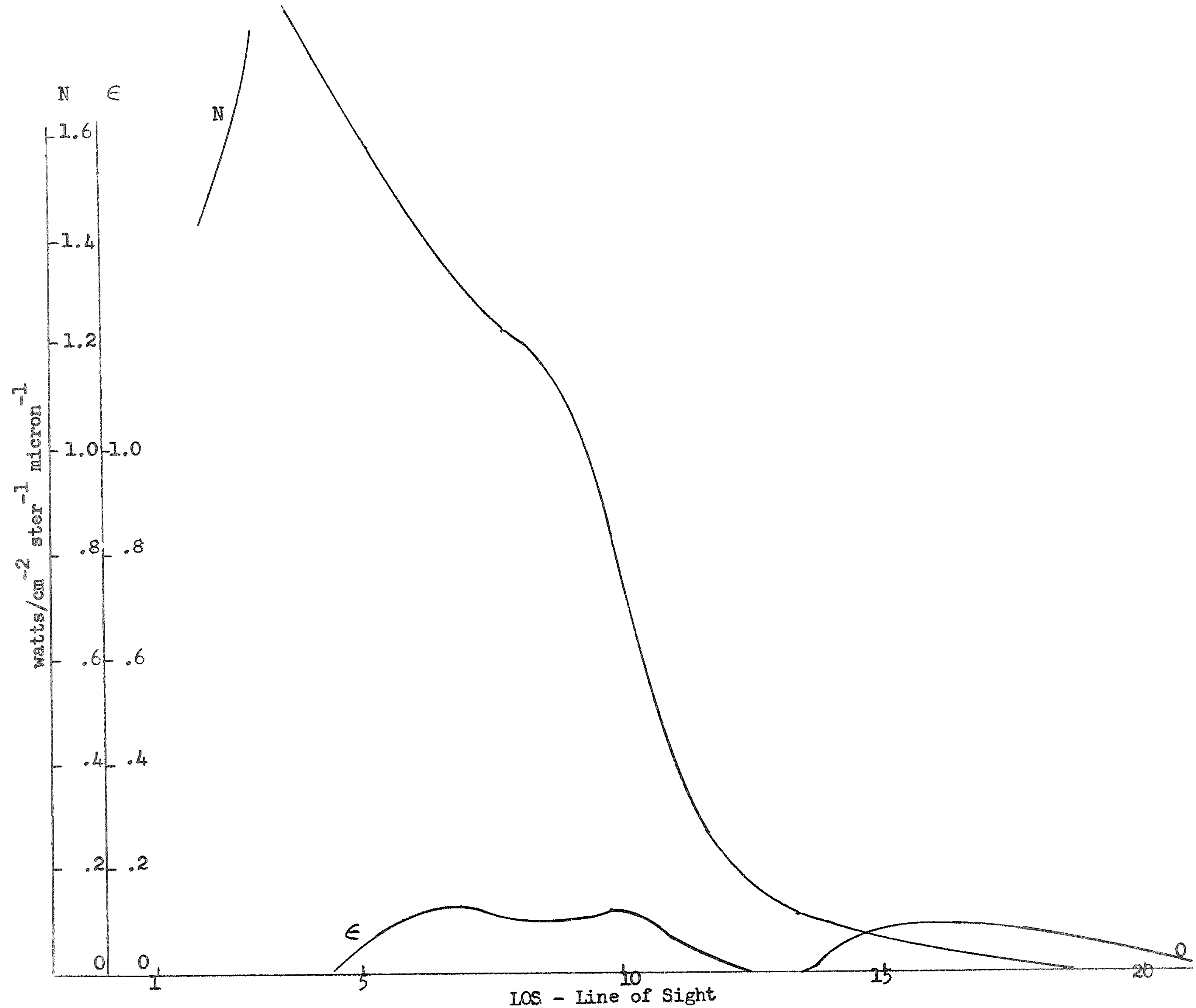

Figure 3-17 Flame radiance and emissivity - Run 26 Position 1

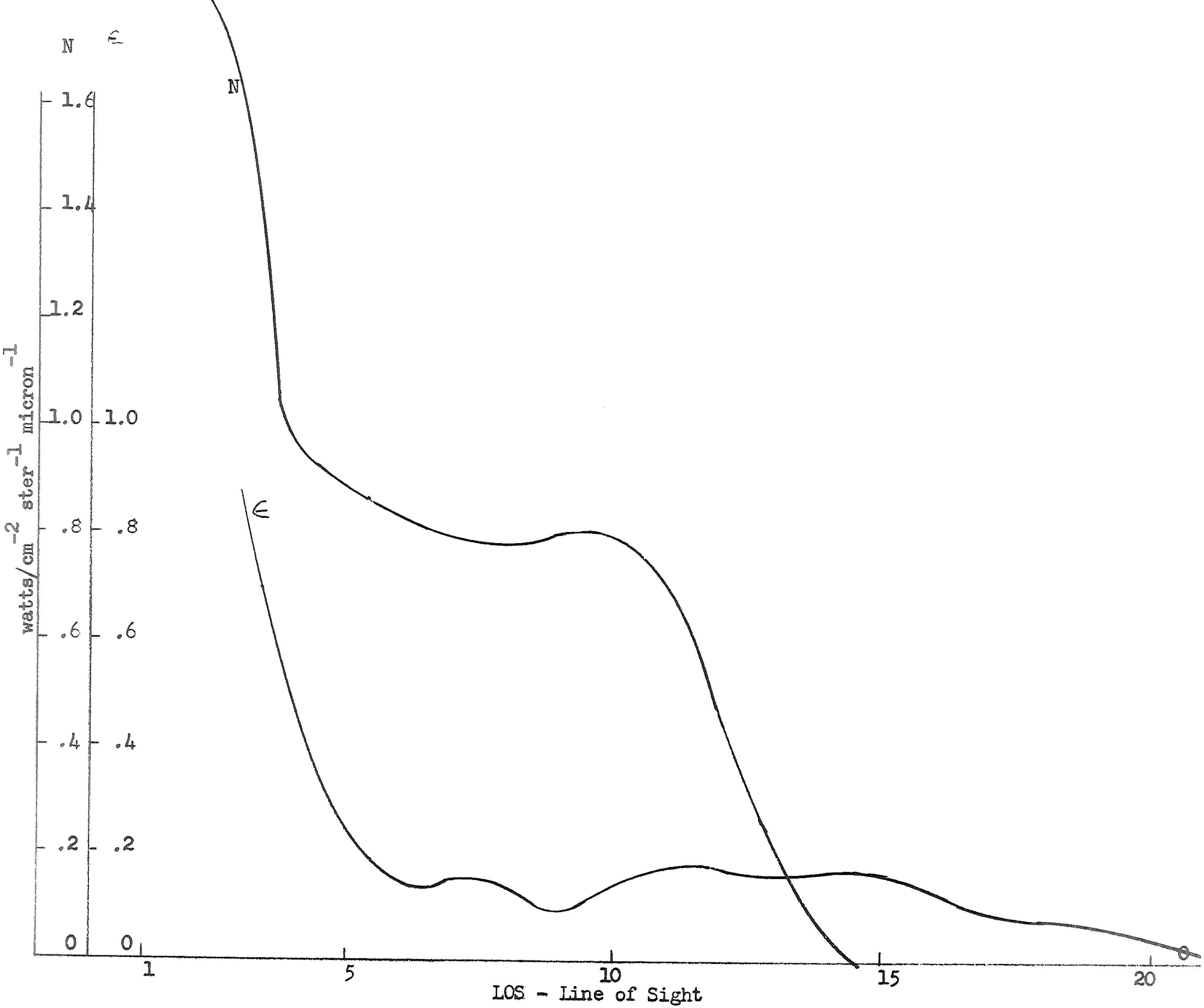

Figure 3-18 **Flame radiance and emissivity - Run 27 Position 5**

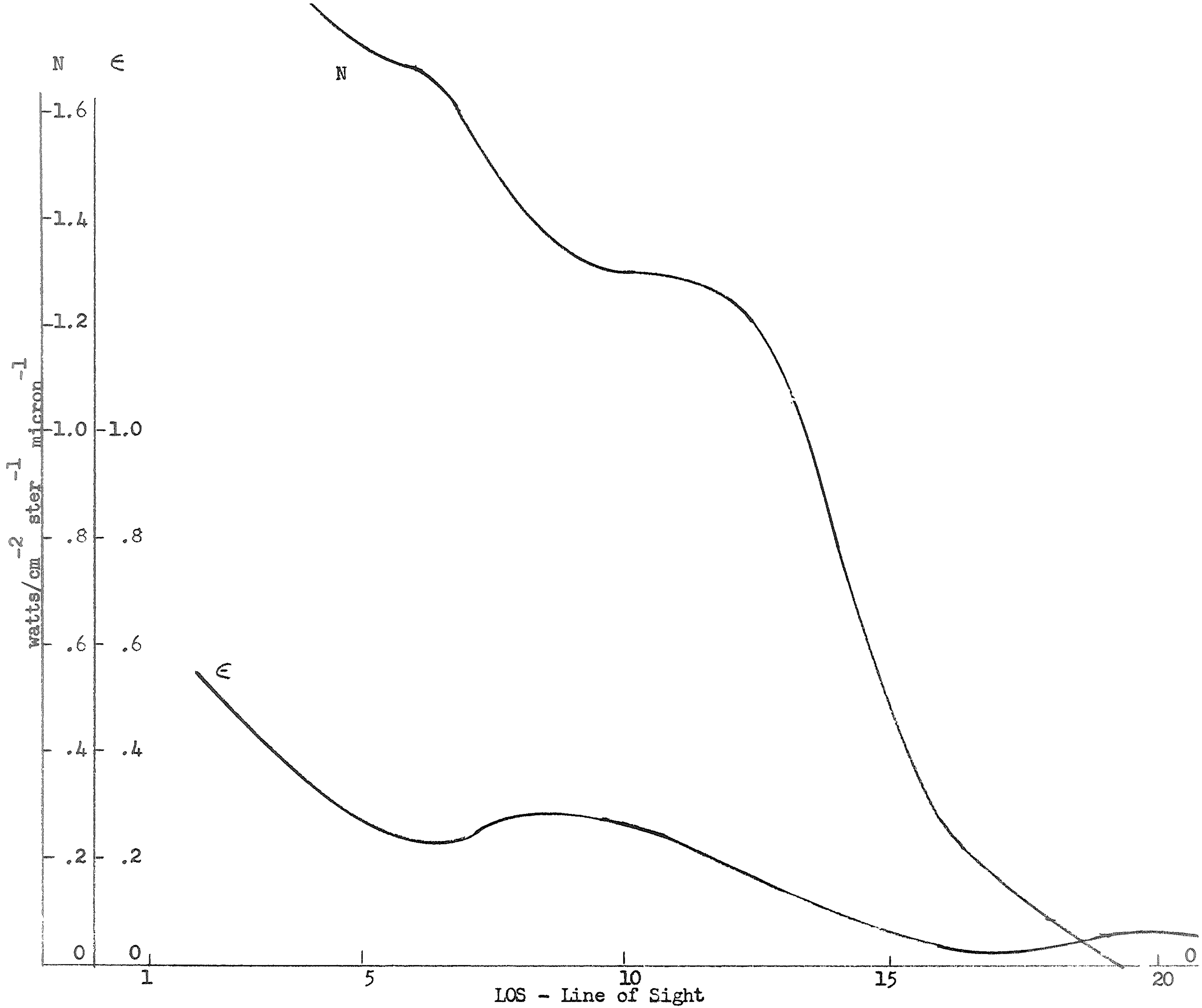

Figure 3-19 Flame radiance and emissivity - Run 28 Position 8

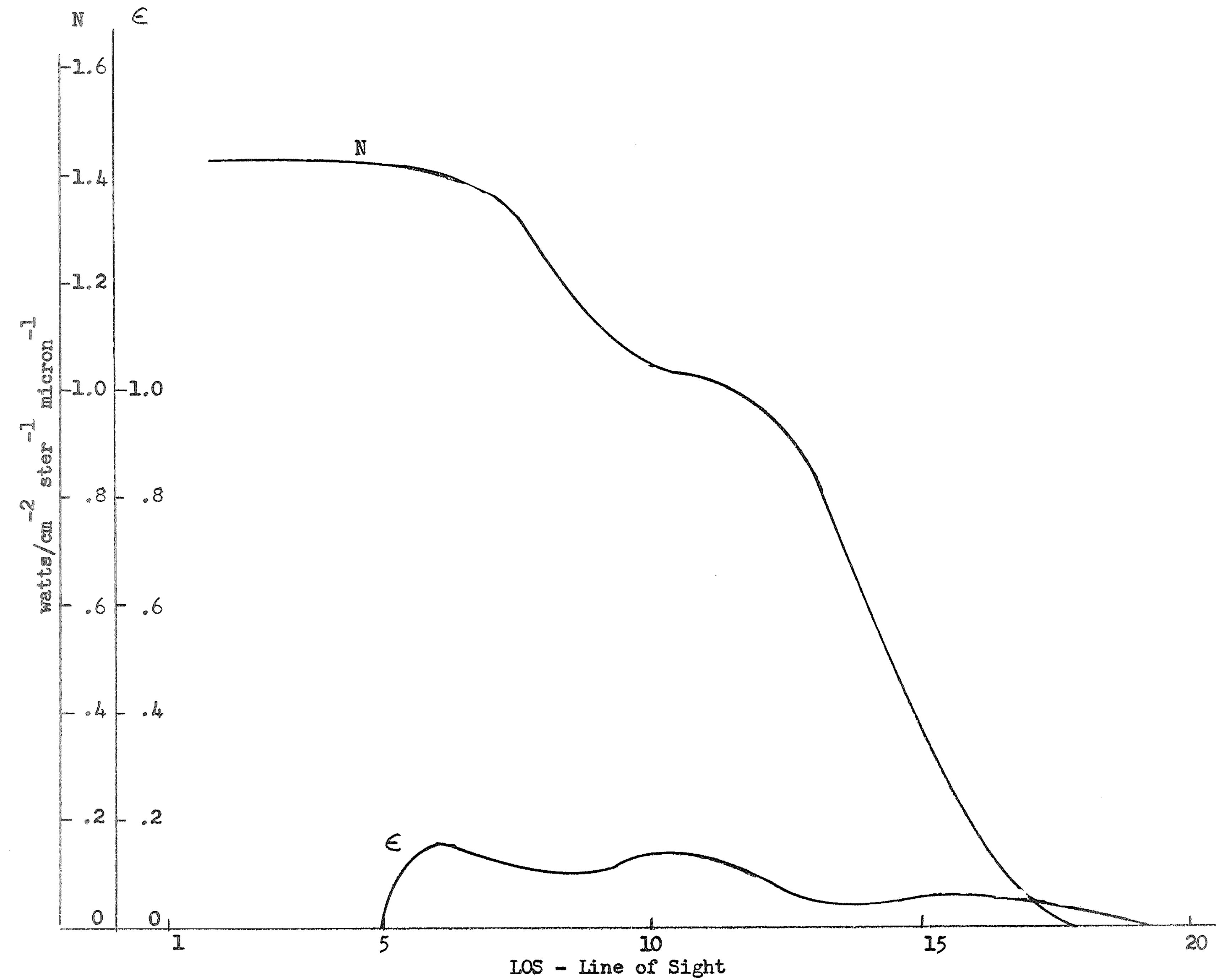

Figure 3-20 Flame radiance and emissivity - Run 30 Position 7

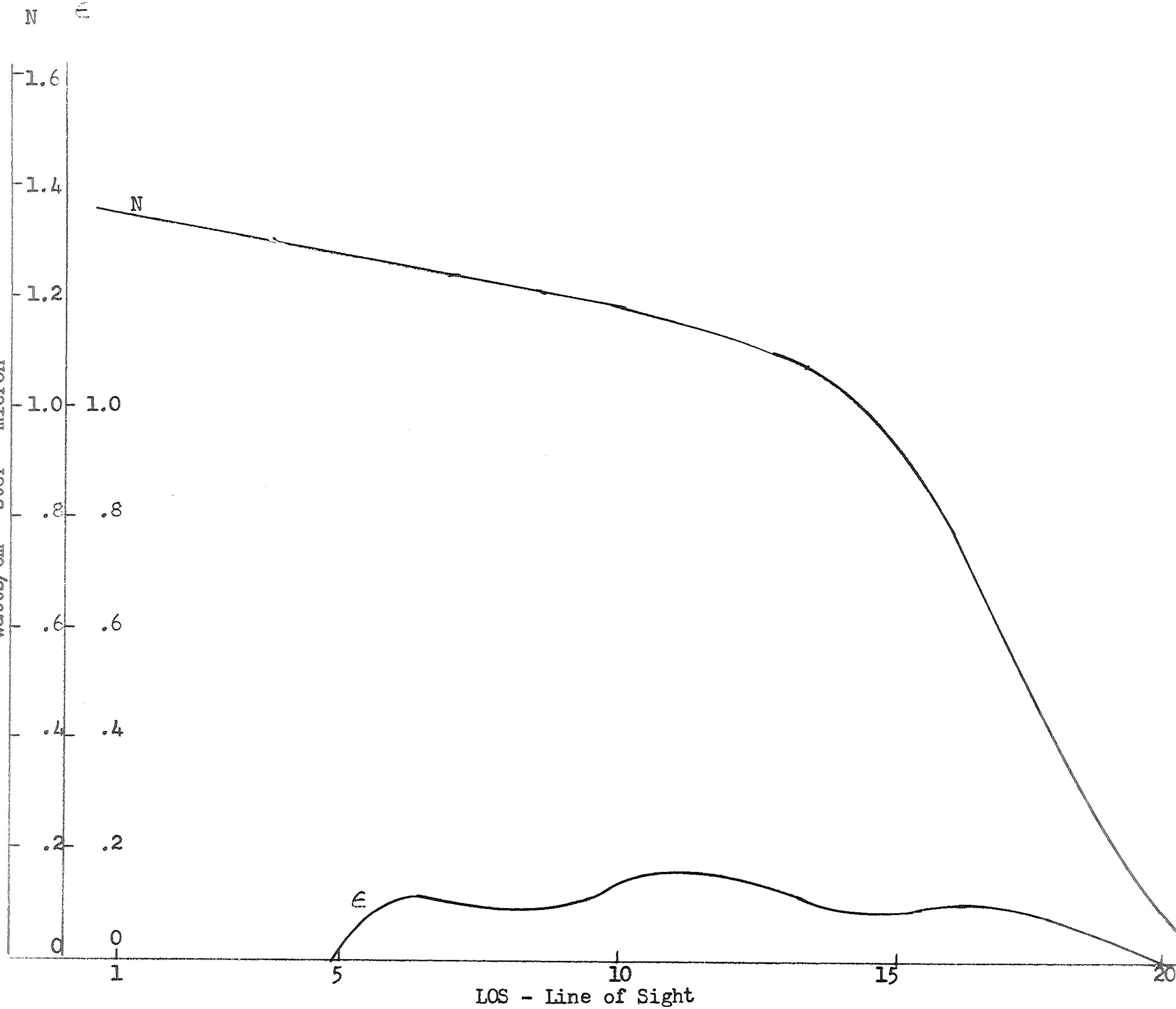

Figure 3-21 Flame radiance and emissivity - Run 31 Position 10

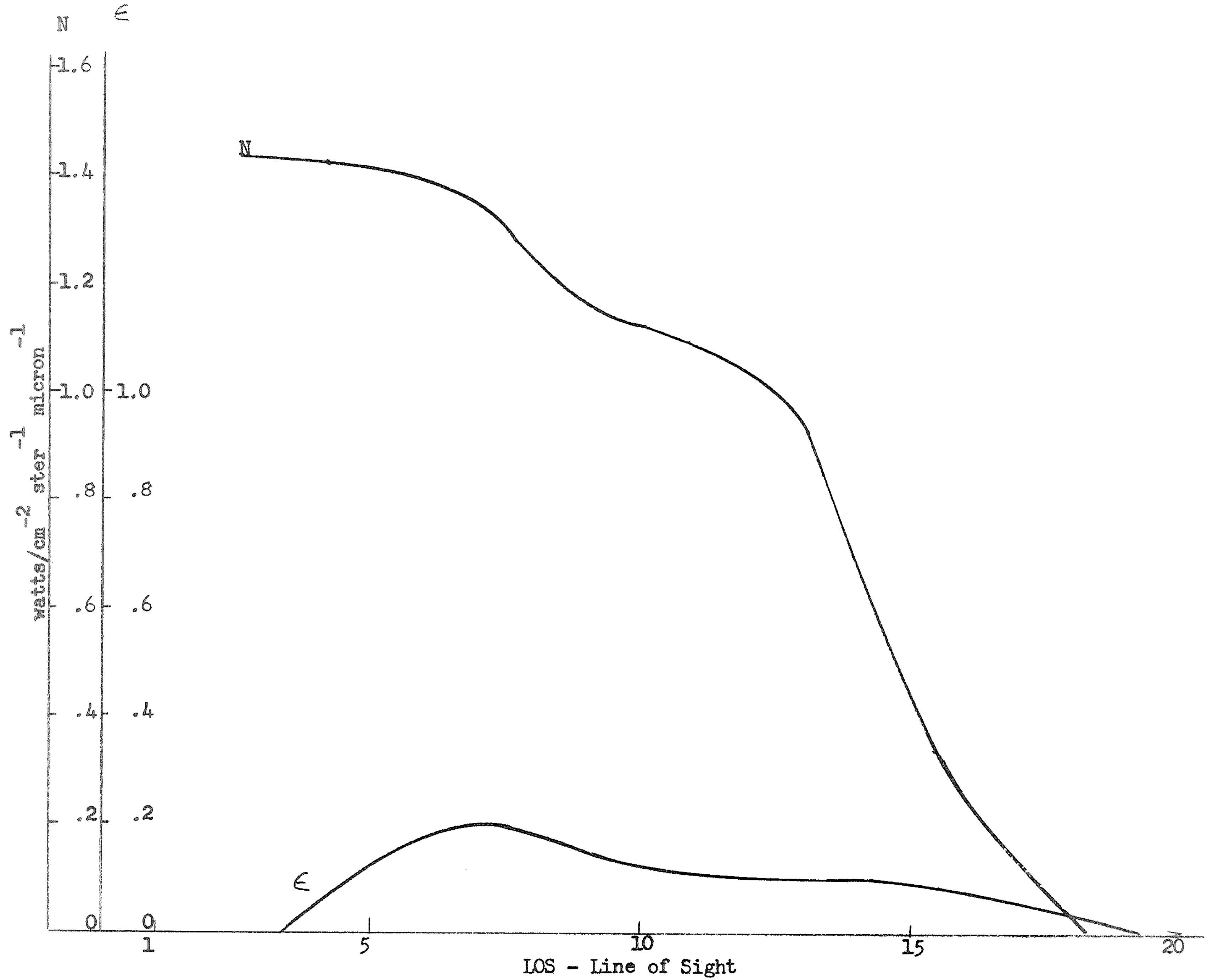

Figure 3-22. Flame Radiance and Emissivity - Run 32 Position 8

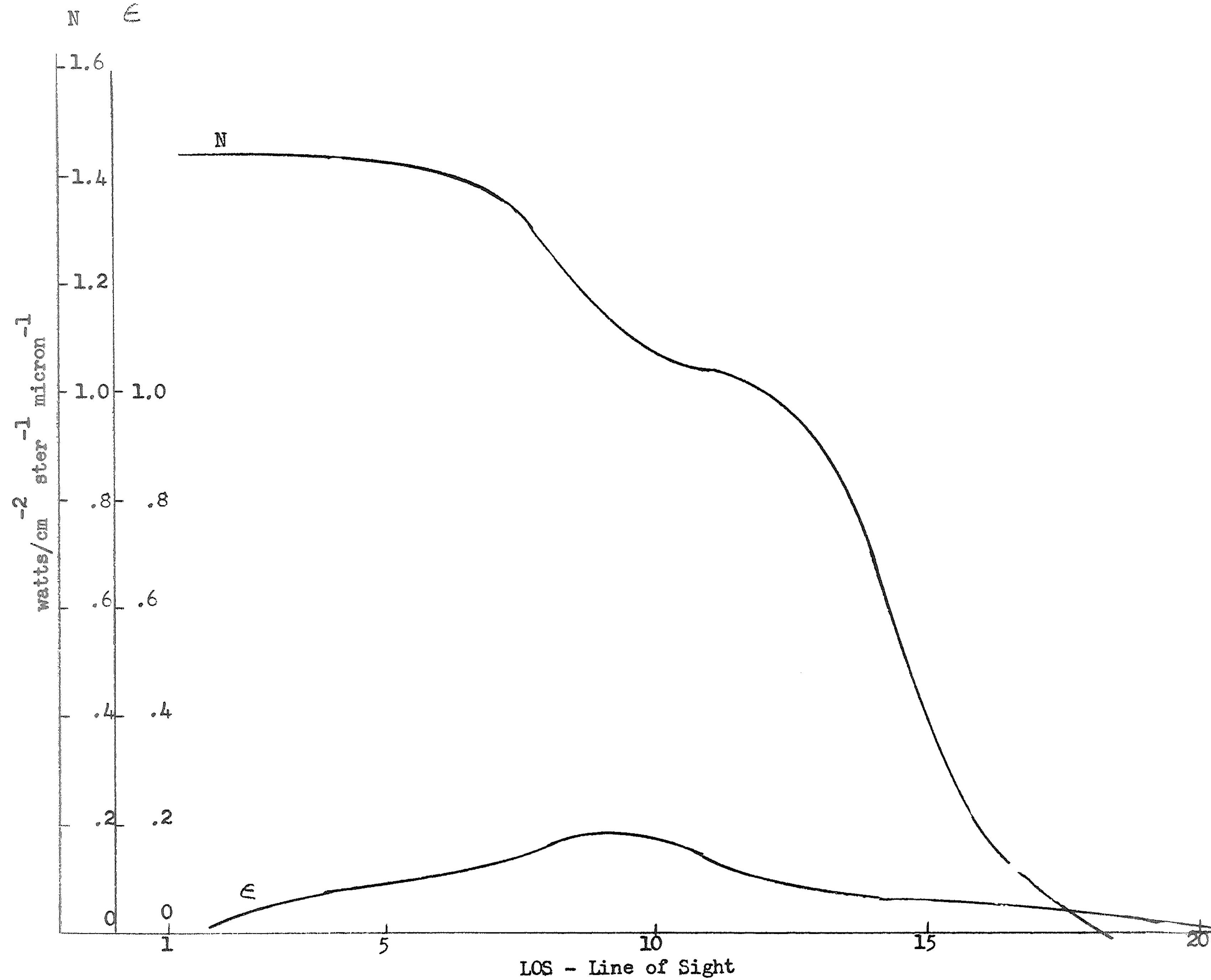

Figure 3-23 Flame Radiance and Emissivity - Run 34 Position 8

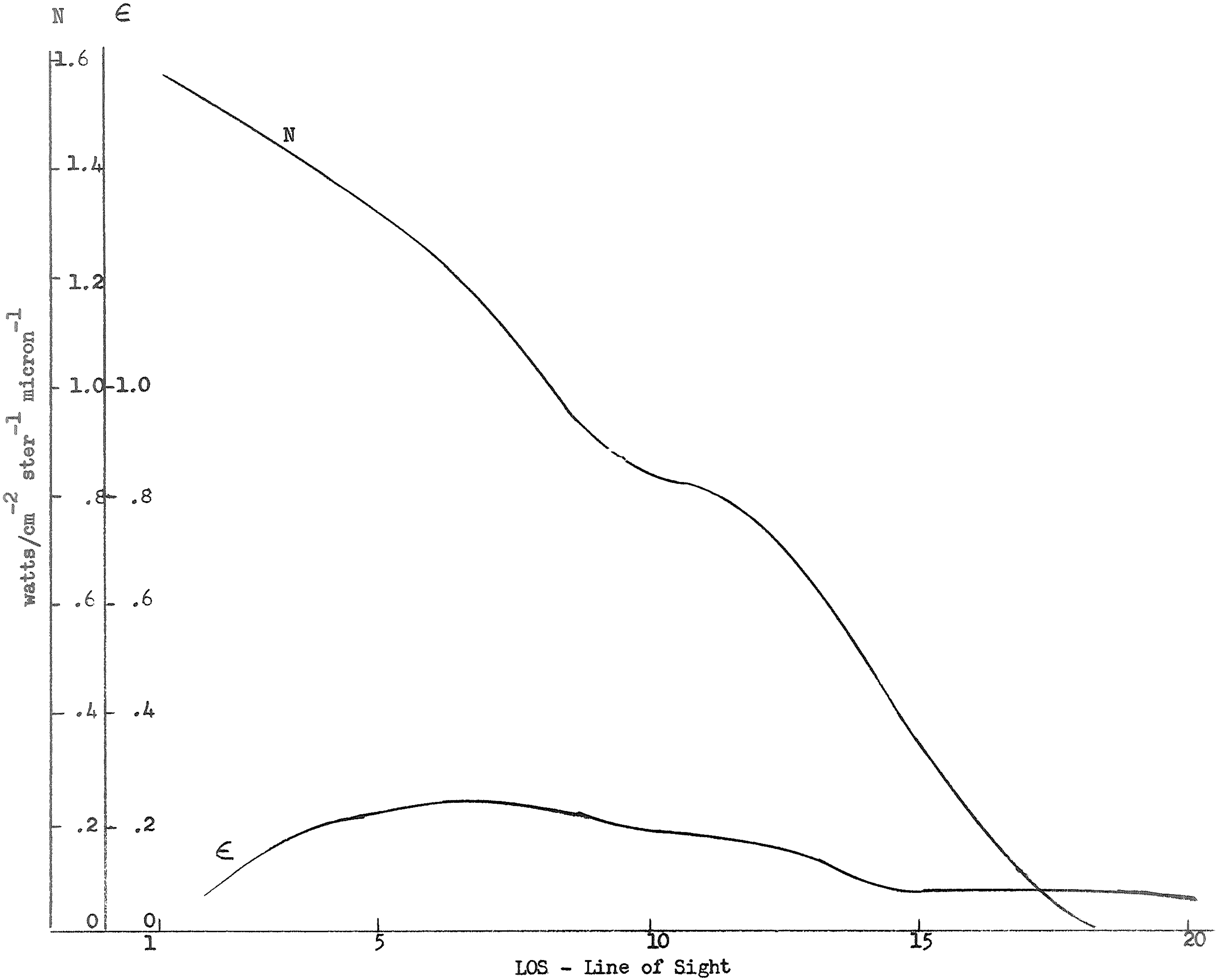

Figure 3-24 Flame Radiance and Emissivity - Run 35 Position 8

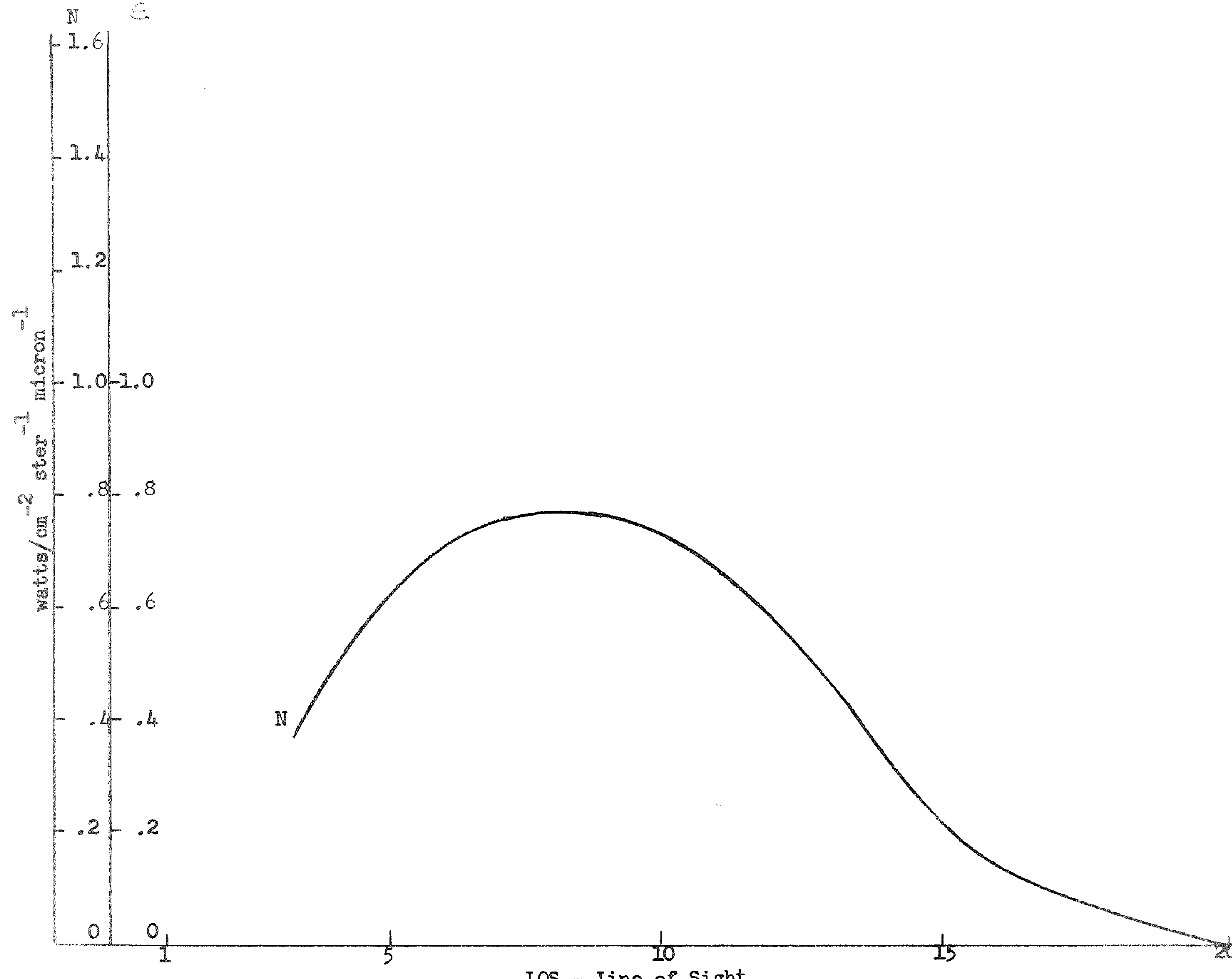

Figure 3-25 Flame Radiance and Emissivity - Run 36 Position 8

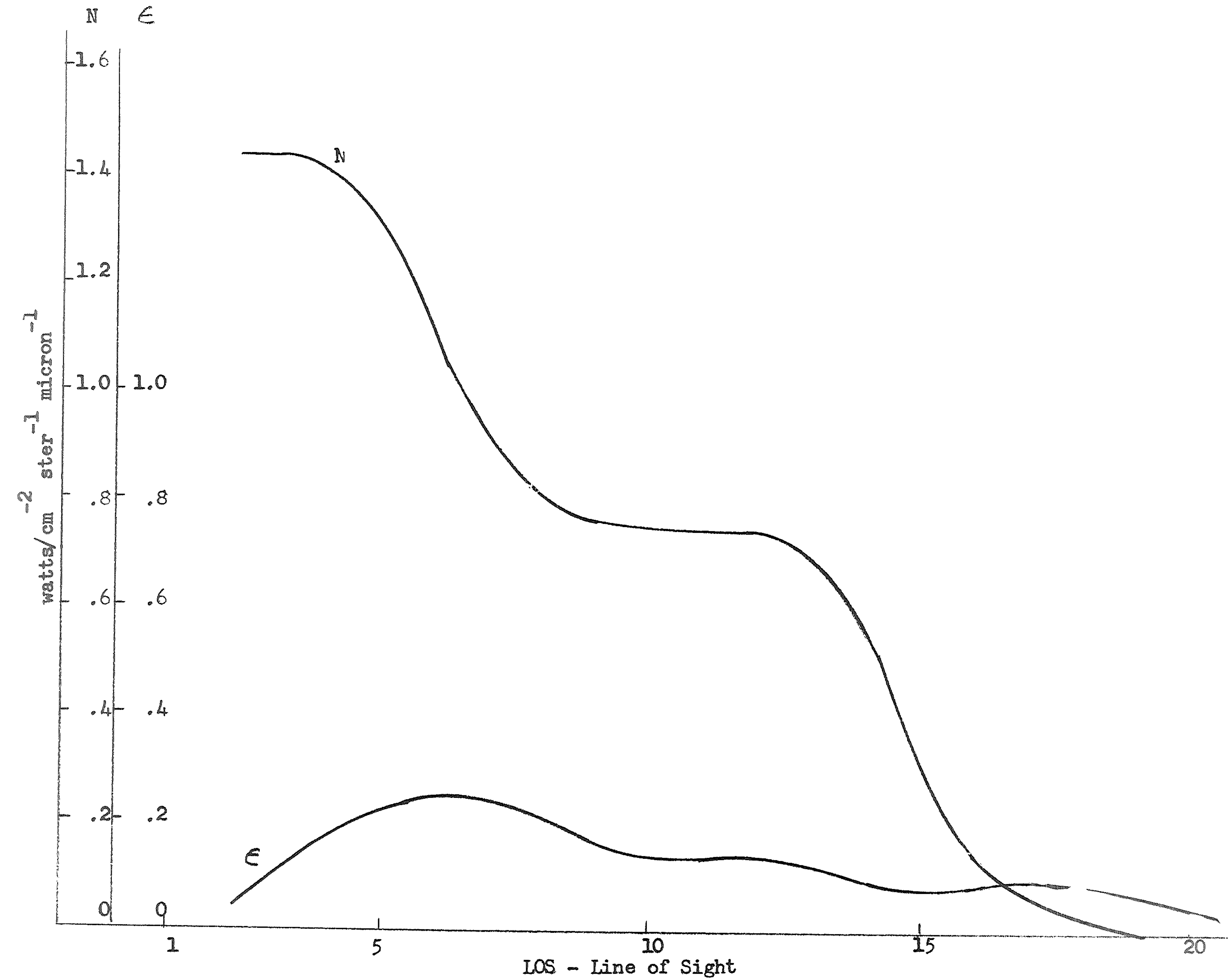

Figure 3-26 Flame Radiance and Emissivity - Run 37 Position 8

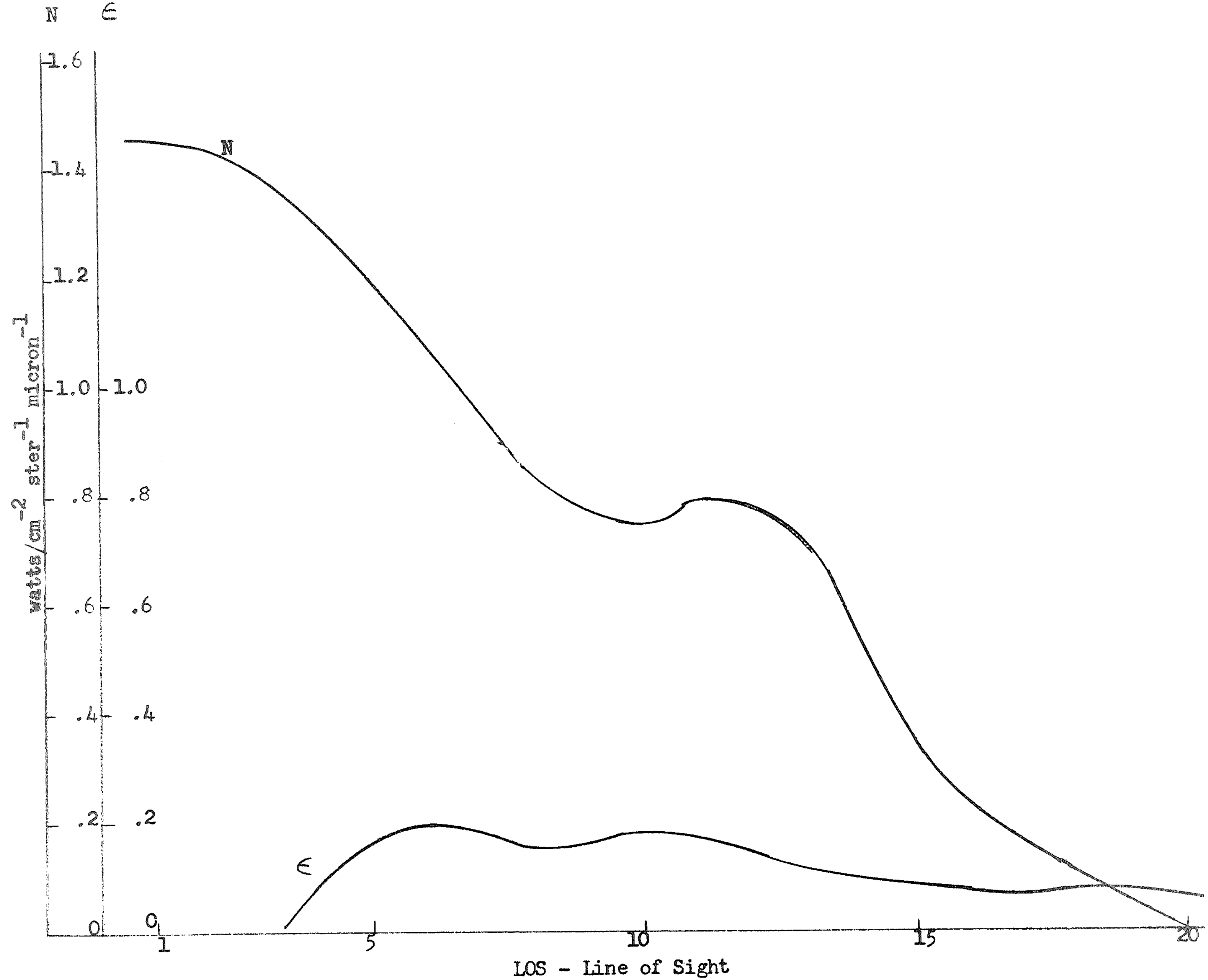

Figure 3-27 Flame Radiance and Emissivity - Run 38 Position 8

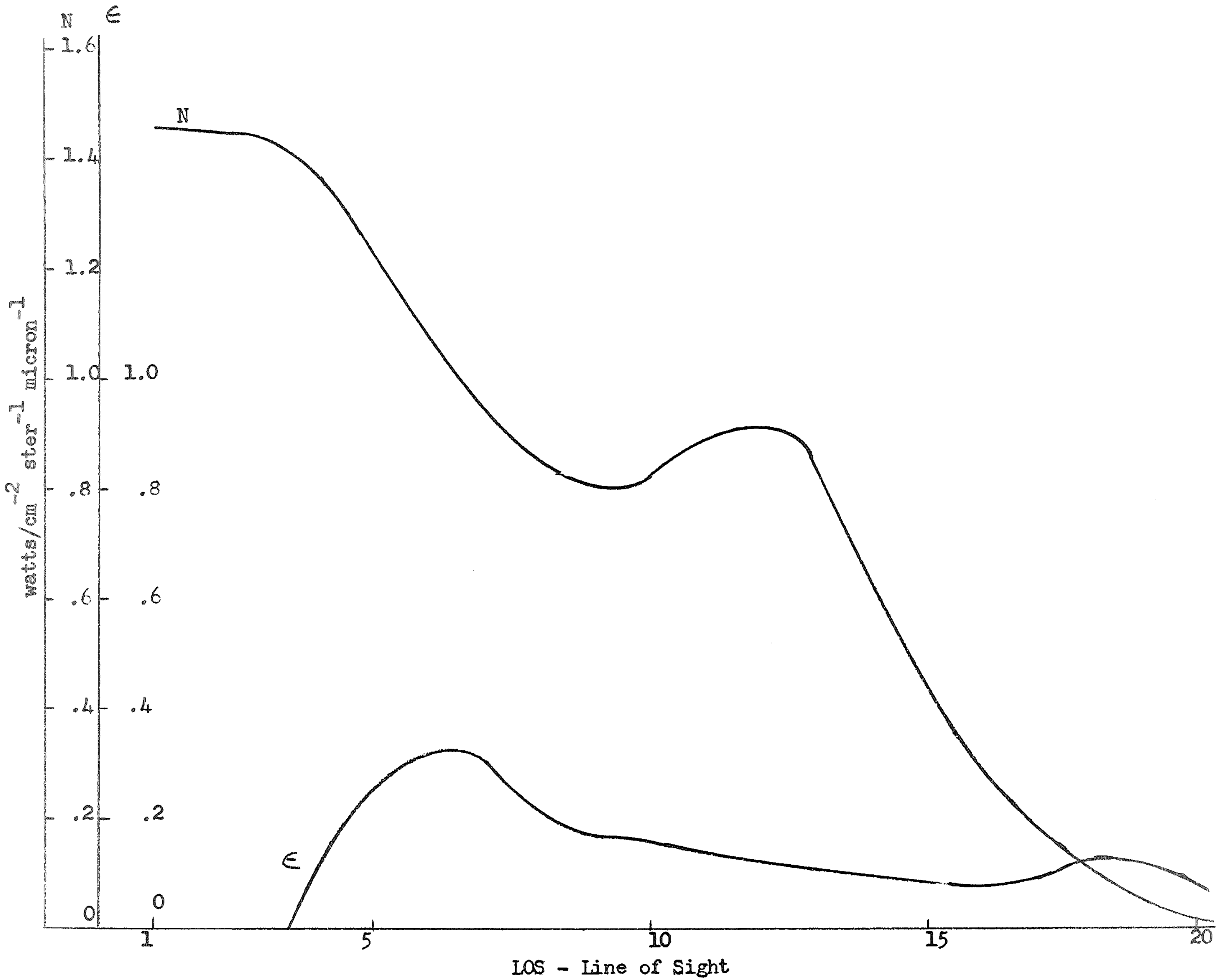

Figure 3-28 Flame Radiance and Emissivity - Run 39 Position 9

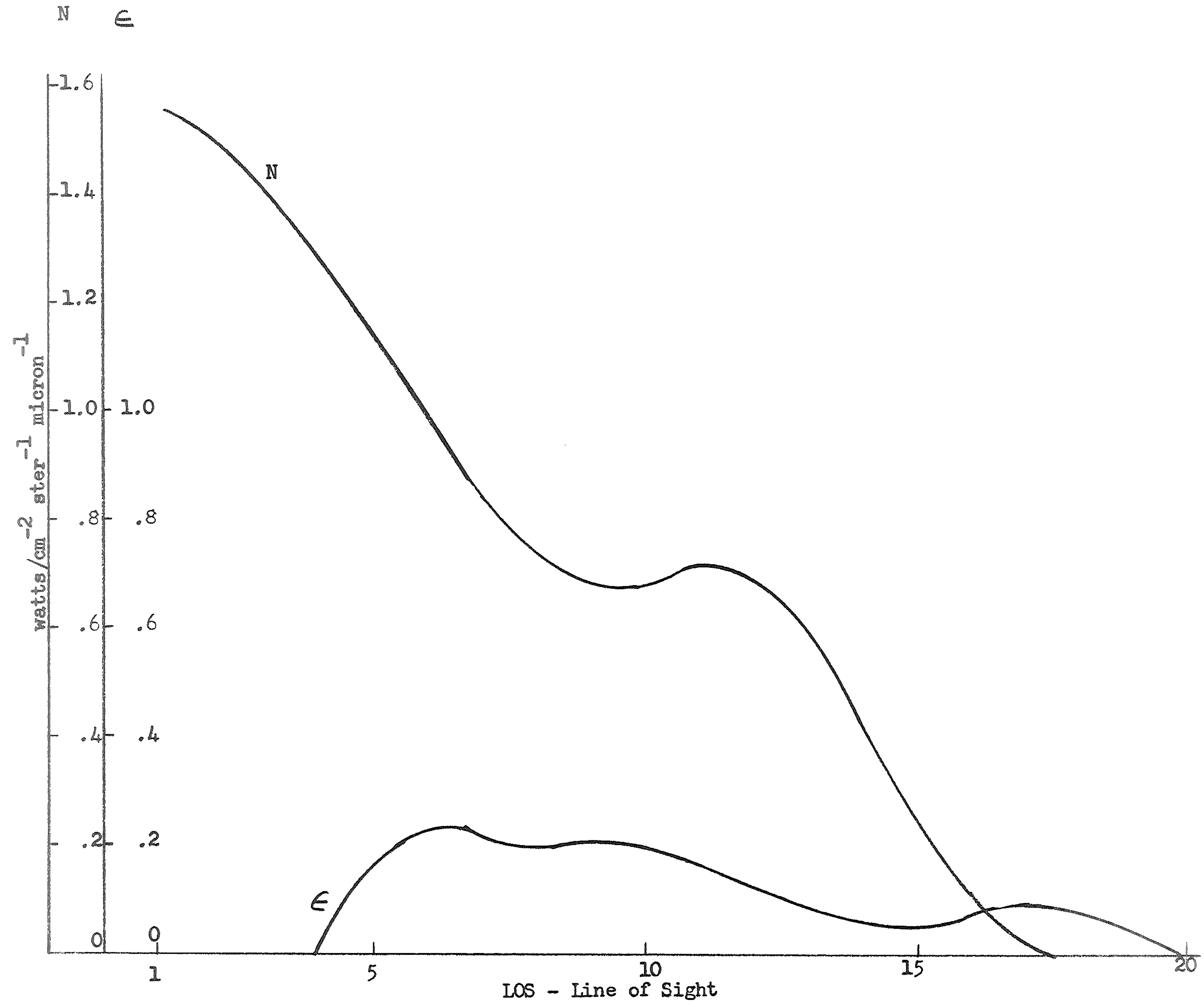

Figure 3-29 Flame Radiance and Emissivity - Run 40 Position 8

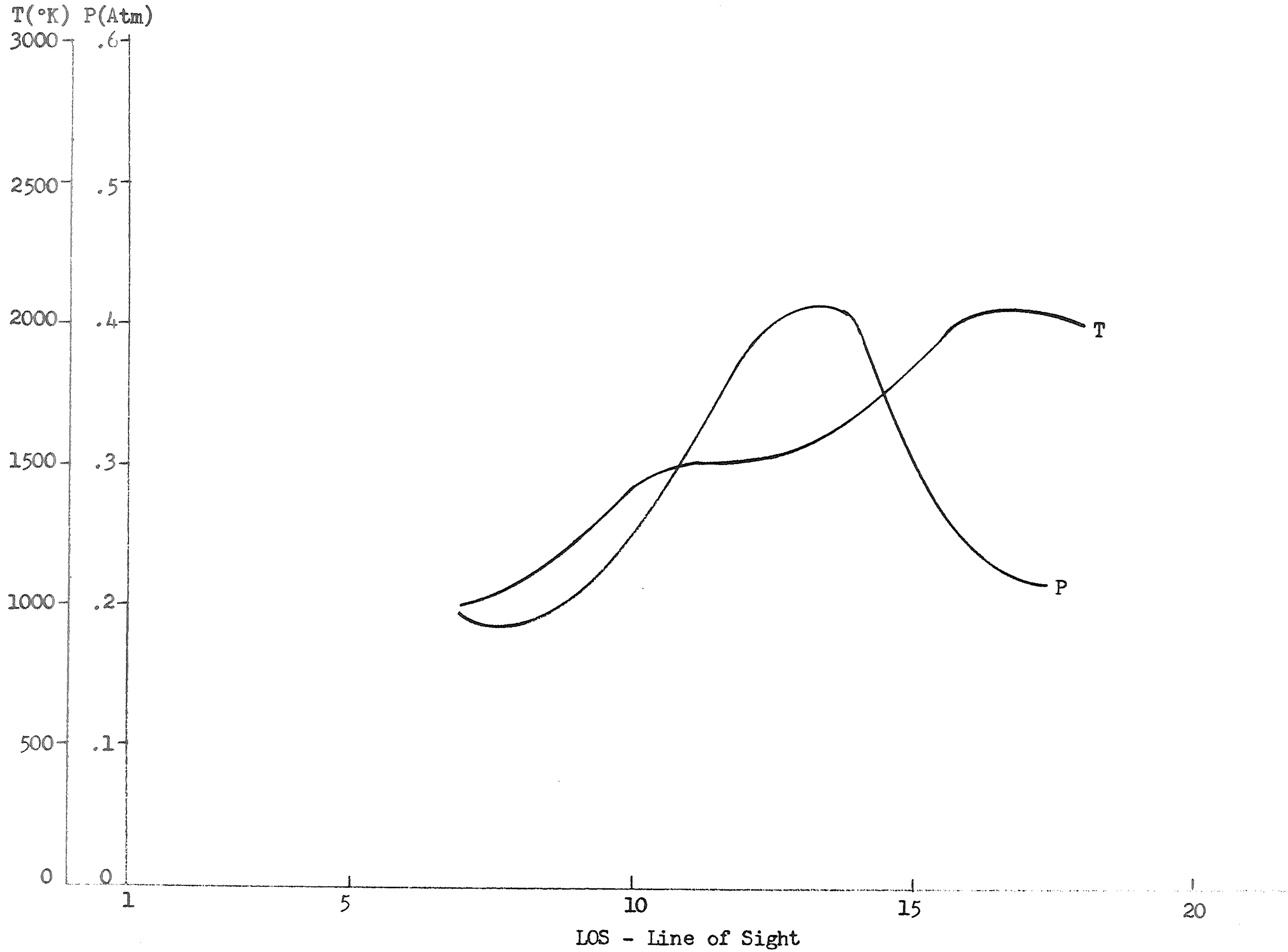

Figure 3-30 Apparent Flame Temperature and H_2O Partial Pressure - Run 021 Position 8

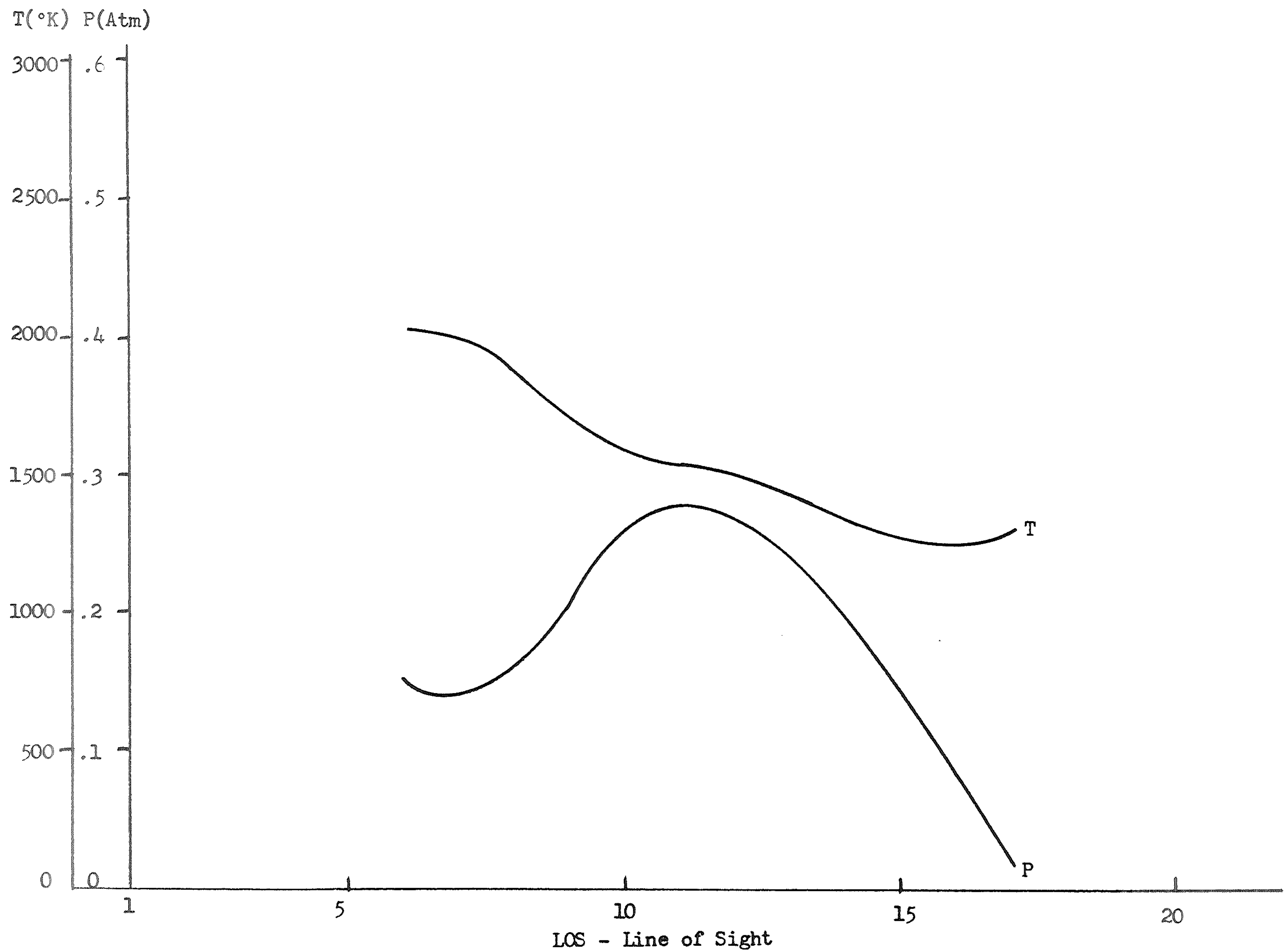

Figure 3-31 Apparent Flame Temperature and H_2O Partial Pressure - Run 10 Position 8

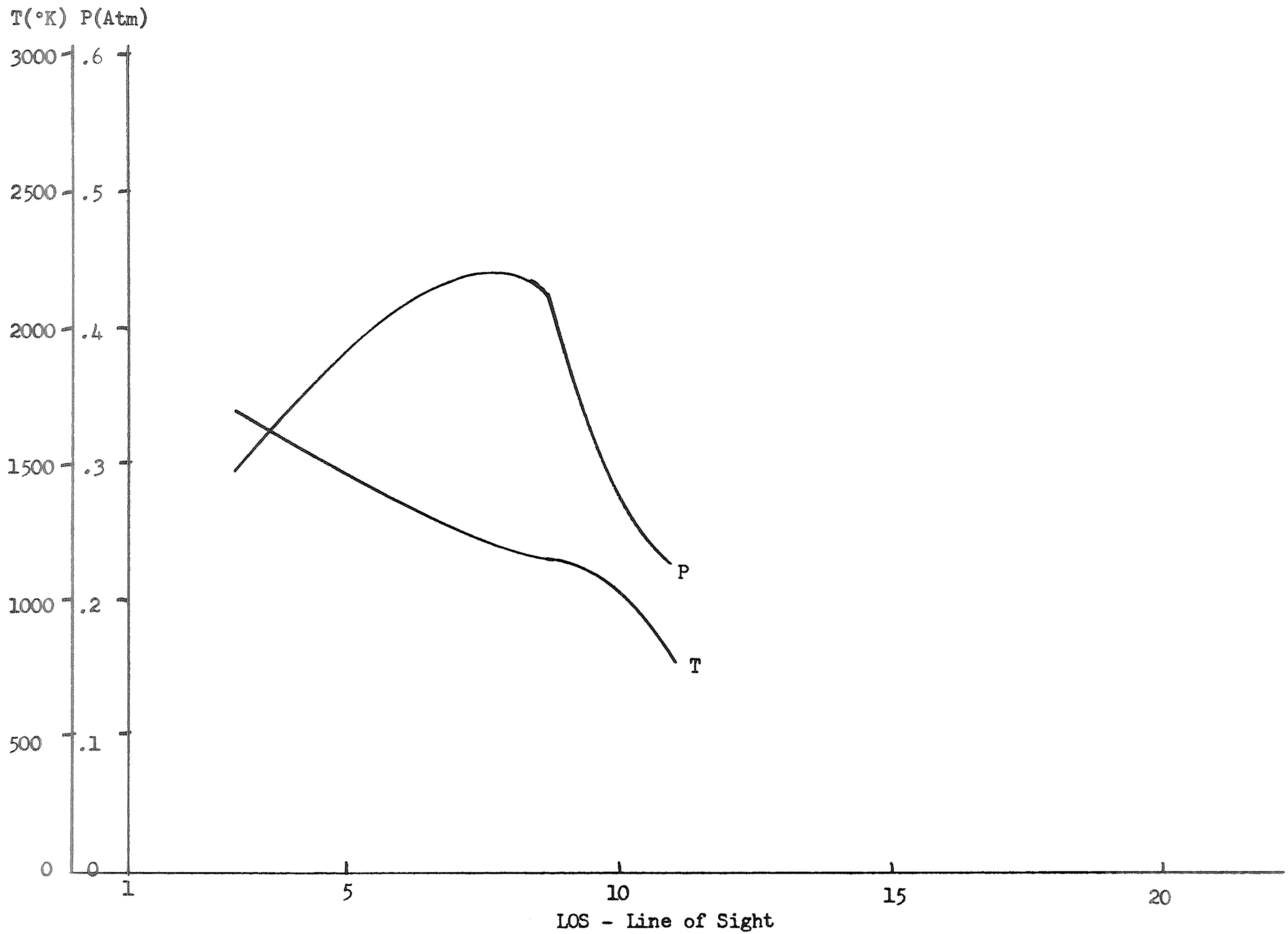

Figure 3-32 Apparent Flame Temperature and H_2O Partial Pressure - Run 11 Position 3

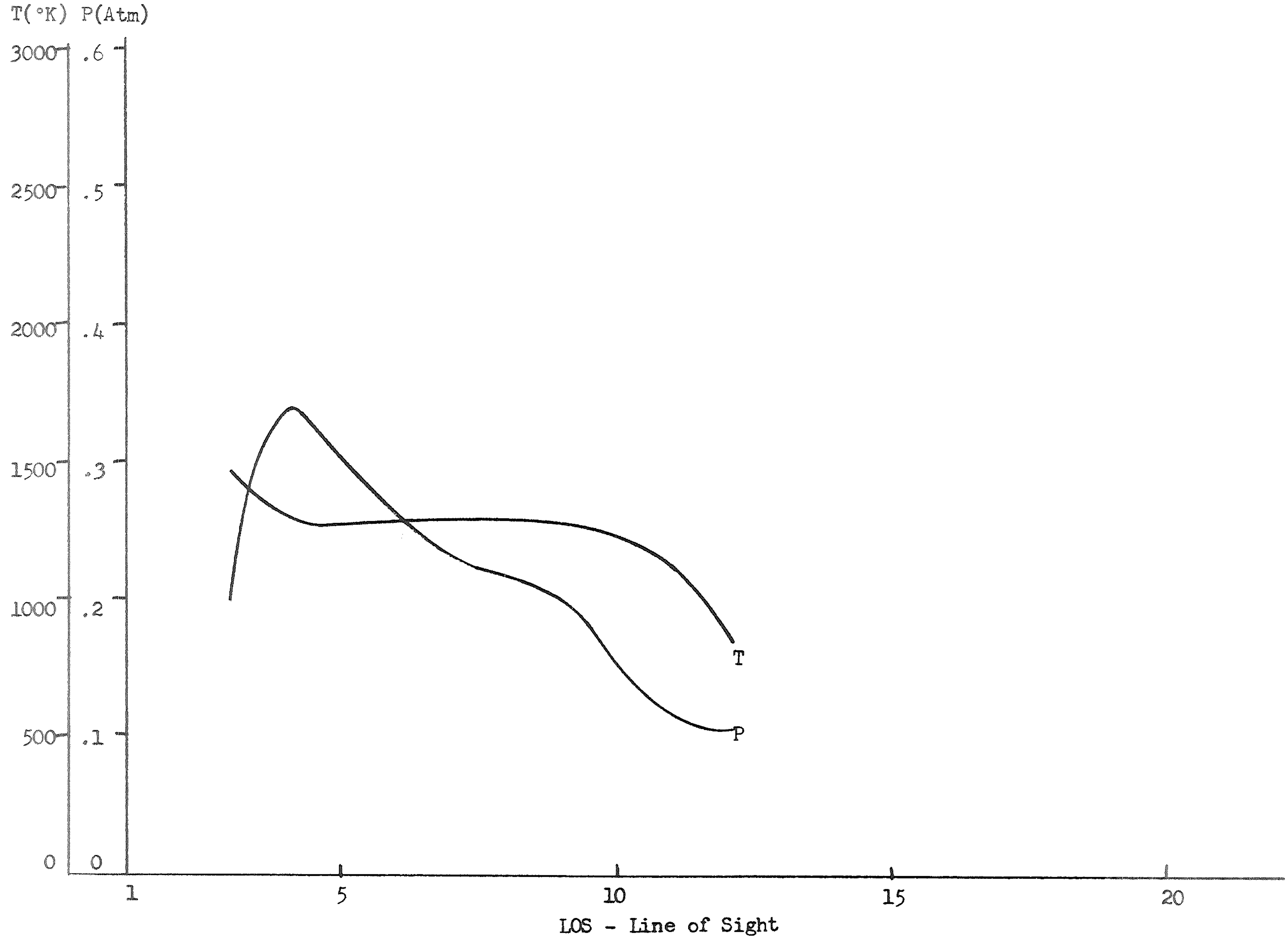

Figure 3-33 Apparent Flame Temperature and H_2O Partial Pressure - Run 12 Position 6

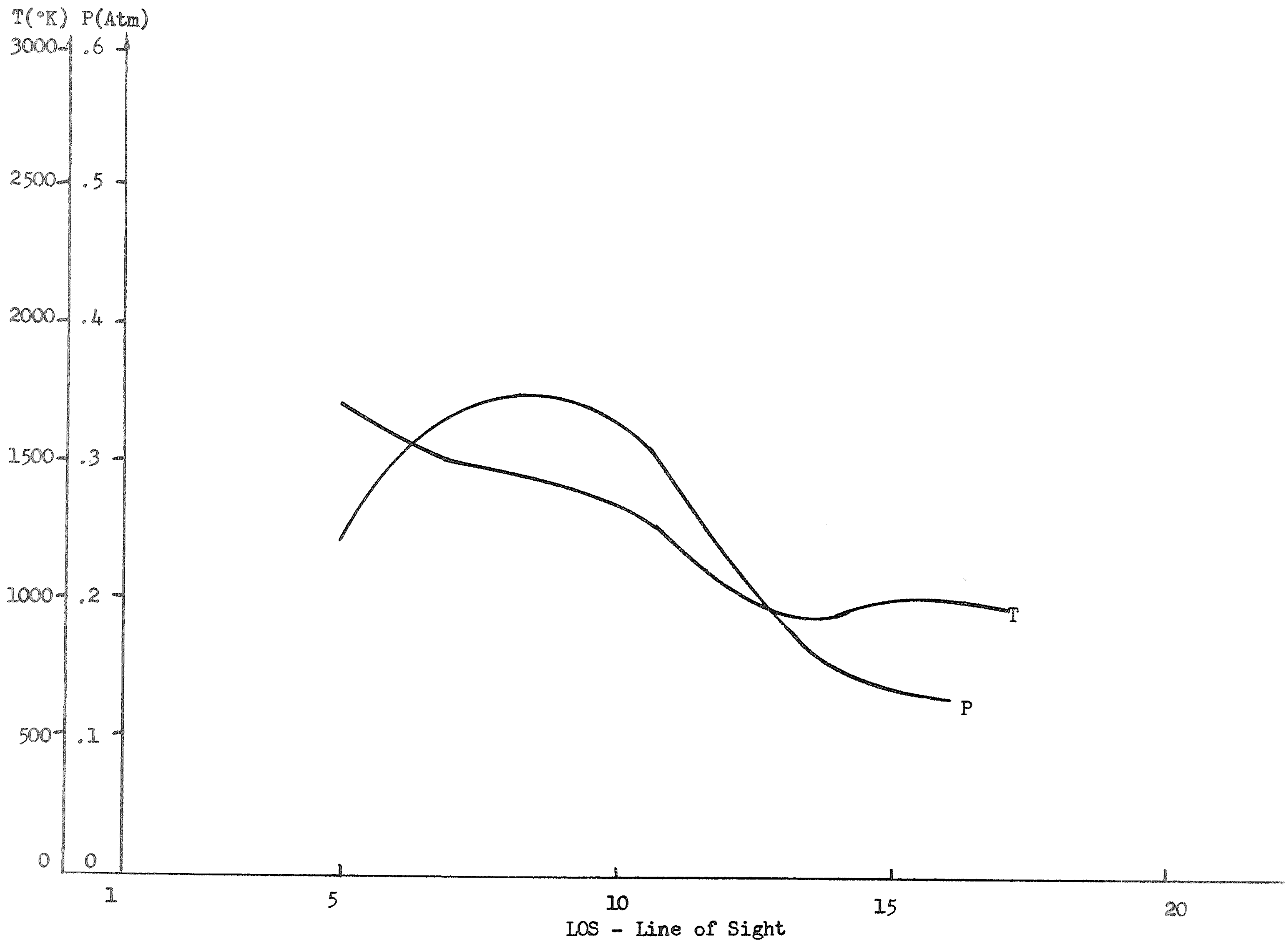

Figure 3-34 Apparent Flame Temperature and H_2O Partial Pressure - Run 13 Position 4

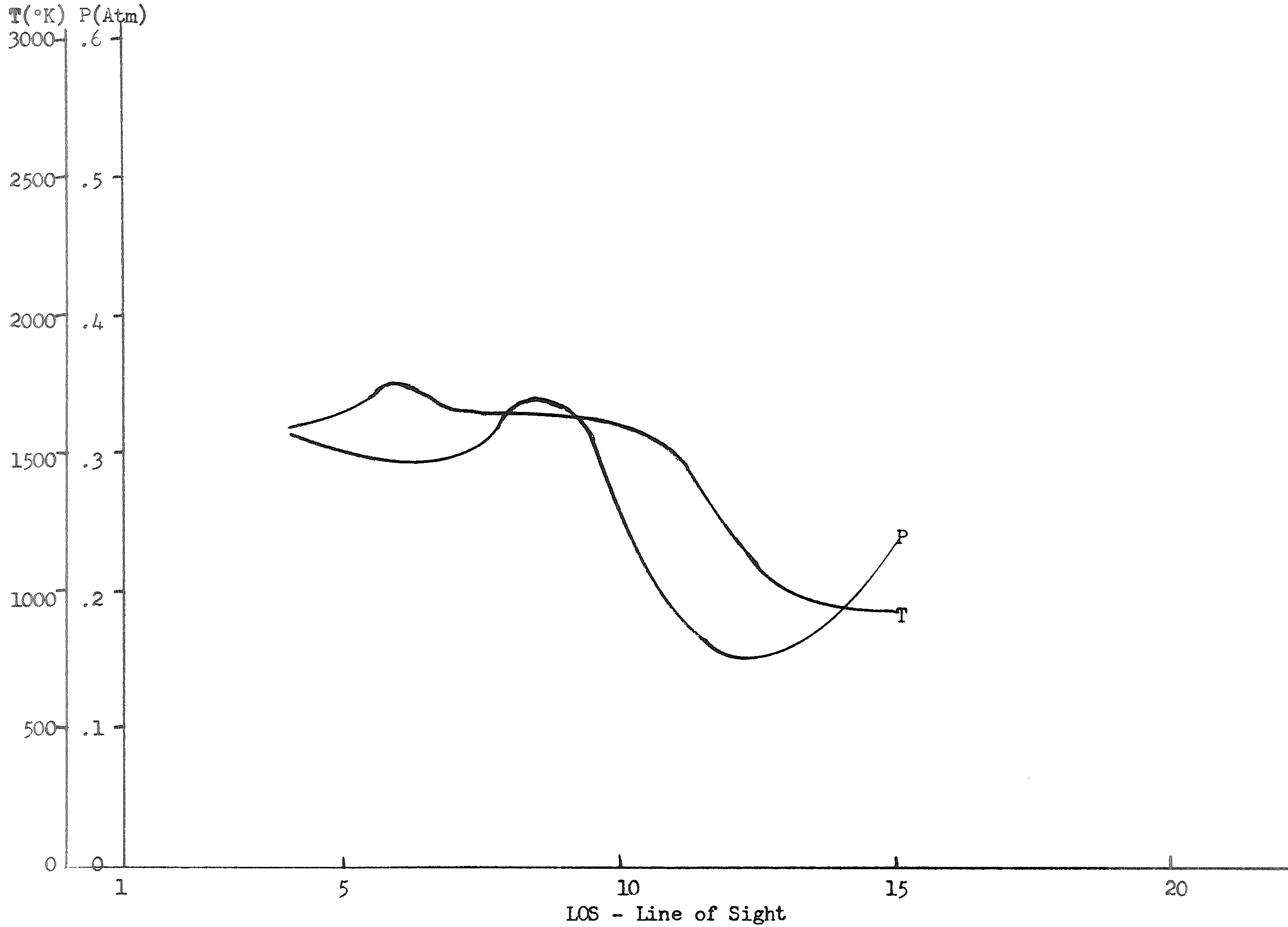

Figure 3-35 Apparent Flame Temperature and H_2O Partial Pressure - Run 14 Position 5

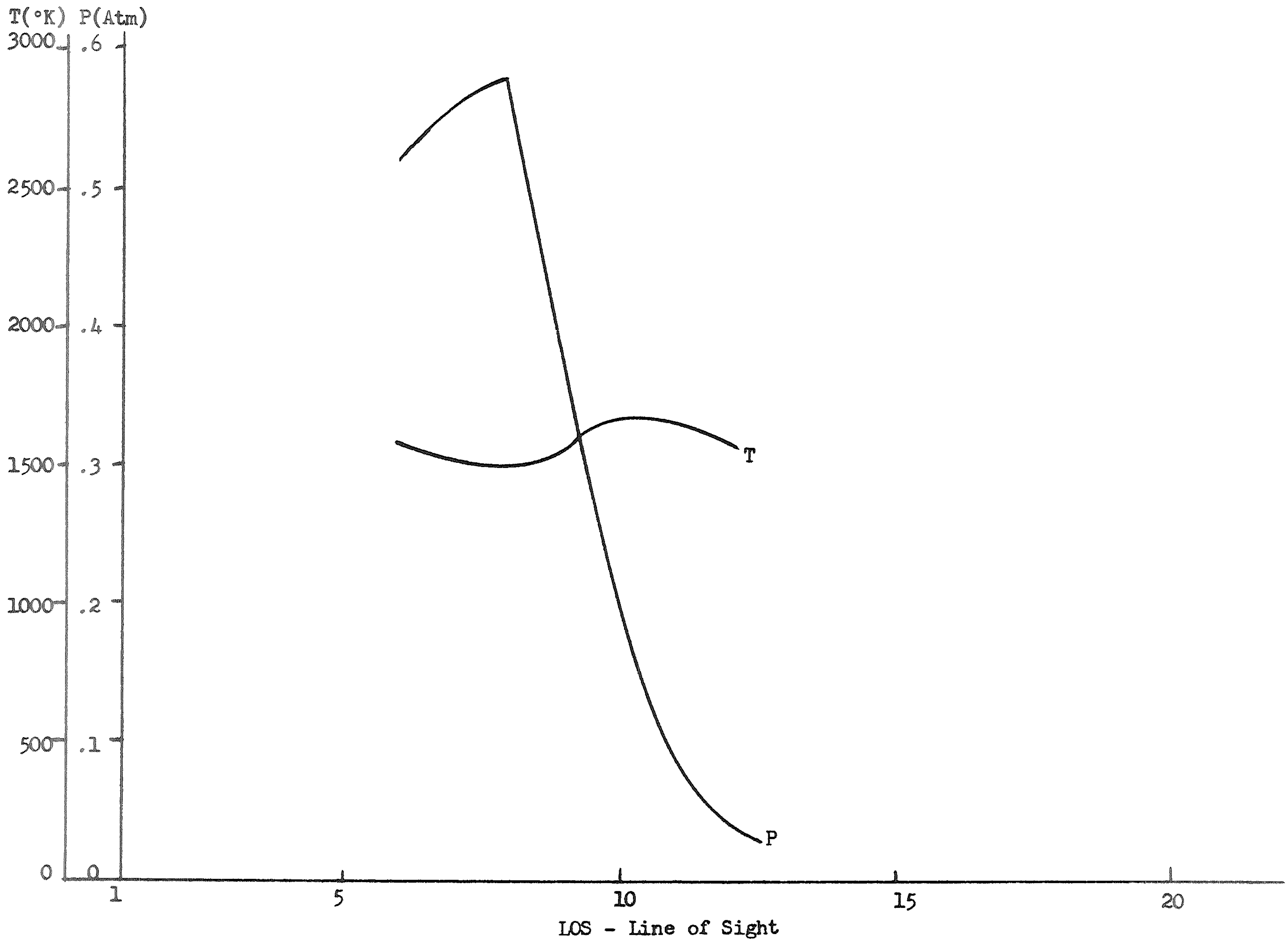

Figure 3-36 Apparent Flame Temperature and H_2O Partial Pressure - Run 17 Position 1

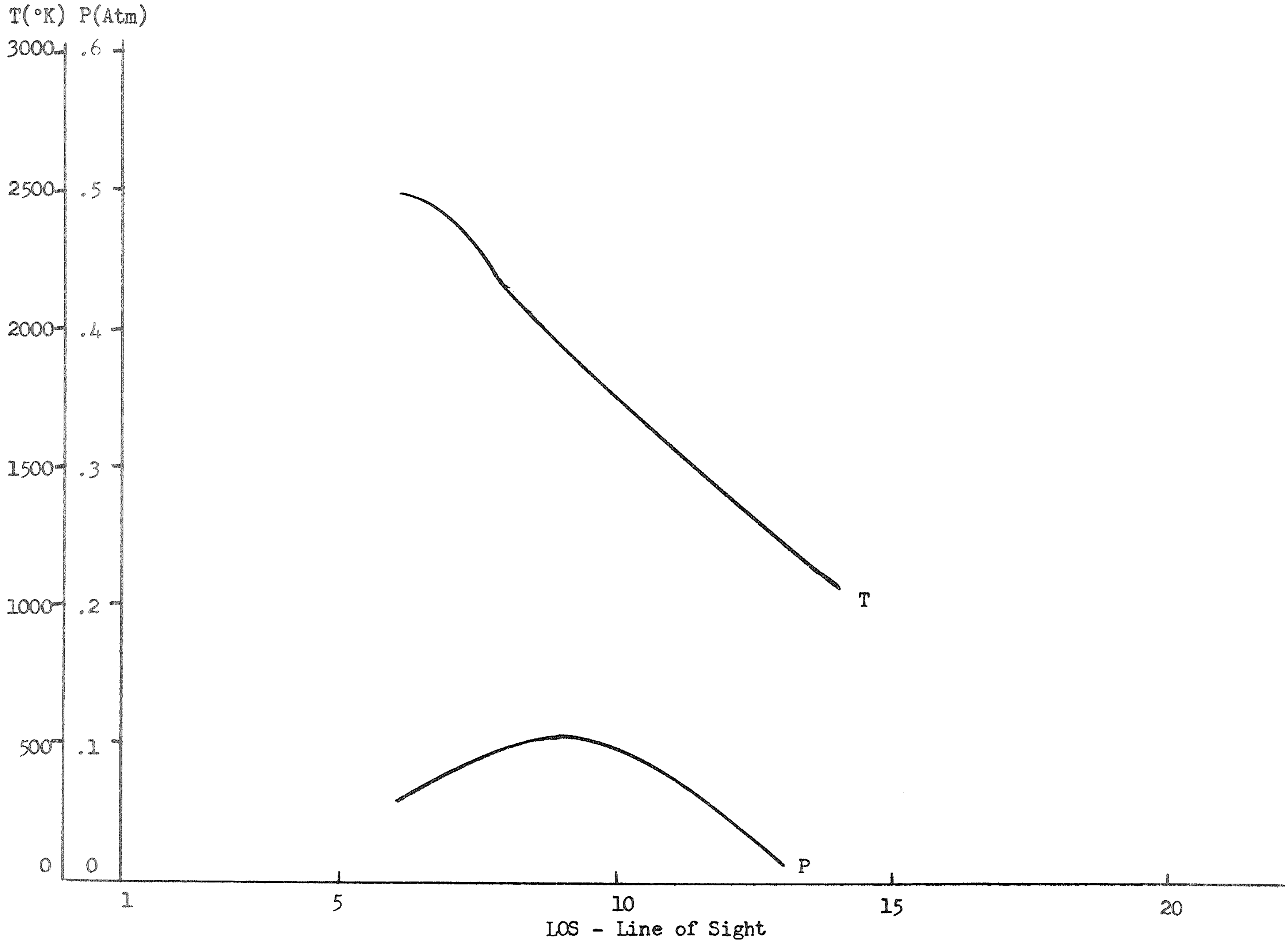

Figure 3-37 Apparent Flame Temperature and H_2O Partial Pressure - Run 18 Position 2

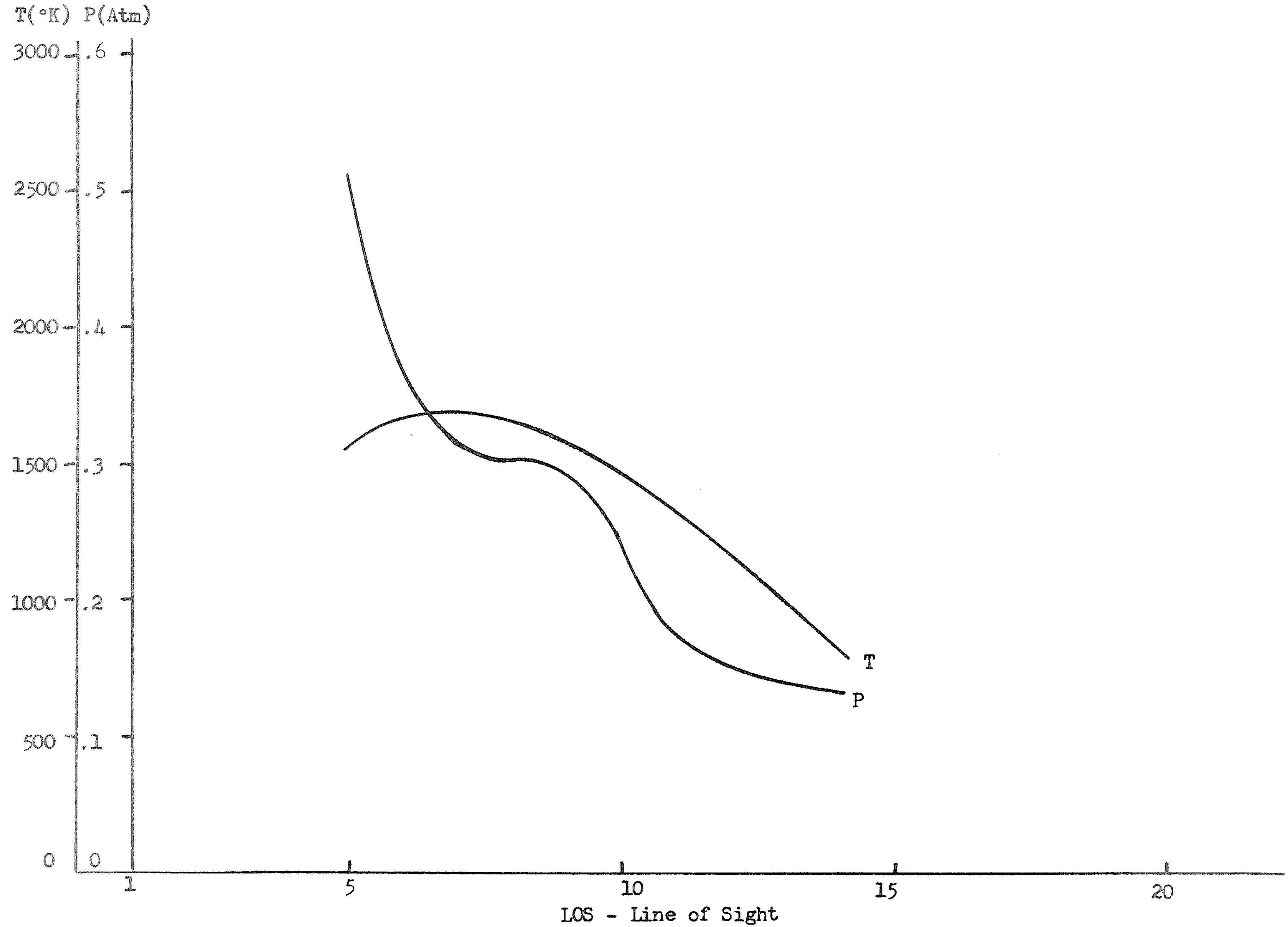

Figure 3-38 Apparent Flame Temperature and H_2O Partial Pressure - Run 20 Position 2

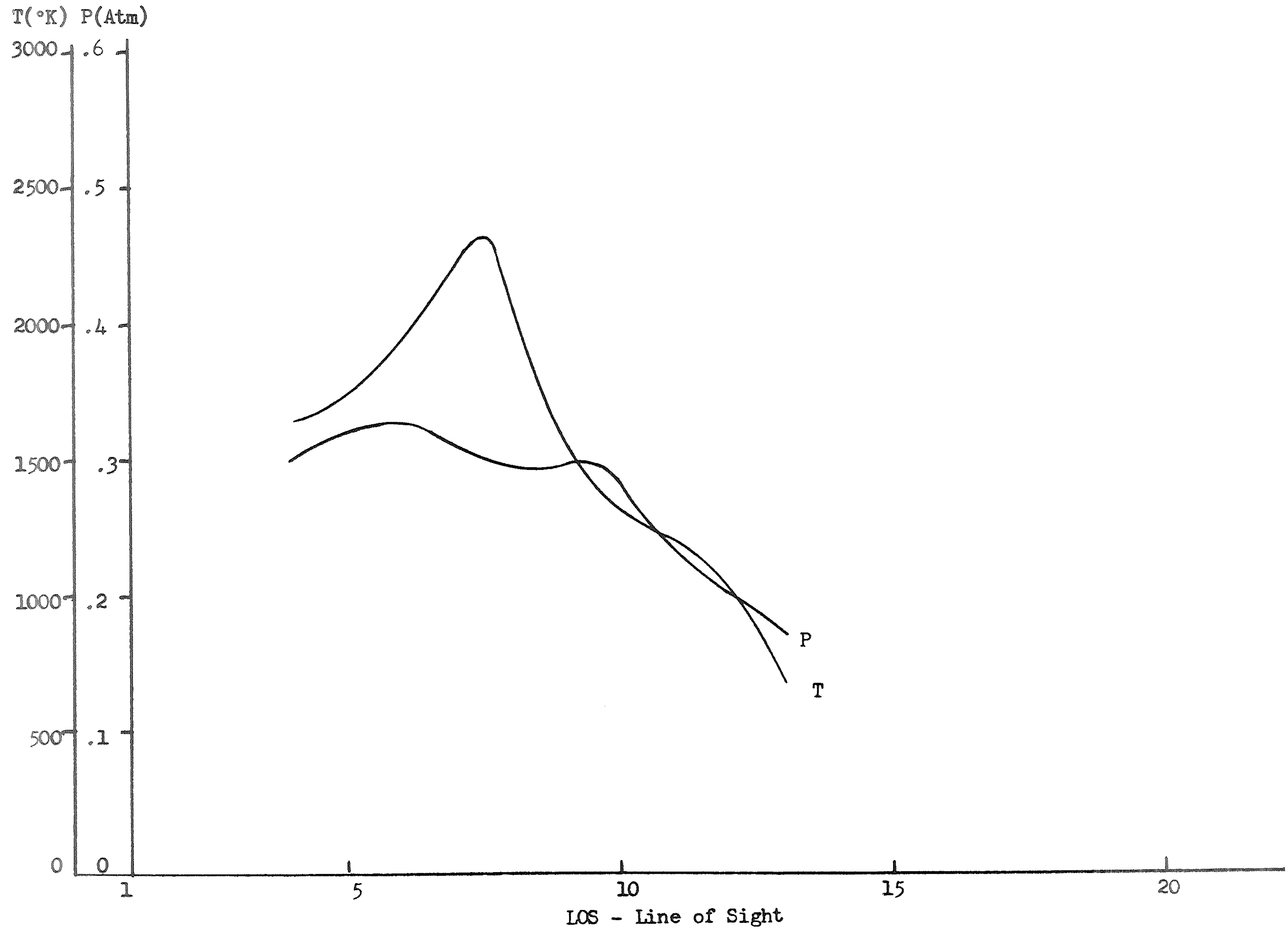

Figure 3-39 Apparent Flame Temperature and H_2O Partial Pressure - Run 21 Position 3

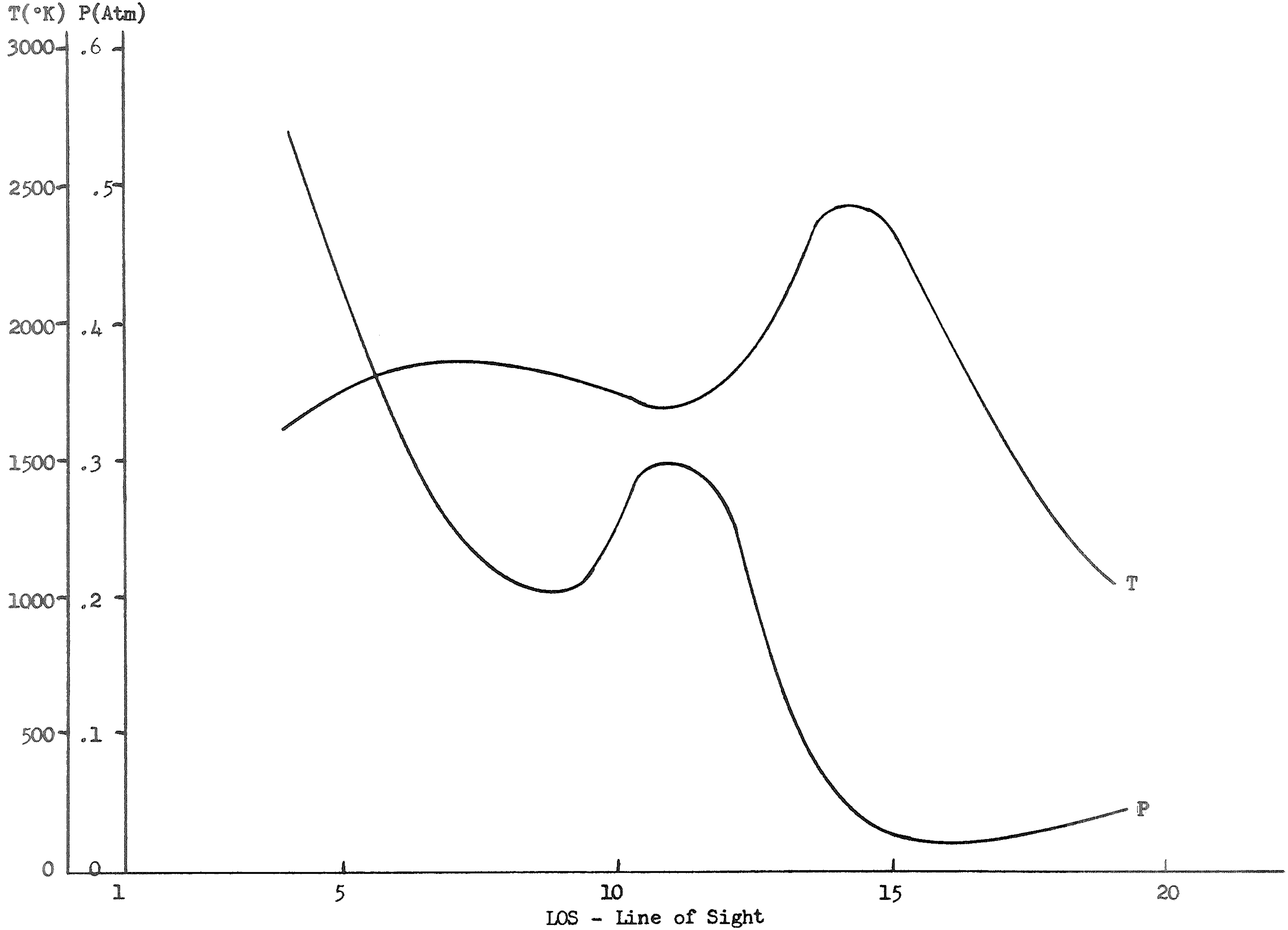

Figure 3-40 Apparent Flame Temperature and H_2O Partial Pressure - Run 22 Position 8½

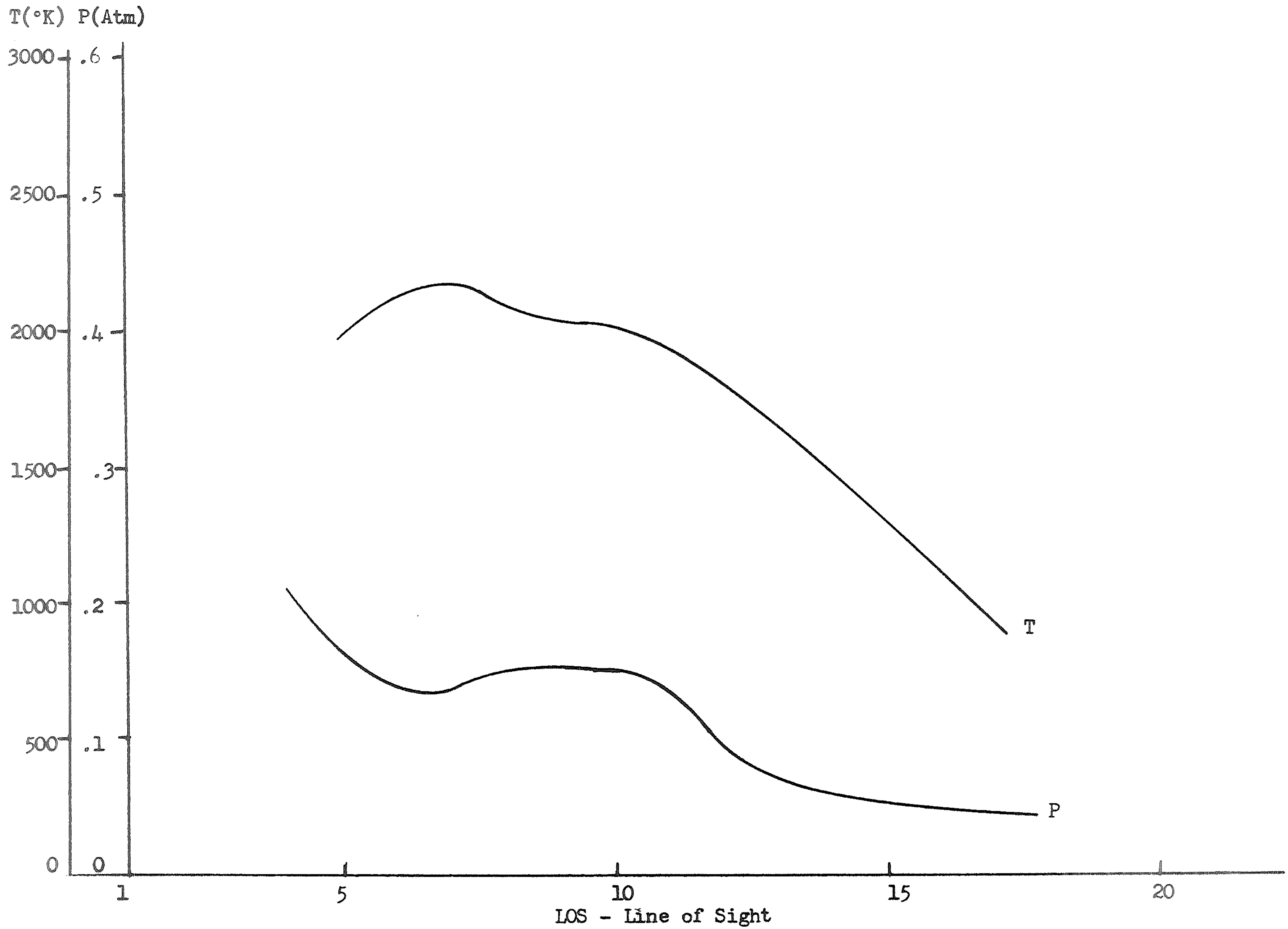

Figure 3-41 Apparent Flame Temperature and H_2O Partial Pressure - Run 23 Position 5

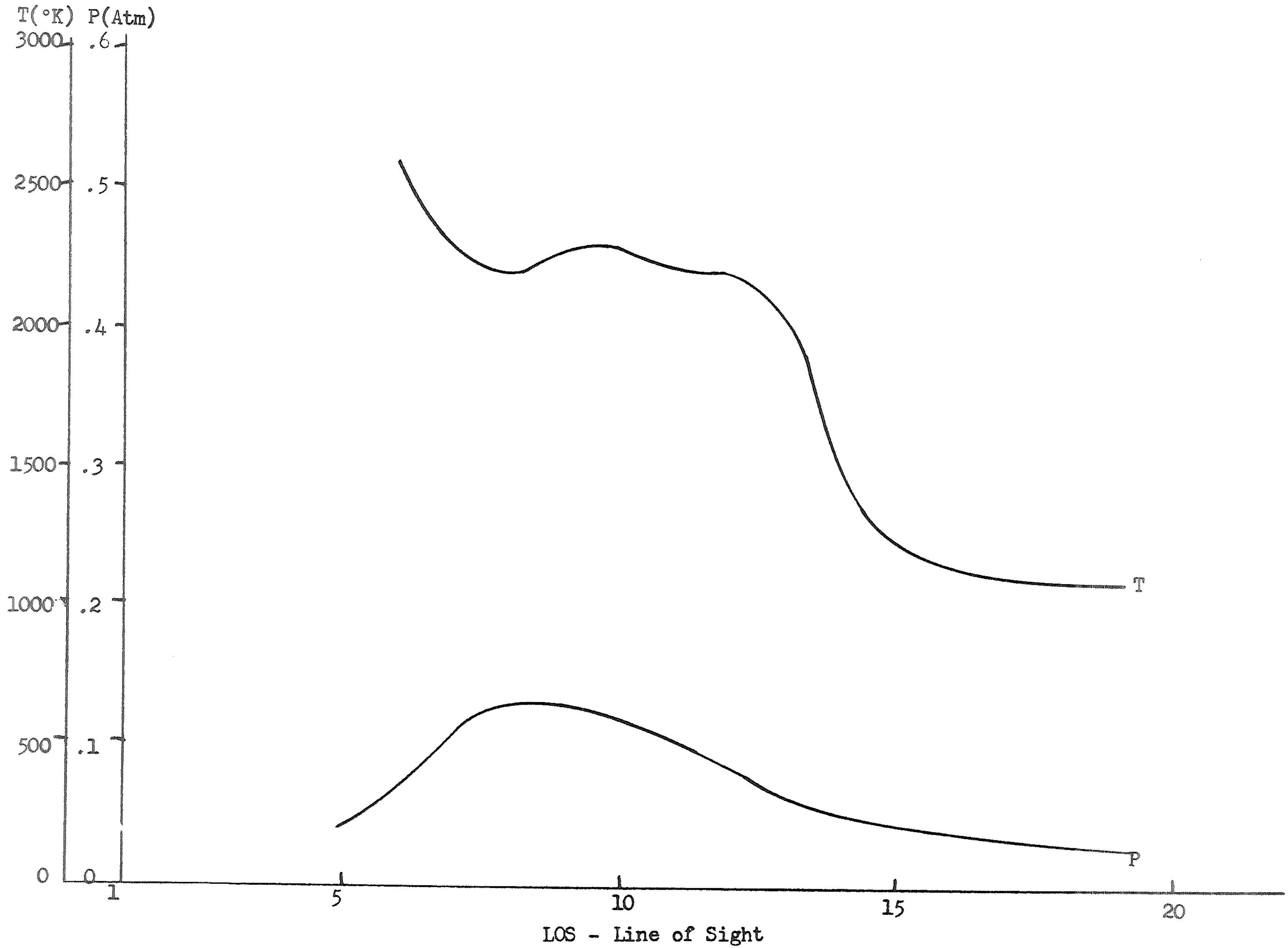

Figure 3-42 Apparent Flame Temperature and H_2O Partial Pressure - Run 24 Position 6

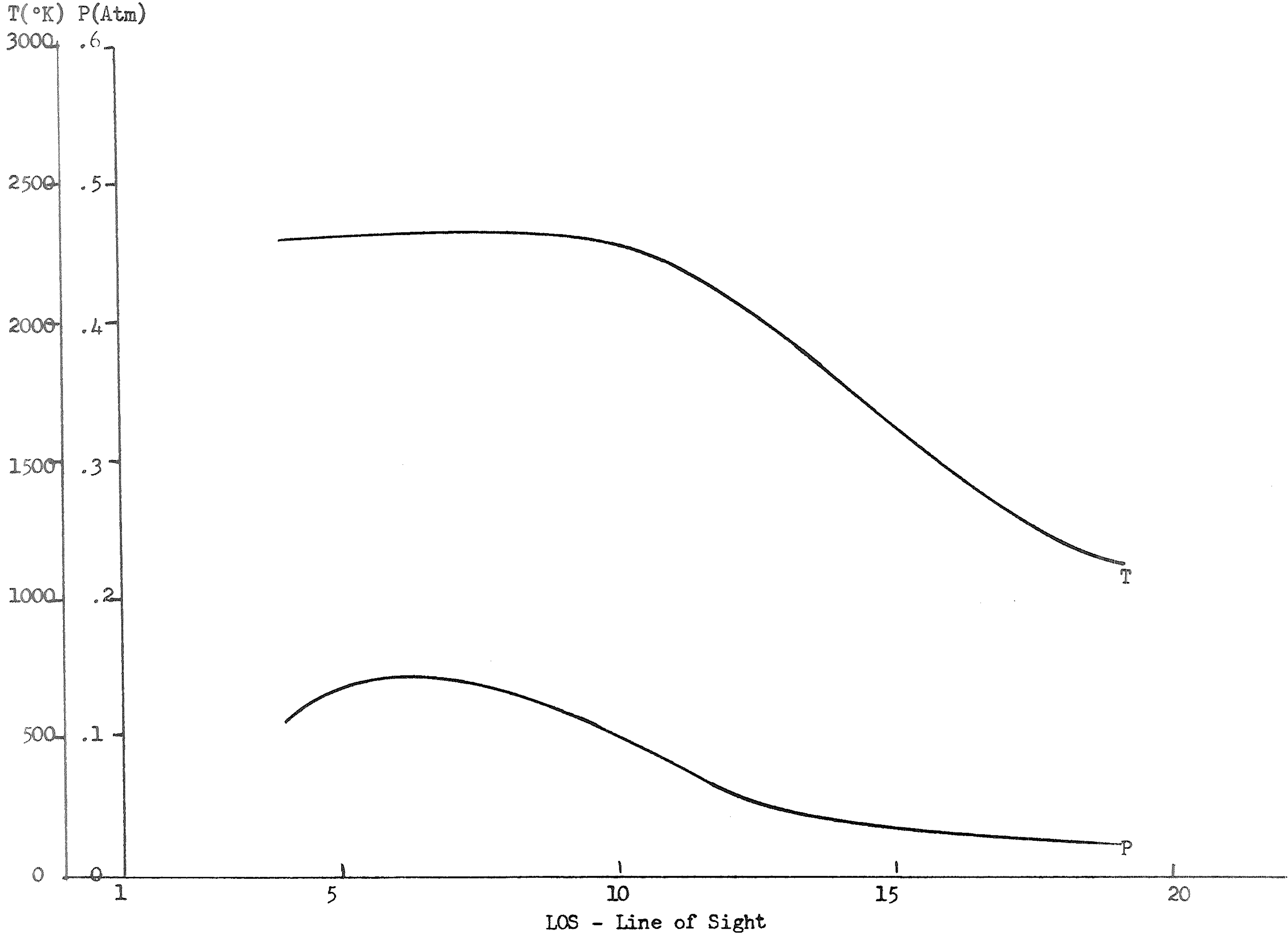

Figure 3-43 Apparent Flame Temperature and H_2O Partial Pressure - Run 25 Position 7

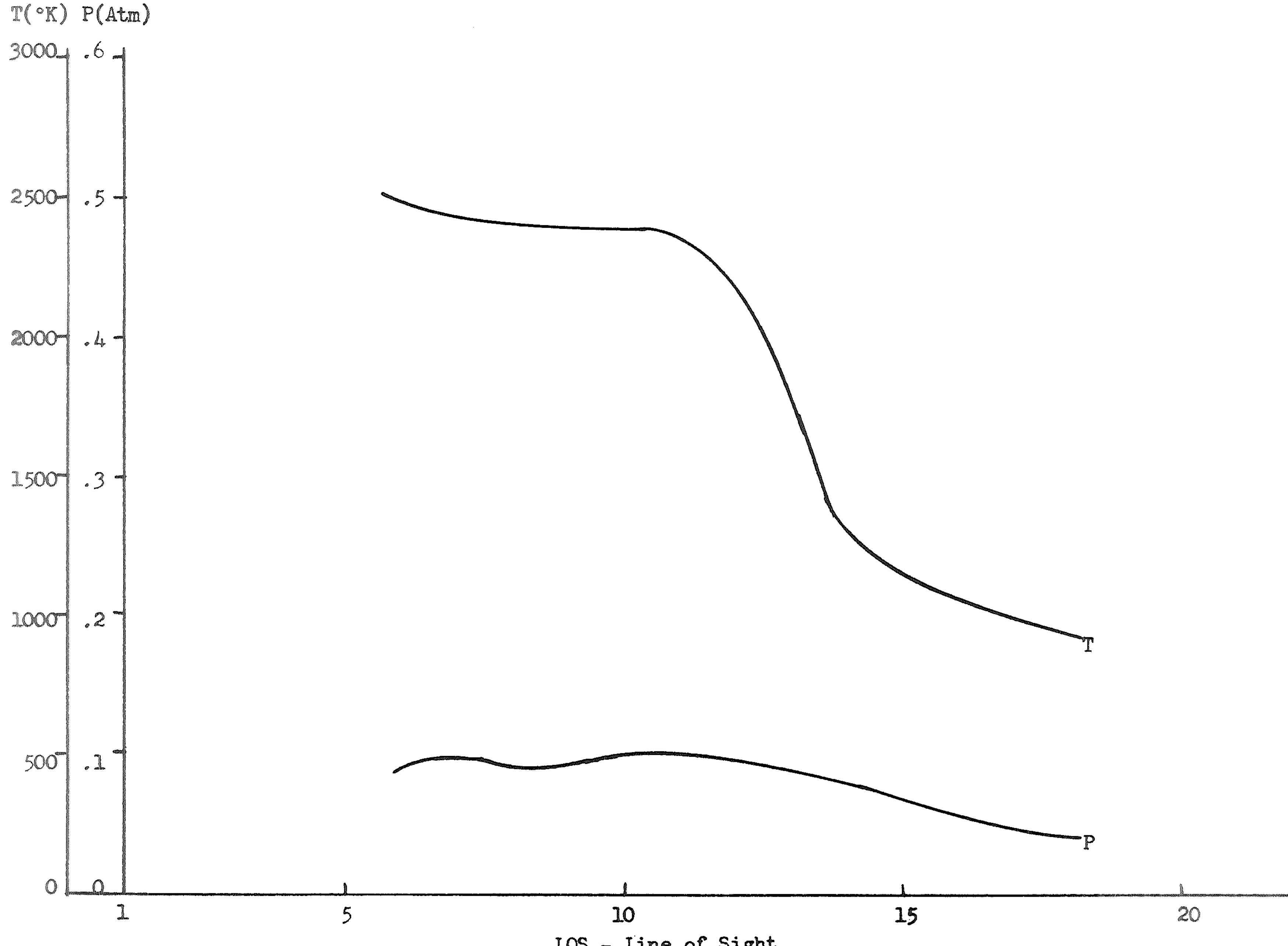

Figure 3-44 Apparent Flame Temperature and H_2O Partial Pressure - Run 26 Position 1

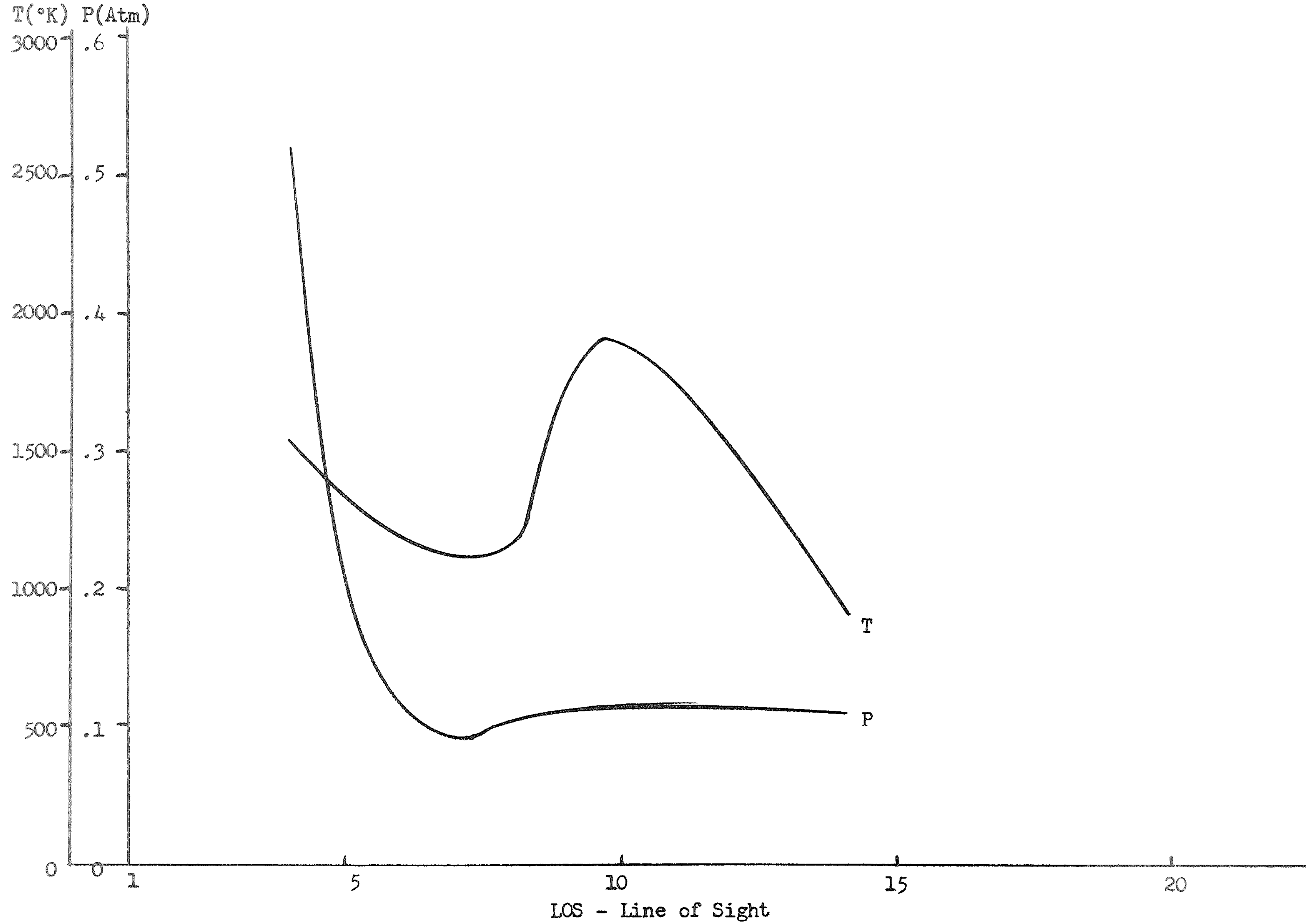

Figure 3-45 Apparent Flame Temperature and H_2O Partial Pressure - Run 27 Position 5

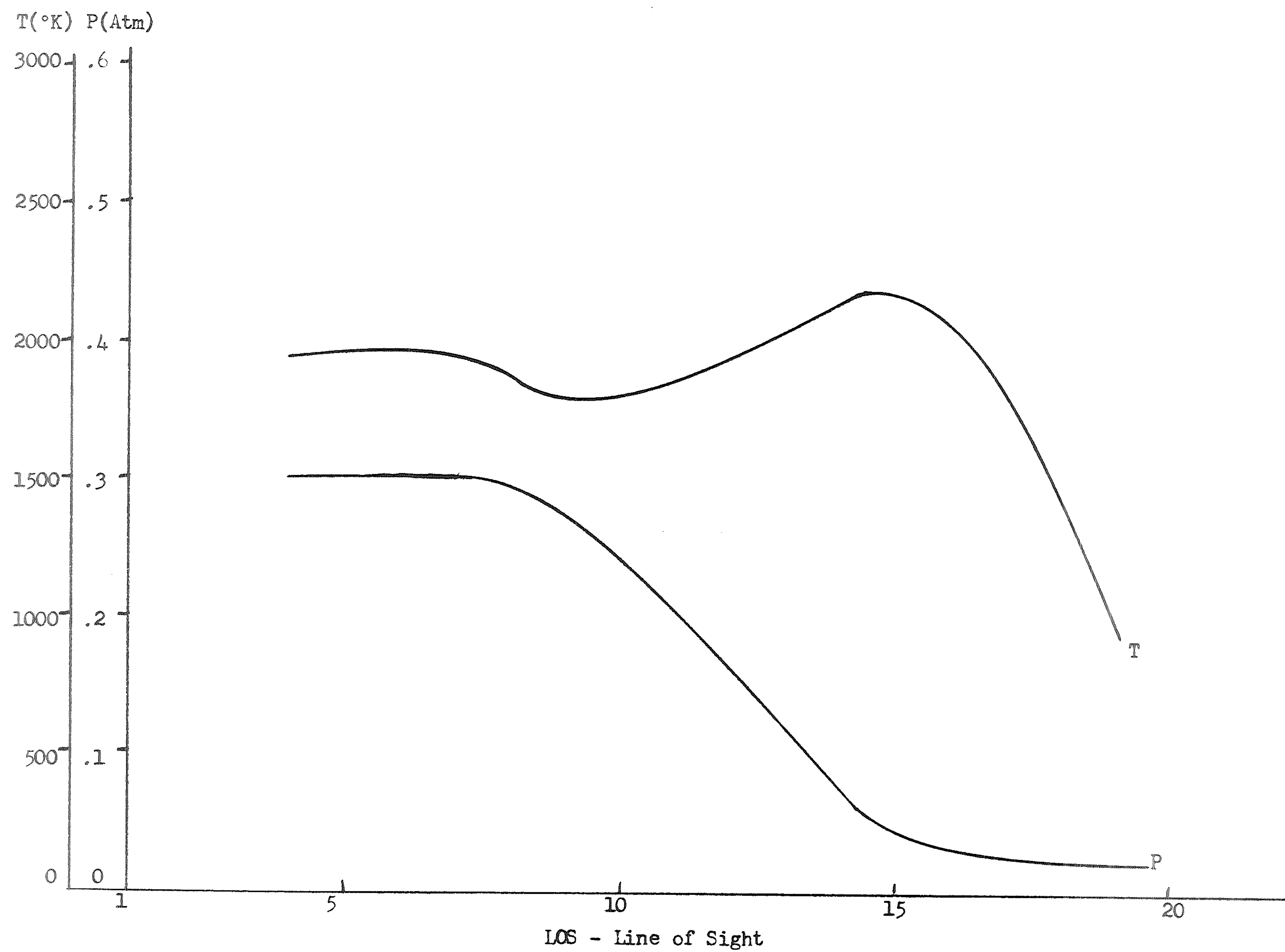

Figure 3-46 Apparent Flame Temperature and H_2O Partial Pressure - Run 28 Position 8

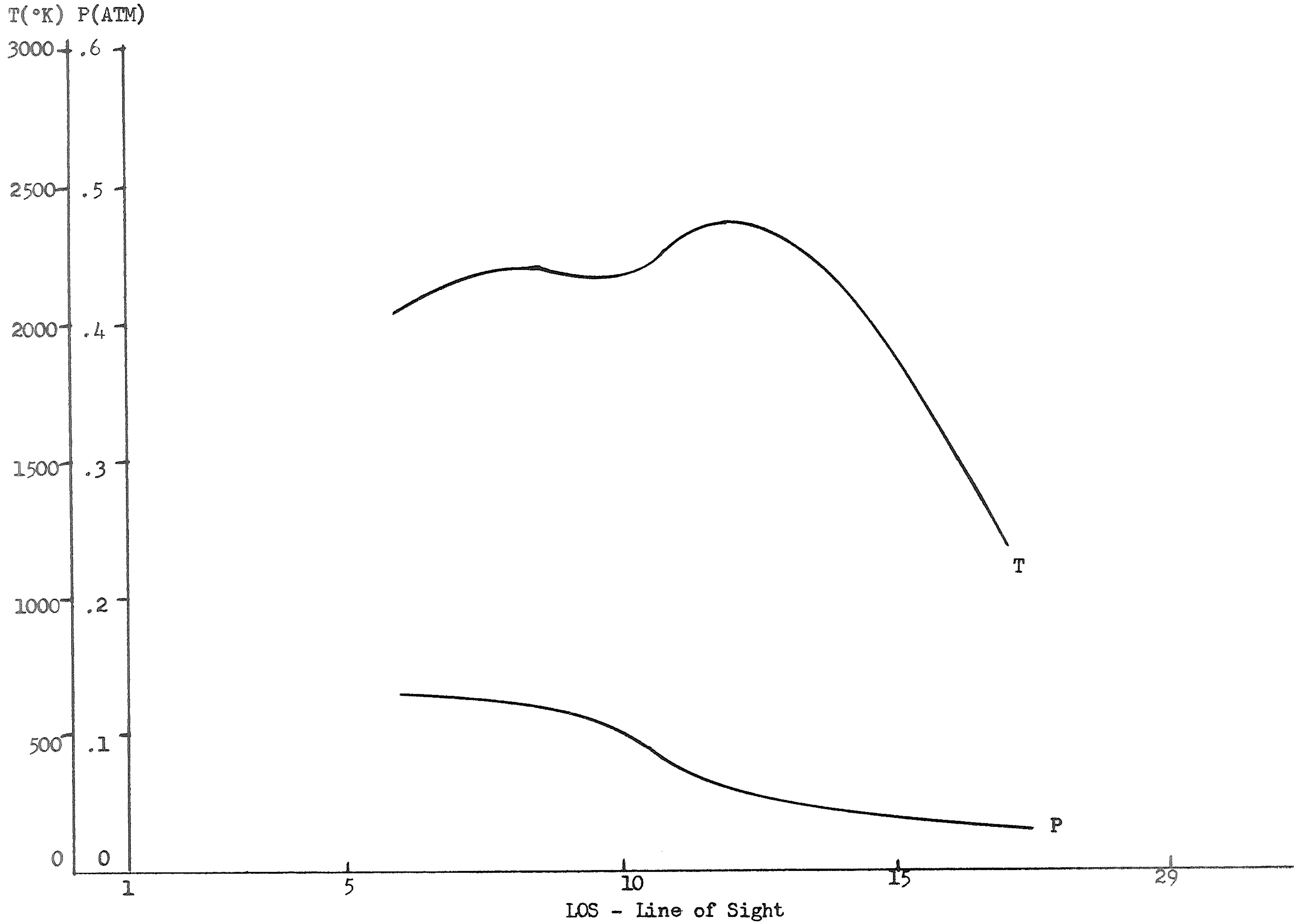

Figure 3-47 Apparent Flame Temperature and H_2O Partial Pressure - Run 30 Position 7

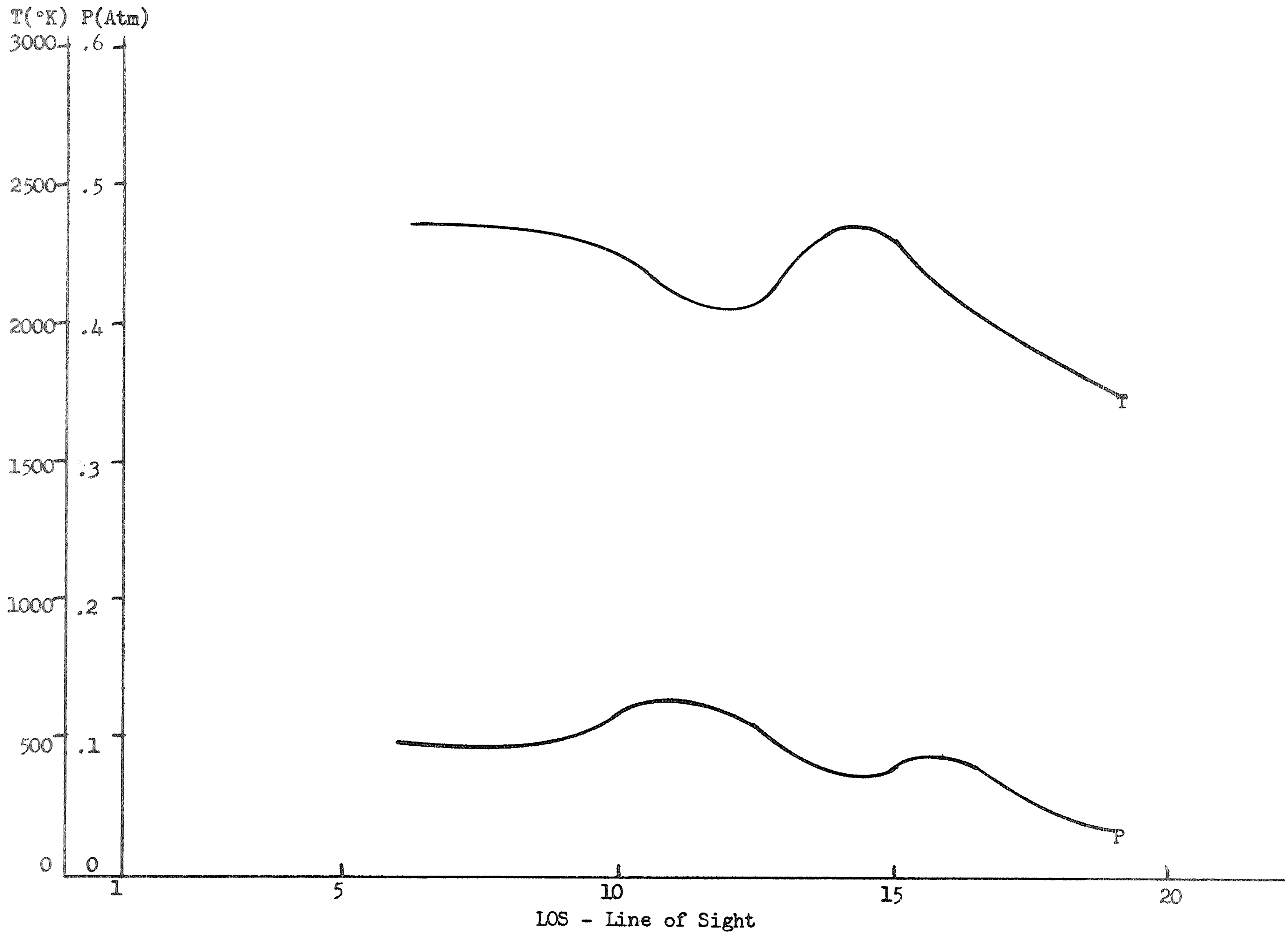

Figure 3-48 Apparent Flame Temperature and H_2O Partial Pressure - Run 31 Position 10

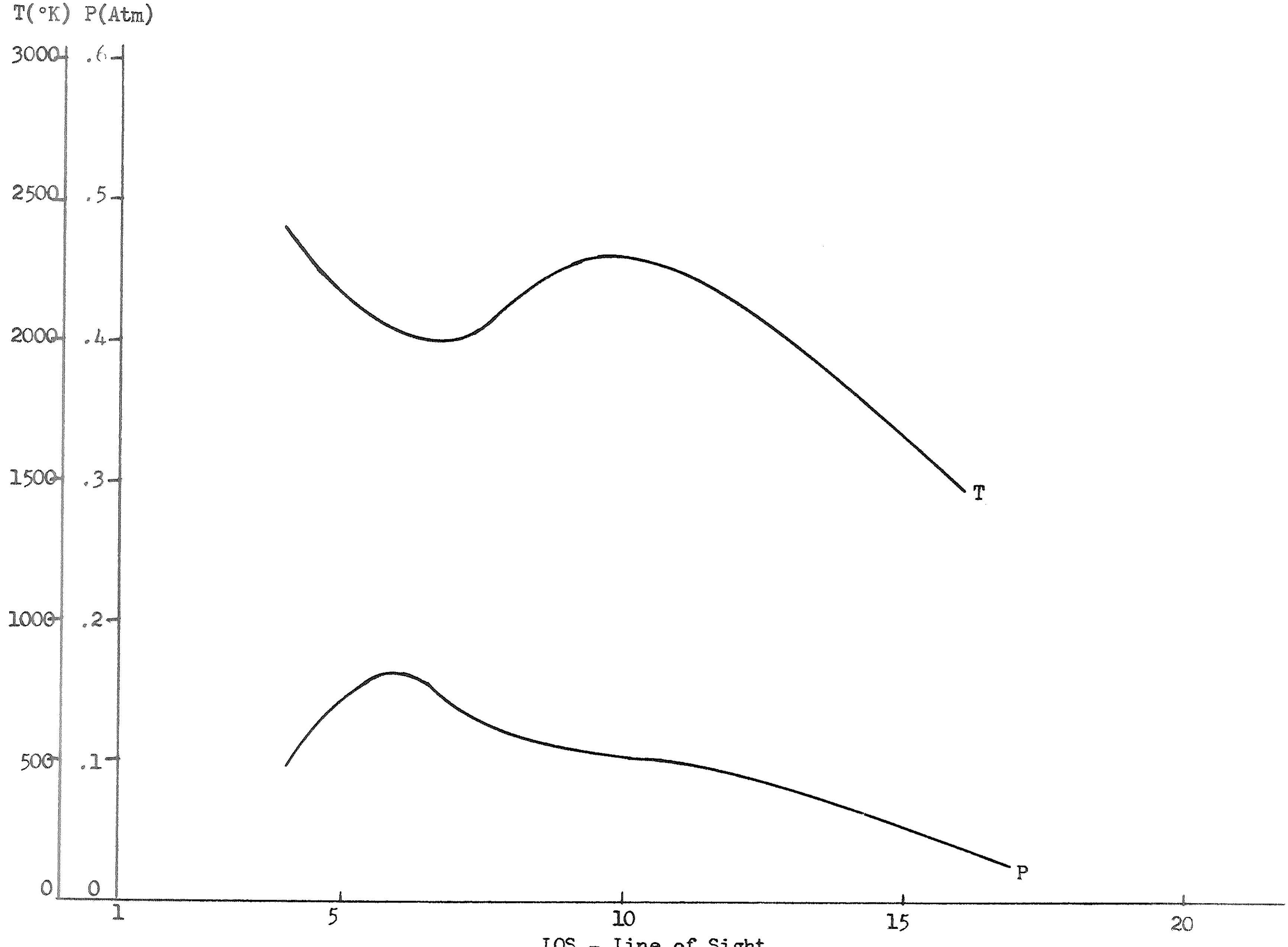

Figure 3-49 Apparent Flame Temperature and H_2O Partial Pressure - Run 32 Position 8

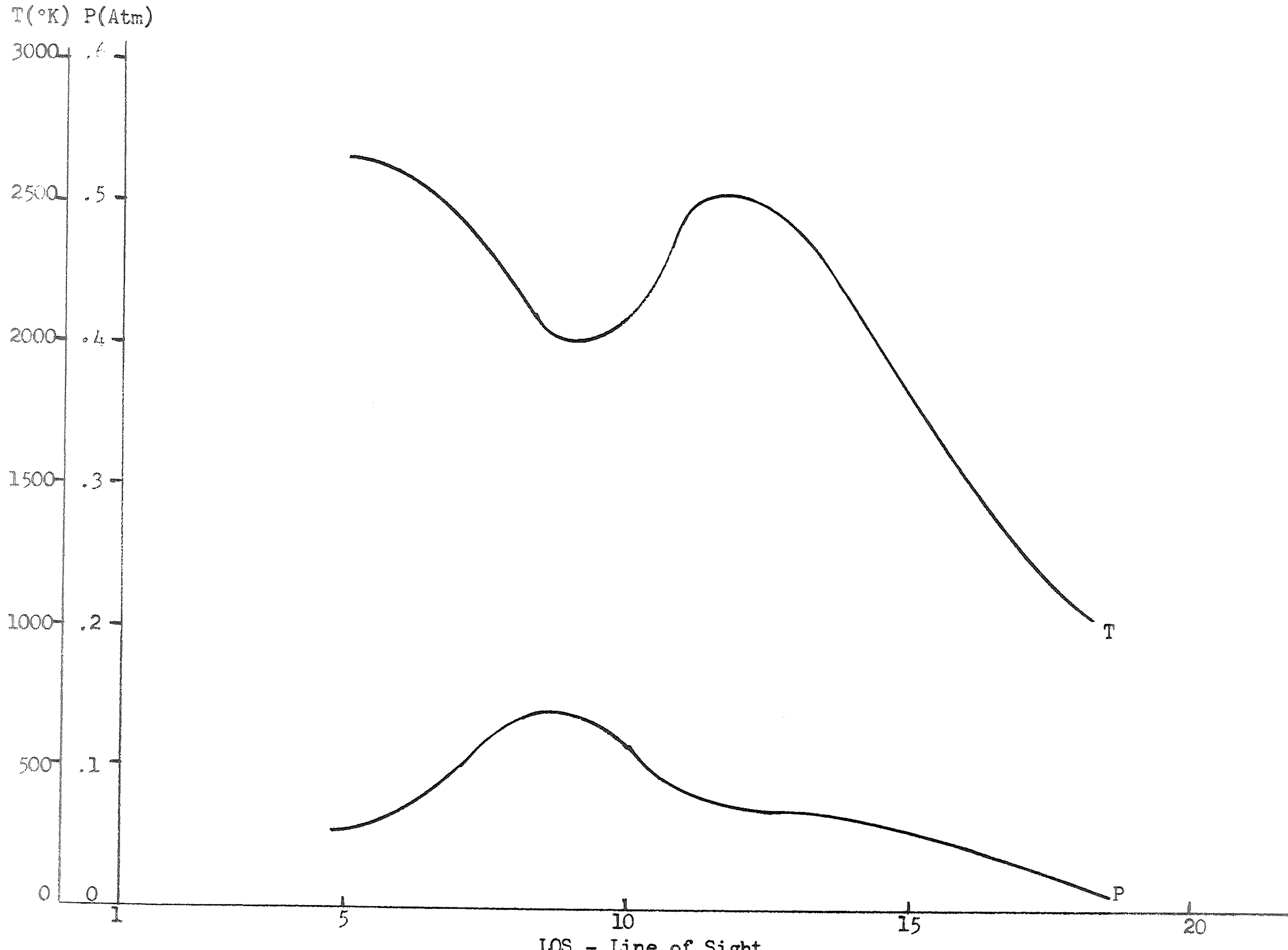

Figure 3-50 Apparent Flame Temperature and H_2O Partial Pressure - Run 34 Position 8

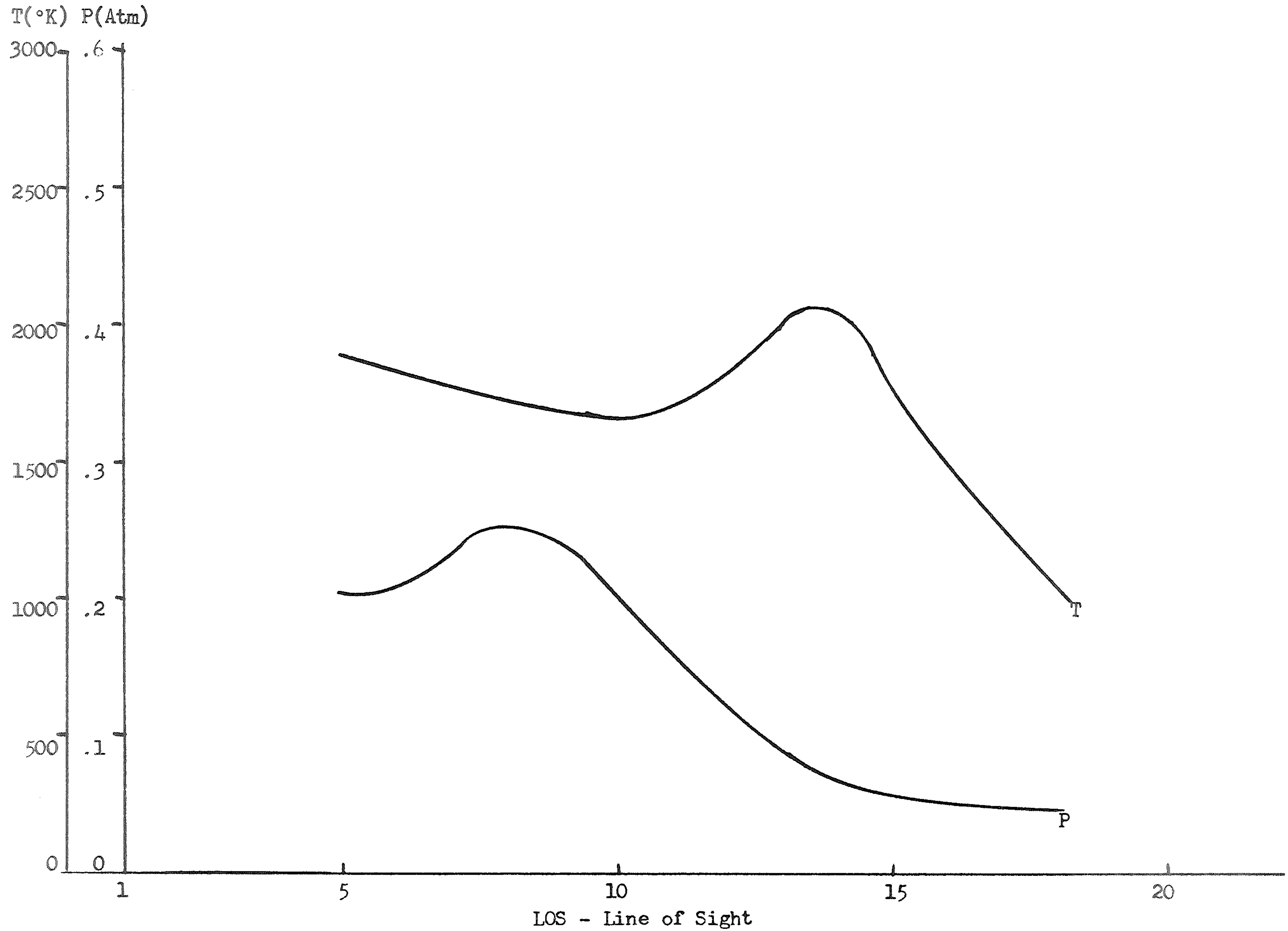

Figure 3-51 Apparent Flame Temperature and H_2O Partial Pressure - Run 35 Position 8

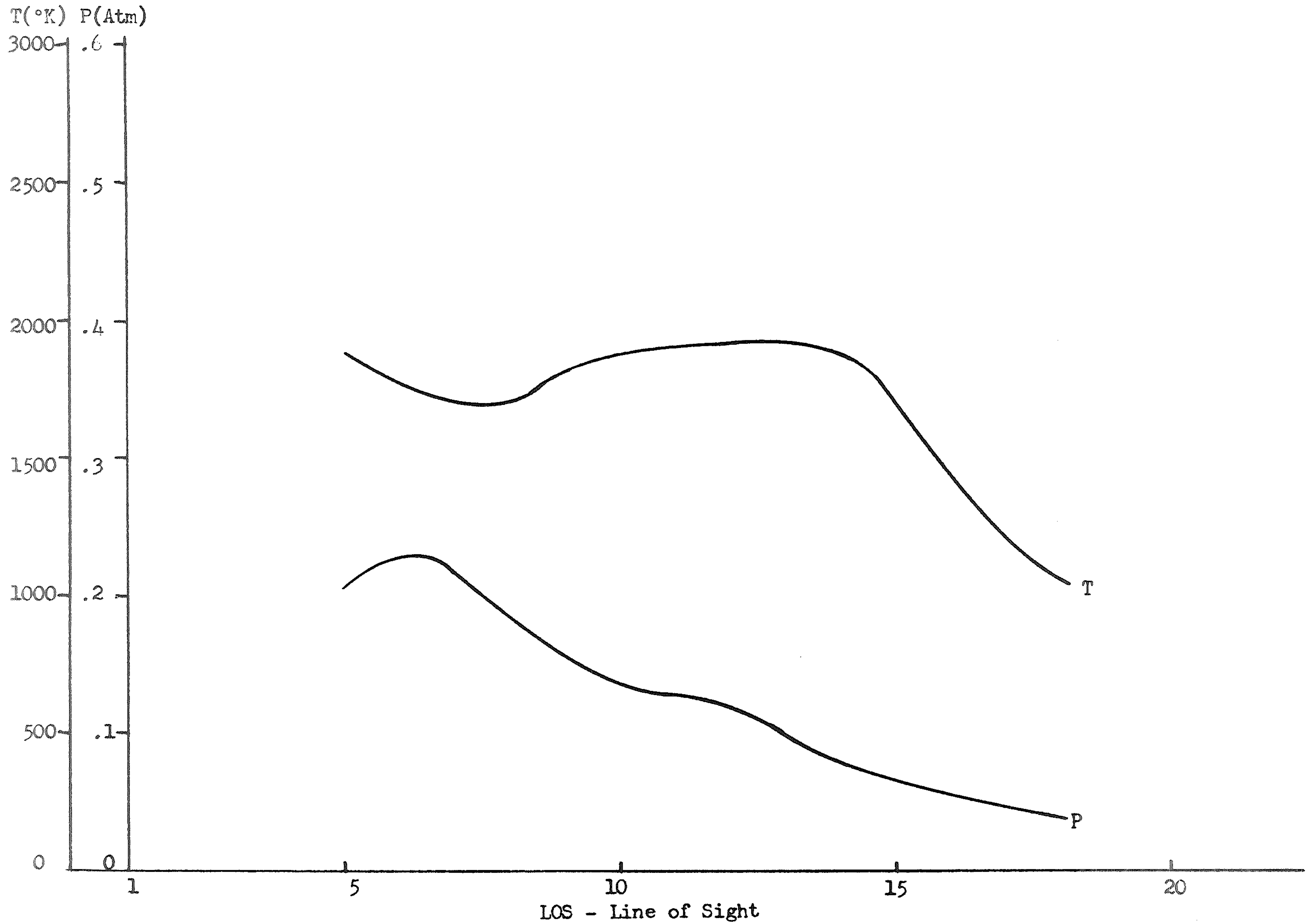

Figure 3-52 Apparent Flame Temperature and H_2O Partial Pressure - Run 37 Position 8

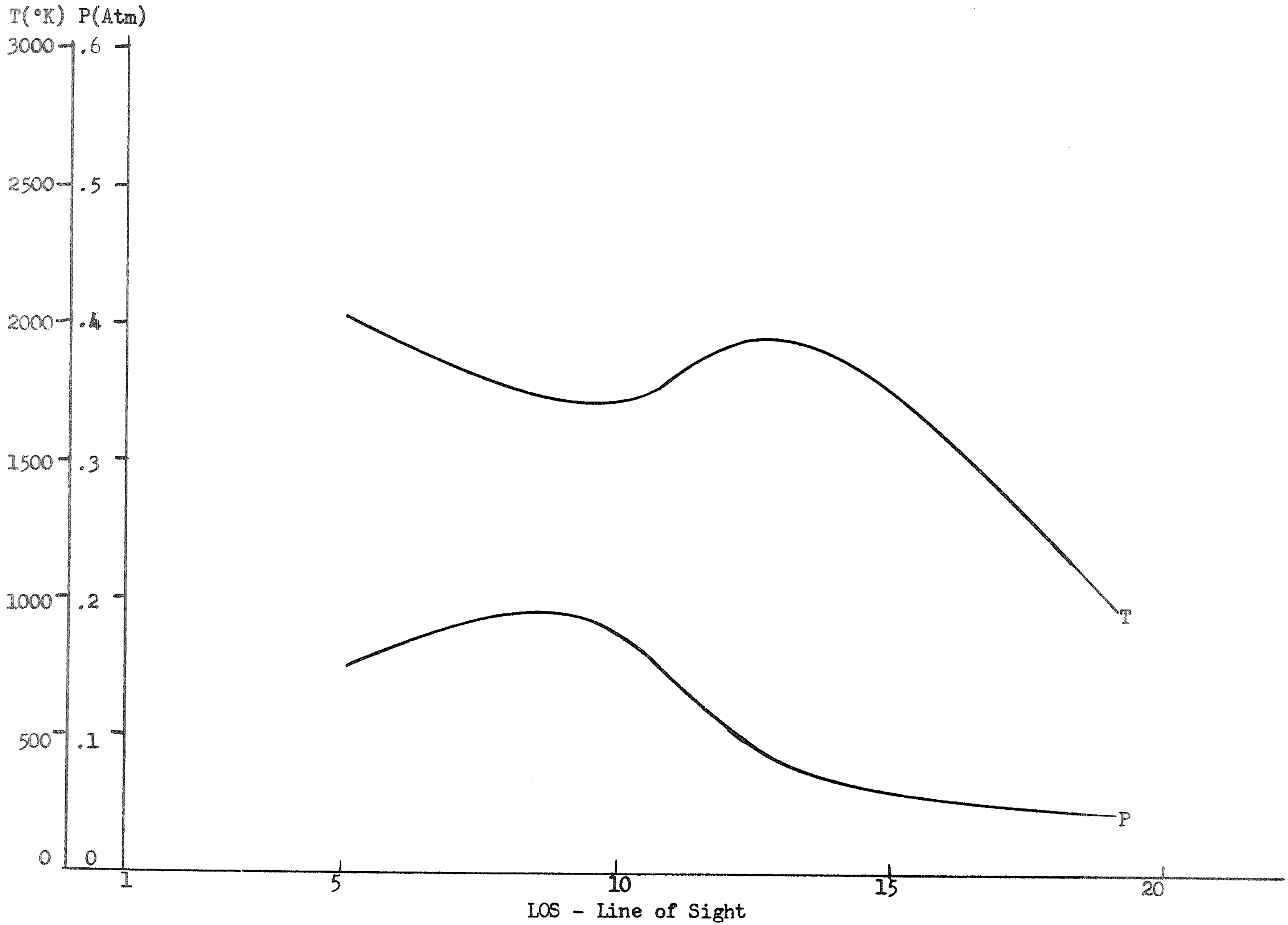

Figure 3-53 **Apparent Flame Temperature and H_2O Partial Pressure** - Run 38 Position 8

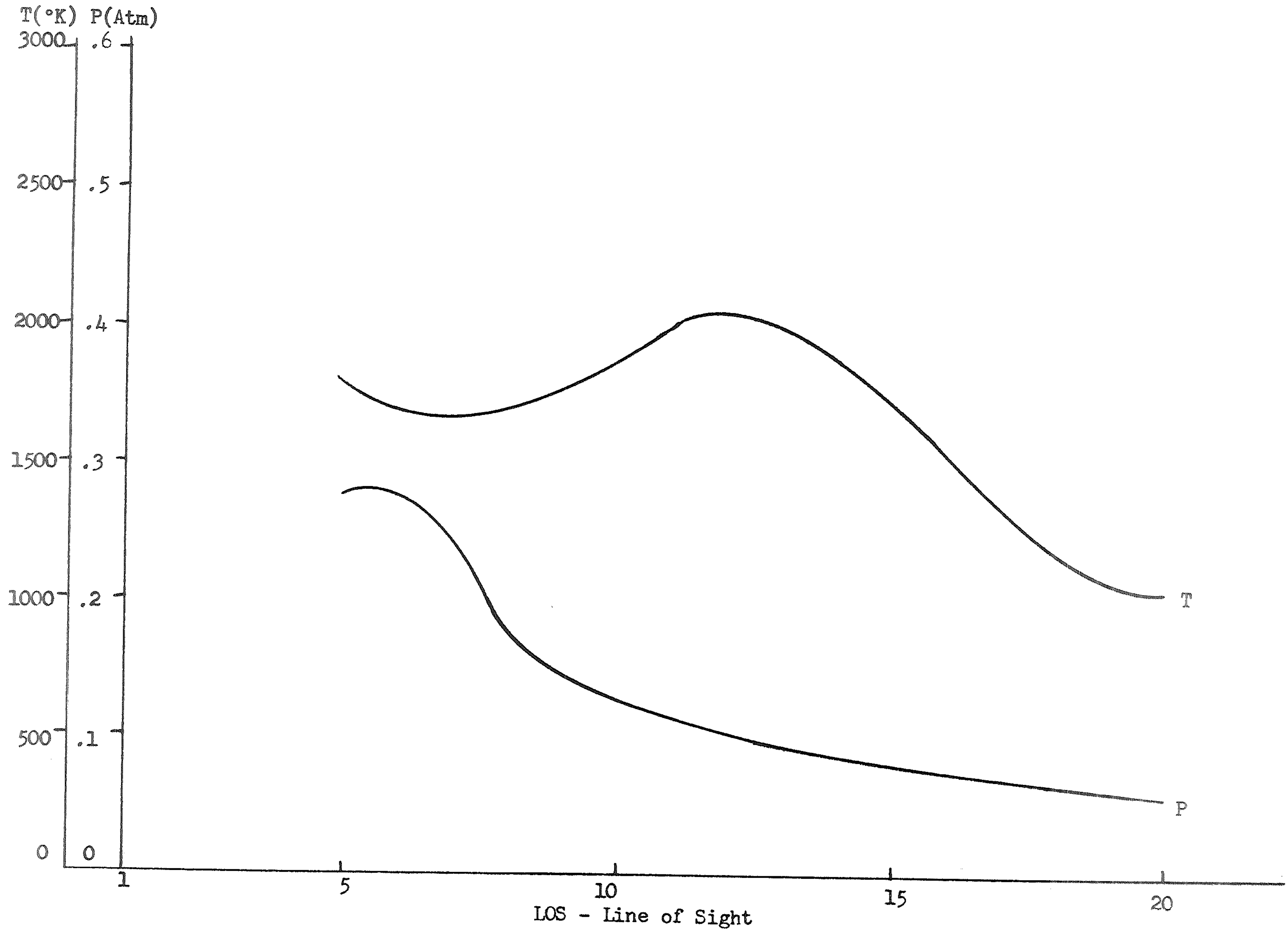

Figure 3-54 Apparent Flame Temperature and H_2O Partial Pressure - Run 39 Position 9

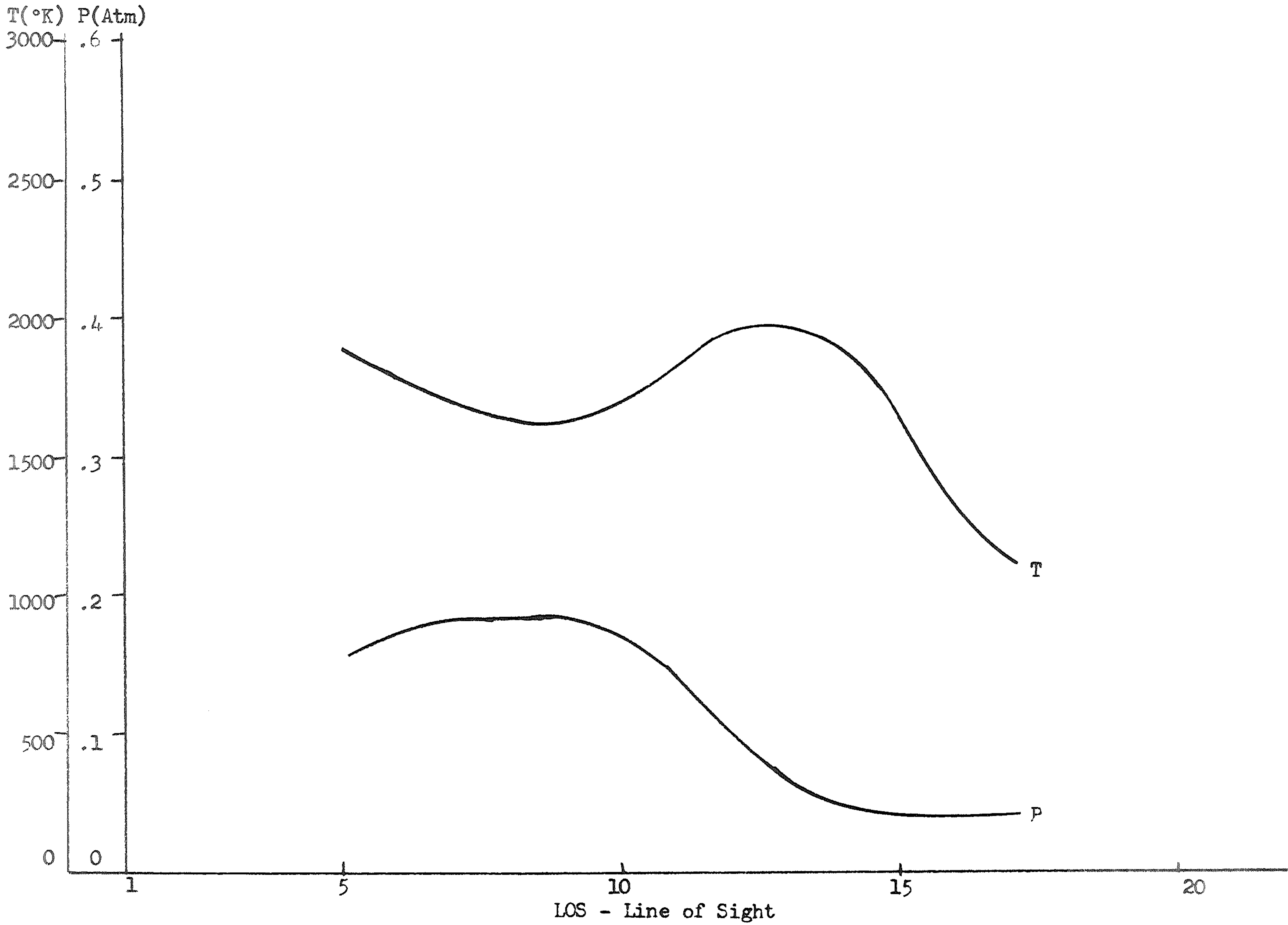

Figure 3-55 Apparent Flame Temperature and H_2O Partial Pressure - Run 40 Position 8

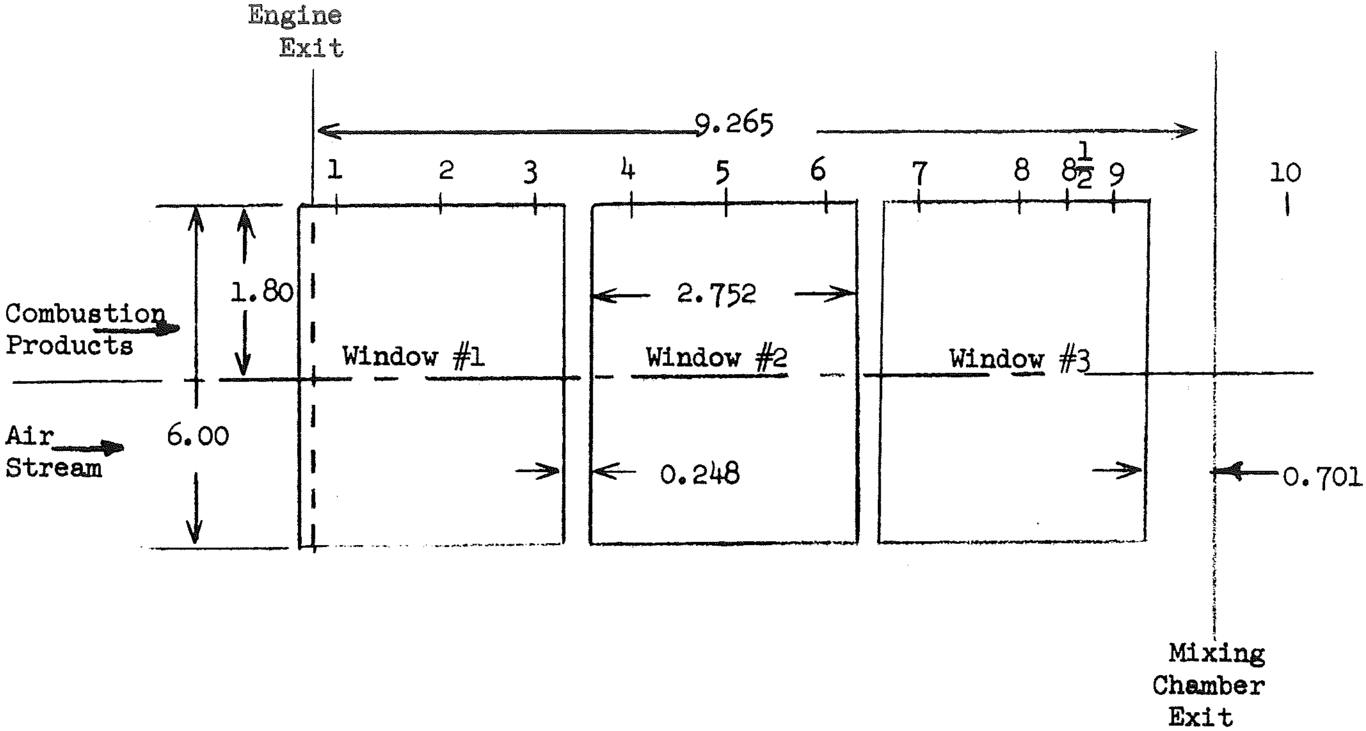

Position	Distance from Start of Mixing Region, inches
1	0.438
2	1.219
3	2.000
4	3.438
5	4.259
6	5.000
7	6.438
8	7.219
8-1/2	7.828
9	8.000
10	12.297

Figure 3-56. Instrumentation Positions

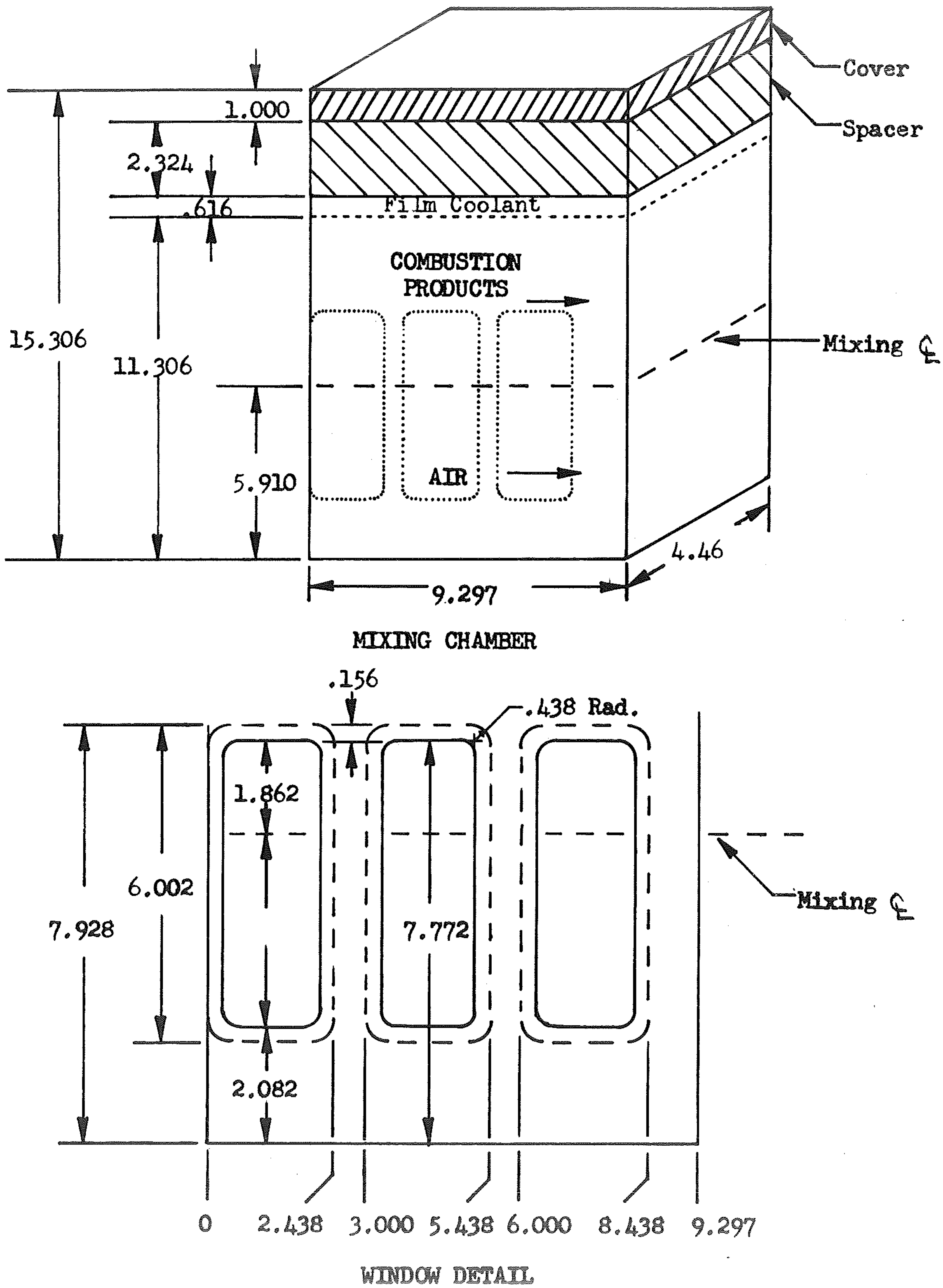

Figure 3-57. Principal Test Section Dimensions

TABLE 3-1

CONVERSION OF LOS TO PHYSICAL ENGINE DIMENSIONS

Line of Sight LOS	Run 021, in.	Run 16, in.	All Other Runs, in.
0	1.62	5.26	----
1	1.93	4.95	----
2	2.24	4.64	8.12
3	2.56	4.32	7.79
4	7.87	4.01	7.47
5	3.18	3.70	7.15
6	3.49	3.39	6.83
7	3.80	3.08	6.50
8	4.12	3.76	6.18
9	4.43	2.45	5.86
10	4.74	2.14	5.54
11	5.05	1.83	5.22
12	5.36	1.52	4.90
13	5.68	1.20	4.57
14	5.99	0.89	4.25
15	6.30	0.58	3.93
16	6.61	0.27	3.61
17	6.92	-.04	3.28
18	7.24	-.36	2.96
19	7.55	-.67	2.64
20	7.86	-.98	2.32
21	8.17	----	2.00
22	8.48	----	1.68

APPENDIX 4

PHOTOGRAPHIC DATA

As mentioned previously a number of photographic measurements were utilized to provide visual information supplemental to the optical data collection. These measurements include schlieren, ultra-violet, infrared, color, and photo-pyrometry photography. A presentation of these data follows.

SCHLIEREN PHOTOGRAPHY

Schlieren photography was utilized to gather data on the gross effects produced by changes in test conditions upon the momentum boundary layer between the subsonic and supersonic streams. The knife edge was horizontal in order to accentuate gradients in the vertical direction. Photographs representing the experiments are shown in Figs. 4-1 to 4-10. The field of view of the schlieren camera was approximately 3-inches by 3-inches. The data extracted from the films together with a definition of the test conditions is given in Table 4-1.

Figures 4-1 and 4-2 represent a top view of the mixing region at the mid-stream and at the edge, respectively. These views indicate that the sidewall film coolant layer has been completely penetrated by the combustor exhaust stream, i.e., the 2-dimensionality of the combustor exhaust products stream has been augmented by mixing with the film coolant. Also shown in Fig. 4-2 is the mixing between the mixing chamber exhaust with the ambient environment. The angle is approximately 11-degrees which is similar to the angles observed for mixing between the combustor exhaust products and air streams. The coarse texture of these prints is indicative of the turbulence scales.

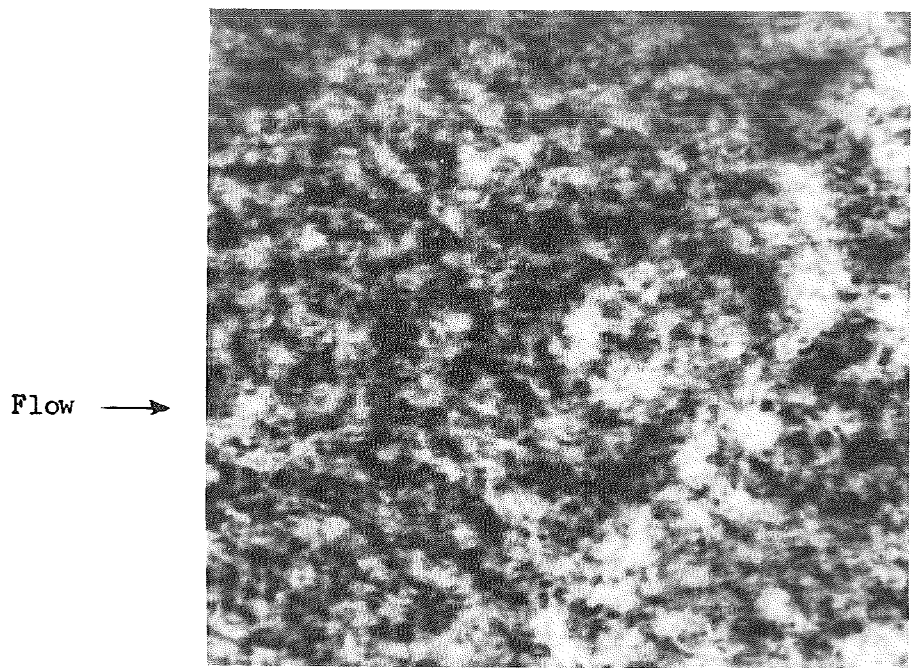

Figure 4-1. Schlieren From Top,Aft of Mixing Chamber Exit - Midstream - Run 5

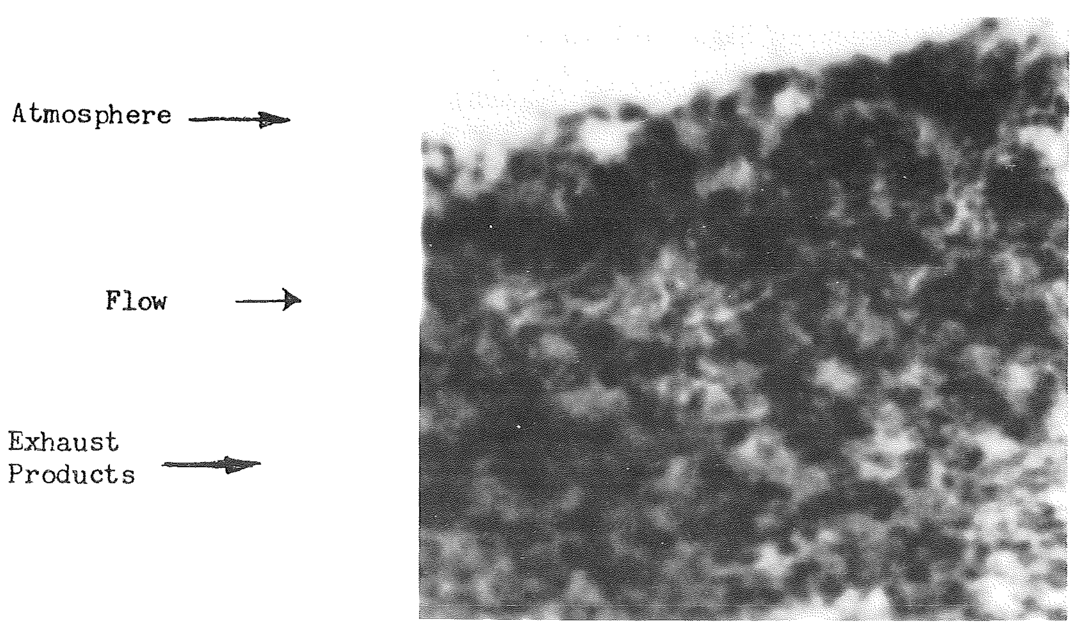

Figure 4-2. Schlieren From Top,Aft of Mixing Chamber Exit - Edge - Run 11

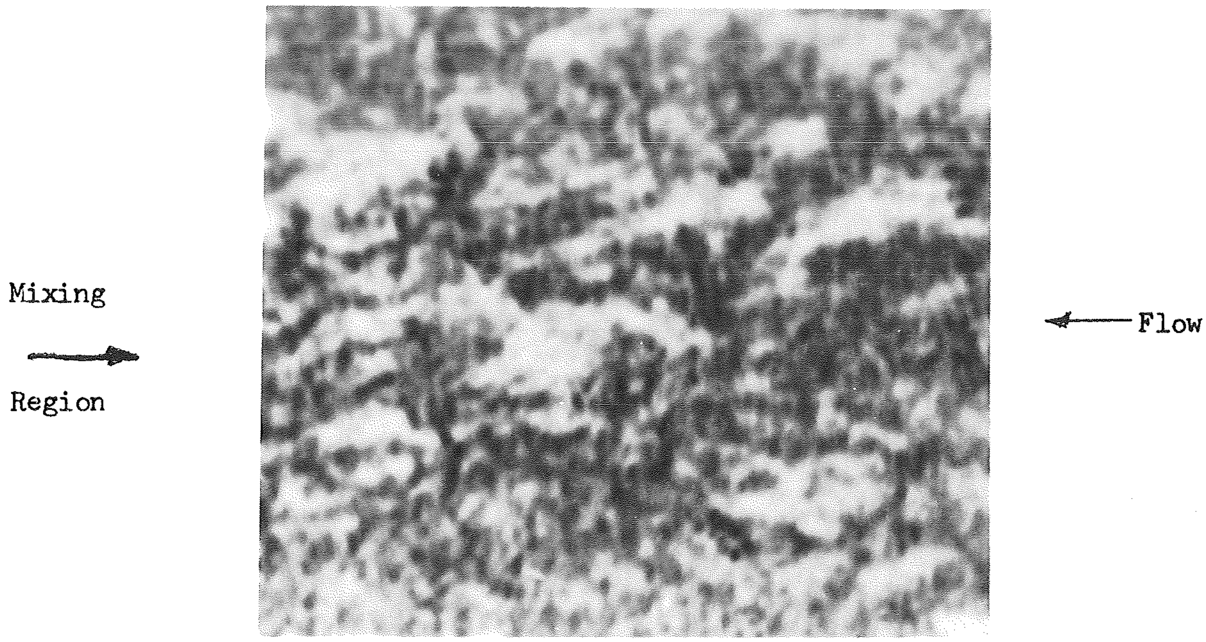

Figure 4-3. Schlieren From Side - Aft of Mixing Chamber Exit - Flow Axis - Run 13

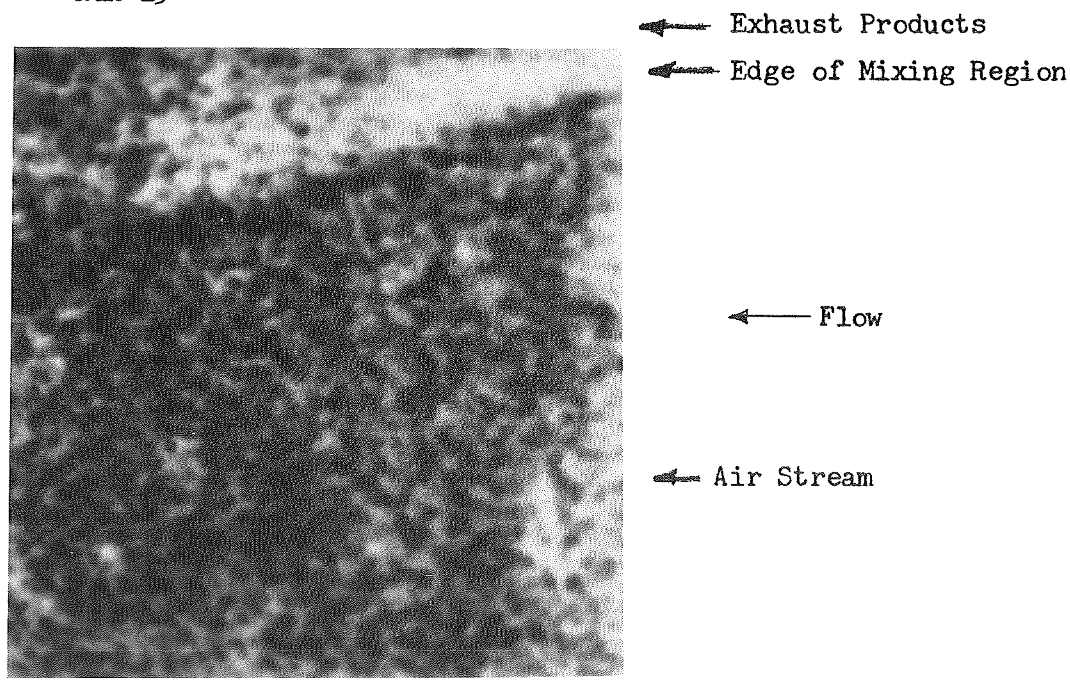

Figure 4-4. Schlieren From Side - Upstream Window - Air Stream - Run 39

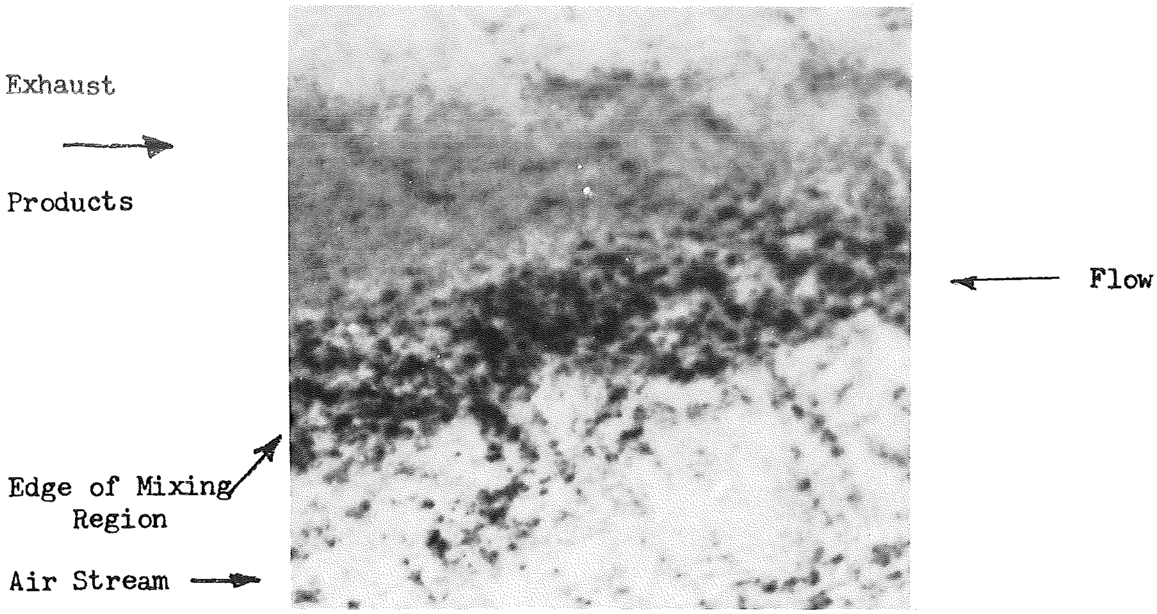

Figure 4-5. Schlieren From Side - Middle Window - Air Stream - Run 19

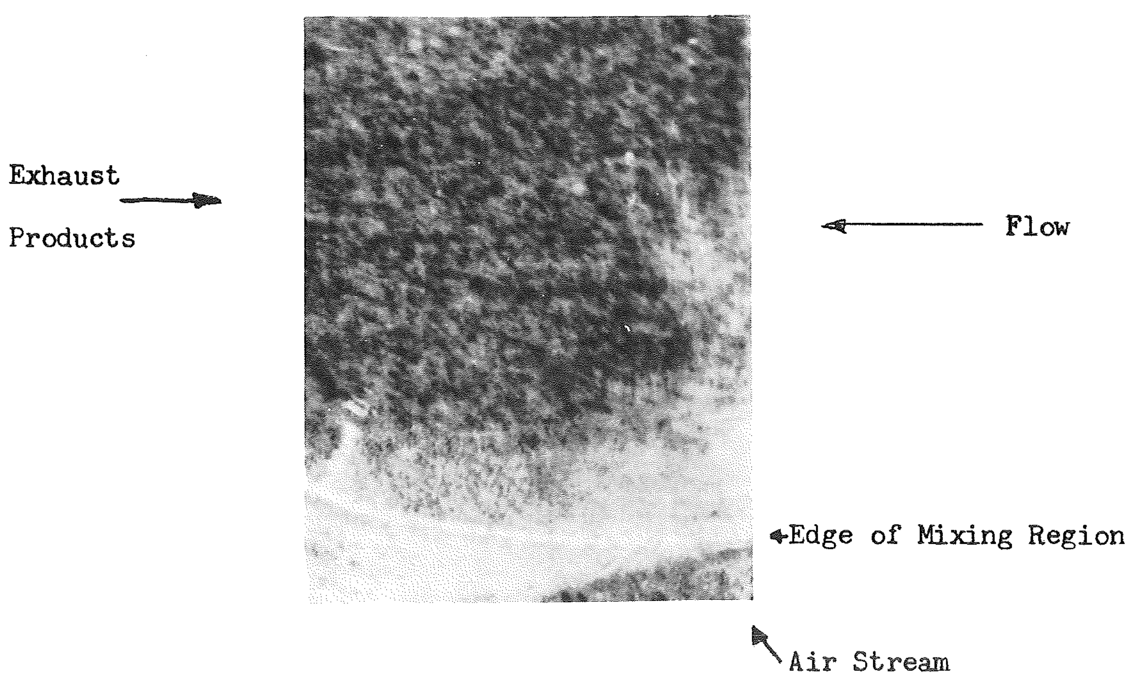

Figure 4-6. Schlieren From Side - Upstream Window - Flow Axis - Run 22

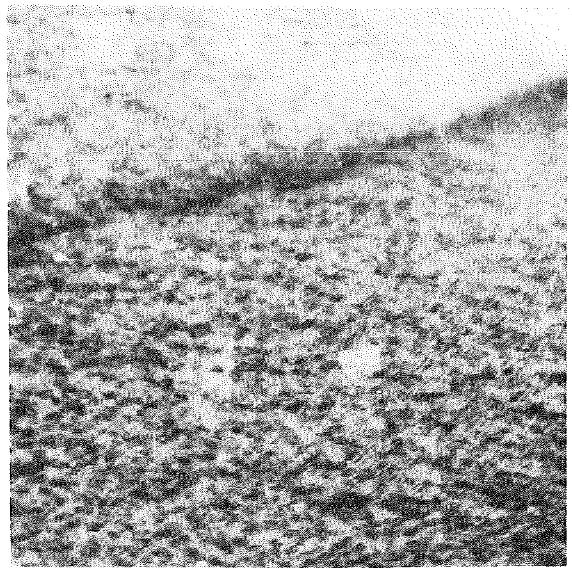

Figure 4-7. Schlieren From Side - Upstream Window - Air Stream - Run 34

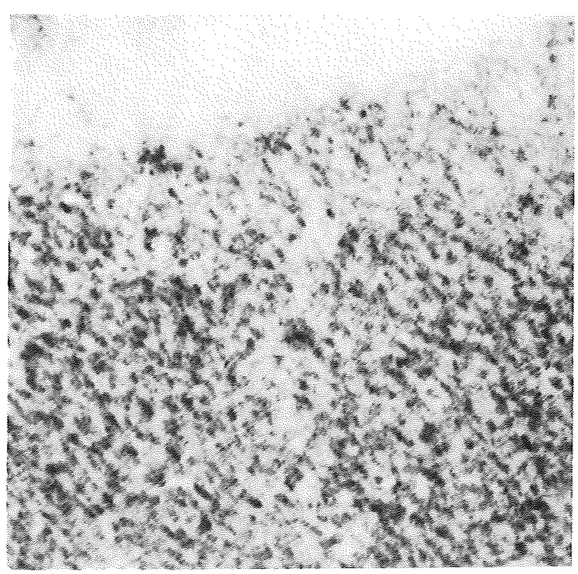

Figure 4-8. Schlieren From Side - Upstream Window - Air Stream - Run 33

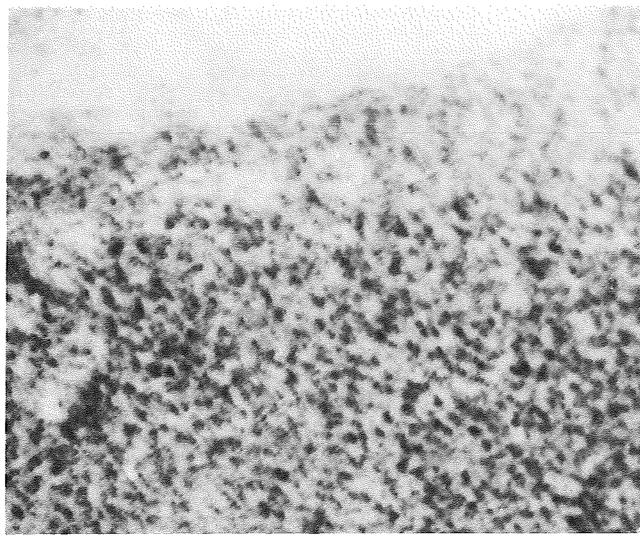

Figure 4-9. Schlieren From Side - Upstream Window - Air Stream - Run 32

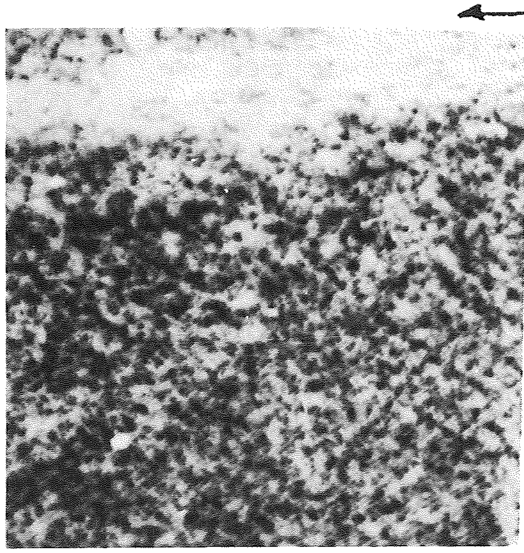

Figure 4-10. Schlieren From Side - Upstream Window - Air Stream - Rur 40

TABLE 4-1

SCHLIEREN DATA

Run #	Test Type	Defined Lines* 1 Deg.	2 Deg.	Fig. #
5	High Temperature Air	---	---	4-1
11	High Temperature Air	11°	---	4-2
13	High Temperature Air	---	---	4-3
19	Medium Temperature Air	10°	8°	4-5
22	Medium Temperature Air	9°	2°	4-6
32	High Velocity Air	11°	8°	4-7
33	Low Velocity Air	14°	13°	4-8
34	Low Temperature Air	15°	---	4-7
39	High Temperature Air	14°	8°	4-4
40	1/4" Dam	6°	5°	4-10

* Schematic

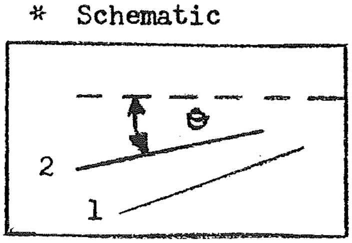

1 Edge of Mixing Region

2 Inner Boundary of Reaction Zone

All of the remaining schlieren figures represent the mixing between the combustor exhaust products and air streams. Figure 4-3 shows a side view of the mixing region near the idealized axis of flow (line between the two streams and mixing centerline) at the same plane utilized for the top view measurements. Relatively uniform mixing was indicated and the scale of turbulence appeared in good agreement with that observed in the top views.

Grouping all of the tests as a function of air temperature (Figs. 4-4 to 4-7) indicated no clear trend for the angle observed for the momentum boundary layer (the angle ranges being 9 to 15 degrees). Although data reduction is relatively crude, these data indicate that changes in air temperature of approximately 700°F have no appreciable effect on the mixing region. The average of these four measurements was 12 degrees which agrees quite well with that observed for the mixing between the exhaust and the environment. Of particular interest is the obvious change in the scale of turbulence between data collected aft and through the mixing chamber. The scale of turbulence is much smaller or finer inside the chamber.

The velocity tests (Figs. 4-8 and 4-9) yielded data that was within the range of the air temperature tests; however, these data indicated that air velocity is a significant mixing parameter; the lower the air velocity the more rapid the mixing. A 240 ft/sec decrease in velocity produced a 3-degree increase in the angle between the mixing layer and the air stream.

Comparison of the schlieren data for the 1/2-inch dam data (Fig. 4-10) with the previously described data indicates that a thin physical boundary is a prerequisite for valid mixing experiments. What normally would be considered an insignificant change in thickness of the lip halved the mixing rate.

No correlation of the data for the inner boundary (the second defined line) that was indicated on a number of the schlieren figures was obtained. The observed angle ranged from 2 to 13 degrees and the difference in angle between the two lines ranged from 1 to 7 degrees.

INFRARED PHOTOGRAPHY

Infrared photography in the 7000-8500A band was utilized to record H_2O emission in the mixing chamber. This coverage was utilized on any firings where optical access was available. Photographs representing the experiments are shown in Figs. 4-11 to 4-22. The field of view of the camera was approximately 12-inches by 12-inches. The data extracted from these films together with a definition of the test conditions is given in Table 4-2. The soft texture of the photographs is an inherent problem in field type IR and UV photography. In addition, black and white reproduction of the color prints promotes further softening. The high temperature zones in the prints are the darkest regions; however, it should be noted that objects that are in shadows also appear dark. Therefore, great care must be exercised so that incorrect information will not be read into the analysis.

In general, three defined lines appear on the prints at the most upstream position. The lower line defines the extent of mixing into the air stream. The second line appears to be the upper boundary of the reaction zone and the

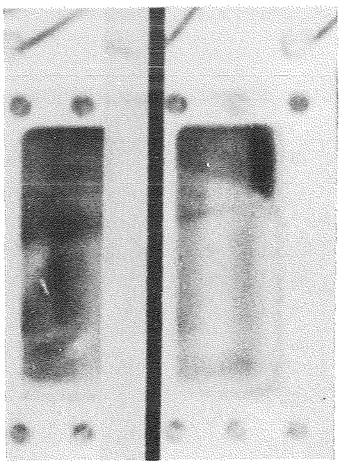

← Flow

Figure 4-11. Infrared Print - Upstream and Middle Windows - Run 16

← Flow

Figure 4-12. Infrared Print - Downstream Window and Aft of Exit - Run 17

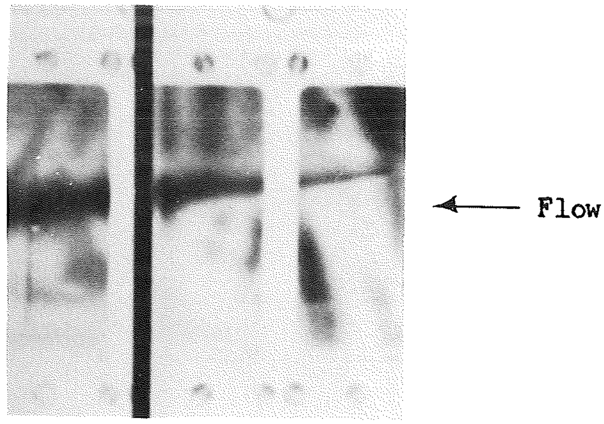

Figure 4-13. Infrared Print - Mixing Chamber - Run 31

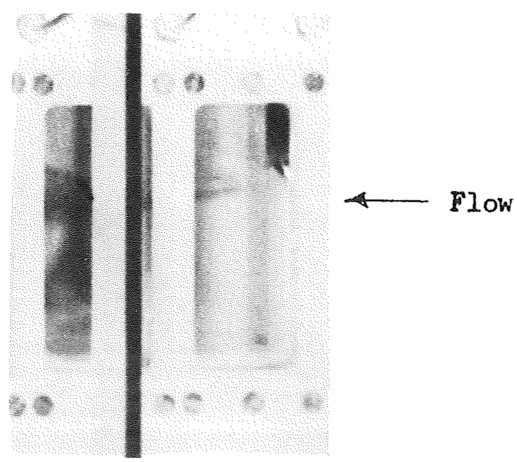

Figure 4-14. Infrared Print - Upstream and Middle Window - Run 19

Flow

Figure 4-15. Infrared Print - Downstream Window and Aft of Exit - Run 20

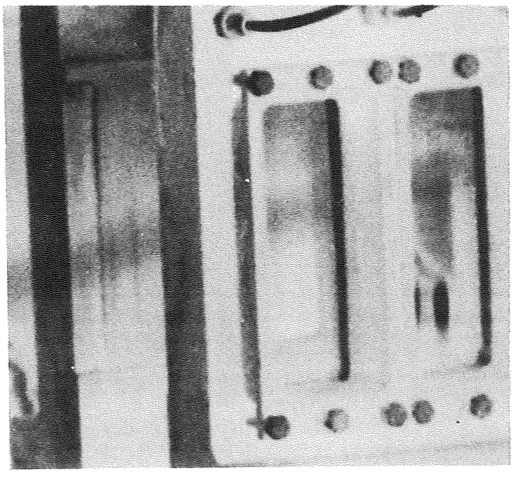

Flow

Figure 4-16. Infrared Print - Middle and Downstream Windows - Run 26

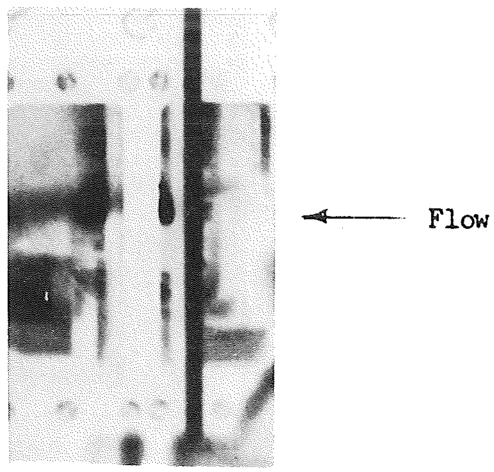

Figure 4-17. Infrared Print - Upstream and Middle Window - Run 34

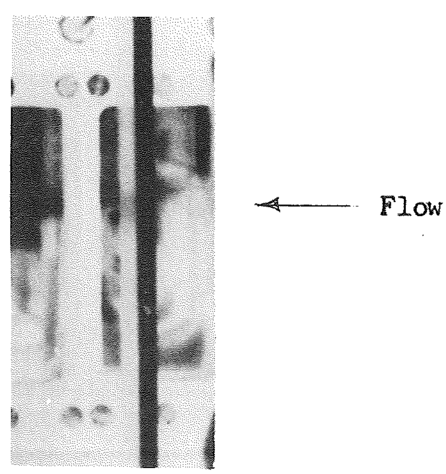

Figure 4-18. Infrared Print - Upstream and Middle Window - Run 32

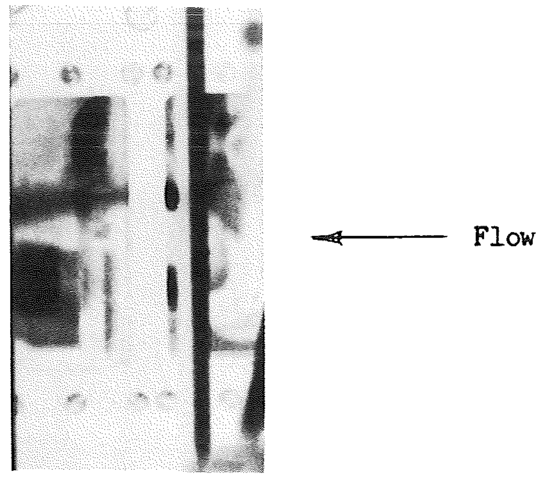

Figure 4-19. Infrared Print - Upstream and Middle Window - Run 33

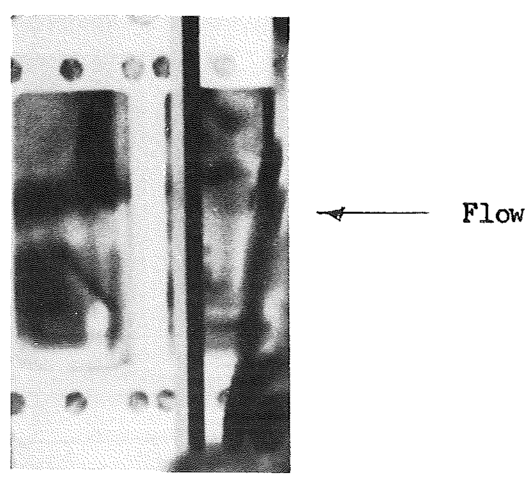

Figure 4-20. Infrared Print - Upstream and Middle Window - Run 35

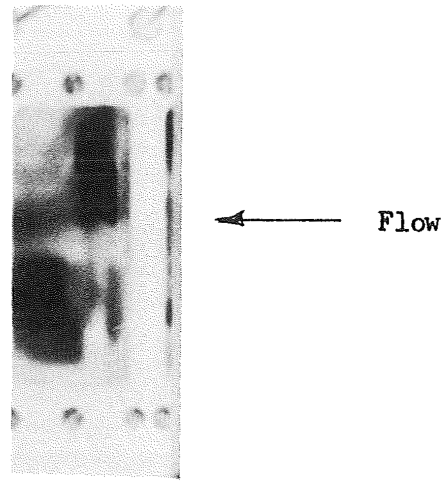

Figure 4-21. Infrared Print - Middle Window - Run 38

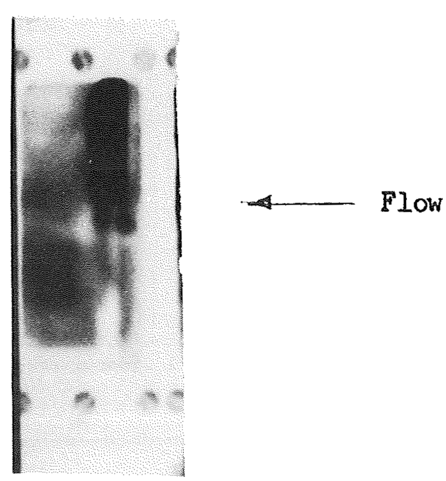

Figure 4-22. Infrared Print - Middle Window - Run 40

TABLE 4-2

INFRARED PHOTOGRAPHIC DATA

Run #/ Fig. #	Test Type	Defined Lines and Location* Deg. (1) Inch	Deg. (2) Inch	Deg. (3) Inch	Deg. (4) Inch
16/4-11	High Temperature Air	10 - 1.96	4 - 1.66	70 - .77	-----
17/4-12	High Temperature Air	10** 2.94	8 - 2.20	-----	-----
19/4-14	Medium Temperature Air	11 - 2.11	6 - 1.90	-----	-----
20/4-15	Medium Temperature Air	6** 2.56	2 - 1.93	-----	-----
26/4-16	Medium Temperature Air	9** 2.95	6 - 2.00	-----	-----
31/4-13	High Temperature Air	9 - 2.17	4 - 1.81	-----	-----
32/4-18	High Velocity Air	9 - 2.08	5 - 1.67	69 - .60	-----
33/4-19	Low Velocity Air	9 - 2.28	1 - 2.03	-----	78 - 3.85
34/4-17	Low Temperature Air	8 - 2.19	2 - 1.73	-----	78 - 3.83
35/4-20	1/2" Screen	11 - 2.27	-----	-----	76 - 3.85
38/4-21	1/8" Screen	6 - 2.41	-----	-----	74 - 3.92
40/4-22	1/2" Dam	-----	-----	-----	78 - 3.68

* Schematic

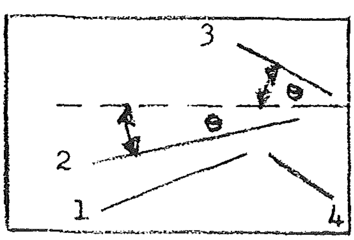

1 Edge of Mixing Region
2 Inner Boundary of Reaction Zone
3 Supersonic Plume Expansion Fan
4 Upper Edge of Transient Eddy

Spatial locations are referenced to the top of the upstream window frame on the downstream edge

**Reference downstream window downstream edge third line defines the plume expansion fan eminating from the nozzle tip. In some cases, Figs. 4-17 to 4-22, a fourth line appears that has a slope in the same direction as the expansion fan; however, it is located in the middle of the air stream and does not appear to be attached to any physical object. Initially, no explanation could be offered for its existence; however, a more detailed analysis of the prints, and in particular Figs. 4-13 and 4-14, led to the following postulation. An eddy exists in the air stream causing a recirculation pattern to exist; therefore, the line that appears in the air stream indicates the presence of the eddy. Since the eddy does not appear in all prints, it is further postulated that it is relatively weak and very sensitive to small changes in the run to run test conditions. The theoretical justification for the existence of this eddy is given in Abramovitch, Ref. 12.

Representation of the tests that were concerned with temperature effects in the mixing process are given in Figs. 4-11 to 4-13 for high temperature air, Fig. 4-14 to 4-16 for medium temperature air, and Fig. 4-17 for low temperature air. No strong effect of air temperature on the mixing process was evident as the change in the angle representing the edge of mixing was only 2 degrees, i.e., approximately 10, 9, and 8 degrees for high, medium, and low temperature air tests. Correlation of the spatial locations was not as clearly defined as some overlapping occurred.

The mixing rate as a function of velocity (Figs. 4-18 and 4-19) defined by the angle of the mixing line did not appear to change (9-degrees for both cases); however, examination of the spatial location did present evidence that mixing is enhanced by lowering the velocity of the air stream (2.08 inches for the high velocity stream and 2.28 inches for the low velocity stream). A more detailed examination of the print revealed that for the low velocity test the postulated eddy was present which could explain why no apparent change in the angle of the mixing line was observed.

The infrared prints representing the studies that incorporated screens in the air stream were inconclusive, Figs. 4-20 and 4-21. On the basis of the angle of the mixing line the data indicated that the finer the turbulence the better the mixing; however, on the basis of the spatial location of the mixing line the opposite appeared true. It should be noted that the eddy discussed above was present in both of these prints and may have "washed out" the true indications.

None of the three previously defined lines were apparent in the test utilizing a 1/4-inch dam, Fig. 4-22; however, the eddy was again present. Since this configuration promotes the formation of eddies, one would expect a stronger eddy for this condition and it appears to be in more intimate contact with the subject mixing process.

No correlation of the inner boundary of the reaction zone could be made due to the wide spread in the data. The value of the angle ranged from 1 to 8 degrees and the angular difference between lines 1 and 2 ranged from 2 to 8 degrees. The high degree of scatter is most probably due to the relatively weak definition of the line. Good agreement was obtained for the angle of line 3; however, spatial resolution was rather poor.

ULTRAVIOLET PHOTOGRAPHY

The ultraviolet photography in the 2850 to 3150A band was utilized to record OH emission in the mixing chamber. As with the infrared photographic coverage, it was utilized on all firings where optical access was available. Two types of ultraviolet coverage were utilized, i.e., 16 mm cine photography and 35 mm sequence photography (photopyrometer fudicial photographs). Photographs representing the experiments are shown in Figs. 4-23 to 4-34. The field of view was approximately 12 inches by 12 inches. The data extracted from these films together with a definition of the test conditions are given in Tables 4-3 and 4-4. The extremely soft texture of the cine reproductions, Figs. 4-23 and 4-24, is indegenous to field type operation; therefore, the principal ultraviolet photographic analysis was conducted with the relatively well defined photopyrometer prints. The regions of maximum emission on these prints is the lightest region.

In general, the ultraviolet photographic data agrees with the observations made with the schlieren and the infrared photography. The effect of temperature on the mixing region, Figs. 4-23 to 4-29, is negligible. The measured angles (approximately equal to 10 degrees) in the mixing chamber are essentially the same; therefore, over the air temperature ranges encountered in this program, mixing is essentially constant. It should be noted that the bulk of the photopyrometry data was taken aft of the exit of the mixing chamber because in the majority of cases the zone radiometer interfered with the view of the test section windows. These data yield angles that are greater than those observed

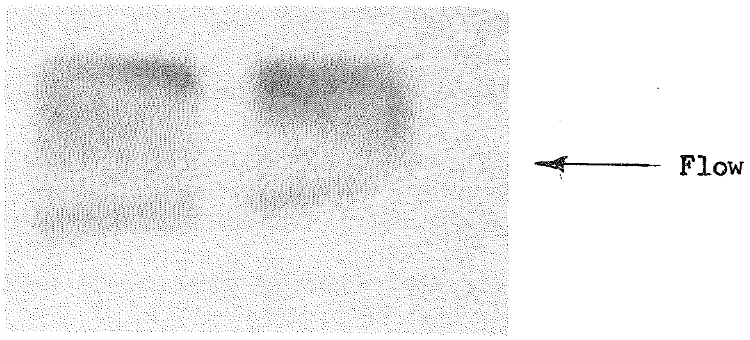

Figure 4-23. Ultraviolet Print - Upstream and Middle Window - Run 10

Figure 4-24. Ultraviolet Print - Middle and Downstream Windows and Aft of Exit - Run 17

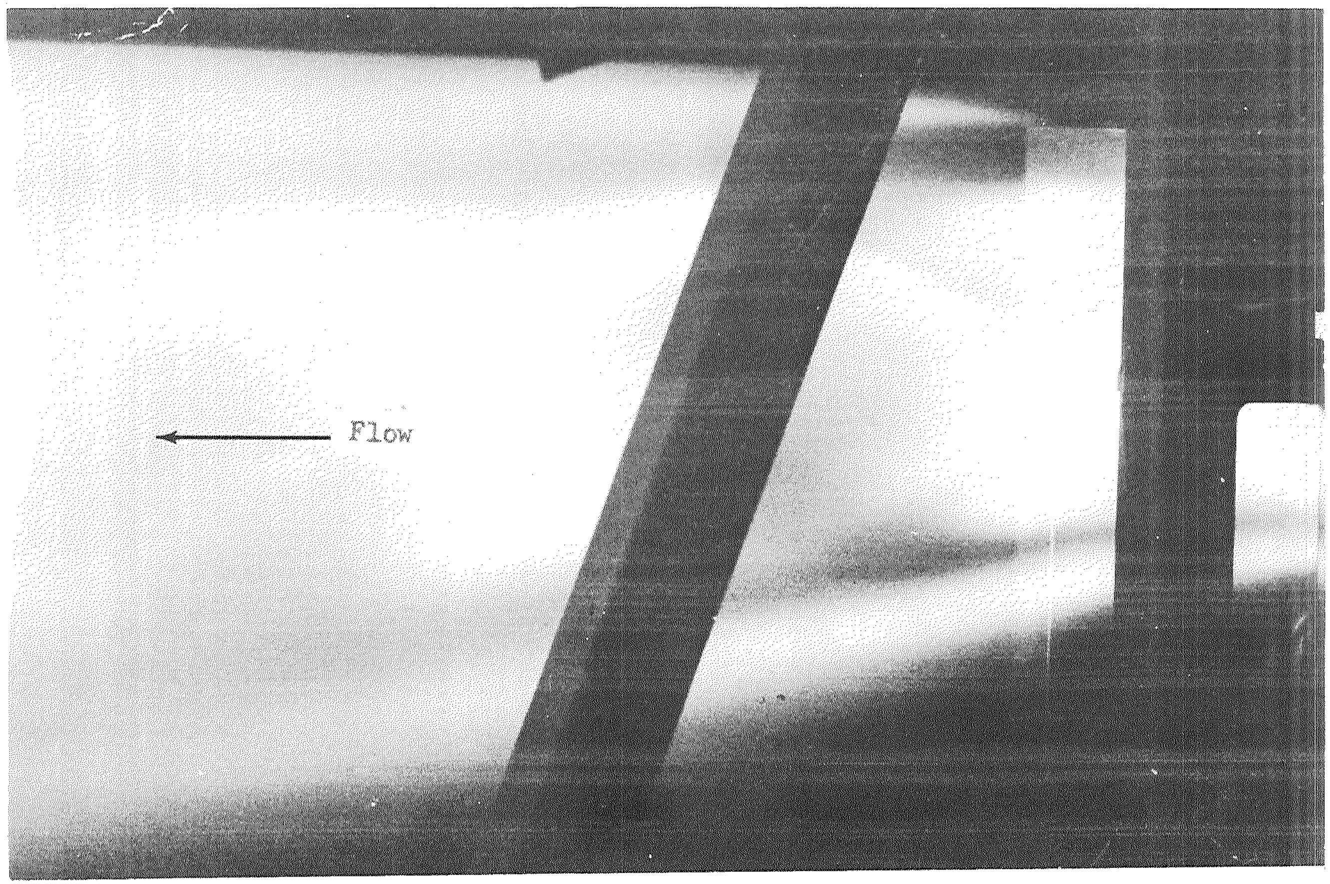

Figure 4-25. Photopyrometer Print - Downstream Window and Aft of Exit - Run 23

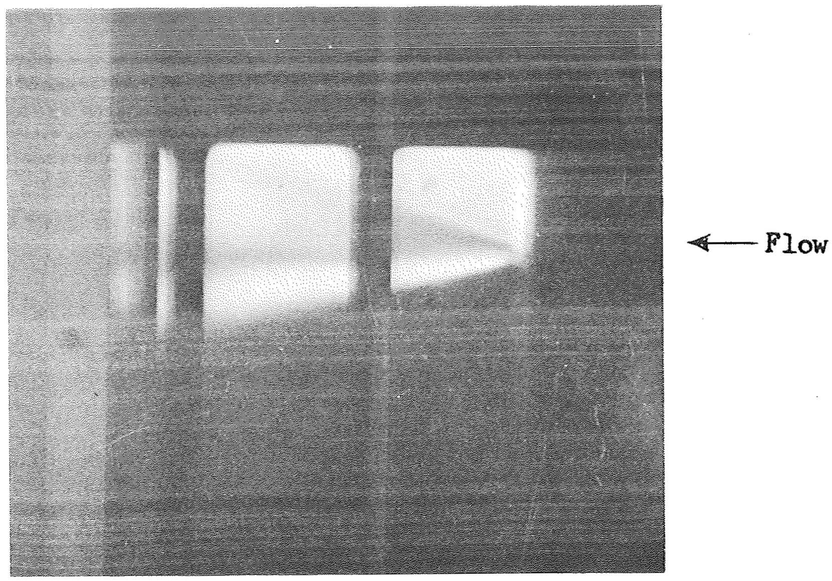

Figure 4-26. Photopyrometer Print - Upstream and Middle Windows - Run 29

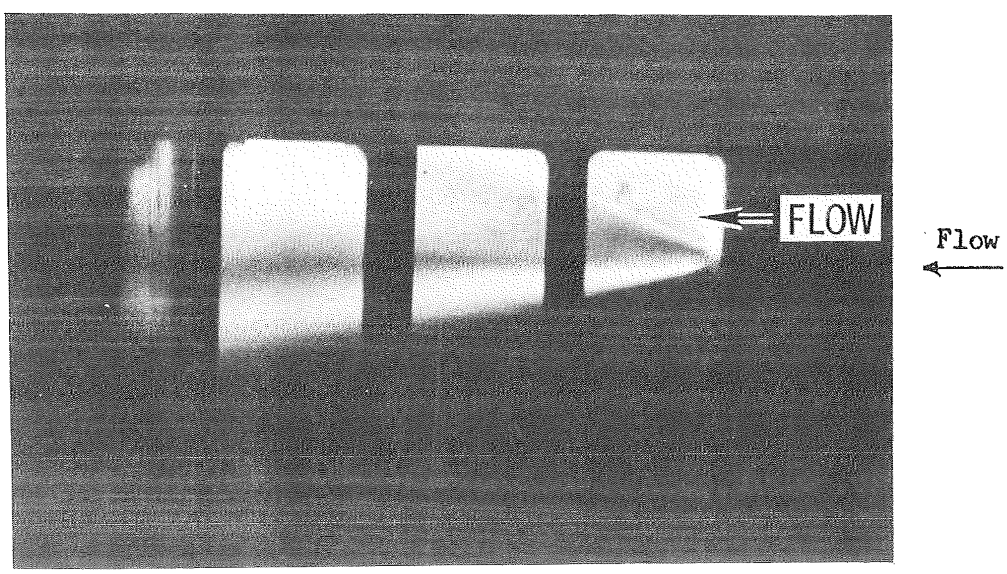

Figure 4-27. Photopyrometer Print - Mixing Chamber - Run 31

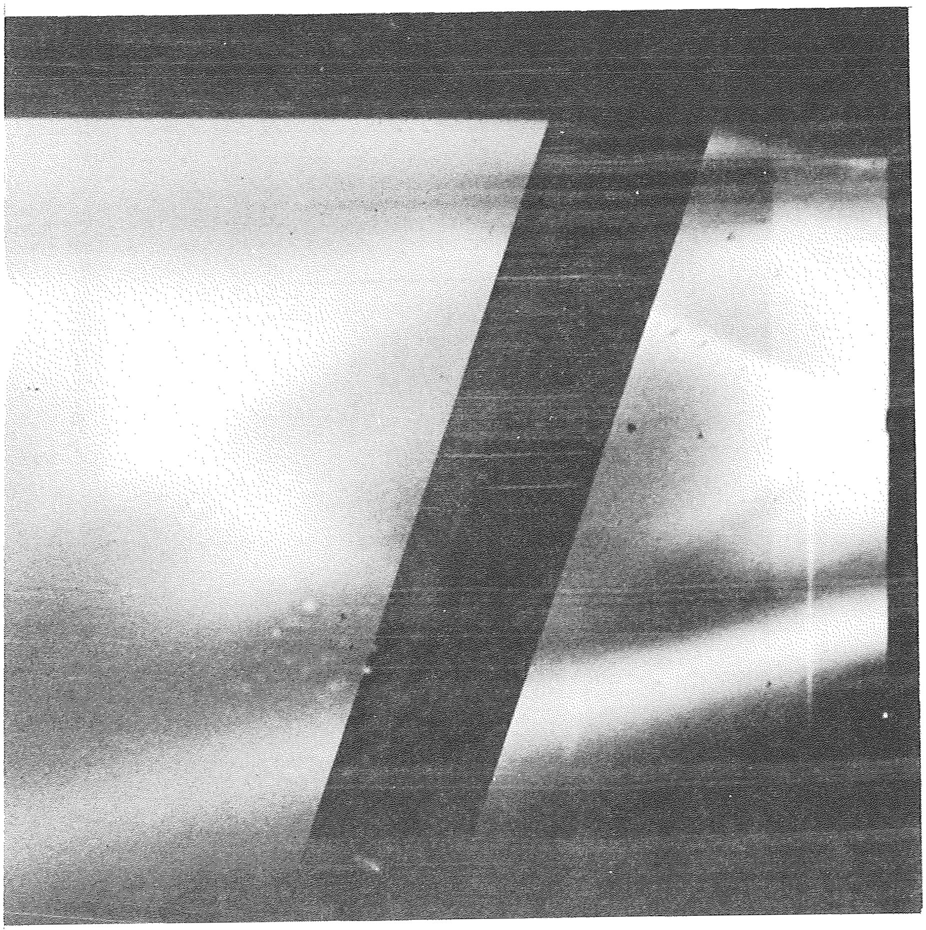

Flow

Figure 4-28. Photopyrometer Print - Aft of Exit - Run 39

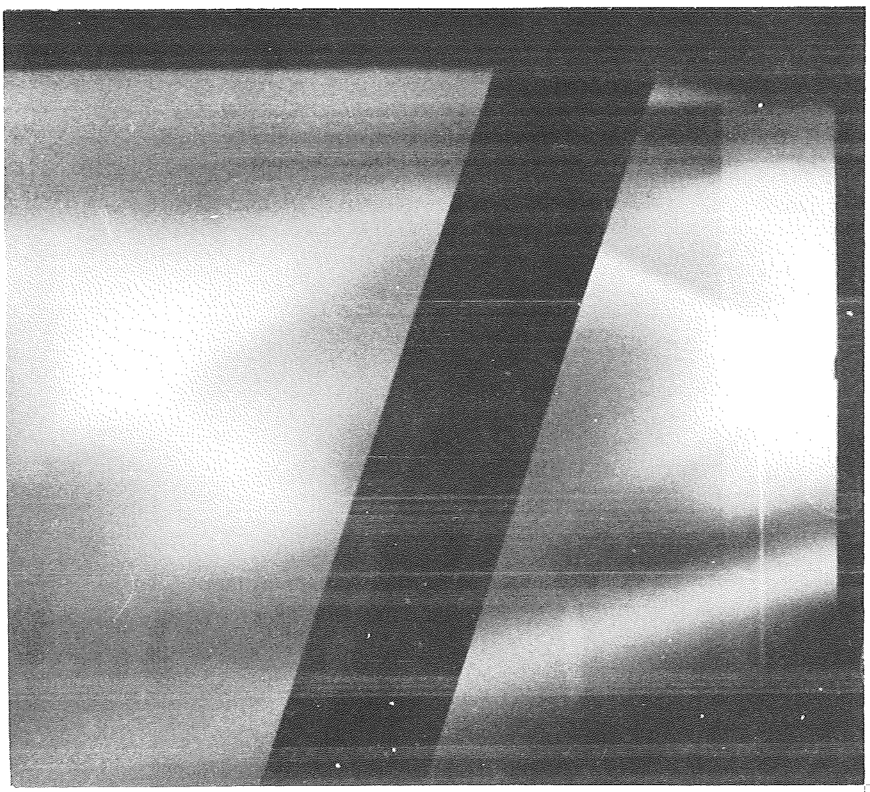

Figure 4-29. Photopyrometer Print - Aft of Exit - Run 34

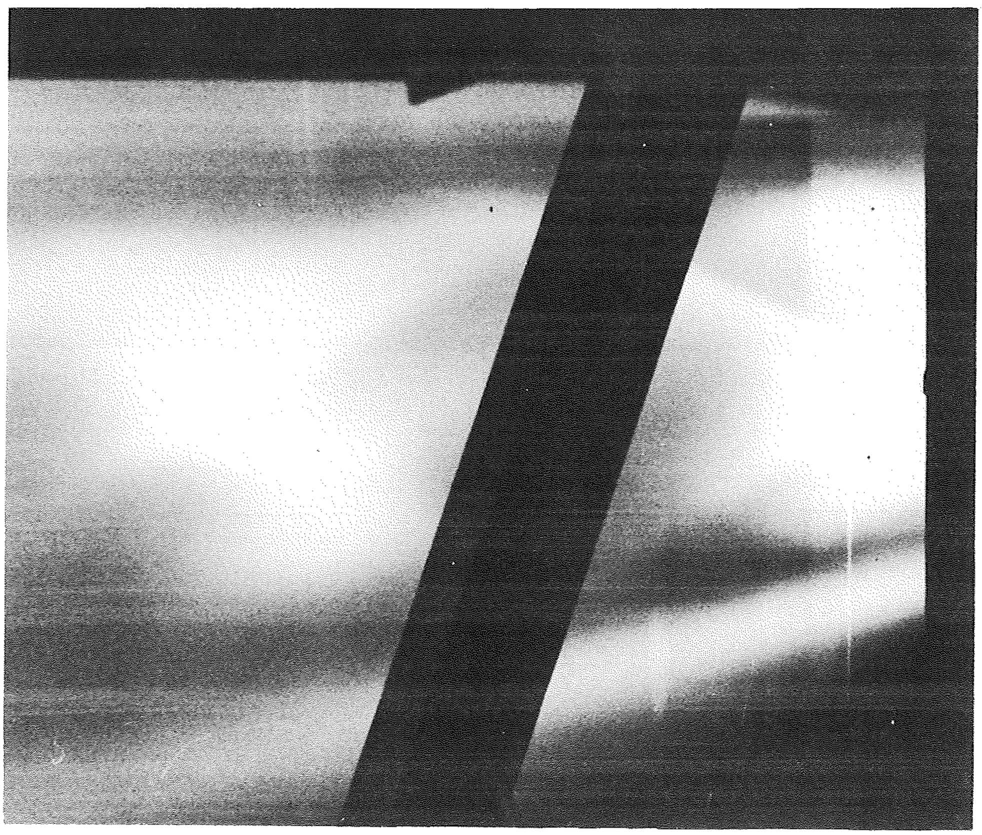

Figure 4-30. Photopyrometer Print - Aft of Exit - Run 32

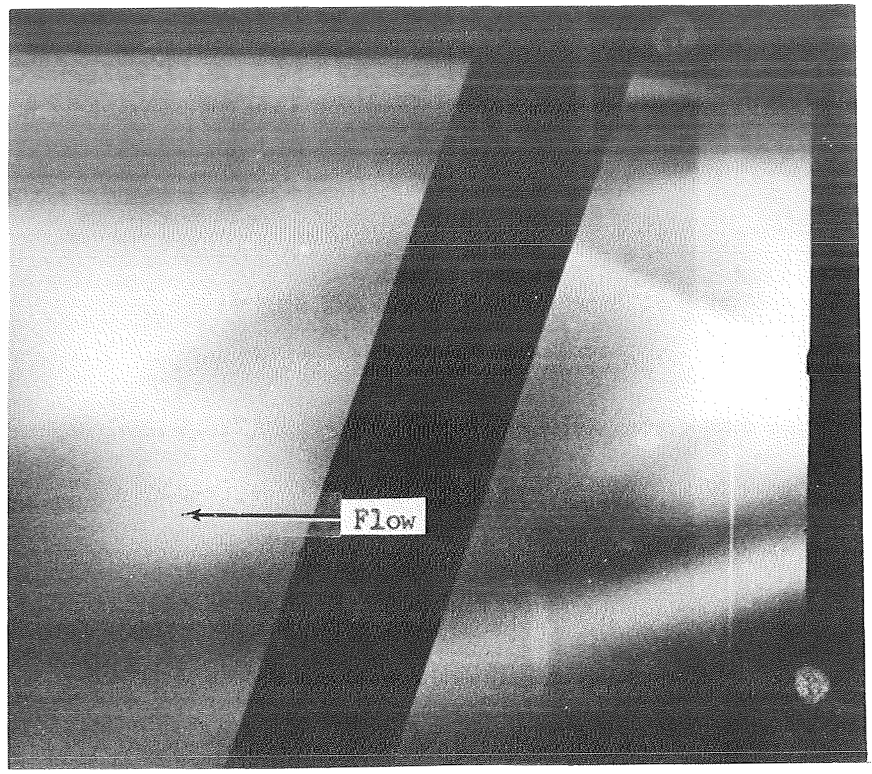

Figure 4-31. Photopyrometer Print - Aft of Exit - Run 33

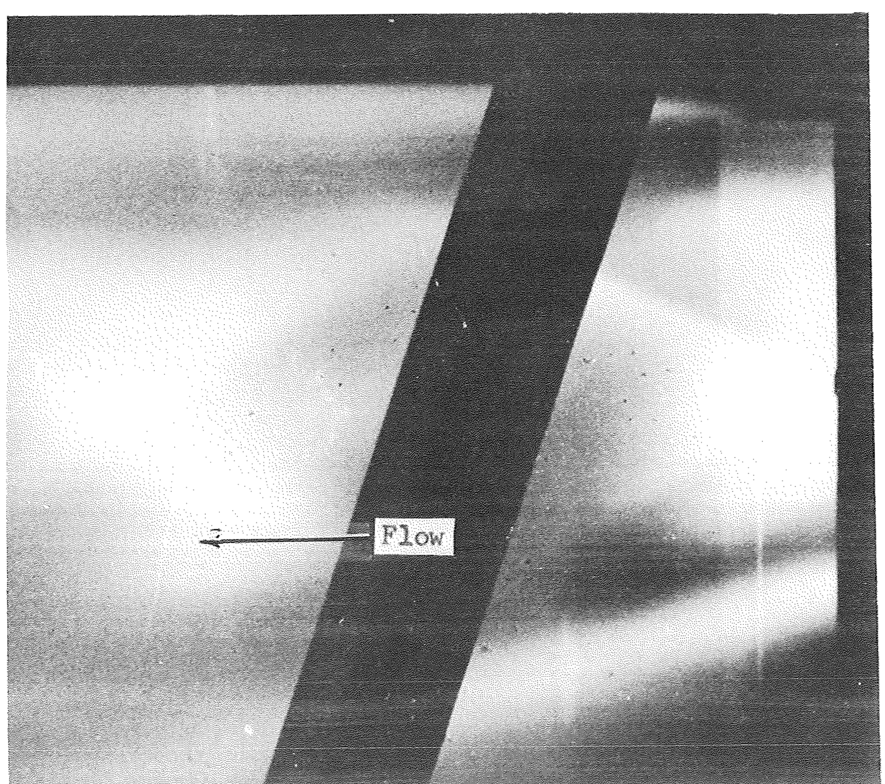

Figure 4-32. Photopyrometer Print - Aft of Exit - Run 35

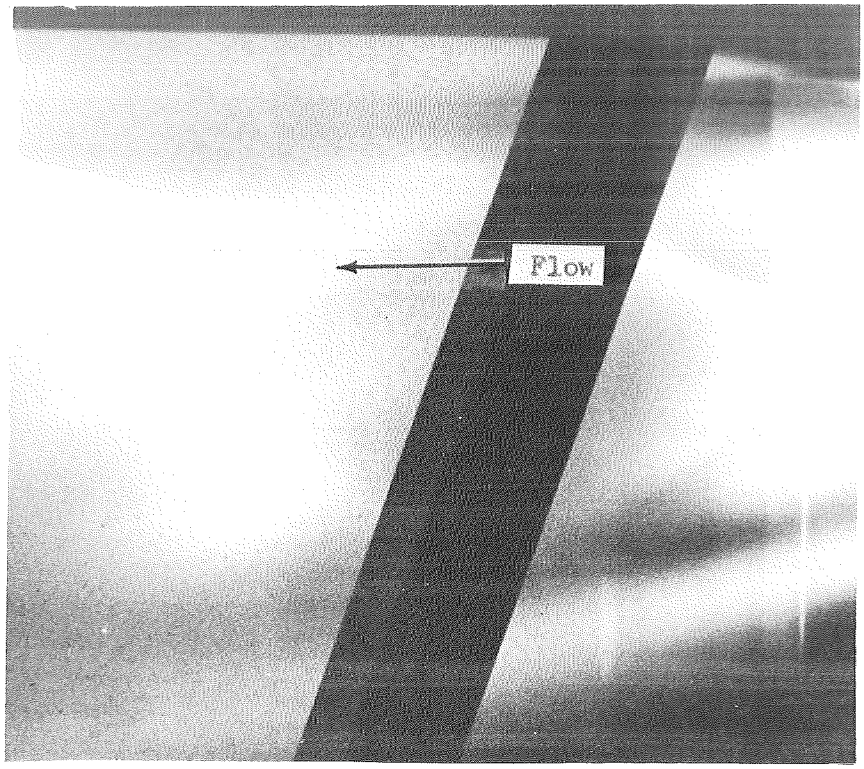

Figure 4-33. Photopyrometer Print - Aft of Exit - Run 38

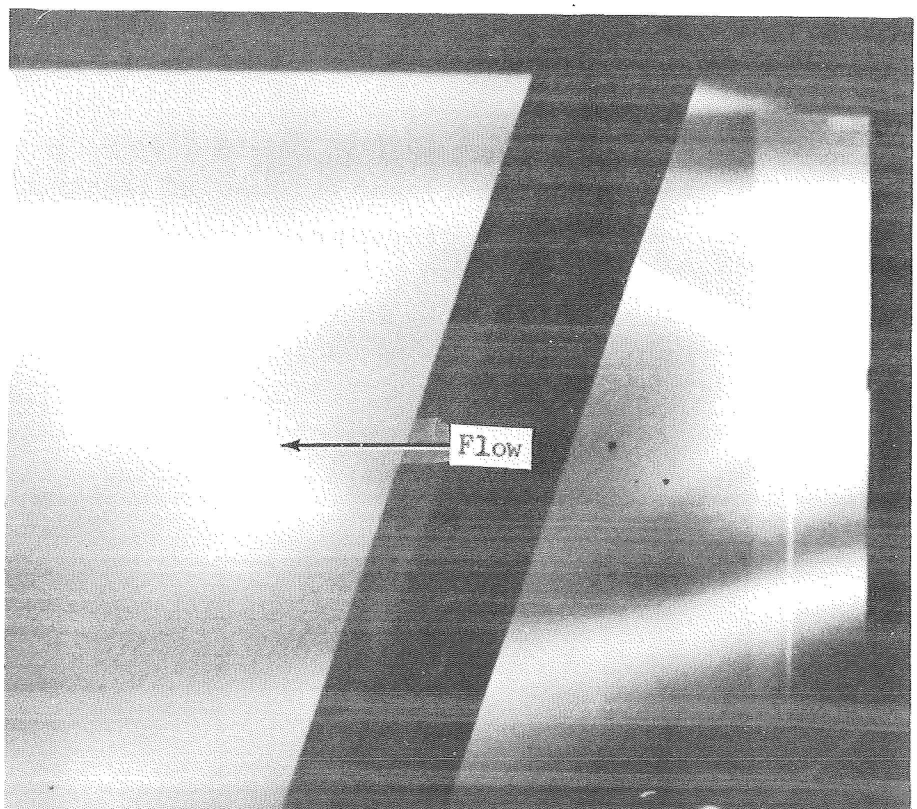

Figure 4-34. Photopyrometer Print - Aft of Exit - Run 40

TABLE 4-3

ULTRAVIOLET PHOTOGRAPHIC DATA

Run No./ Fig. No.	Test Type	Defined Lines* 1 Deg.	2 Deg.	3 Deg.
10/4-23	High Temperature Air	9	4	74
16	High Temperature Air	10	6	72
17/4-24	High Temperature Air	10	7	70
20	Medium Temperature Air	11	6	--
26	Medium Temperature Air	12	9	--

* Schematic

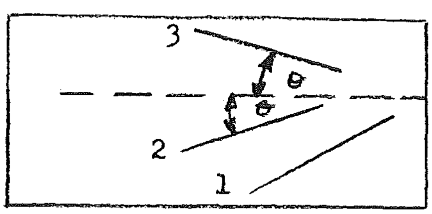

1 Edge of Mixing Region

2 Inner Boundary of Reaction Zone

3 Supersonic Plume Expansion Fan

TABLE 4-4

PHOTOPYROMETER PHOTOGRAPHIC DATA

Run No./ Fig. No.	Test Type	Defined Lines* Deg. 1	Deg. 2	Deg. 3
23/4-25	Medium Temperature Air	6**	4	--
	At Exit	16	14	--
29/4-26	Medium Temperature Air	10**	2	71
31/4-27	High Temperature Air	12**	5	70
32/4-30	High Velocity Air	17	16	--
33/4-31	Low Velocity Air	20	16	--
34/4-29	Low Temperature Air	18	15	--
35/4-32	1/2" Screen	19	17	--
38/4-33	1/8" Screen	15	14	--
39/4-28	High Temperature Air	16	15	--
40/4-34	1/2" Dam	18	16	--

* Schematic

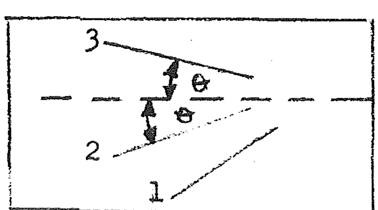

1 Edge of Mixing Layer

2 Inner Boundary of Reaction Zone

3 Supersonic Plume Expansion Fan

** Measurement at window

in the test section due to additional expansion of the flow on exiting the mixing chamber. Therefore, for consistency, data comparisons must be grouped with respect to their general location.

The ultraviolet measurements relating to the effect of velocity upon the mixing processes, Figs. 4-30 and 4-31, agrees well with that described for the schlieren data. Lowering the air velocity increases the rate of mixing. However, no definitive statement can be made about tests with screens and dams, Figs. 4-32 to 4-34. Since the data being compared is aft of the exit of the mixing region it is highly probable that any affect due to these devices has been damped out.

In contrast to the infrared data, a correlation was obtained for a correspondence between lines 1 and 2. The difference between these two angles was constant and approximately equal to 2 degrees. Since no evidence has been gathered indicating any vast differences in mixing rates by the diagnostic experiments conducted one would expect that the reaction zone would have a reproducible thickness as evidenced from this data. The correlation was probably improved because of the considerably narrower wave length band utilized in the UV photographs.

The angles measured for line 3 are approximately equal to 71 degrees for all photographic data and invarient as a function of any of the diagnostic parameters. The postulation that it represents the nozzle lip expansion fan appears valid.

The edge of the mixing zone was compared to a calculation performed by a NASA computer model at conditions similar to those tested in this program, Fig. 4-35. The UV, IR, and schlieren data appears to represent the 1000°K line.

An attempt was made to reduce the photopyrometer fudicial photographs to equivalent brightness temperature maps; however, flaws on the films undetectable to the human eye precluded this. However, relative concentrations could be determined from the photopyrograms. These are presented in Figs. 4-36 to 4-38. The relative correlations are denoted 1 to 3; the lowest to the highest concentrations at a constant step size. See Figs. 4-25 to 4-27, respectively, for spatial orientation.

Examination of these figures reveals that the reaction zone is not continuous, i.e., the reactions take place in discrete pockets. In general, a maximum concentration zone exists in the air and combustion product streams. The region between these two zones exhibits intermediate concentration levels.

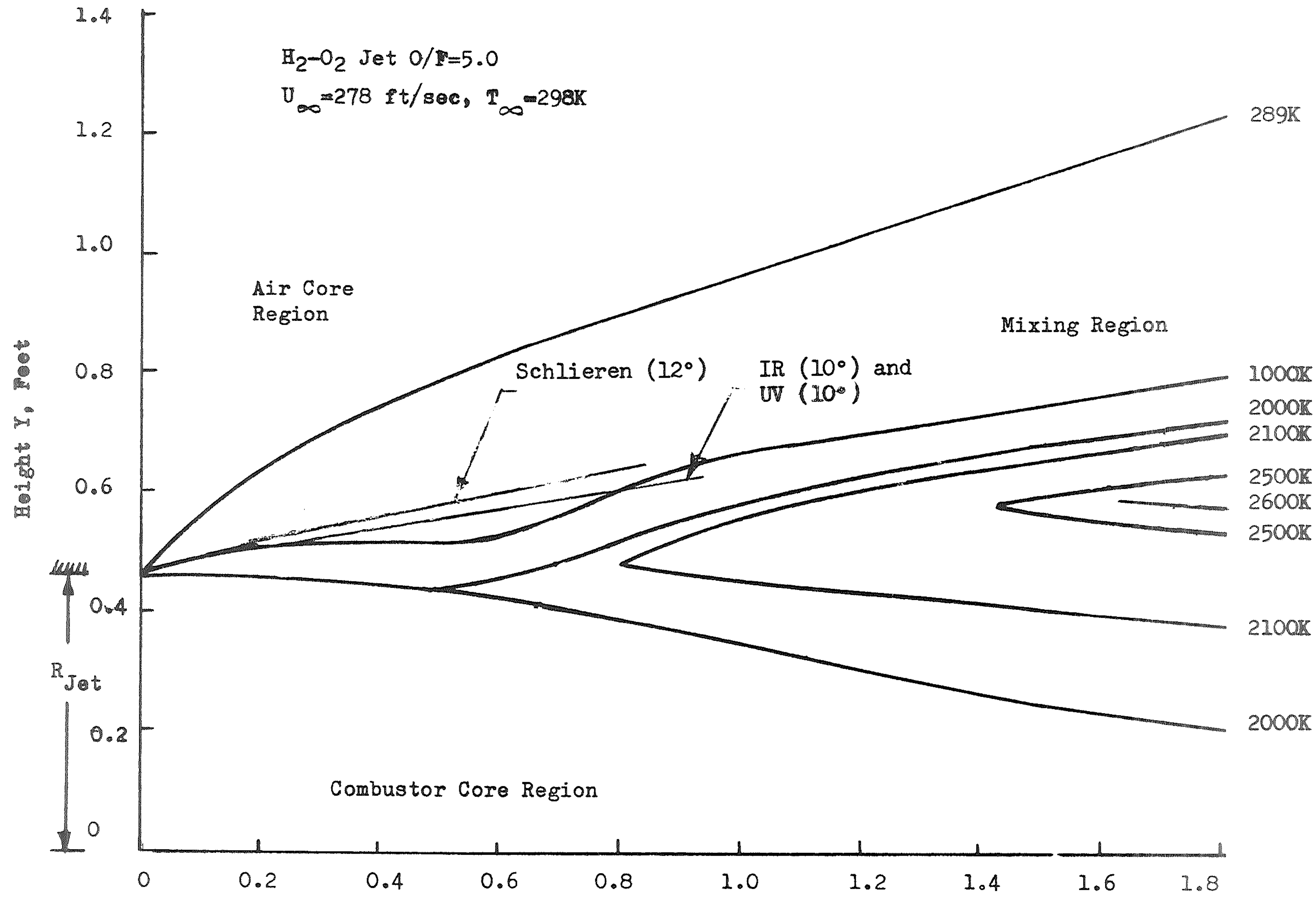

Figure 4-35. Schematic of Mixing Region

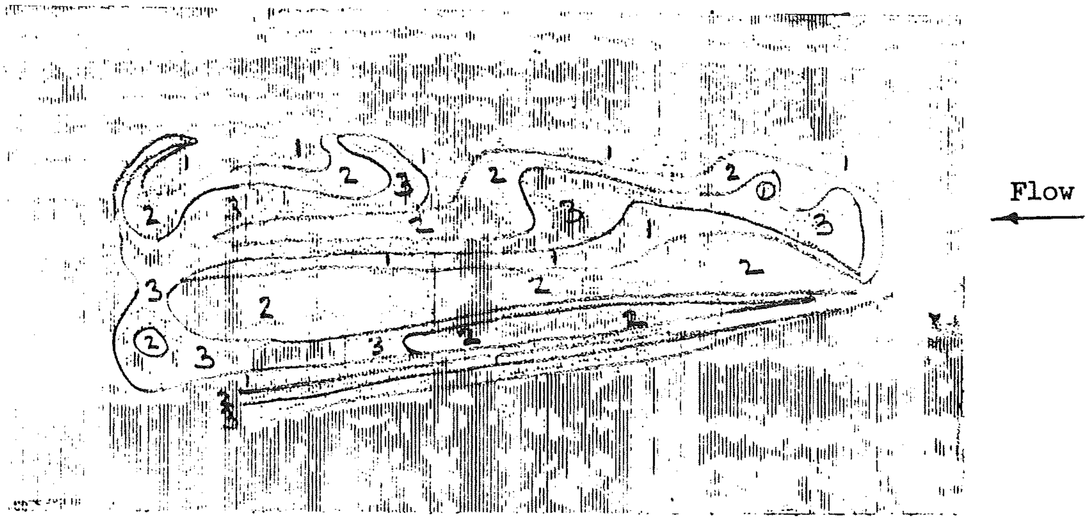

Note: Relative condentrations are denoted 1 to 3
lowest to highest

Figure 4-36. Photopyrogram Showing Relative OH Concentrations - Run 31, T_a = 829 F.

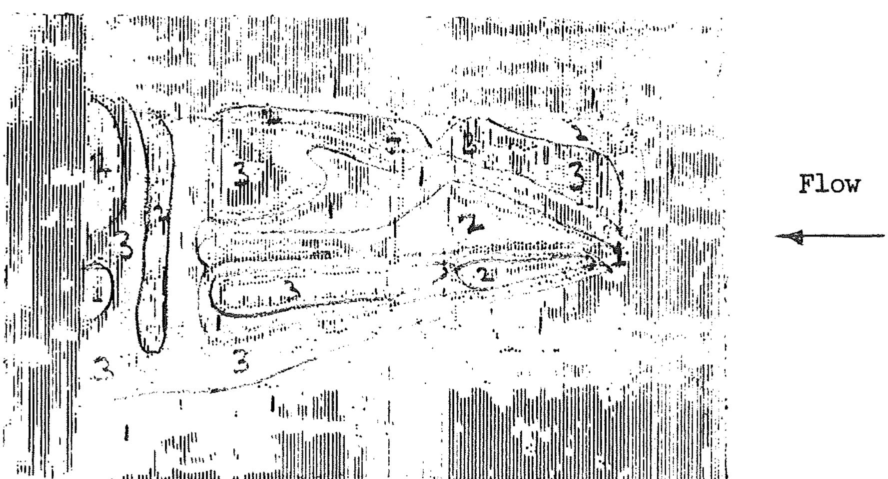

Note: Relative concentrations are denoted
1 to 3 lowest to highest.

Figure 4-37. Photopyrogram Showing Relative OH Concentrations - Run 29, T_a = 612 F.

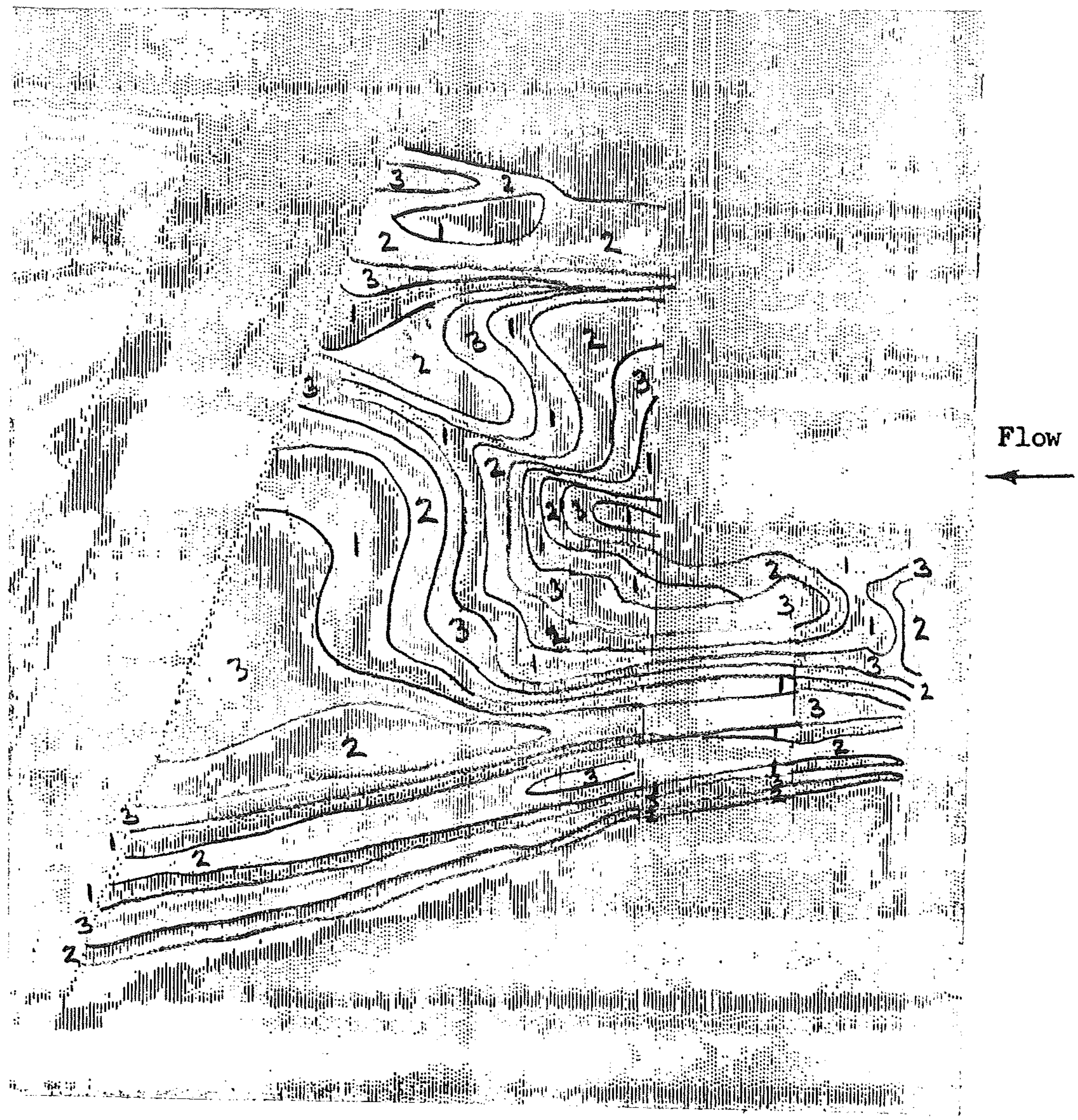

Note: Relative Concentrations are Denoted 1 to 3
Lowest to Highest

Figure 4-38. Photopyrogram Showing Relative OH Concentrations - Run 23, T_a = 612 F.

APPENDIX 5

VELOCITY PROFILES

A determination of the two-dimensional properties of the film coolant and air streams without combustor flow was made. The pressure profiles were measured at the entrance to the mixing chamber with pitot probe rakes (0.060 diameter) used in conjunction with a mercury-filled manometer bank.

The velocity profile data for the air and film coolant streams are presented in Figs. 5-1 and 5-2. The air stream is reasonably two-dimensional except near the bottom wall where a separate flow region exists. The separated flow region is a consequence of the sharp turning angle upstream of the entrance to the mixing chamber. Since this region is relatively far from the theoretically calculated mixing region, it can be assumed to have a negligible influence on the mixing layer of interest.

The film coolants are reasonably two-dimensional at the interfaces of the primary streams, i.e., air and combustor exhaust products. A separated flow region is evident near the side wall for reasons similar to those given above. This, also, can be assumed to have a minimal influence on the mixing region. The tabs depicted on the figures were used to retain the quartz windows.

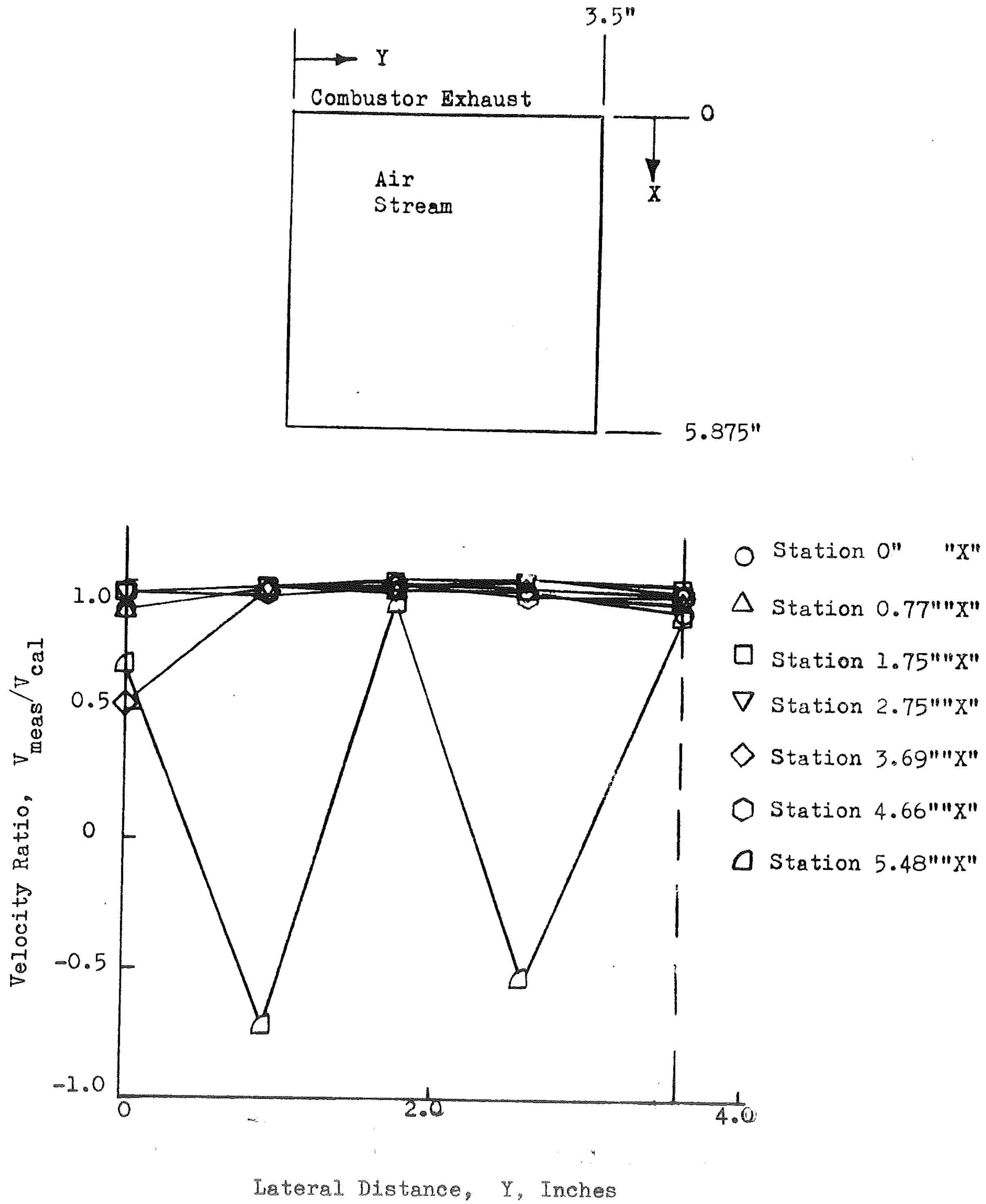

Figure 5-1. Air Stream Velocity Profiles

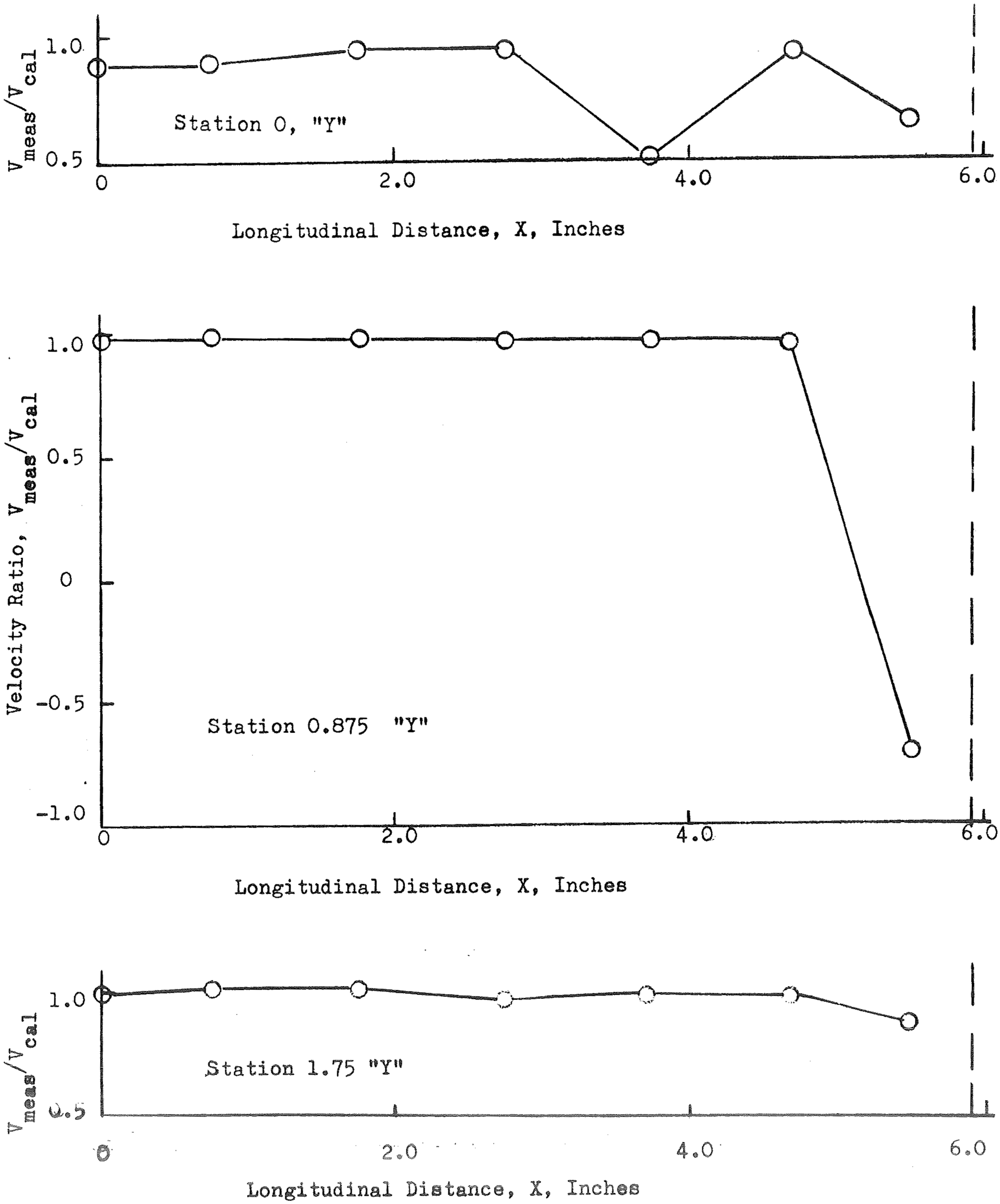

Figure 5-1. (Cont). **Air Stream Velocity Profiles**

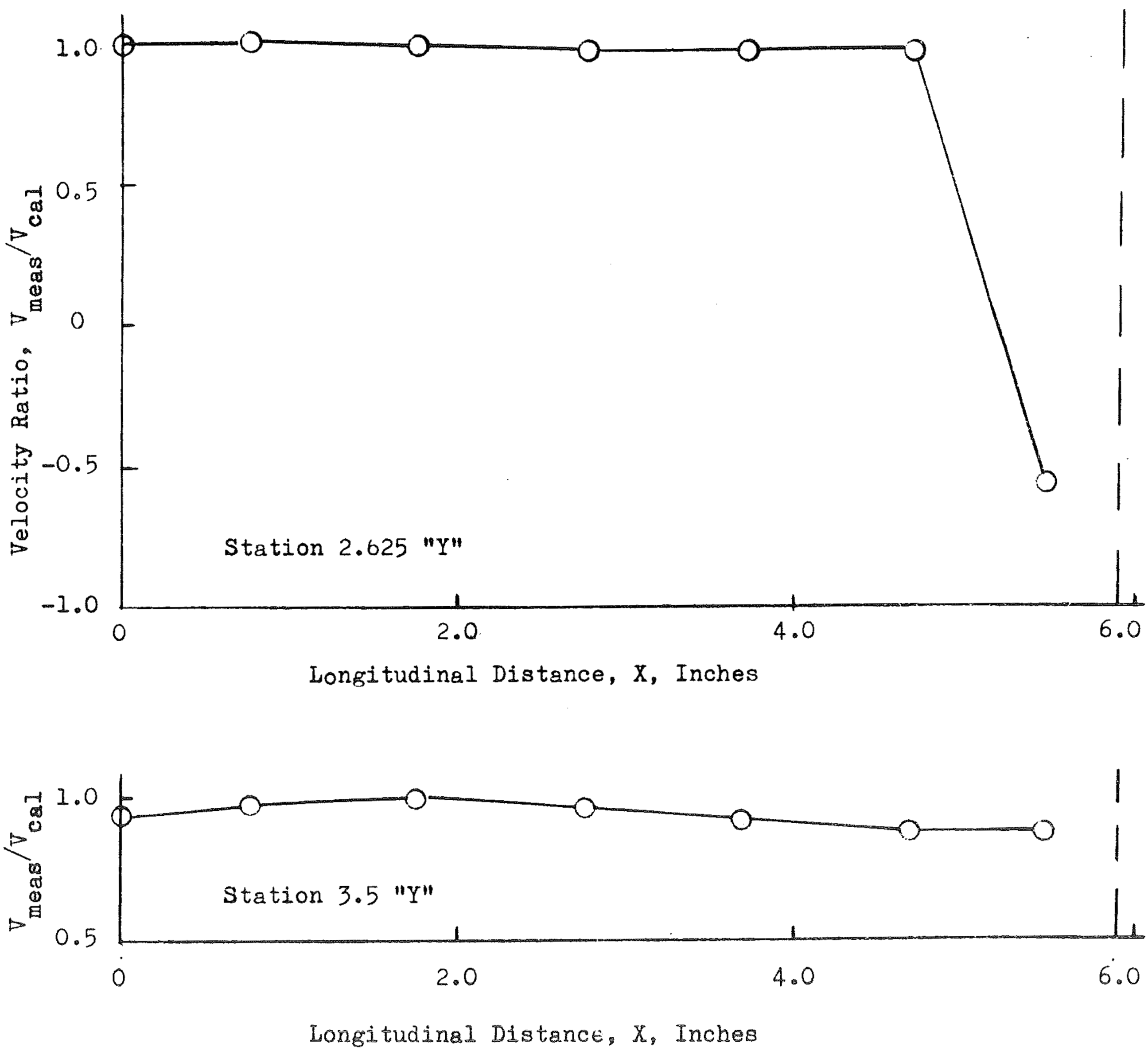

Figure 5-1. (Cont). Air Stream Velocity Profiles

TOP WALL FILM COOLANT

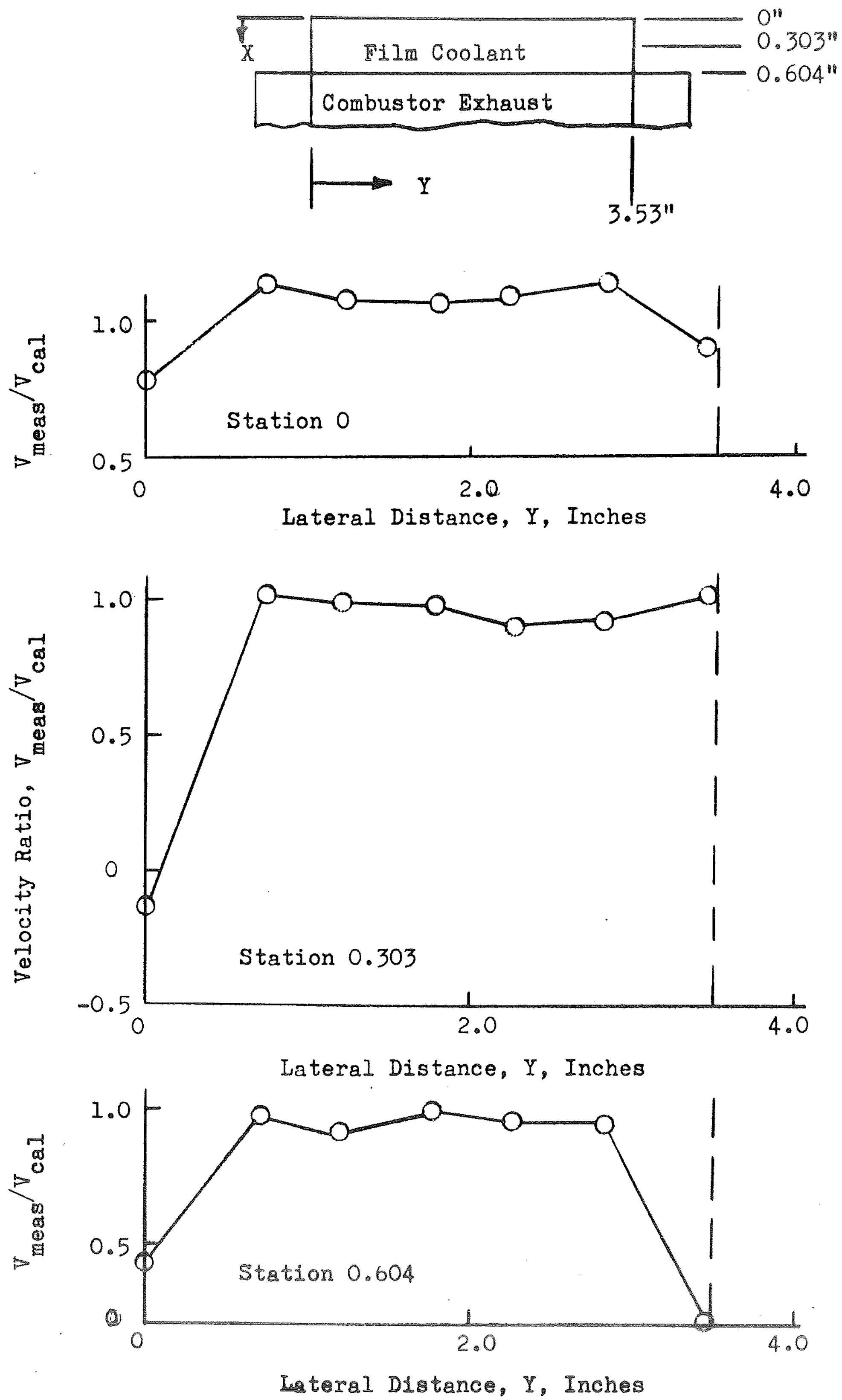

Figure 5-2. **Film Coolant Velocity Profiles**

HIGH PRESSURE FILM COOLANT

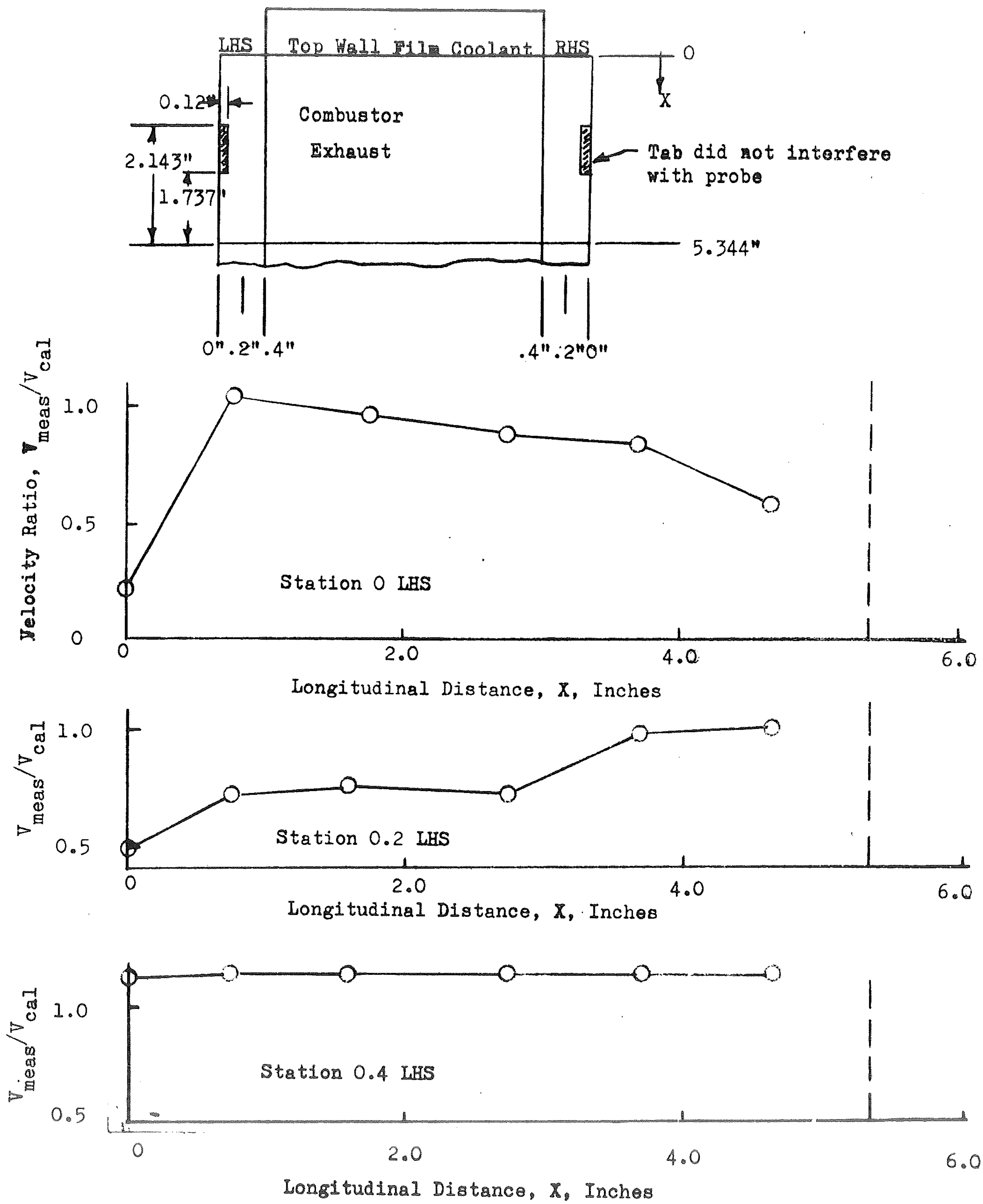

Figure 5-2. (Cont). Film Coolant Velocity Profiles

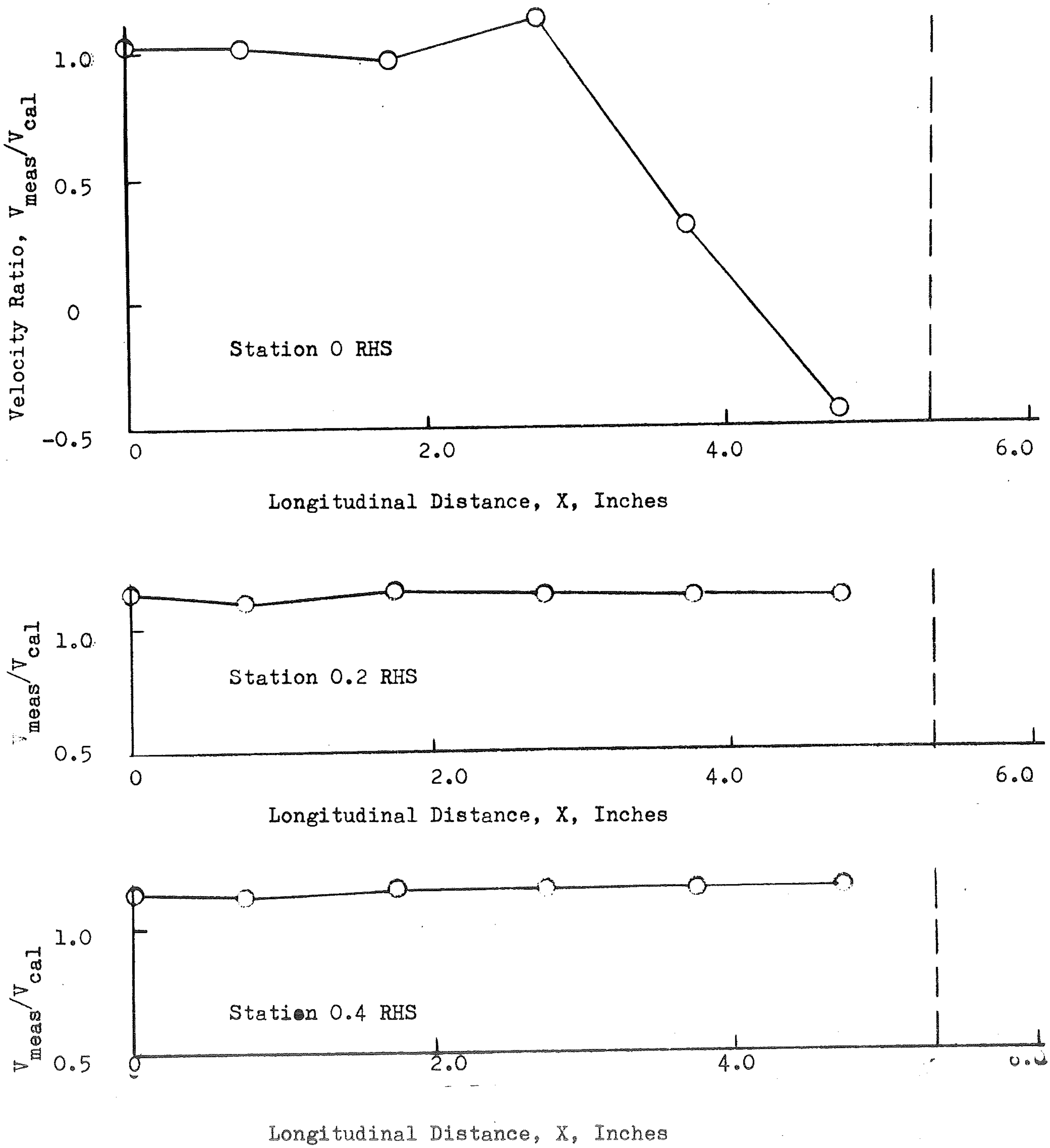

Figure 5-2. (Cont). Film Coolant Velocity Profiles

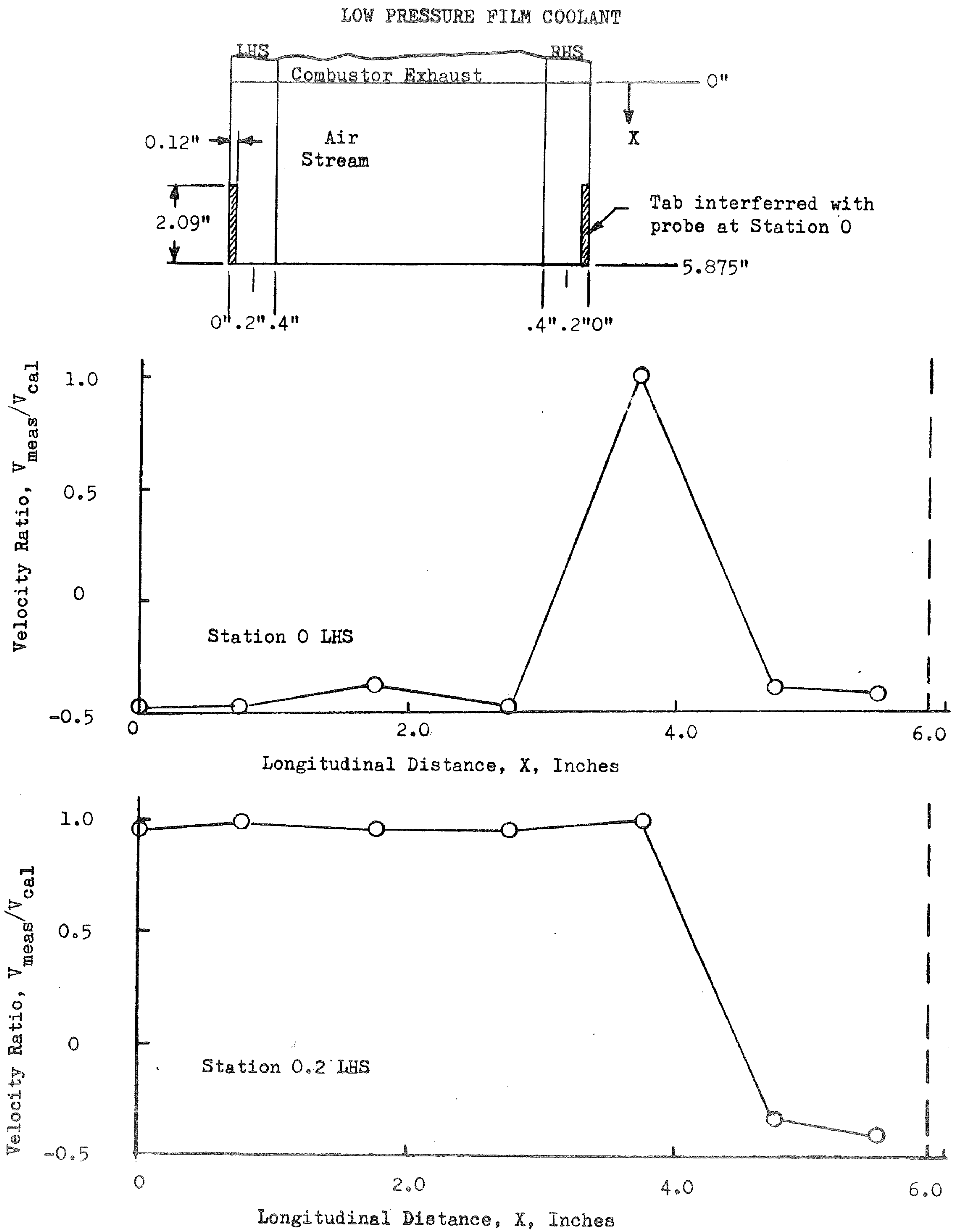

Figure 5-2. (Cont). Film Coolant Velocity Profiles

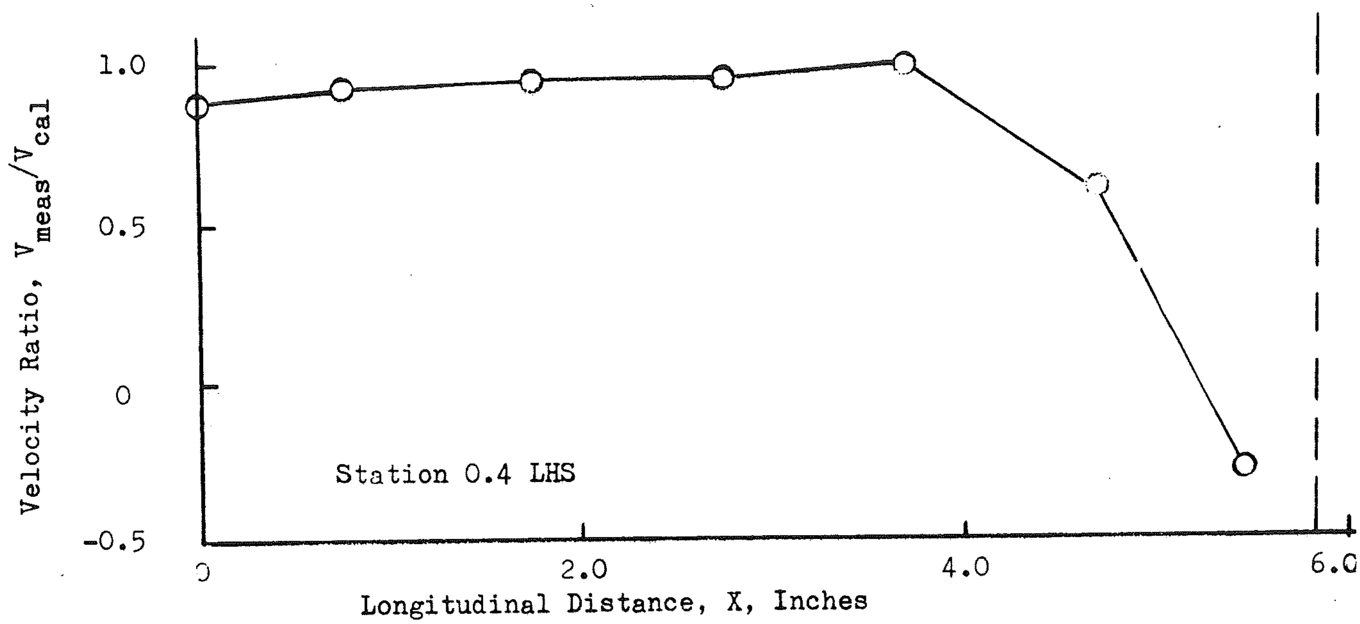

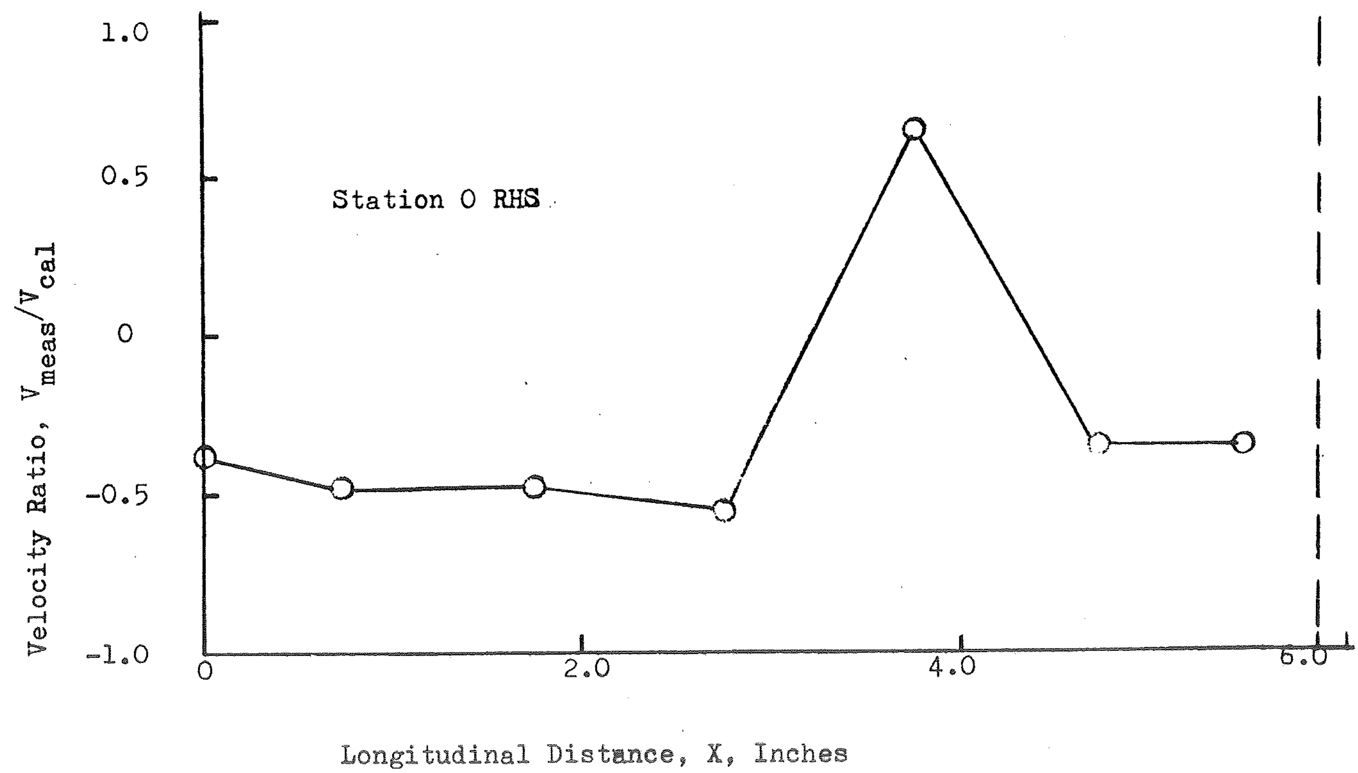

Figure 5-2.(Cont). Film Coolant Velocity Profiles

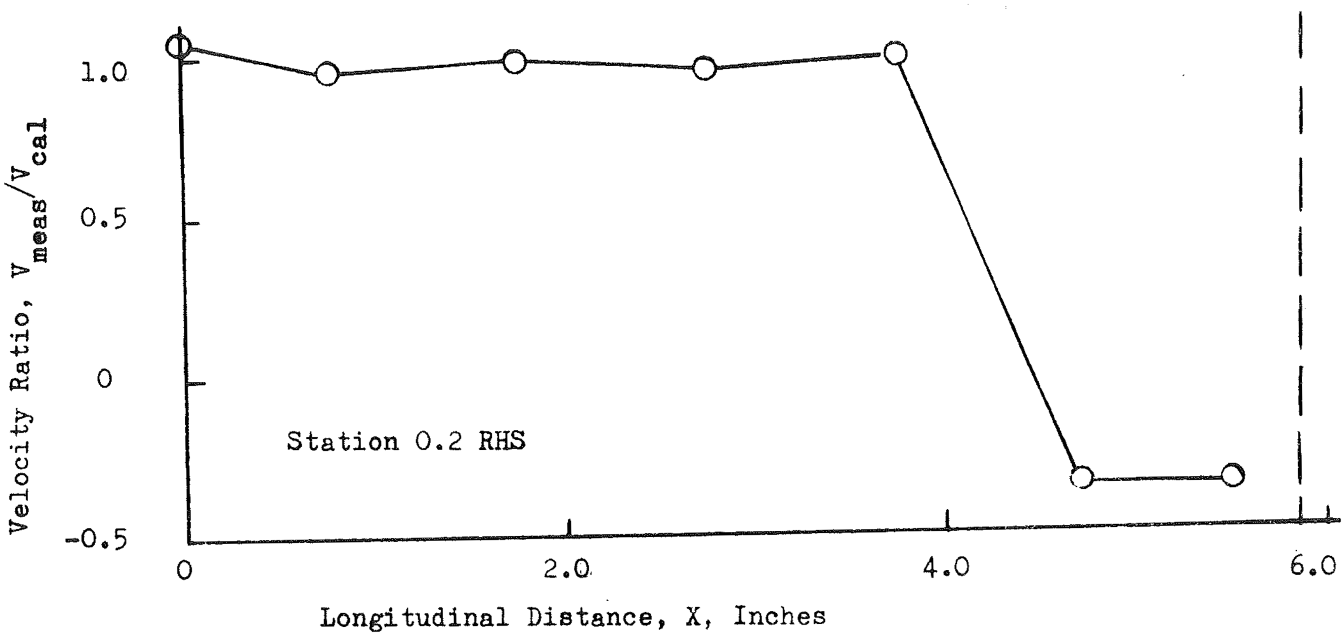

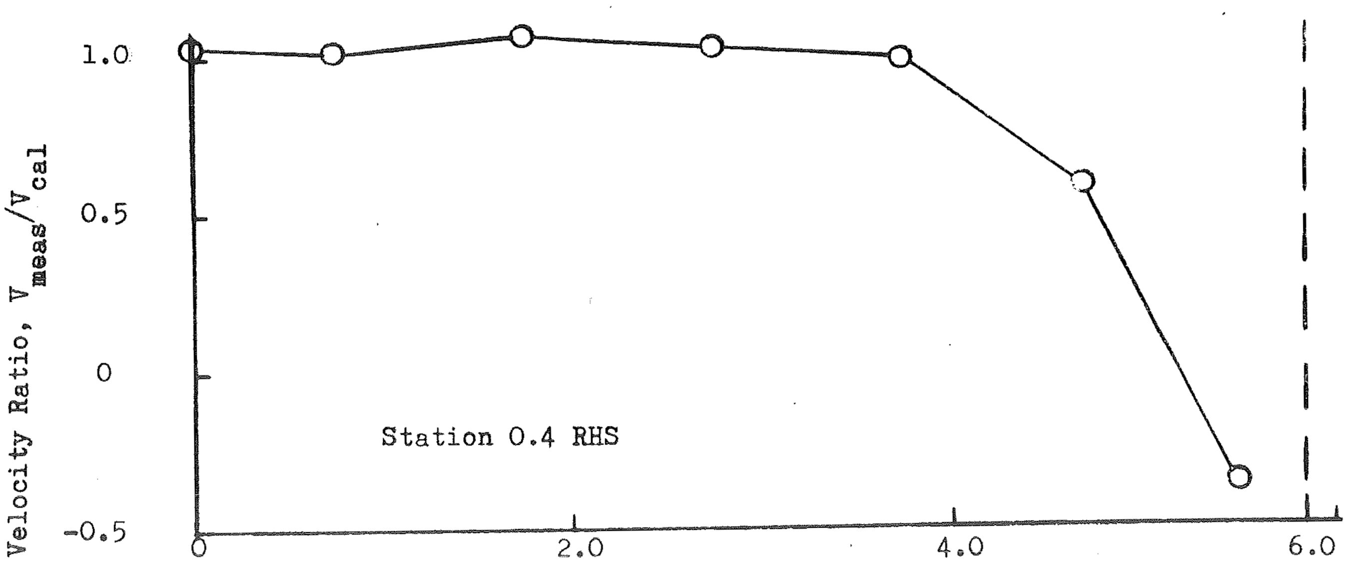

Longitudinal Distance, X, Inches

Figure 5-2 (Cont). Film Coolant Velocity Profiles

APPENDIX 6

TEST FIRING DATA

TABLE 6-1

TEST FIRING DATA

General Conditions

Run No.	Date	P_{ATM} psig	T_{ATM} ^oF	Relative Humidity	P_c, psig	P_c/P_a THEO = 29.35	MR	C^* ft/sec.	η_{c^*}	Duration, Sec.
1	11/19/69	14.02	57	14	398	29.39	5.41	7263	93.2	1.920
2	↓	↓	↓	↓	409	30.17	5.46	7332	94.2	8.045
4	11/26/69	13.92	65	19	396	29.45	5.58	7375	95.3	14.950
021	1/13/70	↓	47	98	402	29.88	5.44	7327	94.1	14.930
041	↓	↓	↓	↓	402	↓	5.50	7398	95.3	8.120
5	↓	↓	↓	↓	399	29.66	5.34	7327	93.8	7.910
10	5/26/70	13.90	54	100	401	29.85	5.39	7301	93.6	9.950
11	↓	↓	↓	↓	397	29.56	5.50	7210	92.8	10.010
12	↓	↓	↓	↓	396	29.49	5.41	7229	92.8	9.970
13	5/28/70	13.81	56	98	399	29.89	5.36	7400	94.8	↓
14	↓	↓	↓	↓	391	29.31	5.08	7708	97.7	↓
15	←				Misfire					→
16	6/9/70	13.90	67	92	398	29.63	5.09	7562	95.9	4.970
17	↓	↓	↓	↓	420	31.22	5.79	7246	94.3	8.410
18	↓	↓	↓	↓	376	28.05	4.72	7619	95.5	9.980
19	6/10/70	13.82	66	72	402	30.09	5.41	7390	94.8	9.970
20	↓	↓	↓	↓	387	29.00	5.16	7516	95.6	9.990
21	↓	↓	↓	↓	↓	↓	5.25	7408	94.5	9.970
22	6/24/70	13.91	80	45	365	27.24	5.01	7119	90.1	9.910
23	↓	↓	↓	↓	388	28.89	5.19	7439	94.7	9.915
24	↓	↓	↓	↓	↓	↓	5.07	7532	95.5	9.925
25	↓	↓	↓	↓	376	28.03	5.08	7270	92.2	9.935
26	6/25/70	↓	↓	34	386	28.75	4.82	7621	95.8	9.915
27	↓	↓	↓	↓	380	28.32	4.89	7619	96.0	9.920
28	↓	↓	↓	↓	378	28.17	4.99	7508	94.9	9.890
29	↓	↓	↓	↓	387	28.82	5.08	7566	95.9	↓
30	↓	↓	↓	↓	↓	↓	5.08	7526	95.4	9.895
31					391	29.11	5.09	7554	95.8	9.905
32	6/26/70	13.82	88	32	383	28.71	5.30	7673	98.1	9.915
33	↓	↓	↓	↓	379	28.42	5.04	7573	95.9	9.935
34	↓	↓	↓	↓	382	28.64	5.08	7545	95.7	9.955
35	7/1/70	13.85	80	42	384	28.73	5.10	7474	94.9	9.925
36	↓	↓	↓	↓	392	29.30	5.09	7596	96.4	9.940
37	↓	↓	↓	↓	386	28.87	5.10	7501	95.2	9.935
38	↓	↓	↓	↓	391	29.23	5.21	7583	96.6	9.915
39	↓	↓	↓	↓	388	29.01	5.05	7732	98.0	9.910
40	↓	↓	↓	↓	382	28.58	4.97	7570	95.6	9.920

TABLE 6-1 (Con't)

TEST FIRING DATA

Water Coolant

Run No.	Tank 1 Flow, lb/sec.	Tank 1 Pressure, psig	Tank 1 Injection Pressure, psig	ΔT_{11}, °F	ΔT_{12}, °F	ΔT_{13}, °F	Tank 2 Flow, lb/sec.	Tank 2 Pressure, psig	Tank 2 Injection Pressure, psig	ΔT_{10}, °F
1	31.61	1030	818	31	18	67	28.65	1043	815	28
2	30.71	1005	802	34	20	136	28.54	1047	809	27
4	28.56	944	760	33	18	143	29.42	980	772	26
021	29.92	980	834	34	25	141	29.75	1028	754	31
041	29.69	974	826	33	21	133	29.53	1008	781	32
5	30.14	1007	848	32	↓	134	30.42	1056	821	30
10	29.81	996	822	31	22	131	30.42	1016	800	33
11	↓	980	820	36	26	137	30.42	1020	799	36
12	28.00	864	740	31	20	133	30.86	1042	820	35
13	↓	874	734	25	17	132	31.08	1060	828	29
14	28.11	846	738	27	19	127	30.86	1042	806	33
15	Misfire									
16	29.81	946	838	27	20	116	31.19	1120	820	23
17	29.13	904	806	28	19	130	29.64	1078	748	25
18	28.00	926	750	24	18	122	28.65	946	700	26
19	29.02	986	798	33	27	138	29.75	1022	740	32
20	29.92	1052	844	↓	25	123	30.75	1090	786	30
21	30.26	1060	848	28	24	126	30.53	1096	↓	27
22	29.58	1056	846	27	22	119	30.08	1056	810	24
23	29.13	1022	840	↓	17	116	↓	1030	804	27
24	29.02	998	806	29	23	121	29.64	1012	780	31
25	29.69	1044	842	25	20	120	30.42	1062	820	24
26	29.81	1052	844	23	18	119	30.86	1066	832	24
27	30.26	1058	852	29	22	114	↓	1086	838	26
28	30.71	1086	894	26	↓	115	31.30	1120	854	26
29	29.92	1082	840	21	17	120	30.53	1068	812	22
30	30.03	1086	842	↓	16	116	30.75	1060	↓	25
31	↓	1092	↓	25	19	122	↓	1062	816	23
32	30.48	1124	860	↓	23	120	30.86	1078	842	26
33	30.37	1122	↓	21	16	111	31.08	1076	844	25
34	30.26	1098	850	19	15	116	30.86	1060	838	22
35	30.48	1078	858	20	16	↓	31.19	1084	860	23
36	30.37	1062	↓	29	22	115	30.97	1050	854	30
37	30.48	1064	854	21	15	116	↓	1098	840	23
38	↓	1060	858	25	22	122	31.08	1096	838	25
39	30.14	1046	834	27	↓	120	30.64	1044	848	29
40	29.81	1004	816	20	14	107	30.30	1042	842	25

TABLE 6-1 (Con't)

TEST FIRING DATA

Water Coolant

Run No.	Tank 1 Flow, lb/sec.	Tank 1 Pressure, psig	Tank 1 Injection Pressure, psig	ΔT_{11}, °F	ΔT_{12}, °F	ΔT_{13}, °F	Tank 2 Flow, lb/sec.	Tank 2 Pressure, psig	Tank 2 Injection Pressure, psig	ΔT_{10}, °F
1	31.61	1030	818	31	18	67	28.65	1043	815	28
2	30.71	1005	802	34	20	136	28.54	1047	809	27
4	28.56	944	760	33	18	143	29.42	980	772	26
021	29.92	980	834	34	25	141	29.75	1028	754	31
041	29.69	974	826	33	21	133	29.53	1008	781	32
5	30.14	1007	848	32	↓	134	30.42	1056	821	30
10	29.81	996	822	31	22	131	30.42	1016	800	33
11	↓	980	820	36	26	137	30.42	1020	799	36
12	28.00	864	740	31	20	133	30.86	1042	820	35
13	↓	874	734	25	17	132	31.08	1060	828	29
14	28.11	846	738	27	19	127	30.86	1042	806	33
15	Misfire									
16	29.81	946	838	27	20	116	31.19	1120	820	23
17	29.13	904	806	28	19	130	29.64	1078	748	25
18	28.00	926	750	24	18	122	28.65	946	700	26
19	29.02	986	798	33	27	138	29.75	1022	740	32
20	29.92	1052	844	↓	25	123	30.75	1090	786	30
21	30.26	1060	848	28	24	126	30.53	1096	↓	27
22	29.58	1056	846	27	22	119	30.08	1056	810	24
23	29.13	1022	840	↓	17	116	↓	1030	804	27
24	29.02	998	806	29	23	121	29.64	1012	780	31
25	29.69	1044	842	25	20	120	30.42	1062	820	24
26	29.81	1052	844	23	18	119	30.86	1066	832	24
27	30.26	1058	852	29	22	114	↓	1086	838	26
28	30.71	1086	894	26	↓	115	31.30	1120	854	26
29	29.92	1082	840	21	17	120	30.53	1068	812	22
30	30.03	1086	842	↓	16	116	30.75	1060	↓	25
31	↓	1092	↓	25	19	122	↓	1062	816	23
32	30.48	1124	860	↓	23	120	30.86	1078	842	26
33	30.37	1122	↓	21	16	111	31.08	1076	844	25
34	30.26	1098	850	19	15	116	30.86	1060	838	22
35	30.48	1078	858	20	16	↓	31.19	1084	860	23
36	30.37	1062	↓	29	22	115	30.97	1050	854	30
37	30.48	1064	854	21	15	116	↓	1098	840	23
38	↓	1060	858	25	22	122	31.08	1096	838	25
39	30.14	1046	834	27	↓	120	30.64	1044	848	29
40	29.81	1004	816	20	14	107	30.30	1042	842	25

TABLE 6-1 (Con't)

TEST FIRING DATA

Low Pressure GN_2 Film Coolant

Run No.	Flow lb/sec.	Duct Pressure P_{sd}, psig	Inlet Pressure P_{mc}, psig	Duct Temp. T_{sd}, °F	Inlet Temp. T_{mc}, °F	Inlet Density ρ_{mc}, lb/ft^3	Inlet Velocity V_{mc}, ft/sec.	Mach No.
1	0.85	1.10	0.050	21	11	0.0779	369.4	0.341
2	0.97	1.45	0.060	27	14	0.0775	421.8	0.388
4	0.96	1.47	↓	33	20	0.0761	428.6	0.392
021	1.02	1.59	0.070	14	0	0.0793	453.6	0.407
041	0.99	1.46	0.060	5	-7	0.0807	414.9	0.391
5	0.96	1.38	↓	10	-2	0.0797	406.5	0.381
10	1.09	1.80	0.080	13	↓	↓	460.5	0.431
11	1.10	1.84	↓	10	-6	0.0803	463.6	0.436
12	1.05	1.65	0.070	9	-5	0.0802	440.9	0.414
13	1.10	1.83	0.080	7	-9	0.0803	462.3	0.436
14	1.11	1.89	↓	13	-3	0.0794	472.1	0.443
15	Misfire							
16	1.13	2.02	0.090	30	12	0.0773	493.5	0.455
17	1.22	2.34	0.110	24	4	0.0788	523.2	0.487
18	1.19	2.19	0.100	17	2	0.0797	504.6	0.472
19	1.22	2.37	0.110	28	7	0.0778	529.6	0.491
20	1.01	1.62	0.070	26	12	0.0769	446.2	0.412
21	1.12	2.02	0.090	35	17	0.0761	497.3	0.456
22	1.17	2.25	0.105	47	27	0.0751	526.2	0.478
23	1.17	2.28	0.107	55	34	0.0740	533.4	0.481
24	1.15	2.19	0.101	54	↓	↓	523.6	0.472
25	1.10	2.01	0.091	51	33	0.0742	502.7	0.454
26	1.12	2.07	0.095	46	27	0.0750	506.7	0.460
27	1.14	2.22	0.103	62	41	0.0729	530.8	0.475
28	0.92	1.43	0.062	↓	48	0.0717	435.6	0.387
29	1.06	1.89	0.085	63	45	0.0723	494.8	0.441
30	1.01	1.71	0.076	59	43	0.0726	471.2	0.421
31	1.09	1.95	0.088	52	34	0.0739	496.4	0.448
32	1.04	1.83	0.082	59	42	0.0723	487.2	0.436
33	0.93	1.47	0.064	64	50	0.0711	443.3	0.393
34	1.04	1.84	0.082	59	42	0.0723	488.4	0.473
35	0.90	1.65	0.424	41	29	0.0761	401.4	0.364
36	1.03	1.74	0.077	50	34	0.0736	471.7	0.425
37	1.03	↓	↓	51	35	0.0735	472.1	↓
38	1.03	1.99	0.313	58	42	0.0737	473.6	0.424
39	1.05	1.88	0.084	62	44	0.0721	494.1	0.441
40	1.02	2.18	0.579	57	42	0.0751	459.1	0.411

TABLE 6-1 (Con't)

TEST FIRING DATA

High Pressure GN_2 Film Coolent

Run No.	Flow lb/sec.	Duct Pressure P_{sd}, psig	Inlet Pressure P_{mc}, psig	Duct Temp. T_{sd}, °F	Inlet Temp. T_{mc}, °F	Inlet Density ρ_{mc}, lb/ft^3	Inlet Velocity V_{mc}, ft/sec.
1	4.43	14.0	0.95	9	-68	0.0997	988.0
2	4.55	14.9	1.46	4	-64	0.1020	993.2
4	↓	15.2	1.66	21	-58	0.1012	1000.5
021	4.58	15.0	1.54	6	-70	0.1036	984.8
041	4.56	14.6	1.32	-3	-78	0.1041	975.3
5	4.58	14.9	1.48	3	-73	0.1039	981.6
10	4.53	14.6	1.33	↓	↓	0.1027	↓
11	↓	↓	1.33	↓	↓	↓	↓
12	4.63	15.1	1.60	-1	-76	0.1054	977.4
13	4.55	14.7	1.43	0	↓	0.1034	978.5
14	4.57	15.0	1.59	5	-71	↓	983.8
15	Misfire						
16	4.40	14.3	1.17	21	-58	0.0978	1000.5
17	4.62	15.5	1.81	14	-64	0.1035	993.2
18	4.58	15.1	1.60	10	-67	0.1030	989.0
19	4.63	15.8	2.01	19	-60	0.1032	998.5
20	4.45	14.6	1.37	17	-61	0.0994	996.4
21	4.36	14.3	1.21	27	-53	0.0964	1006.8
22	4.39	14.7	1.38	36	-45	0.0963	1016.0
23	4.41	14.9	1.47	39	-43	0.0962	1019.1
24	4.48	15.5	1.79	42	-40	0.0976	1022.1
25	4.42	14.9	1.51	39	-43	0.0965	1019.1
26	4.37	14.5	1.29	35	-46	0.0959	1015.0
27	4.30	14.4	1.24	49	-35	0.0929	1029.2
28	4.39	15.0	1.53	47	-36	0.0951	1027.2
29	4.46	15.6	1.85	52	-32	0.0961	1032.3
30	4.40	15.0	1.53	44	-39	0.0957	1024.2
31	4.39	14.8	1.42	41	-41	0.0956	1021.1
32	4.34	↓	1.46	48	-35	0.0940	1028.2
33	4.27	14.4	1.28	53	-31	0.0919	1033.3
34	4.35	14.8	1.49	47	-36	0.0943	1027.2
35	4.43	↓	1.46	30	-50	0.0976	1009.9
36	4.42	15.1	1.63	42	-40	0.0963	1022.1
37	4.43	↓	1.61	39	-43	0.0967	1019.1
38	4.35	14.8	1.46	48	-35	0.0941	1028.2
39	4.38	15.2	1.66	53	-31	0.0944	1033.3
40	↓	14.9	1.51	45	-38	0.0950	1025.2

TABLE 6-1 (Con't)

TEST FIRING DATA

LOX Oxidizer

Run No.	Flow, lb/sec.	Tank Pressure, psig	Injection Pressure, psig	Injection Temp., °F	Injector Temp., °F	ΔP
1	6.22	764	729	-262	-266	331
2	6.34	728	740	-289	-145	↓
4	6.13	750	723	↓	-155	327
021	6.23	744	710	-301	-127	308
041	6.18	746	↓	|	|	↓
5	6.17	738	701	↓	↓	302
10	6.23	750	709	-294	-100	308
11	6.27	740	702	-295	-162	305
12	6.22	742	709	-207	-164	313
13	6.11	722	674	-305	-189	275
14	5.70	726	664	-283	-181	273
15	Misfire					
16	5.92	750	701	-282	-148	303
17	6.64	866	822	-287	-175	402
18	5.49	720	651	-283	-151	275
19	6.17	780	742	-290	-169	340
20	5.81	728	711	-274	-167	324
21	5.91	722	↓	-276	-176	↓
22	5.77	674	663	-289	-183	298
23	5.89	728	716	-288	-173	328
24	5.79	726	703	-289	-180	315
25	5.83	728	701	-287	-186	325
26	5.65	720	679	-276	-174	293
27	5.58	724	680	-285	-171	300
28	5.65	726	679	-281	-183	301
29	5.75	738	688	-276	-184	↓
30	5.79	722	677	-292	-199	290
31	5.82	738	691	-287	-205	300
32	5.66	706	669	↓	-188	286
33	5.63	700	652	-281	-194	273
34	5.70	712	653	-291	-173	271
35	5.79	702	693	↓	-195	309
36	5.81	714	703	-280	-198	311
37	5.79	718	693	-284	-185	307
38	5.82	710	699	-286	↓	308
39	5.64	700	682	-285	-204	294
40	5.66	712	689	-288	-176	307

TABLE 6-1 (Con't)

TEST FIRING DATA

GH_2 Fuel

Run No.	Flow, lb/sec.	Venturi Inlet Pressure, psig	Injection Pressure, psig	Inlet Temp., °F	ΔP
1	1.15	1923	785	58	387
2	1.16	1968	805	72	396
4	1.10	1852	757	69	361
021	1.15	1925	780	63	378
041	1.12	1920	770	82	368
5	1.16	1935	771	60	372
10	↓	1942	760	63	359
11	1.14	1920	752	67	355
12	1.15	1932	761	64	365
13	1.14	1915	760	↓	361
14	1.12	1890	758	66	367
15	Misfire				
16	1.16	1975	794	75	396
17	1.15	1948	806	76	386
18	1.16	1970	787	73	411
19	1.14	1941	792	77	390
20	1.13	1920	776	80	389
21	↓	1925	778	83	391
22	1.15	1989	788	94	423
23	1.13	1977	796	105	408
24	1.14	1992	805	105	417
25	1.15	1983	803	96	427
26	1.17	2019	802	90	416
27	1.14	1983	810	102	430
28	1.13	1977	↓	106	432
29	↓	1980	808	107	421
30	1.14	1974	814	98	427
31	↓	1971	818	91	↓
32	1.07	1862	796	106	413
33	1.12	1959	801	113	422
34	↓	↓	799	107	417
35	1.13	1940	805	83	421
36	1.14	1965	816	91	424
37	↓	↓	↓	95	430
38	1.12	1950	814	106	423
39	↓	1945	815	104	427
40	1.14	1975	822	98	440

APPENDIX 7

DATA REDUCTION COMPUTER PROGRAMS

A hot fire data reduction computer program was written to minimize the time required to reduce the facility operation parameters. Equations and calculations required to reduce the raw data into a workable form were assembled and a computational sequence was formulated. The program performs all the necessary calculations to establish the operating conditions of the various utilities and the initial conditions of the combustion gas, air stream, and film coolants as they enter the mixing chamber. It was written in FORTRAN language and was used in conjunction with a General Electric 440 Timesharing Computer. In addition, a supplementary FORTRAN computer program entitled "Manometer Bank Pressure" was written to shorten the time required for data reduction of the test section static pressure data.

The program, entitled SSMIX, consisted of a main program which handled the majority of the data reduction, two "function" subroutines which convert millivolt values to temperatures in degrees fahrenheit for chromel-alumel and iron-constantan thermocouples, and a subroutine which calculated Mach number by an iterative procedure given values of A/A* (Ref. 8).

Given below are program summaries, a definition of program variables (Table 7-1), program listings (Table 7-2), a data input list, and a printout for a typical run (Table 7-3).

TABLE 7-1

SSMIX PROGRAM VARIABLES

GENERAL

IRUN	-	Run Number	(Integer)
IDATE	-	Run Date	(Integer)
PA	-	Atmospheric Pressure	(psia)
TATM	-	Atmospheric Temperature	(F)
RH	-	Relative Humidity	(Percent)

TANK-1 HIGH PRESSURE WATER SYSTEM

CWH	-	Flowmeter Cycles	(Cycles)
DTWP11	-	Line 11, 3/4-Inch Outlet Delta Temp	(F)
DTWP12	-	Line 12, 1-1/2-Inch Outlet Delta Temp	(F)
DTWP13	-	Line 13, 1/4-Inch Outlet Delta Temp	(F)
PWHI	-	Inlet Pressure	(psig)
PWHT	-	Tank Pressure	(psig)
TWHT	-	Tank Temperature	(F)
TWP11	-	Line 11, 3/4-Inch Outlet Temperature	(F)
TWP12	-	Line 12, 1-1/2-Inch Outlet Temperature	(F)
TWP13	-	Line 13, 1/4-Inch Outlet Temperature	(F)
VWHT	-	Tank Temperature (IC)	(MV)
VWP11	-	Line 11, 3/4-Inch Outlet Temperature (IC)	(MV)
VWP12	-	Line 12, 1-1/2-Inch Outlet Temperature (IC)	(MV)

TABLE 7-1 (Cont'd)

VWP13	-	Line 13, 1/4-Inch Outlet Temperature (IC)	(MV)
WWH	-	Flowrate	(lbs/sec)

TANK 2 - LOW PRESSURE WATER SYSTEM

CWL	-	Flowmeter Cycles	(Cycles)
DTWP10	-	Line 10, 1-Inch Outlet Delta Temperature	(F)
PWLI	-	Inlet Pressure	(psig)
PWLT	-	Tank Pressure	(psig)
TWP10	-	Line 10, 1-Inch Outlet Temperature	(F)
TWLT	-	Tank Temperature	(F)
VWLT	-	Tank Temperature (IC)	(MV)
VWP10	-	Line 10, 1-Inch Outlet Temperature (IC)	(MV)
WWL	-	Flowrate	(lbs/sec)

AIR STREAM

AMC	-	Mixing Chamber Inlet Air Acoustic Velocity	(ft/sec)
AMCAS	-	Dimensionless Area Ratio Equation in Terms of Mach Number in Mixing Chamber	
ASDAS	-	Dimensionless Area Ratio Equation in Terms of Mach Number in the Duct	
AVSD	-	Acoustic Velocity in Duct	(ft/sec)
MMC	-	Mixing Chamber Inlet Air Mach Number	
MSD	-	Mach Number in Duct	
PMC	-	Mixing Chamber Inlet Air Pressure	(psia)
PMCG	-	Mixing Chamber Inlet Air Pressure	(psig)

TABLE 7-1 (Cont'd)

PMCPO	-	Isentropic Pressure Ratio Equation in Mixing Chamber	
PRA	-	Pressure Ratio PA/PSD	
PSD	-	Stream Pressure in Duct	(psig)
PSDA	-	Stream Pressure in Duct	(psia)
PSDPO	-	Isentropic Pressure Ratio Equation in Duct	
RMC	-	Mixing Chamber Inlet Air Density	(lbs/ft^3)
RSD	-	Stream Density in Duct	(lbs/ft^3)
TMC	-	Mixing Chamber Inlet Air Temperature	(R)
TMCF	-	Mixing Chamber Inlet Air Temperature	(F)
TMCTO	-	Isentropic Temperature Ratio Equation in Mixing Chamber	
TSD	-	Stream Temperature in Duct	(F)
TSDA	-	Stream Temperature in Duct	(R)
TSDTO	-	Isentropic Temperature Ratio Equation in Duct	
VMC	-	Mixing Chamber Inlet Air Velocity	(ft/sec)
VSD	-	Stream Temperature in Duct (CA)	(MV)
WA	-	Flowrate	(lbs/sec)
YA	-	Expansion Factor	

LOW PRESSURE NITROGEN SYSTEM

AMCANL	-	Isentropic Pressure Ratio Equation in Mixing Chamber	
AMCNL	-	Mixing Chamber Inlet GN_2 Acoustic Velocity	(ft/sec)
ANLSDV	-	Duct GN_2 Acoustic Velocity	(ft/sec)

TABLE 7-1 (Cont'd)

ASDANL	-	Isentropic Pressure Ratio Equation in Duct	
MNLMC	-	Mixing Chamber Inlet GN_2 Mach Number	
MNLSD	-	Duct GN_2 Mach Number	
PMCNL	-	Mixing Chamber Inlet GN_2 Pressure	(psia)
PMCNLG	-	Mixing Chamber Inlet GN_2 Pressure	(psig)
PMCPNL	-	Isentropic Pressure Ratio Equation in Mixing Chamber	
PNL	-	Manifold Pressure	(psig)
PNLSDA	-	Manifold Pressure	(F)
PRNL	-	Pressure Ratio PA/(PNL + PS)	
PSDPNL	-	Isentropic Pressure Ratio Equation in Duct	
RNLMC	-	Mixing Chamber Inlet GN_2 Density	(lbs/ft^3)
RNLSD	-	Duct GN_2 Density	(lbs/ft^3)
TMCNL	-	Mixing Chamber Inlet Temperature	(R)
TMCNLF	-	Mixing Chamber Inlet Temperature	(F)
TMCTNL	-	Isentropic Temperature Ratio Equation in Mixing Chamber	
TNL	-	Manifold Temperature	(F)
TNLSDA	-	Manifold Temperature	(R)
TSDTNL	-	Isentropic Temperature Ratio Equation in Duct	
VMCNL	-	Mixing Chamber Inlet GN_2 Velocity	(ft/sec)
VNL	-	Manifold Temperature (IC)	(MV)
WNL	-	Flowrate	(lbs/sec)
YNL	-	Expansion Factor	

TABLE 7-1 (Cont'd)

HIGH PRESSURE GN_2 FILM COOLANT

MNH	-	Mach Number in Duct	
PNH	-	Manifold Pressure	(psig)
PNHA	-	Manifold Pressure	(psia)
PNHMC	-	Mixing Chamber Inlet GN_2 Pressure	(psia)
PNHMCG	-	Mixing Chamber Inlet GN_2 Pressure	(psig)
PMCPNH	-	Isentropic Pressure Ratio in Mixing Chamber	
PPONH	-	Isentropic Pressure Ratio in Duct	
RNHMC	-	Mixing Chamber Inlet GN_2 Density	(lbs/ft^3)
TNH	-	Manifold Temperature	(F)
TNHA	-	Manifold Temperature	(R)
TNHMC	-	Mixing Chamber Inlet GN_2 Temperature	(R)
TNHMCF	-	Mixing Chamber Inlet GN_2 Temperature	(F)
TTONH	-	Isentropic Temperature Ratio in Duct	
VNH	-	Manifold Temperature (IC)	(MV)
VNHMC	-	Mixing Chamber Inlet GN_2 Velocity	(ft/sec)
WNH	-	Flowrate	(lbs/sec)

LOX OXIDIZER CALCULATIONS

B	-	Adiabatic Compressibility	
COX	-	Flowmeter Cycles	(Cycles)
DPOXI	-	Injector Delta Pressure	(psi)
PC	-	Chamber Pressure	(psig)
POXI	-	Inlet Pressure	(psig)

TABLE 7-1 (Cont'd)

POXT	-	Tank Pressure	(psig)
PV	-	Vapor Pressure	(psia)
ROX	-	LOX Density	(lbs/ft^3)
RS	-	Saturation Density	(lbs/ft^3)
TK	-	Inlet Temperature	(K)
TOXC	-	Injector Cooldown Temperature	(F)
TOXI	-	Inlet Temperature	(F)
VOXC	-	Injector Cooldown Temperature (IC)	(MV)
VOXI	-	Inlet Temperature (IC)	(MV)
WOX	-	LOX Flowrate	(lbs/sec)

HYDROGEN FUEL CALCULATIONS

DPHI	-	Injection Delta Pressure	(psi)
PHI	-	Inlet Pressure	(psig)
PHIC	-	Inlet Pressure	(psia)
PHVI	-	Venturi Inlet Pressure	(psig)
THI	-	Inlet Temperature	(F)
VHI	-	Inlet Temperature (IC)	(MV)
WH	-	Flowrate	(lbs/sec)
XKH	-	Isentropic Flow Coefficient	
ZH	-	Compressibility Factor	

TABLE 7-1 (Cont'd)

PERFORMANCE PARAMETERS

CN	-	C* Efficiency	(Percent)
CSTAR	-	C*	(ft/sec)
PRPC	-	Pressure Ratio PC/PA	
TCSTAR	-	Theoretical C* @ MR of Test	(ft/sec)
TC4	-	Theoretical C* @ MR = 4.0	(ft/sec)
TC5	-	Theoretical C* @ MR = 5.0	(ft/sec)
TC6	-	Theoretical C* @ MR = 6.0	(ft/sec)
WT	-	Total Flow	(lbs/sec)
XMR	-	Mixture Ratio	

AIR HEATER TEMPERATURES

TAH1	-	Heater Bed Temperature 1	(F)
TAH2	-	Heater Bed Temperature 2	(F)
TAH3	-	Heater Bed Temperature 3	(F)
TAH4	-	Heater Bed Temperature 4	(F)
TAH5	-	Heater Bed Temperature 5	(F)
VAH1	-	Heater Bed Temperature 1 (CA)	(MV)
VAH2	-	Heater Bed Temperature 2 (CA)	(MV)
VAH3	-	Heater Bed Temperature 3 (CA)	(MV)
VAH4	-	Heater Bed Temperature 4 (CA)	(MV)
VAH5	-	Heater Bed Temperature 5 (CA)	(MV)

TABLE 7-2

SSMIX - LOGIC

```
5C * * * PRØGRAM SSMIX        1/9/69      J T. SABØL * * * *
10C
15 REAL MSD,MMC,MNLSD,MNLMC,MNH
20 CALL ØPENF (1,"XDATA",2)
25 READ(1,)IRUN,IDATE,PA,TATM,RH
30C       *****TANK 1 - HIGH PRESSURE WATER SYSTEM*****
35 READ(1,) CWH,PWHT,PWHI,VWHT,VWP11,VWP12,VWP13
40 WWH=.1129*CWH
45 TWHT=ICØN(VWHT)
50 TWP11=ICØN(VWP11)
55 TWP12=ICØN(VWP12)
60 TWP13=ICØN(VWP13)
65 DTWP11=TWP11-TWHT
70 DTWP12=TWP12-TWHT
75 DTWP13=TWP13-TWHT
80C       *****TANK 2 - LØW PRESSURE WATER SYSTEM*****
85 READ(1,) CWL,PWLT,PWLI,VWLT,VWP10
90 WWL=.1102*CWL
95 TWLT=ICØN(VWLT)
100 TWP10=ICØN(VWP10)
105 DTWP10=TWP10-TWLT
110C                 *****AIR SYSTEM*****
115 READ(1,)PSD,VSD
120 TSD=CRAL(VSD)
125 TSDA=TSD+460.
130 PSDA=PSD+PA
135 RSD=2.7*PSDA/TSDA
140 PRA=PA/(PSD+PA)
145 YA=SQRT(((1.-.732**4.)/(1.-.732**4.*PRA**1.42857))*(((3.5*
150&PRA**1.42857)*(1.-PRA**.285714))/(1.-PRA)))
155 WA=16.27*YA*SQRT(PSD*RSD)
160 AVSD=49.*SQRT(TSDA)
165 MSD=3.75*WA/(RSD*AVSD)
170 ASDAS=(1./MSD)*(((2./2.4)*(1.+.2*MSD**2.))**3.)
175 AMCAS=.536*ASDAS
180 CALL MACH(AMCAS,MMC)
185 TSDTØ=1./(1.+.2*MSD**2.)
190 TMCTØ=1./(1.+.2*MMC**2.)
195 TMC=(TMCTØ/TSDTØ)*TSDA
200 TMCF=TMC-460.
205 AMC=49.*SQRT(TMC)
210 VMC=MMC*AMC
215 PSDPØ=1./((1.+.2*MSD**2.)**3.5)
220 PMCPØ=1./((1.+.2*MMC**2.)**3.5)
225 PMC=(PMCPØ/PSDPØ)*PSDA
230 PMCG=PMC-PA
235 RMC=2.7*PMC/TMC
```

TABLE 7-2 (Continued)

```
240C      *****LØW PRESSURE NITRØGEN SYSTEM*****
245 READ(1,)PNL,VNL
250 TNL=ICØN(VNL)
255 TNLSDA=TNL+460.
260 PNLSDA=PNL+PA
265 PRNL=PA/(PNL+PA)
270 YNL=SQRT(((1.-.577**4.)/(1.-.577**4.*PRNL**1.42857))*(((3.5*
275&PRNL**1.42857)*(1.-PRNL**.285714))/(1.-PRNL)))
280 WNL=4.79*YNL*SQRT(PNLSDA*PNL/TNLSDA)
285 RNLSD=2.7*PNLSDA/TNLSDA
290 ANLSDV=49.*SQRT(TNLSDA)
295 MNLSD=11.474*WNL/(RNLSD*ANLSDV)
300 ASDANL=(1./MNLSD)*(((2./2.4)*(1.+.2*MNLSD**2.))**3.)
305 AMCANL=.334*ASDANL
310 CALL MACH(AMCANL,MNLMC)
315 TSDTNL=1./(1.+.2*MNLSD**2.)
320 TMCTNL=1./(1.+.2*MNLMC**2.)
325 TMCNL=(TMCTNL/TSDTNL)*TNLSDA
330 TMCNLF=TMCNL-460.
335 AMCNL=49.9*SQRT(TMCNL)
340 VMCNL=MNLMC*AMCNL
345 PSDPNL=1./((1.+.2*MNLSD**2.)**3.5)
350 PMCPNL=1./((1.+.2*MNLMC**2.)**3.5)
355 PMCNL=(PMCPNL/PSDPNL)*PNLSDA
360 PMCNLG=PMCNL-PA
365 RNLMC=2.61*PMCNL/TMCNL
370C      *****HIGH PRESSURE GN2 FILM CØØLANT*****
375 READ(1,)PNH,VNH
380 TNH=ICØN(VNH)
385 TNHA=TNH+460.
390 PNHA=PNH+PA
395 PPØNH=.988
400 PMCPNH=.528
405 MNH=.122
410 TTØNH=.997
415 WNH=3.38*PNHA/(PPØNH*SQRT(TNHA))
420 TNHMC=.83333*TNHA/TTØNH
425 TNHMCF=TNHMC-460.
430 VNHMC=49.9*SQRT(TNHMC)
435 PNHMC=(PMCPNH/PPØNH)*PNHA
440 PNHMCG=PNHMC-PA
445 RNHMC=2.61*PNHMC/TNHMC
450C      *****LØX ØXIDIZER CALCULATIØNS*****
455 READ(1,)PC,CØX,PØXT,PØXI,VØXI,VØXC
460 TØXI=ICØN(VØXI)
465 TØXC=ICØN(VØXC)
470 TK=(TØXI+459.668)/1.8
```

```
475 RS=62.428227*(1.414202-.001033016*TK-2.23E-5*TK**2.)
480 PV=PA*EXP(5.238279-7.2953481/TK-41958.931/TK**2.)
485 B=6.05790431E-5-1.8993851E-6*TK+1.2860036E-8*TK**2.
490 RØX=RS*(10.*B*(PØXI+PA-PV)+1.)**.1
495 WØX=.17077E-3*CØX*RØX
500 DPØXI=PØXI-PC
505C       *****HYDRØGEN FUEL CALCULATIØNS*****
510 READ(1,)PHVI,PHI,VHI
515 THI=ICØN(VHI)
520 XKH=(((THI+60.)/200.)*.00013)+.01362
525 PHIC=PHI+PA
530 ZH=4.62585E-5*PHIC+.99
535 WH=((PHVI+PA)/SQRT(THI+460.))*SQRT(1./ZH)*XKH
540 DPHI=PHI-PC
545C       *****PERFØRMANCE PARAMETERS*****
550 PRPC=(PC+PA)/PA
555 XMR=WØX/WH
560 WT=WØX+WH
565 CSTAR=130.*(PC+PA)/WT
570 TC4=((((PC+PA)-300.)/200.)*15.)+8146.
575 TC5=((((PC+PA)-300.)/200.)*30.)+7893.
580 TC6=((((PC+PA)-300.)/200.)*40.)+7600.
585 IF(XMR-5.)30,40,50
590 30 TCSTAR=((5.-XMR)*(TC4-TC5))+TC5
595 GØ TØ 55
600 40 TCSTAR=TC5
605 GØ TØ 55
610 50 TCSTAR=TC5-((XMR-5.)*(TC5-TC6))
615 55 CN=(CSTAR/TCSTAR)*100.
620C       *****AIR HEATER TEMPERATURES*****
625 READ(1,)VAH1,VAH2,VAH3,VAH4,VAH5
630 TAH1=CRAL(VAH1)
635 TAH2=CRAL(VAH2)
640 TAH3=CRAL(VAH3)
645 TAH4=CRAL(VAH4)
650 TAH5=CRAL(VAH5)
655C                 *****PRINTØUTS*****
660 PRINT,"           * * * * * * M I X I N G   P R Ø G R A L * *
665&* * * "
670 PRINT,†2,"    NØTE:  DIMENSIØNS FØR PARAMETERS ARE AS FØLLØWS:"
675 PRINT,†,"          TEMPERATURES - F         DENSITIES - #/FT3"
680 PRINT,"          PRESSURES - PSIG         FLØWS - #/SEC"
685 PRINT,"          VELØCITIES - FT/SEC"
690 PRINT,†2,"         * * * * * * * * * * * * * * * * * * * * *
695&* * * *"
```

TABLE 7-2 (Continued)

```
700 PRINT,↑2,"RUN - ",IRUN,"                    ","DATE - ",IDATE
705 PRINT 70,PA,TATM,RH
710 PRINT,↑2,↑,"  .  ***** TANK 1 - HIGH PRESSURE WATER SYSTEM *****"
715 PRINT 75,WWH,PWHT,PWHI,TWHT,DTWP11,DTWP12,DTWP13
720 PRINT,↑2,↑,"        ***** TANK 2 - LØW PRESSURE WATER SYSTEM *****"
725 PRINT 80,WWL,PWLT,PWLI,TWLT,DTWP10
730 PRINT,↑2,↑,"                    ***** AIR SYSTEM *****"
735 PRINT 85,WA,PSD,PMCG,TSD,TMCF,RMC,VMC,AMC,MMC
740 PRINT,↑2,↑,"            ***** LØW PRESSURE NITRØGEN SYSTEM *****"
745 PRINT 90,WNL,PNL,PMCNLG,TNL,TMCNLF,RNLMC,VMCNL,AMCNL,MNLMC
750 PRINT,↑2,↑,"            ***** HIGH PRESSURE NITRØGEN SYSTEM *****"
755 PRINT 100,WNH,PNH,PNHMCG,TNH,TNHMCF,RNHMC,VNHMC
760 65 PRINT,↑2,↑,"         ***** LØX ØXIDIZER CALCULATIØNS *****"
765 PRINT 105,WØX,PØXT,PØXI,TØXI,TØXC,DPØXI
770 PRINT,↑2,↑,"            ***** HYDRØGEN FUEL CALCULATIØNS *****"
775 PRINT 110,WH,PHVI,PHI,THI,DPHI
780 PRINT,↑2,↑,"              ***** PERFØRMANCE PARAMETERS *****"
785 PRINT 115,PC,PRPC,XMR,WT,CSTAR,TCSTAR,CN
790 PRINT,↑2,↑,"         ***** AIR HEATER BED TEMPERATURES *****"
795 PRINT 120,TAH1,TAH2,TAH3,TAH4,TAH5
800 70 FØRMAT(/,"P ATM - "F5.2,5X,"T ATM - "F4.0,5X,"RH - "F4.1,
805&5X,"PC/PA IDEAL - 29.35")
810 75 FØRMAT(/,"FLØW - "F5.2,5X,"P TANK - "F6.1,5X,"P IN - "F6.1,
815&5X,"T TANK - "F4.0,//,"DT 11 - "F4.0,5X,"DT 12 - "F4.0,5X,
820&"DT 13 - "F4.0)
825 80 FØRMAT(/,"FLØW - "F5.2,5X,"P TANK - "F6.1,5X,"P INLET - "
830&F6.1,//,"T TANK - "F4.0,7X,"DT 10 - "F4.0)
835 85 FØRMAT(/,"FLØW - "F4.2,5X,"P SD - "F4.3,5X,"P MC - "F5.3,
840&//,"T SD - "F5.0,5X,"T MC - "F5.0,5X,"RHØ MC - "F5.4,//,
845&"V MC - "F6.1,5X,"A - "F6.1,5X,"M - "F4.3)
850 90 FØRMAT(/,"FLØW - "F4.2,5X,"P N2 - "F4.2,5X,"P MC - "F5.3,//,
855&"T N2 - "F3.0,5X,"T MC - "F3.0,5X,"RHØ MC - "F5.4,//,
860&"V MC - "F6.1,5X,"A - "F6.1,5X,"M - "F4.3)
865 100 FØRMAT(/,"FLØW - "F4.2,5X,"P N2 - "F4.1,5X,"P MC - "F6.2,
870&5X,"T N2 - "F3.0,//,"T MC - "F4.0,5X,"RHØ MC - "F5.4,5X,
875&"VEL N2 - "F6.1)
880 105 FØRMAT(/,"FLØW - "F4.2,5X,"P TANK - "F5.1,5X,"P IN - "F5.1,
885&//,"T IN - "F5.0,5X,"T CØØL - "F5.0,5X,"DP INJ - "F5.1)
890 110 FØRMAT(/,"FLØW - "F4.2,5X,"P VEN IN - "F6.1,5X,"P IN - "F6.1,
895&//,"T H2 - "F4.0,5X,"DP INJ - "F5.1)
900 115 FØRMAT(/,"PC - "F5.1,5X,"PC/PA - "F5.2,5X,"MR - "F5.2,5X,
905&"TØTAL FLØW - "F4.2,//,"C* - "F5.0,5X,"THEØR C* - "F5.0,5X,
910&"ETA C* - "F5.1)
915 120 FØRMAT(/,"T BED 1 - "F5.0,3X,"T BED 2 - "F5.0,3X,
920&"T BED 3 - "F5.0,3X,"T BED 4 - "F5.0,//,"T BED 5 - "F5.0)
925 PRINT,↑2,↑,"            * * * * * * * * * * * * * * * * * * * *
930&* * * * *"
935 PRINT,↑2,↑2
999 END
```

TABLE 7-3

PROGRAM SSMIX - TYPICAL OUTPUT

```
* * * * * * M I X I N G   P R Ø G R A M * * * * *

NØTE:  DIMENSIØNS FØR PARAMETERS ARE AS FØLLØWS:

       TEMPERATURES - F          DENSITIES - #/FT3
       PRESSURES - PSIG          FLØWS - #/SEC
       VELØCITIES - FT/SEC

* * * * * * * * * * * * * * * * * * * * * * * * *

RUN -         30            DATE -     62570

P ATM - 13.91     T ATM -  80.     RH - 34.0     PC/PA IDEAL - 29.35


    ***** TANK 1 - HIGH PRESSURE WATER SYSTEM *****

FLØW - 30.03      P TANK - 1086.0     P IN -  842.0      T TANK -  83.

DT 11 -  21.      DT 12 -  16.      DT 13 - 116.


    ***** TANK 2 - LØW PRESSURE WATER SYSTEM *****

FLØW - 30.75      P TANK - 1060.0     P INLET -  812.0

T TANK -  78.        DT 10 -  25.


              ***** AIR SYSTEM *****

FLØW - 2.27       P SD - .666       P MC - 0.002

T SD -  786.       T MC -  770.      RHØ MC - .0306

V MC -  520.3      A - 1718.2       M - .303
```

TABLE 7-3 (Continued)

***** LØW PRESSURE NITRØGEN SYSTEM *****

FLØW - 1.01 P N2 - 1.71 P MC - 0.076

T N2 - 59. T MC - 43. RHØ MC - .0726

V MC - 471.2 A - 1119.0 M - .421

***** HIGH PRESSURE NITRØGEN SYSTEM *****

FLØW - 4.40 P N2 - 15.0 P MC - 1.53 T N2 - 44.

T MC - -39. RHØ MC - .0957 VEL N2 - 1024.2

***** LØX ØXIDIZER CALCULATIØNS *****

FLØW - 5.79 P TANK - 722.0 P IN - 677.0

T IN - -292. T CØØL - -199. DP INJ - 290.0

***** HYDRØGEN FUEL CALCULATIØNS *****

FLØW - 1.14 P VEN IN - 1974.0 P IN - 814.0

T H2 - 98. DP INJ - 427.0

***** PERFØRMANCE PARAMETERS *****

PC - 387.0 PC/PA - 28.82 MR - 5.08 TØTAL FLØW - 6.93

C* - 7526. THEØR C* - 7885. ETA C* - 95.4

***** AIR HEATER BED TEMPERATURES *****

T BED 1 - 927. T BED 2 - 741. T BED 3 - 958. T BED 4 - 820.

T BED 5 - 936.

PROGRAM SSMIX

This program reduced desired facility parameters from test firing raw data. Three major subsystems were involved: (1) LOX-GH_2 rocket motor, (2) GN_2 film coolant, and (3) heated air. For data reduction purposes these three subsystems are further divided as follows:

1. <u>LOX-GH_2 Rocket Motor</u>
   a. Tank 1 - High Pressure Water System
   b. Tank 2 - Low Pressure Water System
   c. LOX Oxidizer Calculations
   d. Hydrogen Fuel Calculations
   e. Performance Parameters
2. <u>GN_2 Film Coolant</u>
   a. High Pressure GN_2 Film Coolant
   b. Low Pressure Nitrogen System
3. <u>Heated Air</u>
   a. Air Stream
   b. Air Heater Temperatures

Data reduction for each of the above was handled separately in a labeled section of the program.

SSMIX DATA INPUT

Data were entered in permanent file XDATA. Nine lines of data were imputted as shown below.

1. IRUN, IDATE, PA, TATM, RH
2. CWH, PWHT, PWHI, VWHT, VWP11, VWP12, VWP13
3. CWL, PWLT, PWLI, VWLT, VWP10
4. PSD, VSD
5. PNL, VNL
6. PNH, VNH
7. PC, COX, POXT, POXI, VOXI, VOXC
8. PHVI, PHI, VHI
9. VAH1, VAH2, VAH3, VAH4, VAH5

It should be noted that a line number was required and a comma was needed to separate each data variable.

SUBROUTINES

Function Icon

This function performed temperature scaling of millivolt values from iron-constantan thermocouples with a 150F reference junction in the range of -11.2 to +53.2 millivolts (-320 to 1800F). Scaling was accomplished by separating the 64.4 millivolt range into smaller ranges, each being fitted with a third-order polynomial equation. The breakdown was as follows:

.2 MV Range	-11.2 to -11.0 MV
1.0 MV Range	-11.0 to -10.0 MV
2.0 MV Ranges	-10.0 to 0 MV
4.0 MV Ranges	0 to +52.0 MV
1.0 MV Range	+52.0 to +53.0 MV
.2 MV Range	+53.0 to +53.2 MV

The program (Table 7-4) selected the correct equation from the millivolt value and solved for the temperature. Accuracy is within $\pm$ 1.0 F of NBS standards.

Function Cral

This function performed temperature scaling of millivolt values of chromel-alumel thermocouples with a 32F reference junction in the range 0 to 55 millivolts (32 to 2504F). Scaling was accomplished by treating the 55-millivolt range as eleven 5-millivolt ranges, each being fitted with a third-order polynomial equation. The program (Table 7-5) selects the correct equation from the millivolt value and solves for the temperature. Accuracy is within $\pm$ 1.0 F of NBS standards.

Subroutine Mach

This subroutine (Table 7-6) calculates the Mach number for the film coolant and air streams in the range between .01 and 1.00 by an iterative procedure given a value of A/A*. The assumption of a perfect gas (K = 1.4) is utilized. It initially assumes a Mach number of 0.5 and calculates A/A*. Then by comparison to the given value of A/A* it adjusts the Mach number until agreement within 0.0001 is achieved.

PROGRAM MANOMETER BANK PRESSURE

The program, entitled Manometer Bank Pressure, was a simple program that was written to shorten the time required for data reduction of the test section static pressure data. The calibration data was fed into the program together with the raw data by a punched tape. The program then converted the measured liquid level to pressure via the appropriate equation depending on the particular fluid in the

TABLE 7-4

FUNCTION ICON - LOGIC

```
FUNCTIØN ICØN(XMV)
C
C IRØN CØNSTANTAN THERMØCØUPLE MILLIVØLT TØ DEGREES F CØNVERSIØN
C 150 DEGREE REFERENCE JUNCTIØN TEMPERATURE
C      J T. SABØL    12/18/68
C
      IF(XMV.GE.-11.2.AND.XMV.LE.53.2) GØ TØ 5
      T=9999.
      GØ TØ 140
    5 IF(XMV) 10,50,50
   10 IF(XMV.LT.-10..AND.XMV.GT.-11.) GØ TØ 40
      IF(XMV.LE.-11.) GØ TØ 45
      N=IABS(INT(XMV/2))
      I=N+1
      V=XMV+2.*N
      GØ TØ (15,20,25,30,35,35),I
   15 T=-.15*V*V+33.85*V+150.
      GØ TØ 130
   20 T=-.5*V*V+34.5*V+81.7
      GØ TØ 130
   25 T=-.8*V*V+35.9*V+10.7
      GØ TØ 130
   30 T=-1.3*V*V+38.4*V-64.3
      GØ TØ 130
   35 T=-2.65*V*V+43.05*V-146.3
      GØ TØ 130
   40 V=XMV+10.
      T=-8.*V*V+54.*V-243.
      GØ TØ 130
   45 V=XMV+11.
      T=-50.*V*V+65.*V-305.
      GØ TØ 130
   50 IF(XMV.GT.52..AND.XMV.LT.53.) GØ TØ 120
      IF(XMV.GE.53.) GØ TØ 125
      N=INT(XMV/4.)
      I=N+1
      V=XMV-4.*N
      GØ TØ (55,60,65,70,75,80,85,90,95,100,105,110,115,115),I
   55 T=-.0875*V*V+33.525*V+150.
      GØ TØ 130
   60 T=-.05*V*V+32.6*V+282.7
      GØ TØ 130
```

TABLE 7-4 (Cont'd)

```
65  T=.075*V*V+32.2*V+412.3
    GØ TØ 130
70  T=0.*V*V+32.5*V+542.3
    GØ TØ 130
75  T=-.0125*V*V+32.725*V+672.3
    GØ TØ 130
80  T=-.0375*V*V+32.575*V+803.
    GØ TØ 130
85  T=-.0875*V*V+31.975*V+932.7
    GØ TØ 130
90  T=-.1*V*V+31.1*V+1059.2
    GØ TØ 130
95  T=-.1625*V*V+29.975*V+1182.
    GØ TØ 130
100 T=-.1*V*V+28.7*V+1299.3
    GØ TØ 130
105 T=-.025*V*V+28.15*V+1412.5
    GØ TØ 130
110 T=.375*V*V+27.65*V+1524.7
    GØ TØ 130
115 T=-.0375*V*V+30.575*V+1641.3
    GØ TØ 130
120 V=XMV-52.
    T=.4*V*V+29.8*V+1763.
    GØ TØ 130
125 V=XMV-53.
    T=20.*V*V+26.*V+1793.2
130 IF(T) 135,140,140
135 ICØN=INT(T-.5)
    GØ TØ 999
140 ICØN=INT(T+.5)
999 RETURN
    END
```

TABLE 7-5

FUNCTION CRAL - LOGIC

```
      FUNCTIØN CRAL(XMV)
C
C CHRØMEL-ALUMEL THERMØCØUPLE MILLIVØLT TØ DEGREES CØNVERSIØN
C 32 DEGREE REFERENCE JUNCTIØN TEMPERATURE
C      J. T. SABØL      12/27/68
C
      IF(XMV.GE.0.0.AND.XMV.LE.55.) GØ TØ 5
      T=9999.
      GØ TØ 65
    5 N=INT(XMV/5.)
      I=N+1
      V=XMV-5.*N
      GØ TØ (10,15,20,25,30,35,40,45,50,55,60,60),I
   10 T=-.216*V*V+44.94*V+32.
      GØ TØ 65
   15 T=-.048*V*V+45.*V+251.3
      GØ TØ 65
   20 T=-.125*V*V+44.08*V+475.1
      GØ TØ 65
   25 T=-.048*V*V+42.72*V+692.3
      GØ TØ 65
   30 T=-.016*V*V+42.28*V+904.7
      GØ TØ 65
   35 T=.064*V*V+42.36*V+1115.7
      GØ TØ 65
   40 T=.168*V*V+42.74*V+1329.1
      GØ TØ 65
   45 T=.208*V*V+43.88*V+1547.
      GØ TØ 65
   50 T=.176*V*V+45.68*V+1771.6
      GØ TØ 65
   55 T=.240*V*V+47.32*V+2004.4
      GØ TØ 65
   60 T=.240*V*V+50.2*V+2247.
   65 CRAL=INT(T+.5)
   99 RETURN
      END
```

TABLE 7-6

SUBROUTINE MACH - LOGIC

```
SUBRØUTINE MACH(A,XM3)
C
C    THIS PRØGRAM GIVEN AN A/A* VALUE SØLVES FØR MACH NUMBER
C    USING AN ITERATIVE PRØCEEDURE. PRØGRAM WILL SØLVE FØR MACH
C    NUMBERS BETWEEN .01 AND 1.00.
C
XM1=.01
XM2=1.
5 XM3=(XM1+XM2)/2.
AA=(1./XM3)*(((2./2.4)+(.4/2.4)*XM3**2.)**3.)
IF((ABS(AA-A)).LT. .0001) GØ TØ 25
IF(AA-A) 10,25,15
10 XM2=XM3
GØ TØ 5
15 XM1=XM3
GØ TØ 5
25 RETURN
END
```

manometer tube. The measurement of the liquid level was derived from photographs of the manometer bank during testing. Reduction of the film clips to physical dimensions was accomplished through utilization of a Vanguard Motion Analyzer. Manometer bank tubes denoted 1, 2, 3, 6, 7, 9, 13, 20 contained Hydrazine Tetrabromide (s.g. = 2.96, 1 in = .107 psi). Tubes 4, 5, 8, 14, 17 and 18 contained FS-5 a fluorinated oil (s.g. = 1.86, 1 in = .067 psi) and the remaining tubes contained water. All manometer bank fluids were dyed with methylene blue. A program summary is given in Table 7-7 and a typical printout is shown in Table 7-8.

TABLE 7-7

PROGRAM MANOMETER BANK PRESSURE - LOGIC

```
C     MANØMETER BANK PRESSURE PRØGRAM
C
      DIMENSIØN ZERØ(31),RD(31)
      CALL ØPENF(1,"MDATA",2)
      READ(1,)(ZERØ(I),I=1,31)
    1 READ(1,)IRUN,C44,CO
      READ(1,)(RD(I),I=1,31)
      PRINT,"     RUN  - ",IRUN
      PRINT,↑2," NØ.  INCHES   PRESS.",↑
      SPAN=C44-CO
      CAL=44./SPAN
      DØ 10 I=1,31
      XIN=((RD(I)-CO)*CAL)-ZERØ(I)
      GØ TØ(2,2,2,4,4,2,2,4,2,6,6,6,2,4,6,6,4,4,6,2,6,6,6,6,6,6,6,6,
&6,6,6),I
    2 PRESS=XIN*.107
      GØ TØ 8
    4 PRESS=XIN*.067
      GØ TØ 8
    6 PRESS=XIN*.0361
    8 PRINT 20, I,XIN,PRESS
   10 CONTINUE
      PRINT 30,
      GØ TØ 1
   20 FØRMAT(I3,3X,F6.3,2X,F6.3)
   30 FØRMAT(////////////////////////////////////)
      END

READY
```

TABLE 7-8

PROGRAM MANOMETER BANK PRESSURE -

TYPICAL OUTPUT

RUN - 36

NO.	INCHES	PRESS.
1	34.392	3.680
2	43.150	4.617
3	41.132	4.401
4	12.418	0.832
5	-1.627	-.109
6	43.450	4.649
7	41.900	4.483
8	7.608	0.510
9	32.525	3.480
10	-.073	-.003
11	1.271	0.046
12	0.669	0.024
13	39.200	4.194
14	0.925	0.062
15	1.723	0.062
16	0.288	0.010
17	-1.700	-.114
18	-1.650	-.111
19	4.325	0.156
20	41.780	4.470
21	2.398	0.087
22	2.716	0.098
23	3.326	0.120
24	1.388	0.050
25	-.699	-.025
26	-.077	-.003
27	1.386	0.050
28	4.445	0.160
29	-.106	-.004
30	-.077	-.003
31	5.970	0.216

REPORT DISTRIBUTION LIST FOR CONTRACT NAS8-24568

	Copies
NASA Marshall Space Flight Center Marshall Space Flight Center, Alabama 35812	
Attn: Technical Manager, Terry Greenwood, S&E-AERO-AT	5
David Seymour, S&E-AERO-AT	5
Office of Technical Information, MS-IP	2
Keith Chandler, S&E-ASTN-PA	1
Technical Library	1
Hans G. Paul, R-P&VED	2
Purchasing Office, PR-EC	1
Don Thompson, S&E-ASTN-PAA	1
Patent Office, M-PAT	1
Technology Utilization Office, MS-T	1
NASA Headquarters, Washington, D.C. 20546	
Attn: Chief, Liquid Propulsion Technology, OART, RPL	3
Jack Suddreth, OART, RPL	2
Alfred Gessow, OART, RR-2	1
Director, Launch Vehicles and Propulsion, OSSA, SV	1
Director, Advanced Manned Missions, OMSF, MT	1
Chief, Air Breathing Propulsion, RAP	1
Chief, Fluid Dynamics, RRF	1
Director, Technology Utilization Division, OTU	1
NASA Ames Research Center Moffett Field, California 94035	
Attn: Mission Analysis Division	1
Hans M. Mark	2
NASA Scientific and Technical Information Facility P.O. Box 33 College Park, Maryland 20740	10
NASA Goddard Space Flight Center Greenbelt, Maryland 20771	
Attn: Merland L. Moseson, Code 620	2
NASA Pasadena Office 4800 Oak Grove Drive Pasadena, California 91103	
Attn: Henry Burlage, Jr., Propulsion Div., 38	2
JPL Support Contracts Branch, Fred Abbott, Bldg. 150, Rm. 502	1
Patents and Contracts Management	1
Dr. Duane Dippery MS354-357	1

	Copies
NASA Langley Research Center Langley Station Hampton, Virginia 23365 Attn: Edward Cortwright, Director	2
Kenneth Pierpont, MS353	2
NASA Lewis Research Center 21000 Brookpark Road Cleveland, Ohio 44135 Attn: Irving Johnson, MS500-205	2
Paul Herr, MS500-209	1
Office of Technical Information	1
James Dugan, MS501-2	1
NASA Manned Spacecraft Center Houston, Texas 77001 Attn: Joseph G. Thibodaux, Jr., Chief Propulsion and Power Division	2
Office of Technical Information	1
NASA John F. Kennedy Space Center Cocoa Beach, Florida 32921 Attn: Dr. Kurt H. Debus	2
Aeronautical Systems Division Air Force Systems Command Wright-Patterson Air Force Base Dayton, Ohio 45433 Attn: D. L. Schmidt, Code ASRCNC-2	1
Air Force Missile Development Center Holloman Air Force Base, New Mexico Attn: Maj. R. E. Bracken, Code MDGRT	1
Air Force Missile Test Center Patrick Air Force Base, Florida Attn: L. J. Ullian	1
Space and Missile Systems Organization Los Angeles, California Attn: Col. Clark, Technical Data Center	1
Arnold Engineering Development Center Arnold Air Force Station Tullahoma, Tennessee Attn: Dr. H. K. Doetsch	1

	Copies
Bureau of Naval Weapons Department of the Navy Washington, D.C. Attn: J. Kay, RTMS-41	1
Defense Documentation Center Headquarters Cameron Station, Building 5 5010 Duke Street Alexandria, Virginia 22314 Attn: TISIA	1
Headquarters, U.S. Air Force Washington 25, D.C. Attn: Col. C. K. Stambaugh, AFRST	1
Picatinny Arsenal Dover, New Jersey 07801 Attn: I. Forsten, Chief Liquid Propulsion Laboratory, SMUPA-DL	1
Air Force Rocket Propulsion Laboratory Research and Technology Division Air Force Systems Command Edwards, California 93523 Attn: Mr. H. Main, RPRR	1
U.S. Army Missile Command Redstone Arsenal Alabama 35809 Attn: Dr. Walter Wharton	1
U.S. Naval Weapons Station China Lake, California 93557 Attn: Chief, Missile Propulsion Division, Code 4562	1
Chemical Propulsion Information Agency Applied Physics Laboratory 8621 Georgia Avenue Silver Spring, Maryland 20910 Attn: Tom Reedy	1
Aerojet-General Corporation P.O. Box 296 Azusa, California 91703 Attn: W. L. Rodgers	1
Aerojet-General Corporation P.O. Box 1947 Technical Library, Bldg. 2015, Dept. 2410 Sacramento, California 95809 Attn: R. Stiff	1

	Copies
Aeronutronic Division Philco Corporation Ford Road Newport Beach, California 92663 Attn: D. A. Garrison	1
Aerospace Corporation 2400 East El Segundo Blvd. P.O. Box 95085 Los Angeles, California 90045 Attn: John G. Wilder, MS-2293	1
Arthur D. Little, Inc. 20 Acorn Park Cambridge, Massachusetts 02140 Attn: Library	1
Astrosystems International, Inc. 1275 Bloomfield Avenue Fairfield, New Jersey 07007 Attn: A. Mendenhall	1
Atlantic Research Corporation Edsall Road and Shirley Highway Alexandria, Virginia 22314 Attn: Dr. Ray Friedman	1
Avco Systems Division Wilmington, Massachusetts Attn: Howard B. Winkler	1
Beech Aircraft Corporation Boulder Division Box 631 Boulder, Colorado Attn: J. H. Rodgers	1
Bell Aerosystems Company P.O. Box 1 Buffalo, New York 14240 Attn: W. M. Smith	1
Bellcomm 955 L'Enfant Plaza, S.W. Washington, D.C. Attn: H. S. London	1

	Copies
Bendix Systems Division Bendix Corporation 3300 Plymouth Road Ann Arbor, Michigan Attn: John M. Brueger	1
Boeing Company P.O. Box 3707 Seattle, Washington 98124 Attn: J. D. Alexander	1
Boeing Company 1625 K Street, N.W. Washington, D.C. 20006 Attn: Library	1
Boeing Company P.O. Box 1680 Huntsville, Alabama 35801 Attn: Ted Snow	1
Missile Division Chrysler Corporation P.O. Box 2628 Detroit, Michigan 48231 Attn: John Gates	1
Wright Aeronautical Division Curtiss-Wright Corporation Wood-Ridge, New Jersey 07075 Attn: G. Kelley	1
Astropower Laboratory McDonnell-Douglas Aircraft Company 2121 Paularino Newport Beach, California 92663 Attn: Dr. George Moe Director, Research	1
Missile and Space Systems Division McDonnell-Douglas Aircraft Company 3000 Ocean Park Blvd. Santa Monica, California 90406 Attn: R. W. Hallet, Chief Engineer Advanced Space Technology	1
Research Center Fairchild Hiller Corporation Germantown, Maryland Attn: Ralph Hall	1

	Copies
Republic Aviation Corporation Fairchild Hiller Corporation Farmingdale, Long Island, New York Attn: Library	1
General Dynamics/Convair Division Library & Information Services (128-00) P.O. Box 1128 San Diego, California 92112 Attn: Frank Dore	1
Missile and Space Systems Center General Electric Company Valley Forge Space Technology Center P.O. Box 8555 Philadelphia, Penna. Attn: F. Mezger	1
F. E. Schultz	1
Grumman Aircraft Engineering Corporation Bethpage, Long Island New York Attn: Joseph Gavin	1
Honeywell, Inc. Aerospace Division 2600 Ridgway Road Minneapolis, Minnesota Attn: Gordon Harms	1
Hughes Aircraft Co. Aerospace Group Centinela and Teale Streets Culver City, California Attn: E. H. Meier, V.P. and Div. Mgr. Research and Dev. Div.	1
Walter Kidde and Company, Inc. Aerospace Operations 567 Main Street Belleville, New Jersey Attn: R. J. Manfille Dir. of Research Engr.	1
Ling-Temco-Vought Corporation P.O. Box 5907 Dallas, Texas 75222 Attn: Warren C. Trent	1

Copies

Lockheed Missiles and Space Company
P.O. Box 504
Sunnyvale, California 94088
Attn: J. Guill, Technical Information Center 1

Lockheed Missiles and Space Company
Huntsville Research and Engineering Center
4800 Bradford Blvd., N.W.
Huntsville, Alabama 35805
Attn: Mrs. Beverly Audah 1

Lockheed Propulsion Company
P.O. Box 111
Redlands, California 92374
Attn: H. L. Thackwell 1

The Marquardt Corporation
16555 Saticoy Street
Van Nuys, California 91409
Attn: Howard McFarland 1

Baltimore Division
Martin Marietta Corporation
Baltimore, Maryland 21203
Attn: John Calathes (3214) 1

Denver Division
Martin Marietta Corporation
P.O. Box 179
Denver, Colorado 80201
Attn: Dr. Morganthaler 1

Orlando Division
Martin Marietta Corporation
P.O. Box 5837
Orlando, Florida
Attn: J. Ferm 1

McDonnell-Douglas Aircraft Corporation
P.O. Box 516
Municipal Airport
St.Louis, Missouri 63166
Attn: R. A. Herzmark 1

Space & Information Systems Division
North American Rockwell Corporation
12214 Lakewood Boulevard
Downey, California 90241
Attn: Library 1

	Copies
Rocketdyne (Library 586-306) North American Rockwell Corporation 6633 Canoga Avenue Canoga Park, California 91304 Attn: Dr. R. J. Thompson, Jr. S. F. Iacobellis	 1 1
Northrop Space Laboratories 3401 West Broadway Hawthorne, California Attn: Dr. William Howard	 1
Astro-Electronics Division Radio Corporation of America Princeton, New Jersey 08540 Attn: Y. Brill	 1
Reaction Motors Division Thiokol Chemical Corporation Denville, New Jersey 07832 Attn: Dwight S. Smith	 1
Thiokol Chemical Corporation Huntsville Division Huntsville, Alabama Attn: John Goodloe	 1
Space Division Aerojet-General Corporation 9200 East Flair Avenue El Monte, California 91734 Attn: S. Machlawski	 1
Stanford Research Institute 333 Ravenswood Avenue Menlo Park, California 94025 Attn: Dr. Gerald Marksman	 1
TRW Systems Group TRW Incorporated One Space Park Redondo Beach, California 90278 Attn: G. W. Elverum	 1
TAPCO Division TRW, Incorporated 23555 Euclid Avenue Cleveland, Ohio 44117 Attn: P. T. Angell	 1

	Copies
Research Laboratories United Aircraft Corporation 400 Main Street East Hartford, Connecticut 06108 Attn: Erle Martin	1
Hamilton Standard Division United Aircraft Corporation Windsor Locks, Connecticut 06096 Attn: R. Hatch	1
United Technology Center 587 Methilda Avenue P.O. Box 358 Sunnyvale, California 94088 Attn: Dr. D. Altman	1
Florida Research and Development Pratt and Whitney Aircraft United Aircraft Corporation P.O. Box 2691 West Palm Beach, Florida 33402 Attn: R. J. Coar	1
Rocket Research Corporation 520 South Portland Street Seattle, Washington 98108 Attn: Foy McCullough, Jr.	1
Vickers, Inc. P.O. Box 302 Troy, Michigan Attn: Library	1
Louisiana State University Department of Chemical Engineering Baton Rouge, Louisiana Attn: Dr. Richard J. Farmer	1
Sunstrand Aviation 2421 Eleventh Street Rockford, Illinois 61101 Attn: R. W. Reynolds	1
General Applied Science Laboratory, Inc. Merrick and Stewart Avenues Westbury, Long Island New York 11590 Attn: Dr. Ray Edleman	1

UNCLASSIFIED

Security Classification

DOCUMENT CONTROL DATA - R & D

(Security classification of title, body of abstract and indexing annotation must be entered when the overall report is classified)

1. ORIGINATING ACTIVITY (Corporate author) Rocketdyne, a Division of North American Rockwell Corporation, 6633 Canoga Avenue, Canoga Park, California 91304	2a. REPORT SECURITY CLASSIFICATION Unclassified
	2b. GROUP

3. REPORT TITLE

3. REPORT TITLE

PERFORMANCE ANALYSIS OF PROPULSION SYSTEMS

4. DESCRIPTIVE NOTES (Type of report and inclusive dates)

Final Report (17 June 1969 through 18 October (1970)

5. AUTHOR(S) (First name, middle initial, last name)

Wrubel, J. A.

6. REPORT DATE January 1971	7a. TOTAL NO. OF PAGES 308	7b. NO. OF REFS 14
8a. CONTRACT OR GRANT NO. NAS8-24568	9a. ORIGINATOR'S REPORT NUMBER(S) R-8390	
b. PROJECT NO.		
c.	9b. OTHER REPORT NO(S) (Any other numbers that may be assigned this report)	
d.		

10. DISTRIBUTION STATEMENT

11. SUPPLEMENTARY NOTES	12. SPONSORING MILITARY ACTIVITY George C. Marshall Space Flight Center Marshall Space Flight Center, Alabama 35812

13. ABSTRACT The improved understanding of gas stream turbulent mixing is contingent upon obtaining a more comprehensive description of the resultant flow field and a more precise evaluation of the turbulent transport properties.

Under Contract NAS7-521, a facility for study of this phenomenon was constructed and checked out. Characterization and diagnostic experiments, together with some data analysis were accomplished under the present contract, NAS8-24568, and are described herein.

The flow field experimentally studied was the two-dimensional mixing of fuel-rich supersonic hydrogen-oxygen combustion products and a subsonic heated air stream. The mixing was accomplished in a chamber accessible to both optical- and probe-type instrumentation systems.

A total of 36 tests has been conducted which included studies of (1) film coolant interaction, (2) the two-dimensionality of the flow, (3) air temperature effects, (4) velocity ratio effects, (5) air stream turbulence effects, and (6) configuration effects. The data gathered consisted of (1) test section static pressure, (2) mixing layer temperature, (3) partial pressure of H_2O, (4) photographic information (UV, IR, and schlieren), and (5) facility operation.

14. KEY WORDS	LINK A		LINK B		LINK C	
	ROLE	WT	ROLE	WT	ROLE	WT
Gas Stream Turbulent Mixing						
Turbulent Transport Properties						
Supersonic Hydrogen-Oxygen Combustion Products						
Subsonic Heated Airstream						
Film Coolants						
Two-Dimensional Flow						
Temperature Measurements						
Partial-Pressure Measurements						
Photography						